

# **DISCOVERY AND BIOSYNTHESIS OF THE REDOX COFACTOR MYCOFACTOCIN**

## **Dissertation**

zur Erlangung des akademischen Grades  
**„doctor rerum naturalium“ (Dr. rer. nat.)**

vorgelegt dem Rat der Fakultät für Biowissenschaften  
der Friedrich-Schiller-Universität

von Luis Alberto Peña Ortiz  
geboren am 07.03.1987 in Bogotá, Kolumbien

Gutachter 1: Prof. Dr. Christian Hertweck (Jena, Deutschland)

Gutachter 2: Prof. Michael Freeman (Minnesota, Vereinigten Staaten von Amerika)

Gutachter 3: Dr. Gerald Lackner (Jena, Deutschland)

Datum der öffentlichen Verteidigung: 29.09.2021

*Un noble espíritu agradece al hombre más pequeño*

TABLE OF CONTENT

1.	TABLE OF FIGURES .....	1
2.	DECLARATION FOR THE OPENING OF THE DOCTORAL EXAMINATION PROCESS ..	5
3.	SUMMARY.....	6
4.	ZUSAMMENFASSUNG .....	8
5.	LIST OF ABBREVIATIONS AND ACRONYMS.....	11
6.	INTRODUCTION .....	13
6.1.	The genus <i>Mycobacterium</i> and <i>Mycobacterium tuberculosis</i> : disease, treatment, and perspectives .....	13
6.2.	The role of cofactors in antibiotic susceptibility and resistance of mycobacteria .....	16
6.3.	Cofactors are indispensable for cellular biochemistry.....	19
6.3.1.	Biogenesis of the chemical core and tail moieties of organic cofactors .....	21
6.3.2.	Biosynthesis of cofactors containing quinone moieties. ....	25
6.3.3.	Endogenous (polypeptide-derived) quinone cofactors. ....	27
6.3.4.	Pyroloquinoline quinone (PQQ) - a ribosomally-produced and post-translationally modified quinone cofactor.....	28
6.4.	Mycofactocin is a predicted RiPP cofactor .....	31
6.4.1.	Discovery of MFT: gene organization and distribution.....	31
6.4.2.	Biosynthesis of MFT .....	32
6.4.3.	The biological role of MFT.....	35
7.	AIMS OF THIS WORK.....	43
8.	MANUSCRIPTS.....	44
8.1.	Structure elucidation of the redox cofactor mycofactocin reveals oligo-glycosylation by MftF .....	44
8.2.	Impact of Oxygen Supply and Scale-Up on <i>Mycobacterium smegmatis</i> Cultivation and Mycofactocin Formation .....	56
9.	SUPPLEMENTARY RESULTS .....	71
9.1.	The role of mycofactocin in lactate metabolism .....	71
9.2.	The enzymatic activity of MFT-dependent alcohol dehydrogenase and glucose-methanol-choline oxidoreductase .....	77
9.3.	Process development for mycofactocin production in mineral media with supplementation	80



## TABLE OF CONTENT

9.4. Completeness of MFT extraction from complex media broths .....	88
10. DISCUSSION.....	91
10.1. Structure elucidation of the redox cofactor mycofactocin .....	91
10.2. Mycofactocin glucosyltransferase catalyzes an unusual <i>O</i> -glucosylation of a modified <i>N</i> -terminal tyrosine .....	96
10.3. Methylated mycofactocin and the biosynthetic order of mycofactocin production.....	97
10.4. Impact of Oxygen Supply and Scale-Up on <i>Mycobacterium smegmatis</i> Cultivation and Mycofactocin Formation .....	102
11. CONCLUSION & OUTLOOK .....	107
12. REFERENCES .....	109
13. ANNEX.....	123
13.1. Protocol for proteomic analysis of Mycobacterial strains.....	123
13.1.1.Reagents.....	123
13.1.2.Protocol.....	124
13.1.3.Proteomics protocol.....	125
14. ACKNOWLEDGMENTS .....	127
15. SELBSTÄNDIGKEITSERKLÄRUNG.....	129
16. CURRICULUM VITÆ .....	130

**1. TABLE OF FIGURES**

Figure 1: Antibiotics commonly used in tuberculosis treatment. Note that INH (B), EMB (C), ETH (D), and PZA (E) are structurally related to the B<sub>3</sub> vitamers nicotinamide (F), niacin (G), and nicotinamide riboside (H). .....16

Figure 2: Molecular structure of (A) glutathione, (B) bacillithiol, and (C) mycothiol. The cysteine residue in each thiol is highlighted in blue, glutamyl moiety is highlighted in purple. ....18

Figure 3: Coenzyme F<sub>420-1</sub> oxidized (A, redox core in red) and reduced (B, redox core in blue). Pink indicates L-glutamate side chain.....19

Figure 4: Hierarchical classification of cofactors. Redox core highlighted in red when present. Modified from Fischer (2010) [85]. .....20

Figure 5: Organic cofactors and their shared moieties. Cofactors with AMP handle (blue atoms): adenine triphosphate (ATP, A), nicotinamide adenine dinucleotide (NAD<sup>+</sup>, B), nicotinamide adenine dinucleotide phosphate (NADP<sup>+</sup>, C), coenzyme A (D), flavin adenine dinucleotide (FAD<sup>+</sup>, E). The pyridine redox core (black bold bonds and atoms) is highlighted in the black square. Flavin-related cofactors: FAD<sup>+</sup>, flavin mononucleotide (FMN<sup>+</sup>), and the deazaflavin factor 420 (F<sub>420-n</sub>, G). The isoalloxazine redox core (red bold bonds and atoms) is highlighted in the red square. The quinone redox core (green bonds and atoms) can have a quinone conformation as in ubiquinone (H) or menaquinone (I), or a catechol conformation as in topaquinone (TPQ, J) and other endogenous cofactors, or pyrroloquinoline quinone (PQQ, K). Quinone redox core and half-reactions are highlighted in the green square. ....24

Figure 6: Endogenous peptide cofactors, catechol redox core atoms and bonds in green. ....27

Figure 7: Pyrroloquinoline quinone (PQQ) biosynthesis according to [151]. Redox-active atoms are highlighted in red.....30

Figure 8: Clustal Omega [188, 189] alignment of the MftA precursor in 47 species with the MFT cluster, demonstrating highly conserved C-terminal residues. The *M. orygis* sequence most likely represents a variant inactivated by mutation. ....32

Figure 9: Phylogenetic tree of the MFT radical SAM protein (MftC) and the MFT biosynthetic gene cluster. MftC protein alignment was done with the Clustal Omega algorithm [188, 189] and used as input for a maximum likelihood phylogenetic tree using PHYML [190], both in a Geneious

## TABLE OF FIGURES

environment. The LG substitution model was used [191], and branch support is SH-like (values in nodes). The scale bar indicates substitutions per site; six substitution rate categories were allowed, and the tree was optimized to topology/length/rate. All other parameters were estimated automatically. The surrounding gene neighborhood was drawn manually and annotated according to the most up-to-date NCBI annotation. Genes length is not drawn to scale.....33

Figure 10: Current model of PMFT and mature mycofactocin biosynthesis. The MftA precursor undergoes two rSAM-mediated reactions that result in its decarboxylation and cyclization, forming MftA\*. The peptidase MftE cleaves AHDP from the precursor polypeptide, which is then oxidatively deaminated by MftD. This reaction forms the redox-active core of premycofactocin (PMFT, active atoms in red). A predicted glycosyltransferase catalyzes the addition of a glycosyl moiety to form mature MFT. ....37

Figure 11: Gene cluster MSMEG\_6234 to MSMEG\_6242 in *M. smegmatis* mc<sup>2</sup> 155, containing the MFT-dependent alcohol dehydrogenase Mno (MSMEG\_6242). Homologs of these CDS can be found in proteins from *M. tuberculosis* H37Rv (cyan) and *S. erythraea* NRRL2338 (blue). Parentheses indicate the identity percentage with a cutoff of >40%.....41

Figure 12: KEGG metabolic pathway enrichment (A) of features with ratio significance level <0.05 OR annotated as MFT maturases. Lac = lactate, Glc = glucose. (B) Butterfly plot of features in lactate as sole carbon source. Statistically significant features upregulated in the mutant strain appear in the top right side of the chart. *P*-value calculated by two-tailed Student' t-test. ....73

Figure 13: Lactate dehydrogenase activity of MftD. (A): purification by affinity chromatography of the MBP: *M. smegmatis* MftD fusion protein. Protein marker size units in kDa (PageRuler Unstained Protein Ladder) (B) *M. smegmatis* MftD with various  $\alpha$ -hydroxy acids and DCPIP as the final electron acceptor. (C): growth curve of the *E. coli* BL21(DE3)  $\Delta$ *lldD* (courtesy Dr. Daniel Braga). (D): *M. smegmatis*, and *M. bovis* MftD and LldD2 with various  $\alpha$ -hydroxy acids and DCPIP as the final electron acceptor. ....76

Figure 14: Production and enzymatic assay of MSMEG\_6242 in *E. coli* BL21(DE3). (A) SDS-PAGE depicting the fractions of the recombinant enzyme purification by affinity chromatography. Lane 1: crude lysate; 2: NiNTA column flowthrough; 3: 20 mM imidazole wash; 4: 50 mM imidazole wash; 5:

## TABLE OF FIGURES

eluted fraction with 300 mM imidazole; 6: centrifugal concentrator (MWCO 3 kDa) flowthrough; 7: concentrated protein. Protein marker size units in kDa (PageRuler Unstained Protein Ladder). Alcohol dehydrogenase oxidation with recombinant MSMEG\_6242 and NDMA (B) or DCPIP (C) as artificial redox acceptor. (D). Decoloration of oxidized DCPIP only occurs in the presence of reduced NADH.

.....79

Figure 15: Oxygen-unlimited batch culture of MSMEG in a 3 L mineral media filling volume stirred tank reactor. (A) Oxygen transfer rate (OTR) and respiratory quotient. (B) Offline metabolites ethanol, acetate, lactate. (C) the peak area of MFT by the sum of reduced and oxidized species PMFT(H<sub>2</sub>), MMFT-2b(H<sub>2</sub>), MMFT-8(H<sub>2</sub>). Areas were normalized to sample volume. Experimental conditions: stirring rate = system controlled – max 488 rpm, gas flow rate = 0.75 L min<sup>-1</sup>, total reactor volume = 7 L, filling volume = 3 L, temperature 37°C, HdB medium with 10 g L<sup>-1</sup> ethanol, pH 7, controlled with 100 g L<sup>-1</sup> NaOH or H<sub>3</sub>PO<sub>4</sub>. ....84

Figure 16: Oxygen-unlimited batch culture of MSMEG in a 3 L mineral media supplemented with iron and sulfur. (A) Oxygen transfer rate (OTR) and respiratory quotient. (B) Offline metabolites ethanol, acetate, lactate. (C) the peak area of MFT by the sum of reduced and oxidized species PMFT(H<sub>2</sub>), MMFT-2b(H<sub>2</sub>), MMFT-8(H<sub>2</sub>). Areas were normalized to sample volume. Experimental conditions: stirring rate = system controlled – max 421 rpm, gas flow rate = 0.75 L min<sup>-1</sup>, total reactor volume = 7 L, filling volume = 3 L, temperature 37°C, HdB medium with 10 g L<sup>-1</sup> ethanol, iron and sulfur according to text. pH 7, controlled with 100 g L<sup>-1</sup> NaOH or H<sub>3</sub>PO<sub>4</sub>. ....85

Figure 17: Oxygen-unlimited batch culture of MSMEG in a 3 L mineral media supplemented with vitamins and amino acids. (A) Oxygen transfer rate (OTR) and respiratory quotient. (B) Offline metabolites ethanol, acetate, lactate. (C) the peak area of MFT by the sum of reduced and oxidized species PMFT(H<sub>2</sub>), MMFT-2b(H<sub>2</sub>), MMFT-8(H<sub>2</sub>). Areas were normalized to sample volume. Experimental conditions: stirring rate = system controlled, gas flow rate = 0.75 L min<sup>-1</sup>, total reactor volume = 7 L, filling volume = 3 L, temperature 37°C, HdB medium with 10 g L<sup>-1</sup> ethanol, vitamins, and amino acids according to text. pH 7, controlled with 100 g L<sup>-1</sup> NaOH or H<sub>3</sub>PO<sub>4</sub>. ....86

Figure 18: Estimation of the MFT yield in the different steps of the extraction process. MFT was extracted from (A): 5 mL culture; (B): 10 mL culture; (C): 20 mL culture. ....89

## TABLE OF FIGURES

Figure 19: Impact of incubation time on the MFT yield from a 5 mg frozen MSMEG pellet. ....	90
Figure 20: Molecular networking of mycofactocin, generated with GNPS [270] and data visualization by Cytoscape [271]. Nodes are colored based on the carbon source in the culture media, red in ethanol and green in glucose. Edge thickness represent the cosine score, a value of how identical the spectra are. As a representative mycofactocin, MMFT-8H <sub>2</sub> structure is indicated with redox core atoms and bonds in red with the premycofactocin (PMFT) precursor in blue. Position of the methyl moiety in 2- <i>O</i> -methylglucose in bold. ....	93
Figure 21: Mycofactocin and methylmycofactocin biosynthesis. Dashed lines indicate side-reactions. Atoms and bonds in the redox active moiety are highlighted in red (diketone) or blue (dihydroxyl). A bold bond indicates methyl moieties. Relative abundance mutant strains $\Delta mftC$ , $\Delta mftE$ , $\Delta mftD$ , or $\Delta mftF$ , is shown in color scale: white: wild-type, red: lower abundance than in the wild-type, green: higher abundance than in wild-type. SAM: S-adenosylmethionine. SAH: S-adenosylhomocysteine. NDP: nucleotide diphosphate. ....	95
Figure 22: Proposed order of mycofactocin biosynthesis and (methyl) oligoglucosylation. ....	100

## **DECLARATION FOR THE OPENING OF THE DOCTORAL EXAMINATION PROCESS**

### **2. DECLARATION FOR THE OPENING OF THE DOCTORAL EXAMINATION PROCESS**

Hereby I, Luis Alberto Peña Ortiz, born March 7<sup>th</sup>, 1987, author of the present document, state that:

1. I am familiar with valid doctoral examination regulations.
2. I am the sole author of the doctoral thesis project.
3. I did not use any text passage from third parties nor a previous thesis without proper citation, and all tools, personal communications and sources have been effectively used.
4. The people named in the acknowledgements of my dissertation supported me in the selection and evaluation of the material, and the preparation and critical review of the manuscripts and the present thesis.
5. I did not receive external assistance from specialized consultants, and no third party will receive direct or indirect financial benefits from the applicants for work connected with the doctoral thesis.
6. I have not already submitted the present thesis as a final thesis for state or scientific examination.
7. I have not submitted the same or a substantially similar thesis to another higher education institution or any other faculty as a doctoral thesis.

---

Luis Alberto Peña Ortiz

### 3. SUMMARY

*Mycobacterium tuberculosis*, the etiological agent of tuberculosis (TB), can survive as an intracellular pathogen residing in a granulomatous lesion in the lungs. Current TB treatments comprise a long course of several antibiotics with various side effects. Incomplete treatment is leading to antibiotic resistance, a growing threat worldwide. It has been recognized that both antibiotic inactivation and intracellular survival is often mediated by organic cofactors. Furthermore, novel therapeutic compounds in use are prodrugs that require cofactors for *in vivo* conversion into an active pharmaceutical entity. Mycobacterial cofactors are an up-and-coming field of research for developing novel therapeutic compounds. As such, novel cofactors offer an exciting opportunity to discover novel aspects in the pathogen's physiology and pathology as well as inspiring novel avenues for TB management.

Mycofactocin (MFT) is a novel redox cofactor, part of the family of natural products termed ribosomally produced and post-translationally modified peptides and a universal genomic feature of the *Mycobacterium* genus. Its discovery was spurred from the bioinformatic observation of a gene locus in the vicinity of a radical SAM maturase, containing a small peptide precursor, a chaperone, a peptidase, and a glycosyltransferase, alongside putative MFT-dependent redox enzymes and other genes encoding proteins of unknown function. *In-vitro* investigation of the biosynthesis pathway showed the formation of the redox-active precursor premycofactocin. In addition, *in-vivo* studies with the model organism *Mycobacterium smegmatis* have associated MFT to the metabolism of primary alcohols for assimilation as a carbon source. Critical questions remained, such as whether the *in vitro* biosynthetic model is valid *in vivo*, the function of the putative glycosyltransferase, the enzymology of MFT-dependent oxidoreductases and dehydrogenases, and the role of MFT in mycobacterial pathogenesis.

The first project of this thesis published in the article “**Structure elucidation of the redox cofactor mycofactocin reveals oligo-glycosylation by MftF**” identified *in vivo* the previously described precursors and resolved the structure of mature mycofactocin in *M. smegmatis*. With a combination of state-of-the-art techniques, including high-resolution mass spectrometry, isotopic labelling, and nuclear magnetic resonance we identified the role of the putative glycosyltransferase MftF, catalyzing the formation of an oligosaccharide consisting of up to nine glucose units linked by a  $\beta$ -1,4 glycosidic bond, installed at the phenol moiety of premycofactocin. The new mycofactocin congeners, which we consider to be the mature form of the cofactor, are redox-active and form a novel pool enriched during ethanol cultivation as a sole carbon source. Furthermore, we unexpectedly discovered methyl-mycofactocin, in which

the second unit in this oligoglucoside chain is a 2-*O*-methylglucose. The enzyme responsible for this modification is still unknown. Our results close an important gap of knowledge about mycofactocin biosynthesis and provide final evidence for the existence of this cofactor, postulated almost ten years ago.

The second article of this thesis, titled “**Impact of Oxygen Supply and Scale-Up on *Mycobacterium smegmatis* Cultivation and Mycofactocin Formation**” proposes a protocol for mycofactocin production in *M. smegmatis*. By modelling the aeration conditions in complex Lysogeny Broth (LB) and a transfer-rate online measurement, we observed a direct correlation between an increase in long-chain mycofactocin yield and decreased oxygen transfer rate. The ratio of premycofactocin precursor and short-chain mycofactocin, however, remained stable between conditions. We upscaled these parameters based on volumetric power input, from a 40 mL scale to 3 L volume in a 7 L stirred tank reactor, and we observed similar results. Interestingly, we observed higher long-chain mycofactocin yield in Hartman’s de Bont mineral media. With this research, we offer a protocol for achieving MFT production in the milligram scale that will advance our research on the three-dimensional structure and the enzymology of MFT-dependent oxidoreductases.

Bringing these two articles together, it comes to our attention that the previously proposed biosynthetic pathway does not fully explain the novel congeners identified. Based on observations with mutant strains and the enrichment and depletion of pathway-dependent MFT congeners, we propose a biosynthetic route in which glucosylation occurs before premycofactocin formation and methylation, however further studies are required. In conclusion, we have revealed important information about the occurrence and structure of mycofactocin. While critical questions remain open regarding the MFT role in pathogenesis and the interaction with MFT-dependent dehydrogenases/oxidoreductases, this thesis offers not only a characterization of the mature mycofactocin cofactor *in vivo* but opens a practical solution for the problem of yield that will help resolve critical questions regarding the novel cofactor mycofactocin.



#### 4. ZUSAMMENFASSUNG

*Mycobacterium tuberculosis*, der Erreger der Tuberkulose (TB), kann als intrazelluläres Pathogen in granulomatösen Läsion in der Lunge überleben. Die derzeitigen Behandlungsstrategien umfassen eine lange Kur mit mehreren Antibiotika und verschiedenen damit verbundenen Nebenwirkungen. Unvollständige Behandlung kann zu einer Antibiotika-Resistenz führen, eine weltweit wachsende Bedrohung. Es ist bekannt, dass sowohl die Inaktivierung von Antibiotika als auch das intrazelluläre Überleben oft durch organische Kofaktoren vermittelt wird, chemische Moleküle, die für die Enzymaktivität erforderlich sind. Darüber hinaus sind einige neuartigen therapeutischen Verbindungen Prodrugs, die Kofaktoren für die Umwandlung in eine aktive pharmazeutische Form *in vivo* benötigen. Mykobakterielle Kofaktoren sind ein aufstrebendes Forschungsgebiet für die Entwicklung neuer therapeutischer Verbindungen. Daher bieten neuartige Kofaktoren die spannende Möglichkeit, neue Aspekte in der Physiologie und Pathologie des Erregers sowie neue Wege für das TB-Management zu entdecken.

Mycofactocin (MFT) ist ein neuartiger Redox-Cofaktor, der zur Naturstoff-Familie der ribosomal produzierten und posttranslational modifizierten Peptide gehört und ein universelles genomisches Merkmal der Gattung *Mycobacterium* darstellt. Seine Entdeckung wurde durch die bioinformatische Beobachtung eines Genlocus in der Nähe einer radikalen SAM-Maturase angestoßen, der neben putativen MFT-abhängigen Redox-Enzymen und anderen Genen, die für Proteine unbekannter Funktion kodieren, einen kleinen Peptidvorläufer, ein Chaperon, eine Peptidase und eine Glykosyltransferase enthält. *In-vitro*-Untersuchungen des Biosyntheseweges zeigten die Bildung des redoxaktiven Vorläufers Prämycofactocin. Darüber hinaus haben *In-vivo*-Studien mit dem Modellorganismus *Mycobacterium smegmatis* MFT mit dem Metabolismus primärer Alkohole zur Assimilation als Kohlenstoffquelle in Verbindung gebracht. Es blieben kritische Fragen offen, z. B. ob das *In-vitro*-Biosynthesemodell *in vivo* gültig ist, sowie die Funktion der putativen Glykosyltransferase, die Enzymologie der MFT-abhängigen Oxidoreduktasen und Dehydrogenasen sowie die Rolle von MFT in der mykobakteriellen Pathogenese.

Das erste Projekt dieser Arbeit, veröffentlicht im Artikel „**Structure elucidation of the redox cofactor mycofactocin reveals oligo-glycosylation by MftF**“ identifizierte die zuvor beschriebenen Vorstufen erstmal *in vivo* und klärte die chemische Struktur des reifen Mycofactocins aus *M. smegmatis* auf. Mit einer Kombination zeitgemäßer Techniken, einschließlich hochauflösender Massenspektrometrie, Isotopenmarkierung und

kernmagnetischer Resonanz, identifizierten wir die Rolle der putativen Glykosyltransferase MftF, die die Bildung eines Oligosaccharids aus und bis zu neun Glukoseeinheiten mit  $\beta$ -1,4-glykosidischer Bindung am Phenolring des Prämycofactocins katalysiert. Die neuen Mycofactocin-Derivate, die wir als die reife Form des Cofaktors ansehen, sind redoxaktiv und bilden einen Redox-Pool, der bei der Kultivierung von Ethanol als einziger Kohlenstoffquelle angereichert wird. Außerdem entdeckten wir unerwartet Methyl-Mycofactocin, bei dem die zweite Einheit in der Oligoglucosidkette eine 2-O-Methylglucose ist. Das Enzym, das für diese Modifikation verantwortlich ist, ist noch unbekannt. Unsere Ergebnisse schließen eine wichtige Wissenslücke über die Gene der Mycofactocin-Biosynthese und liefern den Nachweis eines unbekanntes Kongeners mit einer einzigen Methylierung, für die das verantwortliche Enzym noch nicht identifiziert wurde.

Im zweiten Artikel dieser Arbeit mit dem Titel „**Impact of Oxygen Supply and Scale-Up on *Mycobacterium smegmatis* Cultivation and Mycofactocin Formation**“ wird ein Protokoll für die Mycofactocin-Produktion in *M. smegmatis* vorgeschlagen. Durch die Modellierung der Sauerstoff-Übertragung in komplexer Kulturbrühe (LB) und einer Online-Messung der Sauerstoff-Transferrate wurde ein direkter Zusammenhang zwischen einem Anstieg der Ausbeute langkettigem Mycofactocin und einer verringerten Sauerstoff-Transferrate beobachtet. Das Verhältnis von Prämycofactocin-Vorläufer und kurzkettem Mycofactocin blieb jedoch zwischen den Bedingungen stabil. Wir skalierten diese Parameter basierend auf dem volumetrischen Leistungseintrag hoch, von einem 40 mL Maßstab auf 3 L Volumen in einem 7-L-Rührkesselreaktor und erhielten ähnliche Ergebnisse. Interessanterweise beobachteten wir eine höhere Ausbeute an langkettigem Mycofactocin in Hartman's de Bont Mineralmedium. Damit bieten wir ein Protokoll zur Produktion von MFT im Milligramm-Maßstab an. Dieser Fortschritt wird die Forschung an der dreidimensionalen Struktur und der Enzymologie von MFT-abhängigen Oxidoreduktasen voranbringen.

Wenn wir diese beiden Artikel zusammenbringen, fällt uns auf, dass der zuvor vorgeschlagene Biosyntheseweg die neu identifizierten Kongenere nicht vollständig erklärt. Basierend auf den Beobachtungen mit mutierten Stämmen und der Anreicherung und Abreicherung von Pfad-abhängigen MFT-Kongeneren schlagen wir einen Biosyntheseweg vor, bei dem die Glucosylierung vor der Bildung von Premycofactocin und der Methylierung stattfindet, jedoch sind weitere Studien zur Absicherung dieser Hypothese erforderlich. Zusammenfassend lässt sich sagen, dass wir wichtige Informationen über das Vorkommen und die Struktur von Mycofactocin aufgedeckt haben. Während kritische Fragen bezüglich der

## ZUSAMMENFASSUNG

Rolle von MFT in der Pathogenese und der Interaktion mit MFT-abhängigen Dehydrogenasen/Oxidoreduktasen offen bleiben, bietet diese Arbeit nicht nur eine Charakterisierung des reifen Mycofactocin-Cofaktors *in vivo*, sondern eröffnet eine praktische Lösung für das Problem der Ausbeute, die helfen wird, kritische Fragen bezüglich des neuartigen Cofaktors Mycofactocin zu lösen.

## LIST OF ABBREVIATIONS AND ACRONYMS

### 5. LIST OF ABBREVIATIONS AND ACRONYMS

<b>AHDP</b>	3-amino-5[( <i>p</i> -hydroxyphenyl)methyl]-4,4-dimethyl-2-pyrrolidinone
<b>AHDP-n</b>	AHDP with <i>n</i> glucosylations
<b>AMP</b>	Adenosine monophosphate
<b>ATP</b>	Adenine triphosphate
<b>BSH</b>	Bacillithiol
<b>CCM</b>	Central carbon metabolism
<b>CTR</b>	Carbon transfer rate
<b>dAdo•</b>	5'-deoxyadenosine
<b>DCPIP</b>	2,6-dichlorophenolindophenol
<b><i>E. coli</i></b>	<i>Escherichia coli</i>
<b>ETH</b>	Ethambutol
<b>FO</b>	8-hydroxy-5-deazaflavin
<b>GAHDP</b>	Glycyl-AHDP
<b>GAHDP-n</b>	Glycyl-AHDP with <i>n</i> glucosylations
<b>GlcNAc-Mal</b>	Malyl N-acetyl-glucosaminine
<b>GlcN-Ins</b>	Inositol N-glucosamine
<b>GLP</b>	Glycopeptidolipids
<b>GMC</b>	Glucose-methanol-choline oxidoreductase
<b>GSH</b>	Glutathione
<b>GT</b>	Glycosyltransferase
<b>HdB</b>	Hartman's de Bont mineral media
<b>HPLC</b>	High-performance liquid chromatography
<b>iLDH</b>	NAD <sup>+</sup> -independent lactate dehydrogenase
<b>INH</b>	Isoniazid
<b>LB</b>	Lysogeny Broth
<b>LC-MS/MS</b>	Tandem liquid chromatography-mass spectrometry
<b>MDR-TB</b>	Multidrug-resistant tuberculosis
<b>MFT</b>	Mycofactocin / mycofactocinone
<b>MFTH<sub>2</sub></b>	Mycofactocinol
<b>MGPL</b>	Methylglucose polysaccharides
<b>MMFT-n</b>	Methyl-mycofactocinone with <i>n</i> glycosylations
<b>MMFTH<sub>2</sub>-n</b>	Methyl-mycofactocinol with <i>n</i> glycosylations
<b>MMP</b>	Methylmannose polysaccharides

## LIST OF ABBREVIATIONS AND ACRONYMS

<b>MSH</b>	Mycothioli
<b>MSMEG</b>	<i>Mycolicibacterium smegmatis</i> (basonym <i>Mycobacterium smegmatis</i> ) mc <sup>2</sup> 155
<b>MTB</b>	<i>Mycobacterium tuberculosis</i>
<b>m/z</b>	Mass-to-charge ratio
<b>NAD<sup>+</sup></b>	Nicotinamide adenine dinucleotide
<b>NADP<sup>+</sup></b>	Nicotinamide adenine dinucleotide phosphate
<b>N-AcGlcIns</b>	N-methyl-mycothioli
<b>NDMA</b>	N-nitrosodimethylamine
<b>NMR</b>	Nuclear magnetic resonance
<b>NMP</b>	Nucleotide monophosphate
<b>nLDH</b>	NAD <sup>+</sup> -dependent lactate dehydrogenase
<b>OTR<sub>max</sub></b>	Maximum oxygen transfer rate
<b>OTR<sub>min</sub></b>	Minimum oxygen transfer rate
<b>RAMOS</b>	Respiratory activity monitoring system
<b>RIF</b>	Rifampicin
<b>RiPP</b>	Ribosomally produced and post-translationally modified peptide
<b>ROS</b>	Reactive oxygen species
<b>RQ</b>	Respiratory quotient
<b>rSAM</b>	Radical <i>S</i> -adenosyl methionine enzymes
<b>SAM</b>	<i>S</i> -adenosyl methionine
<b>SDH</b>	Short-chain dehydrogenases/reductases
<b>STR</b>	Stirred tank reactor
<b>PMFT</b>	Premycofactocin / Premycofactocinone
<b>PMFTH<sub>2</sub></b>	Premycofactocinol
<b>PMPS</b>	Polymethylated polysaccharides
<b>PMS</b>	1-methoxy-5-methylphenazinium methylsulfate
<b>Pta-AckA</b>	Phosphate acetyltransferase-acetyl kinase pathway
<b>PQQ</b>	Pyrruloquinoline quinone
<b>PZA</b>	Pyrazinamide
<b>TB</b>	Tuberculosis
<b>TOM</b>	Transfer-rate online measurement
<b>VY</b>	Valyl-tyrosine dipeptide
<b>XDR-TB</b>	Extensively multidrug-resistant tuberculosis

**6. INTRODUCTION****6.1. THE GENUS *MYCOBACTERIUM* AND *Mycobacterium tuberculosis*: DISEASE, TREATMENT, AND PERSPECTIVES**

The *Mycobacteriaceae* family comprises the *Hoyosella* genus of environmental microbes, but the more widely known members belong to the *Mycobacterium* genus and amended genera (*Mycolicibacterium*, *Mycolicibacter*, *Mycolicibacillus*, and *Mycobacteroides*). All-in-all, more than 180 species are in this family within the phylum Actinobacteria. Morphologically, these are aerobic or microaerophilic rods. The cell wall in these organisms contains mycolic acid, long-chain fatty acids modified by cyclopropane, methoxy, or ketone groups. This composition makes the wall resistant to decolorization of crystal violet with acid or alcohol, and as such, Gram-staining is an unreliable technique for their determination. Instead, alternative methods such as the Ziehl-Neelsen staining are employed. Most species are environmental microbes and are rarely pathogenic such as *Mycolicibacterium smegmatis* mc<sup>2</sup> 155 (MSMEG). Other highly pathogenic and medicinally relevant species are still placed in the modified *Mycobacterium* genus due to their medical and economic interest [1, 2]. *M. tuberculosis* (MTB) is an intracellular pathogen and the most important organism in the genus by being the etiological agent of tuberculosis (TB) [3, 4]. Other relevant organisms like *M. leprae* and *M. ulcerans* are causative agents of leprosy and Buruli ulcers. *M. bovis* infection in cattle results in bovine TB, which can spread to animals or humans.

TB is an infectious pulmonary disease, one of the top 10 major causes of illness-related death, and the leading infectious disease worldwide from a single infectious agent [5, 6]. Infection occurs by dispersion of contagious bacilli from the cough droplets of an infected individual. The bacilli establish themselves in the alveoli of an uninfected host. The mycolic acids are easily recognized by the innate immune system, a possible outcome of the >70,000 years of coexistence with humans [7-9]. The cells involved in this process, first phagocytic macrophages and, two to three weeks post-infection, antigen-specific lymphocytes are recruited to the infection site, and a granuloma is formed. The granuloma formation stops the extracellular growth of the bacilli; however, these can still survive inside the macrophage as intracellular pathogens. Survival is mediated by the ability of the pathogen to adapt to this environment: gene expression changes in these conditions to express pathways related to hypoxia, oxidative, and nitrosative stress tolerance, heavy metal toxicity, and low nutrient availability [10]. In this stage, termed latent TB, the bacilli survive for long periods of time on very scarcely available carbon sources. Metabolic profiling of MTB-infected lung granulomas has identified tricarboxylic acid cycle intermediates (citrate, isocitrate, succinate, fumarate),

## INTRODUCTION

### The genus *Mycobacterium* and *Mycobacterium tuberculosis*: disease, treatment, and perspectives

free amino acids and peptides (tyrosine, tryptophan, and others), lactate, acetate, and a wide variety of fatty acids, among others, as possible substrates that MTB could possibly survive from [11-14]. Notably, glucose is absent in this environment, and gene up-regulation has been identified in pathways encoding for fatty acid and cholesterol assimilation, and gluconeogenesis [10, 13].

Latent TB is asymptomatic and non-transmissible. Although most infections remain latent, individuals remain at a 5 - 10% risk of developing active TB within two years post-infection [5, 15]. In this further stage the bacilli are released from the granuloma, leading to further dissemination through the body and possibly onto new hosts. Common symptoms are fever, chronic cough that could include blood clots, chest pain, weight loss, and general fatigue, among others. On a more chronic stage tissue necrosis appears, while pulmonary and extrapulmonary lesions develop in bones and joints [8, 15, 16]. Without treatment, up to 60% of active TB cases result in death [6].

A typical TB treatment regimen is a 4 to 6-month therapy composed of the combination of three or more antituberculosis compounds, mainly rifampicin (RIF), isoniazid (INH), ethambutol (ETB), ethionamide (ETH), and/or pyrazinamide (PZA, Figure 1A-E). Resistance to RIF and INH indicates the emergence of multidrug-resistant (MDR-TB) and extensively multidrug resistant TB (XDR-TB) strains [17]. RIF is a semi-synthetic derivative of rifamycin, a polyketide produced by *Amycolatopsis rifamycinica*. It is the only first-line treatment able to act on both dormant and metabolically active bacilli. Its mechanism of action is binding to the  $\beta$ -subunit of the RNA polymerase, thereby preventing mRNA synthesis for translation [18]. Mutations in the  $\beta$ -subunit encoding *rpoB* gene are responsible for most rifampicin-resistant clinical isolates [19, 20]. PZA, ETH, and INH, on the other hand, are structurally related to the B<sub>3</sub> vitamers nicotinamide, niacin, and nicotinamide riboside (Figure 1F-H). Their use arises from the observation that high doses of nicotinamide positively affected mycobacterial infection treatment on a murine model [21, 22]. This effect is particularly relevant because the B<sub>3</sub> vitamers are precursors of the cofactors nicotinamide adenine dinucleotide (NAD<sup>+</sup>) and the phosphorylated congener, nicotinamide adenine dinucleotide phosphate (NADP<sup>+</sup>).

INH and PZA are compounds termed prodrugs, compounds that on their own have little or no pharmaceutical activity. However, a chemical reaction *in vivo* converts the molecule into an active drug. This approach is useful because it serves as a mechanism to improve pharmacokinetic properties such as adsorption. A cleavable tag can then be added to improve

## INTRODUCTION

### **The genus *Mycobacterium* and *Mycobacterium tuberculosis*: disease, treatment, and perspectives**

distribution, which is then removed to elicit the desired action. Despite their structural similarities, the bacteriostatic effect of these compounds is not by competition with the  $\text{NAD}^+$  binding site [23]. INH is activated by the catalase-peroxidase KatG; the resulting product can form an  $\text{NAD}^+$ -adduct to inhibit InhA, an enoyl-ACP reductase catalyzing elongation of the fatty acid chain of mycolic acids. Its inactivation leads to the accumulation of precursors, inhibition of mycolic acid biosynthesis, and cell death [24]. PZA is activated by PncA, a nicotinamidase involved in  $\text{NAD(P)}^+$  metabolism with pyrazinamidase activity, converting PZA to pyrazonoic acid. An efflux pump expels it from the cell; however, in the extracellular space, the molecule is protonated and re-enters the cell by passive diffusion. As the cell tries to detoxify the cytoplasm, pyrazonoic acid accumulates, resulting in cytoplasm acidification and membrane transport deficiency [25, 26]. Inhibition of cell wall biosynthesis has also been investigated, pointing to a plethora of additional deleterious mechanisms not yet completely understood [27-30]. EMB, on the other hand, binds to 5'-hydroxyl groups in D-arabinose, blocking the polymerization and transfer of arabinogalactan and lipoarabinomannan into the cell wall [31-33]. INH and EMB act synergistically *in vivo* and are used simultaneously during TB treatment. It has been proposed that they share a molecular target, possibly by binding EMB to the transcriptional repressor EtbR, which regulates the expression of the enoyl-acyl-carrier protein reductase encoded in the *inhA* gene. This effect prevents its expression and further enhances the bacteriostatic effect of INH on cell wall biosynthesis [23, 34-39].

Resistance to the four anti-TB first-line medications is widespread and an emerging threat to healthcare worldwide [40]. The length of the treatment, poor compliance, comorbidities like HIV, and related drug interactions have contributed to MDR-TB and XDR-TB strains [5, 41]. These cases are treated with longer antibiotic courses (6-24 months) and second-line, novel pharmacological compounds such as ethionamide or pretomanid with various secondary effects [5, 40, 42]. All in all, the interaction of anti-TB drugs with  $\text{NAD}^+$ , and possibly with other, less common cofactors present in MTB, offers a promising avenue for the development of novel anti TB drugs, as well as furthering our understanding of the biochemistry, pathogenesis, and resistance mechanism of this deathly microorganism.



## The role of cofactors in antibiotic susceptibility and resistance of mycobacteria

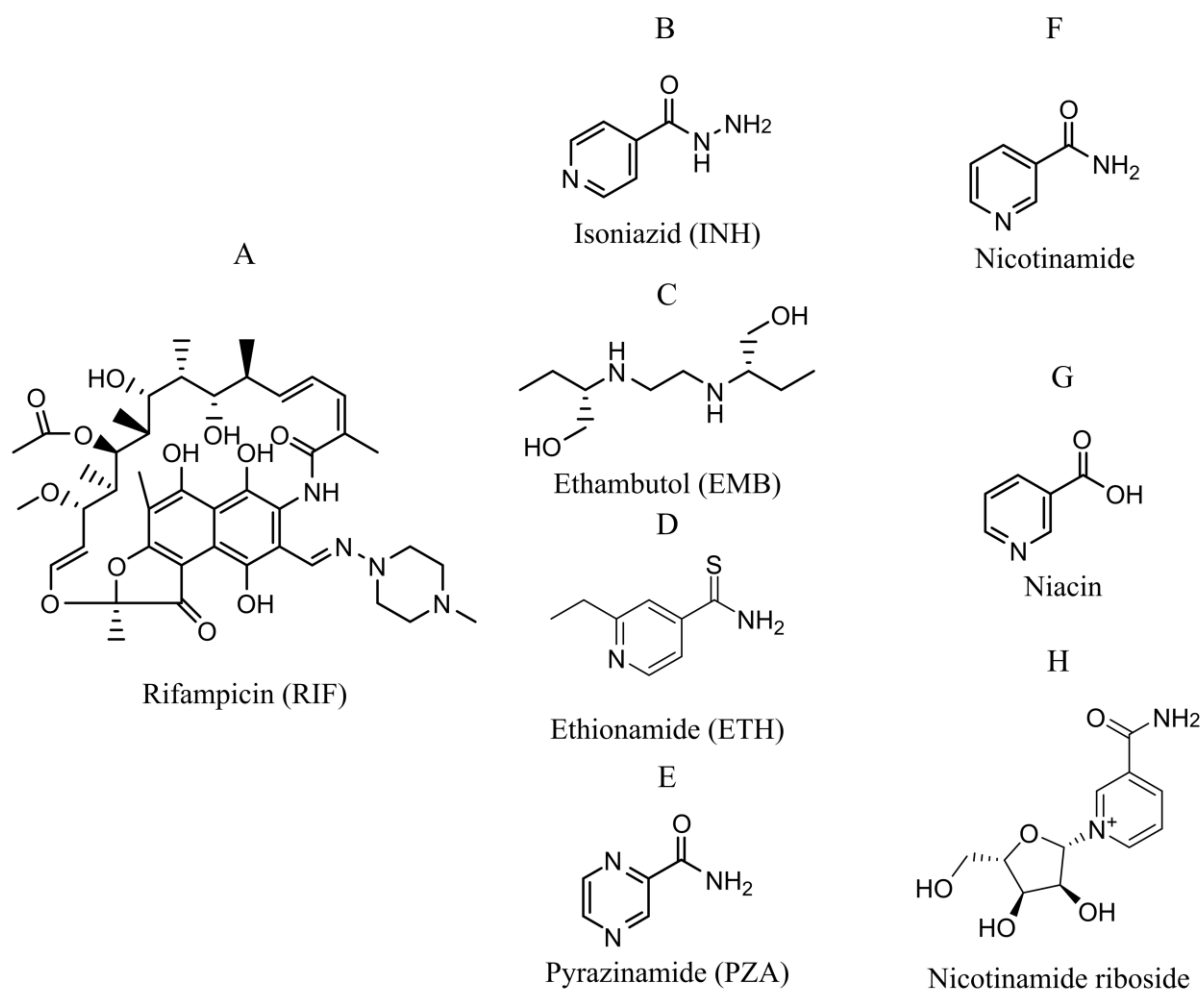


Figure 1: Antibiotics commonly used in tuberculosis treatment. Note that INH (B), EMB (C), ETH (D), and PZA (E) are structurally related to the B<sub>3</sub> vitamins nicotinamide (F), niacin (G), and nicotinamide riboside (H).

## 6.2. THE ROLE OF COFACTORS IN ANTIBIOTIC SUSCEPTIBILITY AND RESISTANCE OF MYCOBACTERIA

All living organisms must detoxify reactive oxygen species (ROS) and maintain intracellular redox balance to support electron flow between two species. ROS are oxygen adducts in which an unpaired electron is free in the outer shell, making it highly reactive and toxic. In bacteria, most of the ROS species are formed from uncoupled electrons passing through the electron transport chains, reducing oxygen to superoxide anion ( $O_2^-$ ). This anion can inactivate proteins by oxidation of solvent-accessible cysteine residues, iron-sulfur clusters, and DNA nucleotides. Inorganic mechanisms such as ionizing radiation and toxins are also involved in ROS formation [43, 44]. ROS are also formed in chloroplasts, mitochondria, and the phagosome in macrophages, where  $O_2^-$  and nitric oxide are part of the chemical arsenal to produce peroxynitrite ( $ONOO^-$ ) and combat bacterial infections [44, 45], an innate immunity mechanism to which MTB can survive in a latent infection phase [16]. Intracellular ROS mediates INH activation, and ROS detoxification agents are involved in both the resistance and

**The role of cofactors in antibiotic susceptibility and resistance of mycobacteria**

sensitivity to first- and second-line anti-TB drugs [46]. Cofactors, defined as “ions or organic molecules required by an enzyme for its activity” [47], are essential for ROS inactivation, redox balance, enzyme activity, and in general life on Earth. While some chemical reactions can occur spontaneously, without enzymes, life, as we know, would be impossible [48, 49].

Low molecular-weight thiols, some amino acids (cysteine and homocysteine) or dipeptides (cysteinylglycine), and coenzyme A all contain thiol groups and protect organisms by acting as a dispensable oxidation target for ROS, a “cellular redox buffer” [50, 51]. The most-studied small thiol is glutathione (GSH, Figure 2A), a small Glu-Cys-Gly tripeptide cofactor for many peroxidases [52, 53]. In the presence of ROS, two molecules of GSH form a disulfide dimer, neutralizing the offending species in the process [54-56]. Gram-positive bacteria such as *Bacillus* and *Staphylococcus* do not produce GSH, but a small thiol termed bacillithiol (BSH, Figure 2B), a cysteine-glycin dipeptide glycosylated with malyl N-acetyl-glucosamine (GlcNAc-Mal) [57]. Mycobacterial strains and other actinomycetes do not produce GSH nor BSH, but instead mycothiol (MSH, Figure 2C), another thiol redox cofactor composed by N-acetyl-L-cysteine linked to glucosamine and inositol. MSH-mediated inactivation of ROS occurs with the same disulfide bridge formation mechanism as GSH [58-61].

Methylated bacillithiol (N-Me-MSH) is a novel variant modified by N-methylation of the cysteine amino group by a predicted S-adenosyl L-methionine methyltransferase (N-Me-MSH synthase A). N-Me-MSH has been discovered in *Chlorobium tepidum*, *C. phaeobacterioides*, and *Prosthecochloris* sp. strains when grown photoautotrophically under anaerobic conditions, which indicates that it is correlated with oxygen and light levels and growth phase [56]. Based on the genomic spread of the BSH cluster and its correlation with predicted methyltransferases, this bacillithiol variant could be more abundant than expected, even though no putative function has been assigned. Since these strains have no sulfur metabolism, a role here would be unlikely. Furthermore, an H<sub>2</sub>S-rich anaerobic environment in which these organisms thrive would require substantial amounts of N-Me-MSH for it to be considered a primary mechanism to protect against oxidative stress. Two possible functions are detoxification of sulfhydryl reactive agents by thiol-dependent dehydrogenases and metal homeostasis by chelation [62].

This case shows that variants of biologically-relevant molecules are still undiscovered, particularly when biosynthesized by mechanisms such as radical SAM-mediated reactions [63]. For example, while methyl-mycothiol (Me-MSH) has not been discovered *in vivo*, it was produced artificially by solid-phase synthesis containing a methyl-glucosamine moiety instead

## INTRODUCTION

### The role of cofactors in antibiotic susceptibility and resistance of mycobacteria

of methyl cysteine as in *N*-Me-MSH. Kinetic characterization showed that Me-MSH disulfide offers a comparable activity for mycothiol disulfide reductase, showcasing enzyme flexibility and possible screening methods for mycothiol derivatives and inhibitors [64]. Me-MSH could arise from a similar radical SAM methyltransferase mechanism, enzymes which are abundant in the *Mycobacterium* proteome and presumed to participate in the methylation of RNA during ribosome maturation [65], in the synthesis of cell wall components [66], and as a resistance mechanism against antimicrobial compounds [67].

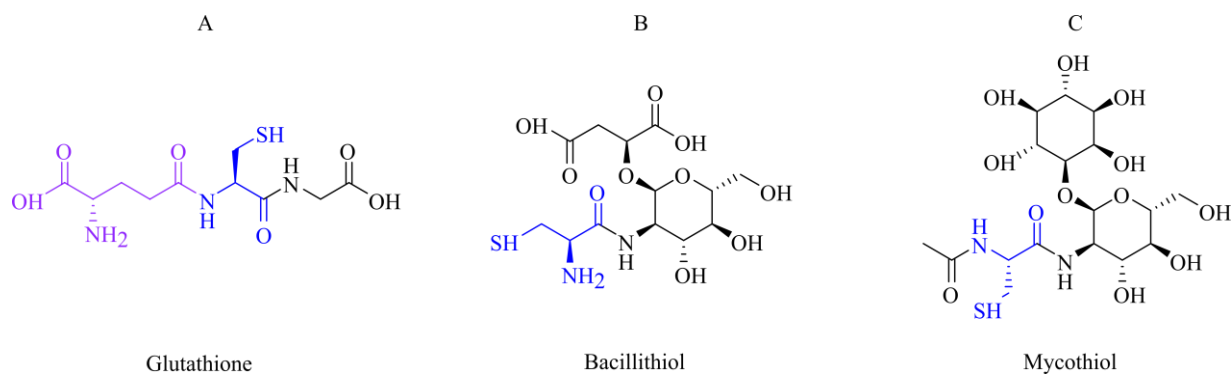


Figure 2: Molecular structure of (A) glutathione, (B) bacillithiol, and (C) mycothiol. The cysteine residue in each thiol is highlighted in blue, glutamyl moiety is highlighted in purple.

Given the role of MSH in the neutralization of reactive electrophilic species, it has been speculated that it could be involved in mycobacterial resistance mechanisms that generate said species. Initial studies in MSMEG confirmed this hypothesis, with the observation that truncated MSH-biosynthesis at various points results in increased sensibility to RIF, in addition to antibiotics not commonly used for the treatment of TB (vancomycin, penicillin, erythromycin, azithromycin) [68]. Conversely, increased resistance to ETH, and INH was also found, which indicates that MSH is an additional factor in anti-TB detoxification [69-72]. Furthermore, oxidative stress is a crucial element of macrophage-mediated defense, and the role of MSH in ROS management could indicate a role in intramacrophage survival during latent TB [44, 73]. Therefore, MSH-competitive inhibitors could boost rifampicin efficiency and open pathways to repurpose other antibiotics not used for TB, with the caveat of preventing simultaneous treatment with other compounds depending on MSH for its activity [68].

Another example of TB treatment influenced by cofactors is the prodrug pretomanid, approved for treating MDR-TB and XDR-TB. It is the first anti-TB medication approved in 40 years, part of a novel group of candidate drugs known as nitroimidazoles [74-78]. The activation of pretomanid results in des-nitroimidazoles and the generation of reactive nitrogen species that interact with the prosthetic group in cytochromes. This alters the coupling of the bacterial

## INTRODUCTION

### Cofactors are indispensable for cellular biochemistry

respiratory chain to the reduction of oxygen in the cell membrane [77]. This activation process is mediated by a deazaflavin-dependent nitroreductase (Ddn) [75, 77] that uses coenzyme F<sub>420</sub>, a lactyl oligoglutamate phosphodiester derivative of 8-hydroxy-5-deazaflavin (FO), as a redox cofactor. This cofactor is, in turn, regenerated by an F<sub>420</sub>-dependent glucose-6-phosphate dehydrogenase (Fgd). Coenzyme F<sub>420</sub> is found in a much more restricted set of bacteria and archaea. It acts as a 2-electron hydride carrier for various enzymes involved in methanogenesis, detoxification, and secondary metabolite production [79-83].

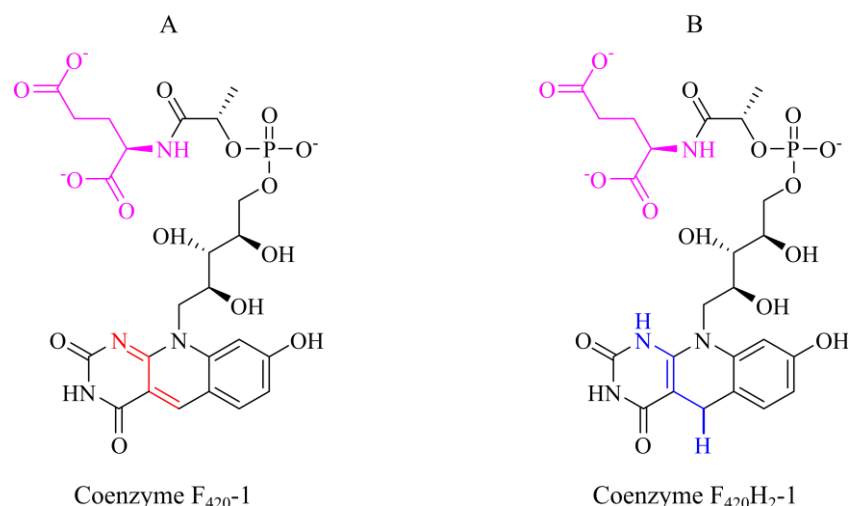


Figure 3: Coenzyme F<sub>420</sub>-1 oxidized (A, redox core in red) and reduced (B, redox core in blue). Pink indicates L-glutamate side chain.

In mutants with  $\Delta fgd$  or  $\Delta ddn$  genotypes, the prodrug is not activated; therefore, these deleterious mutations confer high-level resistance to pretomanid and other nitroimidazoles [74, 75, 84]. Interestingly, similar mutations also enhance sensitivity to other antibiotics and xenobiotics, including first-line anti-TB medications [83]. As outlined for MSH, these results indicate that F<sub>420</sub> and F<sub>420</sub>-dependent enzymes participate in metabolic pathways that result in resistance to anti-TB drugs. Therefore, potential future treatments focused on rare cofactors and their depending on oxidoreductases, or even on novel undiscovered cofactors could open potential avenues into new TB treatments or boost existing first-line medications. Overall, this also highlights the remarkable versatility of cofactors for cellular biochemistry.

### 6.3. COFACTORS ARE INDISPENSABLE FOR CELLULAR BIOCHEMISTRY

A hierarchical classification of cofactors and some examples are given in Figure 4 [85]. Ionic or inorganic cofactors refer specifically to metal ions in metalloproteins or iron-sulfur clusters, forming spatial rearrangements of Fe built around the sulfur atom in a cysteine-rich pocket. Both are widespread and involved in structural stability, catalysis, electron transfer (redox), oxygen transport, nitrogen fixation, hydrolysis, or photosynthesis [86].

## INTRODUCTION

### Cofactors are indispensable for cellular biochemistry

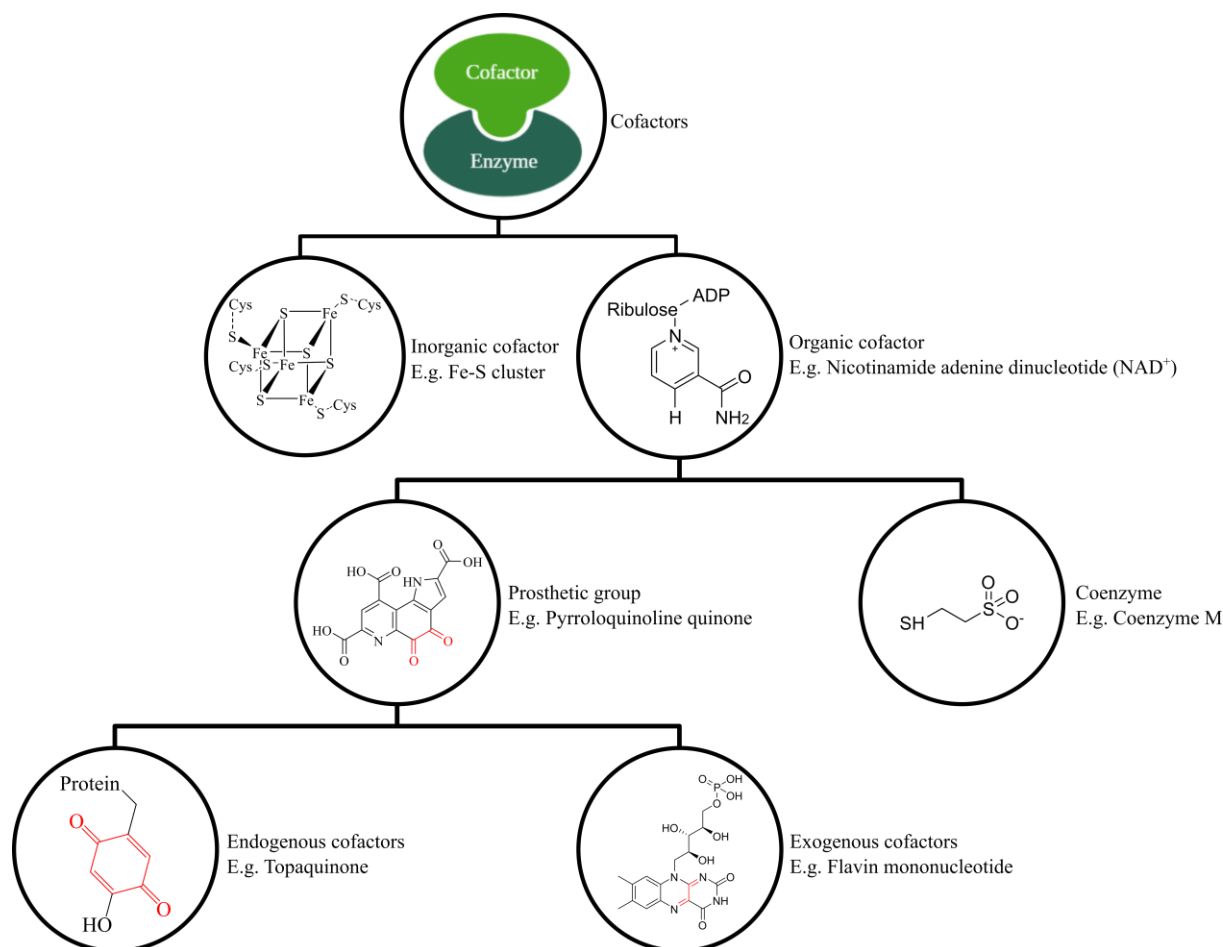


Figure 4: Hierarchical classification of cofactors. Redox core highlighted in red when present. Modified from Fischer (2010) [85].

Organic cofactors comprise a wide variety of molecules that differ from each other greatly in chemical structure, biogenesis, polarity, and size [85]. Structurally, enzymes have a three-dimensional pocket close to the active site where the cofactor is bound. When binding occurs, the enzyme is active, and the enzyme-cofactor complex is termed holoenzyme. An enzyme without its cofactor is inactive and termed apoenzyme. The strength of the bond adds a level of classification to organic cofactors. Most organic cofactors involved in oxidation and reduction are not tightly bound to the enzyme and leave the active site after a catalytic cycle; in this case, the cofactor is termed coenzyme and is regenerated elsewhere. However, prosthetic groups are tightly bound to the enzyme, usually, but not necessarily, by a covalent bond. The cofactor remains in the binding pocket through successive reaction cycles and needs to be regenerated [87]. The majority of cofactors originate externally to the target enzyme (exogenous cofactors). A small proportion is formed from a single residue or a polypeptide precursor and undergoes post-translational modifications [88, 89].

All-in-all, a comprehensive classification of cofactors is fraught with exceptions and examples where a molecule participates with different mechanisms in chemical reactions [85].

## INTRODUCTION

### Cofactors are indispensable for cellular biochemistry

For example,  $\text{NAD}^+$  and  $\text{NADP}^+$  are the archetypical examples of organic cofactors and are essential in metabolic redox reactions. These reactions involve a reversible transfer of electrons (usually hydrogen species  $\text{H}^+$ ,  $\text{H}^-$ ) between the cofactor and a substrate, resulting in either the oxidation (loss of electrons) or reduction (gain of electrons) of a product. However, some processes involving DNA repair, gene expression, and secondary metabolite production depend on a non-redox role of the NAD(P) pool [85].

#### *6.3.1. Biogenesis of the chemical core and tail moieties of organic cofactors*

It is generally challenging to classify cofactors based on their chemical nature and modifications. Nevertheless, a few patterns can be described involving the examples shown in Figure 4. Firstly, the cofactor molecules often consist of a catalytically active “core moiety” and a polar “tail moiety.” The core moieties of cofactors are structurally and biosynthetically more diverse than the tail moieties. Therefore, an introduction of their common structures and biogenesis is limited to some examples but can be a basis of grouping to some extent. For instance, there are a few recurring structural motifs within both the head and tail moieties.

The core of adenosine triphosphate (ATP, Figure 5A), while not considered a cofactor, is an adenosine monophosphate moiety (AMP handle, Figure 5, blue atoms). This moiety is transferred from ATP by a phosphate adenyltransferase to cofactors such as  $\text{NAD}^+$ ,  $\text{NADP}^+$ , coenzyme A, and flavin adenine dinucleotide (FAD, Figure 5B-E). The AMP handle is recognized by an adenine-binding loop in the target enzyme and locks the cofactor/coenzyme. This region is located in the vicinity of hydrophobic residues, which are functionally conserved whether the ligand acts as a cofactor, coenzyme, enzymatic substrate, or allosteric effector [90]. In other, non-redox roles of nucleotide cofactors, the ADP-ribose moiety is consumed during reactions involving ribosyl transferases during protein post-translational modification, calcium signaling, and homeostasis. Therefore, the source molecules are typically not considered cofactors in these specific reactions [85, 91]. Ancestral nucleotide-based coenzymes such as those with an AMP handle are proposed as a relic of a previous “RNA world,” a widespread hypothesis of the origin of life on Earth. In this evolutionary scenario, biocatalysis and the genetic transfer was mediated by RNA and ribozymes, in contrast to the current DNA-protein world [92, 93].

While not specific for cofactors, it should be mentioned that phosphorylation can be seen as a simple tail moiety, as is the case for pyridoxal phosphate (PLP), thiamine pyrophosphate (TPP), and flavin mononucleotide (FMN, Figure 5F). Phosphorylation is a conserved evolutionary mechanism that facilitates interaction with proteins, acts as an expedited way to

regulate function temporally, and increases polarity, preventing molecules from passing biological membranes [94]. Glutamylation or even polyglutamylation (Figure 5, purple atoms) is another common structural theme in tail moieties. It is present in GSH (Figure 2A), F<sub>420</sub> (Figure 5G), tetrahydromethanopterin, and methylofuran [95]; the latter two compounds present as carbon-carrier cofactors in methanogenic archaea and methylotrophic bacteria, respectively [96]. The polyglutamate tail of F<sub>420</sub> is involved in interactions with the enzyme and prevents leakage from the cytoplasm, unlike the less polar and not glutamylated core moiety (FO) [82, 97, 98]. In eukaryotic folates, it is also involved in determining a correct subcellular localization [99].

The length of the F<sub>420</sub> glutamyl moiety was also correlated with different kinetic properties. In general, increased polyglutamylation was correlated with higher substrate affinity and cofactor binding to the enzyme (lower  $k_M$ ) and decreased the turnover rate (lower  $k_{cat}$ ) [100, 101]. This phenomenon was independent of cofactor concentration and possibly explained by electrostatic interactions of the charged glutamyl tail with conserved residues in the F<sub>420</sub>-dependent oxidoreductases, modulating the binding affinity. As a result, chain length might enable aerobic bacteria to control cellular redox reactions at the expense of a reduced catalytic rate [100].

Another common tail moiety is the isoprenyl side chain in ubiquinone, menaquinone, and other cofactors (Figure 5, H and I, cyan atoms). In combination with the quinone redox-active head, these cofactors are part of the respiratory chain and reside in biological membranes. The quinone moiety (Figure 5, green atoms) catalyzes electron transfer between donors and receivers. The prenylated tail moiety of variable length increases the overall hydrophobicity of the entire molecule and acts as an irreversible anchor for insertion in the lipid bilayer [102, 103]. Non-prenylated endogenous quinone cofactors (TPQ, TTQ, CTQ, and LTQ, Figure 6) or PQQ (Figure 5, K) arise from a common biosynthetic theme, the oxidation of the phenol moiety in a tyrosine residue.

Other classification approaches have similar caveats, such as physicochemical properties, structural hierarchy, chemical similarity, or relationship between cofactor and metabolites. Cofactor-specific databases have been developed to establish possible connections between cofactors roles for industrial applications or pathogenesis [85, 104]. In short, the diversity in the structural motives of cofactors not only reflects their importance in cellular biology but serves as markers to find novel cofactors in the most unsuspected places.

## INTRODUCTION

### Cofactors are indispensable for cellular biochemistry

NAD<sup>+</sup> is the best-known redox cofactor, universally present across all taxa, and involved in a staggering number of biochemical reactions as well as regulatory events [105, 106]. An NAD<sup>+</sup> kinase catalyzes the phosphorylation of NAD<sup>+</sup> into NADP<sup>+</sup>, and while the redox pairs (NAD<sup>+</sup>/NADH and NADP<sup>+</sup>/NADPH) have similar redox potential, the deletion of this enzyme is lethal [107]. While some NAD-dependent oxidoreductases can interchangeably use either coenzyme, the vast majority are specific for either cofactor. Therefore, NAD<sup>+</sup> and NADP<sup>+</sup> are considered different redox pools, owing to a compartmentalized location and different biochemical functions. While NAD<sup>+</sup>/NADH is involved in glycolysis and oxidative phosphorylation (catabolism), NADP<sup>+</sup>/NADPH is involved in the biosynthesis of nucleotides and fatty acids (anabolism) [108]. Two *de novo* pathways have been identified for NAD<sup>+</sup> biosynthesis, by chemical specialization of iminoaspartate in most prokaryotes [109] or tryptophan in Eukarya and a minimal subset of prokaryotes [110, 111]. A third pathway produces NAD<sup>+</sup> by direct transfer of the AMP moiety to nicotinamide. Furthermore, the pyridine nucleotide cycle (PNC or salvage) is present in all taxa to recycle the pyrimidine moiety from B<sub>3</sub> vitamins or assimilate exogenous NAD<sup>+</sup> [112-114].

The nucleoside guanosine is a starting point for several core moieties of cofactors. The biosynthesis of the pterin ring of, e.g., in folic acid or the isoalloxazine ring of riboflavin are well-known examples. A pathway branching from riboflavin biosynthesis involving the amino acid tyrosine generates 7,8-dimethyl-8-hydroxy-5-deazariboflavin (FO), which upon ligation with phosphorylated organic acids and polyglutamylation yields the coenzyme F<sub>420</sub> [82].



## INTRODUCTION

### Cofactors are indispensable for cellular biochemistry

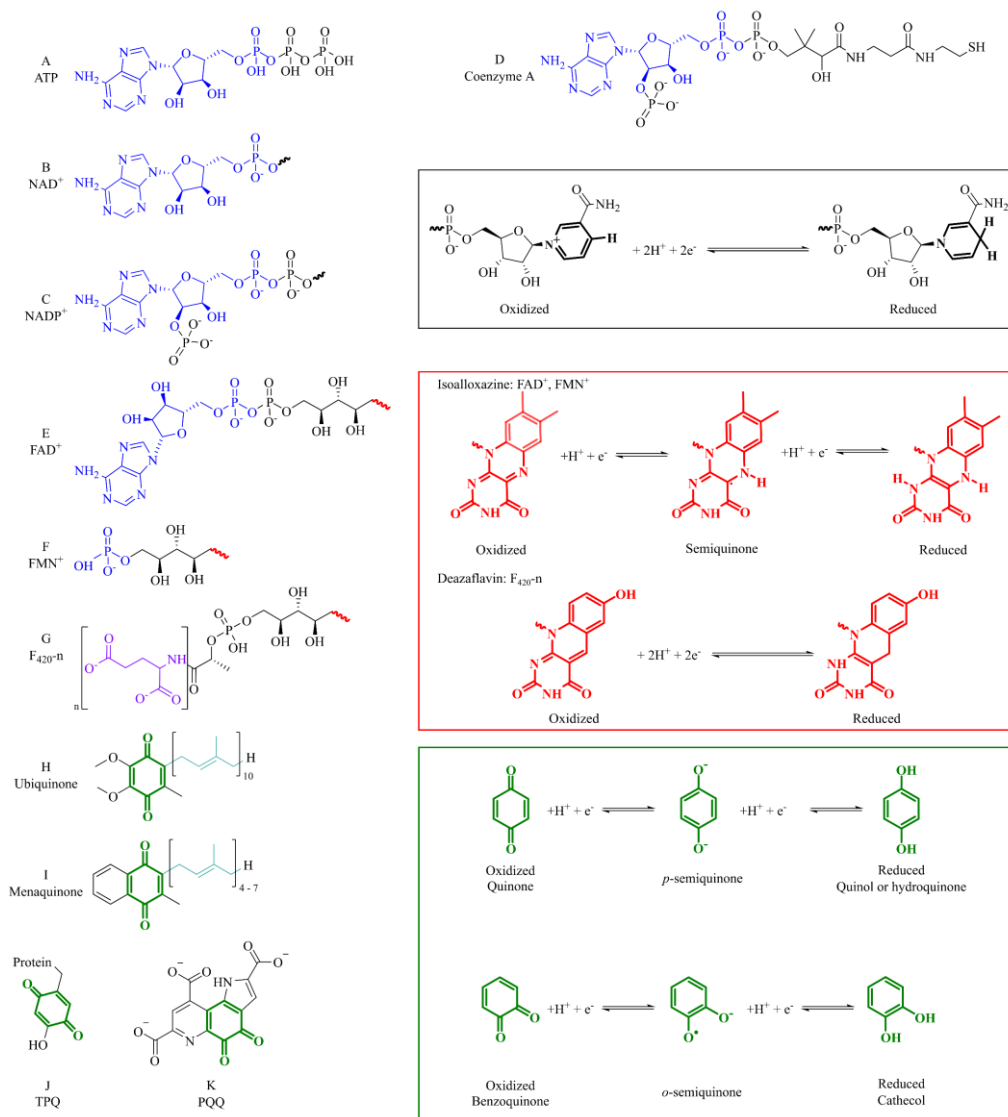


Figure 5: Organic cofactors and their shared moieties. Cofactors with AMP handle (blue atoms): adenine triphosphate (ATP, A), nicotinamide adenine dinucleotide (NAD<sup>+</sup>, B), nicotinamide adenine dinucleotide phosphate (NADP<sup>+</sup>, C), coenzyme A (D), flavin adenine dinucleotide (FAD<sup>+</sup>, E). The pyridine redox core (black bold bonds and atoms) is highlighted in the black square. Flavin-related cofactors: FAD<sup>+</sup>, flavin mononucleotide (FMN<sup>+</sup>), and the deazaflavin factor 420 (F<sub>420-n</sub>, G). The isoalloxazine redox core (red bold bonds and atoms) is highlighted in the red square. The quinone redox core (green bonds and atoms) can have a quinone conformation as in ubiquinone (H) or menaquinone (I), or a catechol conformation as in topoquinone (TPQ, J) and other endogenous cofactors, or pyrroloquinoline quinone (PQQ, K). Quinone redox core and half-reactions are highlighted in the green square.

The redox core of cofactors is the heart and soul required in the oxidation and reduction machinery, indicated by the bold atoms and bonds in Figure 5. The pyridine ring (Figure 5, bold black) on the nicotinamide moiety is the shared redox core for NAD<sup>+</sup> and NADP<sup>+</sup> (Figure 5B, C). The pyridine ring is an obligate two-electron agent, and all redox reactions occur with the transfer of two electrons.

The isoalloxazine redox core (Figure 5, bold red) can present itself in the riboflavin-derived cofactors FAD and FMN (Figure 5E, F), where it can perform one- (half, termed semiquinone)

or two-electron (full) reactions. Most flavin-dependent enzymes (90%) are oxidoreductases, with remaining members classified as transferases, lyases, isomerases, and ligases [115, 116]. By contrast, the coenzyme F<sub>420</sub> (Figure 5G) is involved in redox reactions and methanogenesis, degradation of xenobiotic and natural heterocyclic compounds, and production of secondary metabolites [79-83]. Compared to the isoalloxazine ring in FMN and FAD, the deazaflavin ring of F<sub>420</sub> contains a carbon atom in position 5 of the isoalloxazine ring instead of a nitrogen atom. Furthermore, while C-7 and C-8 are methylated in the flavin-derived FMN and FAD, in F<sub>420</sub> C-7 is hydroxylated, and C-8 is unsubstituted. Because of these changes, this ring is termed 8-hydroxy-5-deazaflavin. F<sub>420</sub> has a lower redox potential than both flavins and nicotinamide cofactors and cannot form a semiquinone; redox reactions involving F<sub>420</sub> are limited to two-electron reductions [117].

Another redox moiety is the one found in quinone cofactors. The redox core can be present in two conformations depending on the substitution pattern on the dihydroxybenzene ring: *para*- found in the quinone ring of ubiquinone, menaquinone (Figure 5H, I), and phyloquinone, and *ortho*- found in the endogenous peptide cofactors topaquinone (TPQ, Figure 5J) triptophanquinone (TTQ), cysteine tryptophylquinone, and lysyl tryptophylquinone (LTQ, Figure 6) or pyrroloquinoline quinone (PQQ, Figure 5K). Quinones can also undergo one- or two-electron reactions, resulting in *p*- or *o*-semiquinone [118]. The full reaction results in reduced quinol or hydroxyquinol from *p*-substituted quinone, or *o*-quinone from the catechol ring [119, 120]. The quinone moiety in TPQ, PQQ, and others is particularly interesting because it can be formed from the oxidation of the phenol moiety in a tyrosine residue. As the starting point for amino acid precursor-derived cofactors, this will be detailed in the following sections.

### 6.3.2. Biosynthesis of cofactors containing quinone moieties

Menaquinone is the primary quinone of the prokaryotic anaerobic electron transport chain, while phyloquinone fulfills a similar role in the photosynthetic system of plants, algae, and cyanobacteria [121, 122]. Ubiquinone is present in bacterial and animal aerobic respiration, such as the respiratory complex of mitochondria. Facultative bacteria such as *E. coli* possess menaquinone, dimethyl menaquinone, or ubiquinone. Not only they act selectively depending on environmental conditions, but the transcription of the required oxidative or fermentative catabolic genes in each condition is regulated by oxidation (deactivated) or reduction (activated) of two cysteine residues in the two-component regulator anoxic redox control (Arc) protein [123-125].

Chorismate, a product of the shikimate pathway, is not only an intermediate to quinones, but precursors in this pathway are also diverted to form folates, aromatic amino acids, and a wide variety of secondary metabolites such as vitamin E and K [126, 127]. The relationship between the biosynthetic genes and menaquinone and ubiquinone pathways is interesting from an evolutionary point of view. Since ubiquinone biosynthesis is membrane-associated and requires oxygen, and its biosynthetic genes are less syntenic compared to menaquinone, it is proposed that archaic menaquinone gave rise to ubiquinone, first in cyanobacteria and then in the common ancestor of alpha, beta, and gammaproteobacteria, bacterial lineages adapted to different oxygen levels [128].

Menaquinone biosynthesis begins from isomerization of chorismate to isochorismate and condensation with 2-oxoglutarate, followed by pyruvate elimination. A naphthoyl-CoA intermediary mediates ring closure; a thioesterase removes CoA before isoprenylation, decarboxylation, and radical SAM-mediated methylation [121]. In ubiquinone biosynthesis, instead of condensation, a chorismate lyase converts chorismate into 4-hydroxybenzoate, which further undergoes prenylation, hydroxylation, decarboxylation, hydroxylation, and methylation [127]. In both cases, the formation of the isoprenyl tail moiety arises from the structural isomers dimethylallyl diphosphate and isopentenyl phosphate, which differ on the isoprenyl position double bond. A prenyltransferase uses the pyrophosphate group to catalyze the consecutive addition of isoprene moieties by isoprenyltransferases in the presence of divalent cations [122, 127, 129, 130]. The length of menaquinone isoprenyl moiety ranges from 4 to 13 depending on both species and growth temperature [122], while the isoprene monomer of ubiquinone in *E. coli* usually contains 8 units and 6 in *S. cerevisiae*, with minor amounts of other lengths possible [127].

The polar head of quinone cofactors is hydrophilic and able to interact with proteins. In contrast, the prenylated nonpolar tail locates the enzyme in the hydrophobic region of the lipid bilayer. As such, prenylquinones are usually membrane-bound, while unprenylated quinones are cytosolic or periplasmic. Furthermore, quinones are exquisitely sensitive to oxygen and become rapidly and non-catalytically oxidized on air. This also points to a probable earlier development in evolution, adapted to function in a more reductive atmosphere under conditions previous to the appearance of photosynthetic oxygen, making transmembrane localization necessary [122]. These properties and the intermediary semiquinone redox state make quinones a critical component of the electron transport chain, sitting comfortably between the obligate one-electron obligate cofactors  $\text{NAD(P)}^+$  or two-electron flavins. The electron transport chain

## INTRODUCTION

### Cofactors are indispensable for cellular biochemistry

is then complete, funneling electrons towards the final electron acceptor, oxygen in aerobic conditions or fumarate, nitrate, and other electron acceptors in anaerobic conditions [125, 131].

#### 6.3.3. Endogenous (polypeptide-derived) quinone cofactors

The *o*-substituted quinone moieties arise from amino acids in the endogenous cofactors topaquinone (TPQ), tryptophan tryptophylquinone (TTQ), cysteine tryptophylquinone (CTQ), and lysine tryptophylquinone (LTQ). A quinone moiety can also be formed in an exogenous cofactor like pyrroloquinoline quinone (PQQ). In all of these cases, a heavily post-translationally modified aromatic amino acid residue is the basis for the quinone redox core. The benzene group from tyrosine or phenylalanine, or the conjugated system in tryptophan, forms an intermediary termed aminosemiquinone, further oxidized to generate an active redox site [132]. Endogenous cofactors, or *in situ* cofactors (Figure 6), are formed by crosslinking amino acids located in their target enzyme's active site, always involving at least an aromatic residue to generate a quinone ring [133].

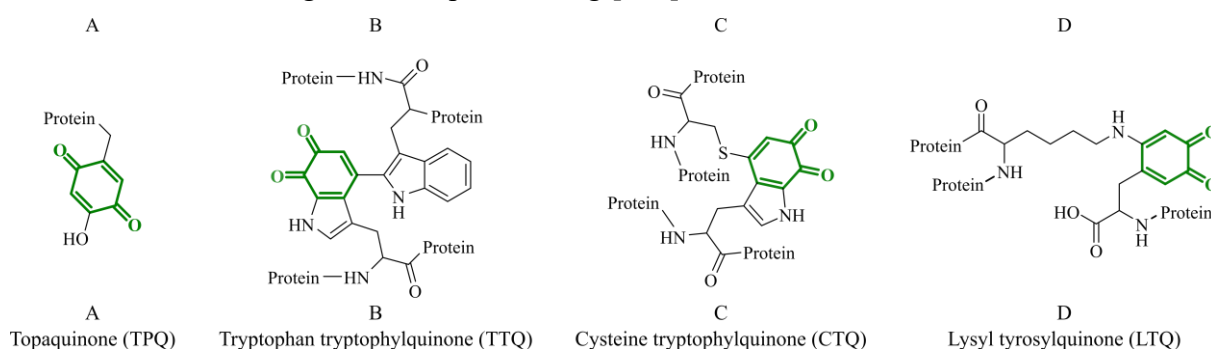


Figure 6: Endogenous peptide cofactors, catechol redox core atoms and bonds in green.

2,4,5-trihydroxyphenylalanine quinone (TPQ, or topaquinone, Figure 6A) was discovered in 1990 as an internal cofactor within copper amine oxidase [134, 135]. The tyrosine oxidation occurs in the conserved region Thr-X-X-Asn-Tyr-Asp/Glu in a spontaneous, aerobic, metal-dependent autocatalytic mechanism [136, 137]. Only TPQ biosynthesis occurs without a second residue; still, it is a model to study the biochemistry and biosynthesis of the other quinocofactors [133]. Tryptophan tryptophylquinone (TTQ, Figure 6B) is a cofactor for oxidases in the methylamine utilization locus (*mau*) and aromatic amine dehydrogenases, allowing the producing organism to grow in methylamines. A covalent bond is formed with a tryptophan residue in addition to a keto group on the indole ring [138]. As TPQ, the introduction of one oxygen atom is spontaneous; further oxidation requires the heme metalloenzyme MauG [139].

A third cofactor, cysteine tryptophylquinone (CTQ, Figure 6C), also requires oxidation of the tryptophan's indole moiety. But instead of a crosslink to a tryptophan residue, a thiol group

in a cysteine residue is involved [140]. While CTQ and TPQ are prokaryotic, TQP can be found in both eukaryotes and prokaryotes. Lysyl tyrosylquinone (LTQ, Figure 6D), on the other hand, has been found exclusively on eukaryotic lysyl oxidases, involved in the maturation and post-translational modification of the extracellular matrix. However, studies suggest that the presence of biosynthetic genes could signal possible existence in both archaeal and bacterial proteins [141]. As TPQ, a similar, spontaneous, copper, and oxygen-dependent biosynthetic mechanism is involved, with a crosslink to a lysine residue [142, 143]. Endogenous cofactors with quinone moieties such as TPQ, TTQ, CTQ, and LTQ are present in a limited set of enzymes, expanding the scope of cofactor-mediated chemistry and their relationship with enzymes.

#### 6.3.4. *Pyroloquinoline quinone (PQQ) - a ribosomally-produced and post-translationally modified quinone cofactor*

Another cofactor with quinone moieties, pyrroloquinoline quinone (PQQ), involves similar crosslinking mechanisms between aromatic residues. Still, instead of occurring in the active site, PQQ is a ribosomally produced and post-translationally modified peptide (RiPP), a class of natural products arising from ribosomally made polypeptide chains acting as a precursor, which undergo further chemical modifications and specialization in the form of post-translational modifications [144, 145]. As the name implies, in RiPPs the precursor sequence is a canonical L-amino acid polypeptide [145]. The *N*-terminal leader peptide serves for recognition by processing enzymes, mature product secretion where appropriate, and protection from proteases [146]. The core peptide region, usually at the *C*-terminus or close to it, contains the residues which comprise the mature product. Artificial variability in both leader and core region of the precursor can generate novel variants of known RiPP pathways [147]. Adjacent to the peptide-encoding gene is one or more open reading frames for enzymes that perform the required post-translational modifications on the core peptide. A chaperone is needed for leader peptide recognition in some instances, such as lassopeptides or sactipeptides [148]. Overall, many types of enzymes could be involved in maturation processes like cyclization, epimerization, methylation, hydroxylation, or glycosylation. Finally, a peptidase is often involved in releasing the mature core peptide from the leader peptide. In bacteriocins, ATP-mediated transporters and self-immunity mechanisms are often present [144, 149, 150]. Due to these shared features RiPP biosynthetic pathways can be inherently employed to generate post-translationally modified peptides, including by combining different pathways. However, an inherent result is that finding novel cryptic pathways is less straightforward. The individual RiPP families are diverse between themselves, and putative BGCs could be

## INTRODUCTION

### Cofactors are indispensable for cellular biochemistry

evolutionarily inactivated. On a technical level, the small precursor size also impairs some commonly used bioinformatics methods. Surpassing these limitations require a combination of bioinformatic prediction and confirmatory analytical techniques, making the discovery of novel RiPPs an active and promising field of research for novel bioactive molecules [144].

Pyrroloquinoline quinone (PQQ) is a RiPP-derived cofactor associated with quinoprotein redox enzymes. Initially described in prokaryotic glucose dehydrogenases that were found to act independently of nicotinamide-based or flavin cofactors, PQQ is a dissociable, non-covalently bound cofactor for Gram-negative bacterial enzymes involved in the metabolism of alcohol, aldehydes, and carbohydrates [151-153]. Divalent metal ions mediate PQQ binding to its apoenzyme [153, 154]. Trace amounts have been found in mammalian tissues and presumed to originate from food sources. Its deficiency has been associated with the pathogenesis of liver fibrosis, stroke, reduced fertility, and *in vitro* and *in vivo* osteoporosis rodent models [155-160]. Initially, it was proposed that this could indicate a possible vitamin role, and later superseded by the concept of longevity vitamin, required for aging and long-term mitochondrial health [161-163].

The PQQ operon, responsible for the biosynthesis of the mature cofactor (Figure 7), contains the genes *pqqABCDEFG*, in which *pqqADE* are essential for PQQ production. PqqA is a short peptide, including the conserved motif -ExxxY- [164]. The glutamate and tyrosine residues are crosslinked by a radical SAM PqqE, in a reaction dependent on the presence of a chaperone termed PqqD [165]. PqqE belongs to the superfamily of radical SAM (rSAM) enzymes, a group of more than 600,000 enzymes (Protein Data Bank, 2020) characterized by the -CX<sub>3</sub>CX<sub>2</sub>C- motif in which an iron-sulfur cluster [4Fe-4S] is present [166-169]. The reduced Fe-S cluster provides an electron for the rSAM to cleave *S*-adenosylmethionine (SAM), in a reaction that releases L-methionine and the reactive electrophile species 5'-deoxyadenosine (dAdo•), which functions as an oxidant by subtracting electrons from susceptible residues [170]. These residues are highly conserved, and variability can result in the inactivation of the pathway. While not essential for the pathway, it has been postulated that *pqqB* encodes an iron-dependent hydroxylase to oxidize tyrosine before or after its crosslinking with glutamate [133, 151, 171]. The modified dipeptide is cleaved from the main polypeptide by a peptidase, encoded as a monomer by *ppqF* or as a dimer *pqqFG* in some species [172]. PqqC is hypothesized to perform the final post-translational modification, including the amino group's cyclization to the phenyl moiety and the implicit 8-electron oxidation [173].

# INTRODUCTION

## Cofactors are indispensable for cellular biochemistry

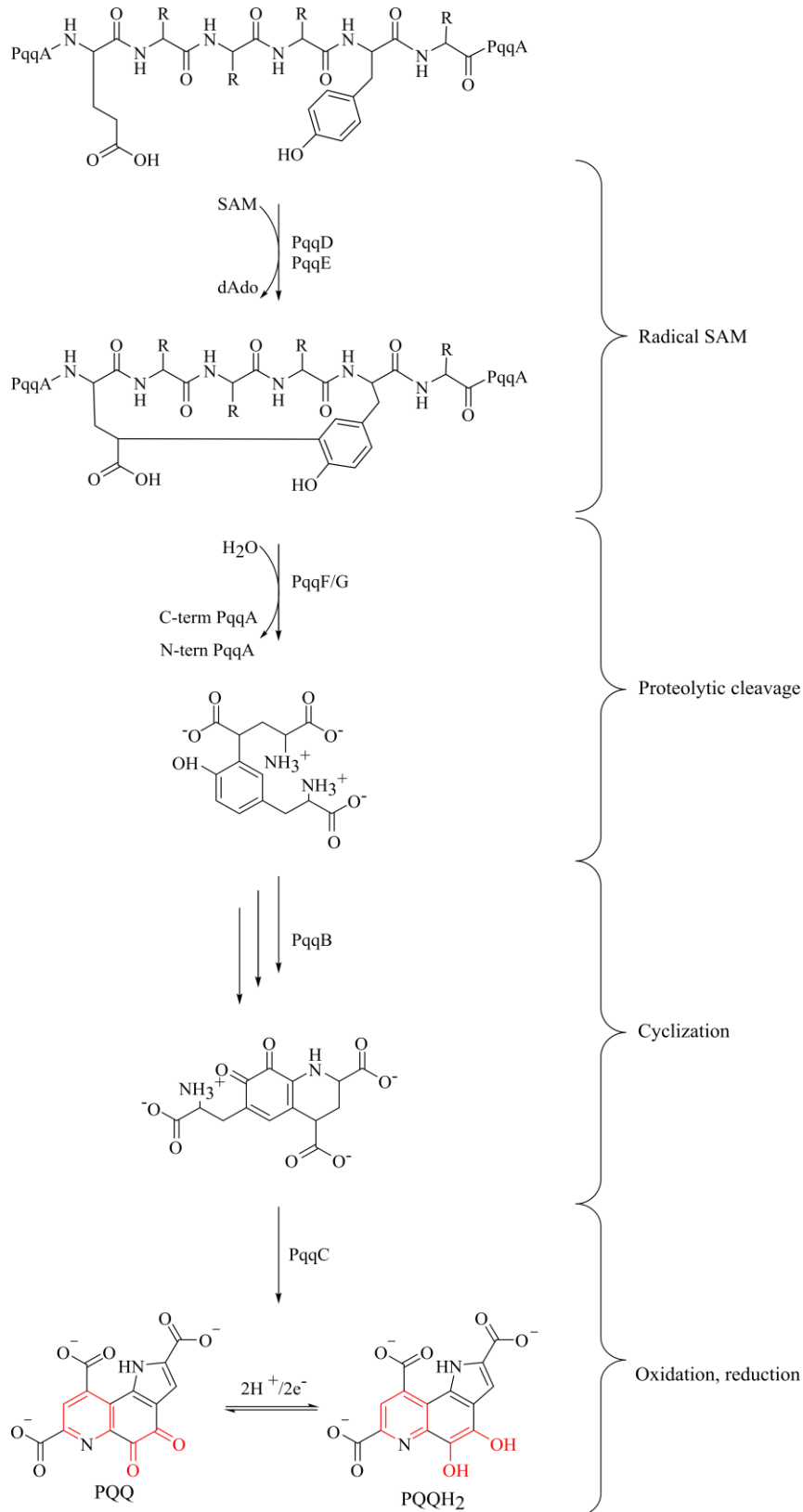


Figure 7: Pyrroloquinoline quinone (PQQ) biosynthesis according to [151]. Redox-active atoms are highlighted in red.

#### 6.4. MYCOFACTOCIN IS A PREDICTED RIPP COFACTOR

##### 6.4.1. Discovery of MFT: gene organization and distribution

The presence of a gene encoding a radical SAM enzyme has been proposed as a target for data mining in the pursuit of novel RiPPs [63]. Some of the reactions that rSAM enzymes catalyze are uniquely enzymatic and difficult to be reproduced by synthetic means, for example, methylations and C-C or C-S bond formation, decarboxylation, and epimerization [170, 174, 175]. To query multiple genomes simultaneously, partial phylogenetic profiling (PPP) was employed, by proposing functional connections between the co-occurrence of genes encoding radical SAM with genes encoding short peptides of unknown function, possibly indicating the RiPP precursor and target of post-translational modification [63]. This relation is scored higher if co-occurrence is present in the same genome locus, and also through similar taxa as expected if the product confers an evolutionary advantage [63, 176-178]. Furthermore, the “bioinformatic grammar” would allow to make an educated guess on the role of the novel RiPP under study. For example, the cluster of the PQQ redox cofactor is characterized by specific conserved residues on the C-terminal core peptide precursor, co-occurrence with cofactor-dependent enzymes, and no putative exporter in the BCG. In contrast, the precursor of the bacteriocin family of antibiotics is conserved in the N-terminal leader peptide region and putative exporters are co-clustered [63, 179]

Using this approach, a novel gene cluster encoding a radical SAM and a putative RiPP precursor was found clustered a glycosyltransferase. This BGC is found sparsely distributed across some Archaea and Chloroflexi, prevalent in Proteobacteria and especially Actinobacteria. It is also found in all species of the genus *Mycobacterium*. The radical SAM enzyme was annotated as a PqqE-like radical SAM, and the “small peptide of unknown function” displayed a highly conserved C-terminus. Notably, the gene cluster was also associated with specific subfamilies of oxidoreductases, as is the case for PQQ. This suggests a scenario where the biosynthetic locus encodes the redox cofactor for said oxidoreductases. Because of its presence in the genus *Mycobacterium* and the similarity of the locus to the PQQ cofactor and bacteriocin biosynthesis, the predicted RiPP product was termed mycofactocin (MFT) [178].

The organization of the cluster and taxonomic tree in a few selected strains is given in Figure 9. The MFT precursor *mftA*, binding protein *mftB*, and radical SAM *mftC* are clustered together and in the same orientation. There is point variability in some genera, for example, between *S. rhizosphaericus* where *mftABC* are together, while in *S. griseoruber*, the locus



## INTRODUCTION

### Mycofactocin is a predicted RiPP cofactor

AOK10\_RS36905 is inserted between *mftB* and *mftC*. This locus encodes a putative xanthine dehydrogenase accessory-like protein (XdhC), a family of enzymes that require molybdenum and ferredoxin as the main electron acceptor in purine degradation [180]. The position of the glycosyltransferase gene varies across genomes. However, it is generally close to a putative peptidase, and an FMN-dependent enzyme annotated initially as L-lactate dehydrogenase but experimentally determined later to act as a deaminase [181]. All in all, this indicates that while the position of *mftABC* is highly conserved through genomes with an MFT cluster, insertions and reorganizations concerning biosynthetic and putative MFT-dependent genes change the structure through the taxonomic tree (Figure 9). Still, their effects cannot be fully predicted by *in-silico* methods [182].

#### 6.4.2. Biosynthesis of MFT

The proposed MFT biosynthesis is indicated in Figure 10. *In vitro* catalytic activities of the enzymes described here have been confirmed in anaerobic conditions [181, 183-187]. MftA is the MFT precursor, analog in its biosynthetic role to PqqA. The C-terminal sequence is highly conserved, with the sequence -[MI]CGVY being practically invariable (Figure 8). Exclusively in the presence of the MftB chaperone, the radical SAM enzyme MftC reductively cleaves *S*-adenosyl-L-methionine (SAM) to generate CO<sub>2</sub>, L-methionine, and the dAdo• [183, 184]. The rSAM reaction was initially proposed to catalyze the oxidative decarboxylation of Tyr30 residue, leading to the unsaturation of the peptide bond in the terminal dipeptide [183, 184]. Upon further mechanistic studies, two rSAM-mediated reactions were found to occur: a first decarboxylated precursor, termed MftA\*\*, present in minor quantities. The main, more abundant isomeric product was termed MftA\*, a decarboxylated, cyclized molecule where the C $\alpha$ /C $\beta$  of Tyr30 is covalently crosslinked with the C $\beta$  of Val29. [185].



Figure 8: Clustal Omega [188, 189] alignment of the MftA precursor in 47 species with the MFT cluster, demonstrating highly conserved C-terminal residues. The *M. oryzae* sequence most likely represents a variant inactivated by mutation.

**INTRODUCTION**  
Mycofactocin is a predicted RiPP cofactor



Figure 9: Phylogenetic tree of the MFT radical SAM protein (MftC) and the MFT biosynthetic gene cluster. MftC protein alignment was done with the Clustal Omega algorithm [188, 189] and used as input for a maximum likelihood phylogenetic tree using PHYML [190], both in a Geneious environment. The LG substitution model was used [191], and branch support is SH-like (values in nodes). The scale bar indicates substitutions per site; six substitution rate categories were allowed, and the tree was optimized to topology/length/rate. All other parameters were estimated automatically. The surrounding gene neighborhood was drawn manually and annotated according to the most up-to-date NCBI annotation. Genes length is not drawn to scale.

## INTRODUCTION

### Mycofactocin is a predicted RiPP cofactor

The modified C-terminal dipeptide from MftA\* is then cleaved from the precursor by the iron-dependent peptidase MftE to generate AHDP (3-amino-5[(*p*-hydroxyphenyl)methyl]-4,4-dimethyl-2-pyrrolidinone) [187]. MftA\*\*, on the other hand, is non-susceptible of proteolytic cleavage by MftE, confirming that MftA\* is the real intermediate in MFT biosynthesis [185]. MftD annotated initially as an L-lactate dehydrogenase was thought to be an MFT-dependent redox enzyme, with a putative role in lactate metabolism coupled to MFT and part of the mycobacterial respiratory chain for energy generation. [178, 192]. Referring back to a possible interaction between MFT and TB pathogenesis, lactate has been proposed as a carbon source in the granuloma, key for the survival of latent MTB.

In the macrophage, two molecular oxygen moles per NADPH are used to produce NADP<sup>+</sup> and the oxidative burst that results in H<sup>+</sup> and the reactive oxygen species (superoxide) O<sub>2</sub><sup>-</sup>. As a highly energetic process, it results in lactate production by the Warburg effect, an overflow mechanism (section 10.4) to relieve the oxidative decarboxylation pathway [193-195]. However, knock-out studies of the MTB genes encoding for L-lactate dehydrogenases identified that while an  $\Delta lldD2$  mutant was unable to grow in lactate, growth in an  $\Delta mftD/lldD1$  strain was not affected in lactate dehydrogenase activity [196]. Metabolomics and transcriptomics studies failed to identify lactate as an essential source for MTB in early macrophage infection, having an uptake frequency of 0.07 when compared with cholesterol (1) or glucose (0.97) [197]. Further studies found the *mftD/lldD1*-encoding locus slightly upregulated with pyruvate as sole *in vitro* carbon sources compared with glucose and lactate, while the *lldD2* transcript was the most abundant in pathways related to CCM, except that upregulation under lactate compared to glucose was not observed. These results suggested that *lldD2* is constitutively expressed in MTB, while *lldD1* is possibly involved in pyruvate metabolism [198]. Furthermore, MftD is downregulated in MTB under DTT-induced reductive stress to simulate the predicted intra-macrophage infection conditions [199].

These hypotheses were put to rest with the *in vitro* demonstration that MftD *in vitro* is not responsible for lactate oxidation. Instead, they catalyzed the oxidative deamination of AHDP in a two-step reaction: the amino group is oxidized in the presence of molecular oxygen to yield an imino group, which can then spontaneously hydrolyze to generate an  $\alpha$ -diketo-amide and release ammonium [181]. The two keto groups in the product, termed premycofactocin (PMFT), can act as a coordinated redox center. This was confirmed by enzymatic assay with a putative MFT-dependent carveol dehydrogenase enzyme, resulting in carveol oxidation to

## INTRODUCTION

### Mycofactocin is a predicted RiPP cofactor

carvone and generation of PMFTH<sub>2</sub> [181, 200]. Midpoint voltammetry quantified a redox potential of PMFT of -255 mV using an Ag/AgCl reference electrode, more negative than the endogenous cofactors TPQ, LTQ, TTQ, and CTQ (-150 to -188 mV) and slightly lower than that of PQQ (-240 mV). The latter values are obtained with a different method, by measurement with a standard hydrogen electrode as reference. Because of its role in the biosynthesis of PMFT MftD has been renamed AHDP oxidase.

As mentioned before, the MFT BGC is defined by the co-occurrent presence of the MftA MFT precursor, the binding protein MftB, the radical SAM MftC, and a putative MFT glycosyltransferase MftF. The function of MftF had not been elucidated until recently and will be addressed in the first article of the present thesis. Most but not all of MFT-containing genomes have an open reading frame encoding for the AHDP oxidase [178] and under the current biosynthetic model [181, 201] is unclear whether in *mftD*-deficient genomes functional mycofactocin is produced. Furthermore, the putative mycofactocin regulator *mftR*, part of the DNA-binding motif based on two-domain transcriptional regulation Tet<sup>R</sup> [202], was found with significant upregulation in MTB (Rv0691c) during macrophage infection in both *in vitro* and an *in vivo* model, signaling a possible role in MFT expression during MTB pathogenesis [203].

#### 6.4.3. *The biological role of MFT*

As previously mentioned, because the mycofactocin BGC is more similar in its bioinformatic grammar to PQQ rather than bacteriocins, the mature product is believed to be a redox cofactor [63, 178]. In the MFT BGC, no transporter, signal peptide, or immunity-conferring protein can be predicted *in silico*. These features are present, for example, in the 34-residue lantibiotic RiPP nisin [204]. In addition, genes encoding two possible families of oxidoreductases were found co-localized with the predicted biosynthetic genes *mftABCF*. These two families are the zinc-dependent and iron-dependent alcohol dehydrogenases and the short-chain dehydrogenase/reductase superfamily (SDR). Furthermore, and while not described as part of the canonical MFT cluster [178], some glucose/methanol/choline oxidoreductase (GMC) members are present in the MFT BGC and considered as putative MFT-dependent oxidoreductases.

Alcohol dehydrogenases catalyze the oxidation of primary alcohols to aldehydes and ketones, which can be further metabolized in the central carbon metabolism (CCM). They can be divided as NAD(P)<sup>+</sup>-dependent, F<sub>420</sub>- or PQQ-dependent, and FAD-dependent. The NAD(P)<sup>+</sup>-dependent clade can be further subdivided into zinc-dependent (group I), short-chain SDR (250 – 350 residues, group II), and iron-dependent (preferably aldehyde reductases, group

## INTRODUCTION

### Mycofactocin is a predicted RiPP cofactor

III) [205-208]. Organic cofactors couple the transfer of electrons to the cellular redox pool: NAD(P) in the alcohol dehydrogenase family while in the GMC family are flavin-derived [207, 209]. The identification of PQQ-dependent alcohol dehydrogenases in methylotrophic bacteria marked the additional recognition of the role of lanthanum and other lanthanides (La – Nd) in electron transfer from the reduced PQQ cofactor to membrane-bound cytochromes. This example is the only known role of these rare earth elements in cellular biochemistry [210].

The GMC family was proposed as a result of sequence alignment from the glucose dehydrogenase (GLD), methanol oxidase (MOX), and choline dehydrogenase (CHD) families. Enzymes in this clade share an *N*-terminal 30-residues region corresponding to the adenosine diphosphate (ADP)-binding  $\beta\alpha\beta$  fold and carry a covalently or non-covalently bound FAD cofactor [211]. Their mode of action is on the hydroxyl moiety of alcohols, carbohydrates, or sterols, yielding an aldehyde group. In some cases, the product is retained in the active site to be further oxidized into a carboxylic acid [211-213]. One of the practical applications of these clades of enzymes is in glycemic sensors. An immobilized glucose oxidase, coupled with peroxidase, can be used to determine glucose levels in the blood. These *in vitro* diagnostics medical devices include immobilized FAD<sup>+</sup> or PQQ cofactors and artificial electron acceptors [214]. In addition, industrial applications have been proposed in lignocellulolytic processes for the biofuel industry and the synthesis of pharmaceutical precursors [213, 215, 216].

Enzymatic characterization of some GMC oxidoreductases has been performed with 2,6-dichlorophenolindophenol (DCPIP), *N*-nitrosodimethylamine (NDMA), or 1-methoxy-5-methylphenazinium methylsulfate (PMS) [217-219]. Not only do artificial electron acceptors complete the catalytic cycle – but they also serve as a colorimetric dye for readout [220]. Because these compounds are xenobiotic, enzymes that show activity towards these compounds but are orphans concerning their natural cofactor are provisionally called NDMA-dependent or DCPIP-dependent dehydrogenases/oxidoreductases.

## INTRODUCTION

### Mycofactocin is a predicted RiPP cofactor

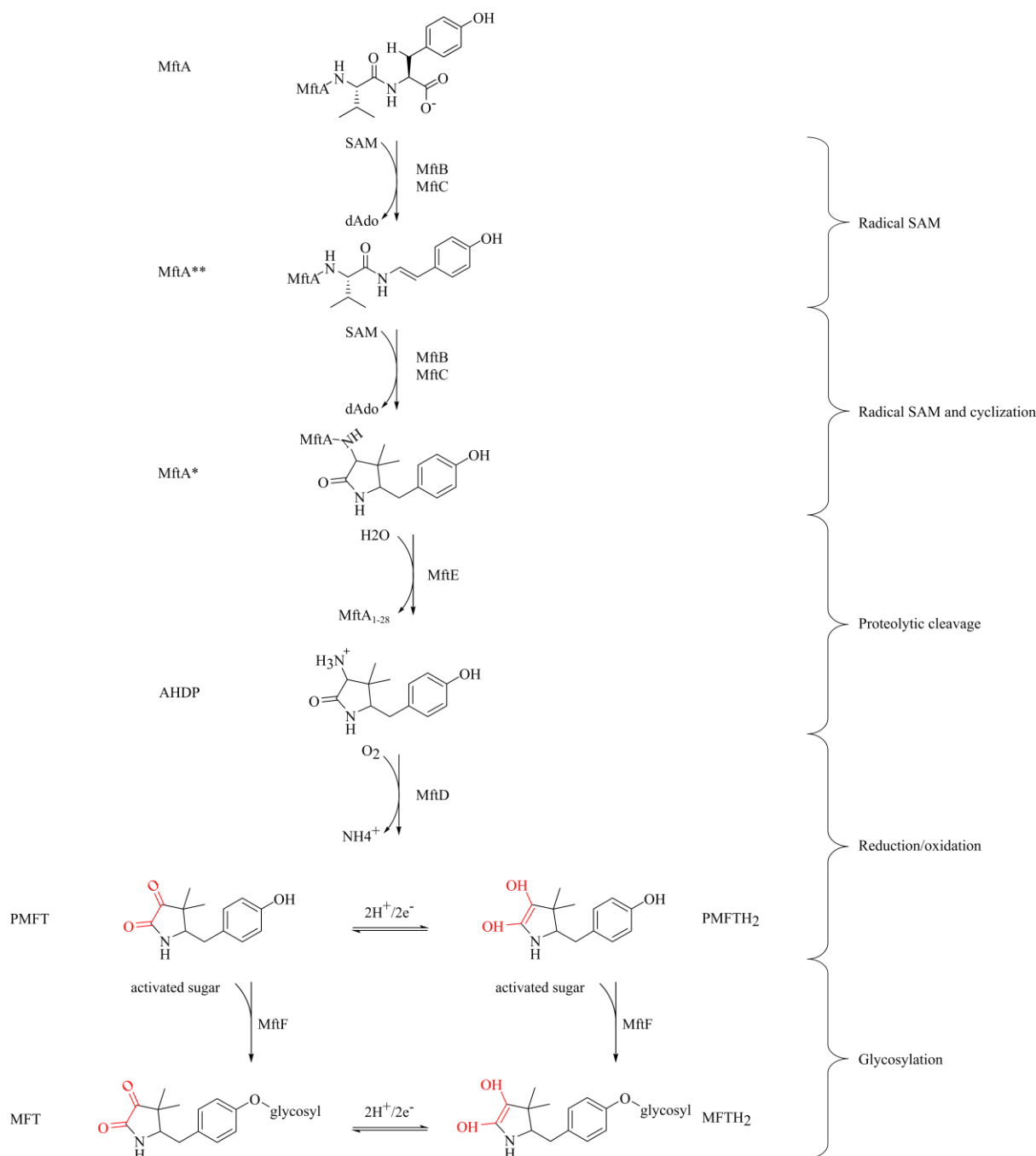


Figure 10: Current model of PMFT and mature mycofactocin biosynthesis. The MftA precursor undergoes two rSAM-mediated reactions that result in its decarboxylation and cyclization, forming MftA\*. The peptidase MftE cleaves AHDP from the precursor polypeptide, which is then oxidatively deaminated by MftD. This reaction forms the redox-active core of premycofactocin (PMFT, active atoms in red). A predicted glycosyltransferase catalyzes the addition of a glycosyl moiety to form mature MFT.

Conventional NAD<sup>+</sup>-dependent dehydrogenases contain a cofactor binding site that is open to the solvent. This enables exchange with the reduced redox pool of NADH and catalytic turnover. The tightly-bound, non-exchangeable NAD<sup>+</sup> cofactor of the stereoselective nicotinoprotein carveol dehydrogenase LimC from *Rhodococcus erythropolis* DCL14 is an outlier from this. Carveol dehydrogenases catalyze the cyclic terpenoid carveol reduction into carvone and are part of the monoterpene pathway that produces volatile compounds, involved

## INTRODUCTION

### Mycofactocin is a predicted RiPP cofactor

in ecological interactions [221]. *In vitro* experimental characterization revealed a tightly bound, non-exchangeable NAD<sup>+</sup> cofactor and an additional loop in the cofactor binding site. However, redox activity was only significant with the artificial terminal electron acceptor DCPIP [222].

Based on Pfam annotation with putative MFT-dependent SDR dehydrogenases identified in the MFT cluster, LimC could be an MFT-dependent enzyme as well [178]. Sequence analysis revealed that said insertion loop is also present in the SDR dehydrogenases associated with the MFT-cluster [222, 223]. To determine the structural features of these enzymes and their tightly bound cofactor, nine putative NAD<sup>+</sup>-dependent mycobacterial dehydrogenases with said insertion and encoded in genomes with the MFT BGC were produced in *E. coli* and crystallized [223]. When compared with other non-MFT SDR dehydrogenases and the position of the insertion relative to the cofactor binding pocket, the insertion loop makes NAD<sup>+</sup> partially inaccessible and leaves only a small portion of it solvent-accessible. This matches the observation of the insert loop in LimC as previously described [222].

With a representative *M. avium* SDR dehydrogenase and using carveol (substrate), carvone (product), DCPIP (artificial redox cofactor), and, for comparison, tricyclazole as an inhibitor, non-covalent binding was observed by saturation transfer difference – nuclear magnetic resonance (STD-NMR). This interaction indicates that the additional loop does not impair substrate or product binding. All-in-all, having NAD<sup>+</sup> as a partially-accessible cofactor and with the binding of an artificial electron acceptor possible, it is possible that, *in vivo*, a second redox cofactor, mycofactocin, is required to connect the internal cofactor with the cellular redox pool [223]. Table 1 describes some of the putative MFT-dependent dehydrogenases/oxidoreductases characterized, either structurally by crystallography or *in vitro* enzymatic assays.

**INTRODUCTION**  
**Mycofactocin is a predicted RiPP cofactor**

Annotation	Species	UniProt ID	Cofactor	PDB ID	Ref.
Carveol dehydrogenase	<i>R. erythropolis</i>	Q9RA05	NAD <sup>+</sup> , DCPIP*	NA	[222]
Carveol dehydrogenase	<i>M. avium</i>	A0QCJ8	NAD <sup>+</sup>	3T7C**	
Carveol dehydrogenase	<i>M. avium</i>	A0QB72	NAD <sup>+</sup>	3UVE	
Putative carveol dehydrogenase	<i>M. avium</i>	A0QDP5	NAD <sup>+</sup>	4RGB	
Carveol dehydrogenase	<i>M. avium</i>	A0QFV1	NAD <sup>+</sup>	3PXX 5EJ2**	[223]
Putative short-chain dehydrogenase	<i>M. abscessus</i>	B1MLR7	NAD <sup>+</sup>	3S55	
Putative carveol dehydrogenase	<i>M. paratuberculosis</i>	Q73SC8	NAD <sup>+</sup>	PGX	
Putative 3-ketoacyl-ACP reductase	<i>M. paratuberculosis</i>	Q73W00	NAD <sup>+</sup>	3SX2	
Short-chain dehydrogenase	<i>M. paratuberculosis</i>	Q73X99	NAD <sup>+</sup>	3TSC	
NDMA-dependent methanol dehydrogenase	<i>M. smegmatis</i>	A0R5M3	NDMA*	NA	[224-226]

Table 1: Putative MFT-dependent oxidoreductases and their level of characterization. Annotation is given as in the original publication [223]. PDB ID NA when not reported as crystalized. \* means enzymatic activity studies performed with an artificial redox acceptor. \*\* indicates the removal of the hexahistidine tag.

Orthogonal evidence for the function of MFT as a redox cofactor involved in primary metabolism has been observed *in vivo* [226]. One research line regarding intracellular MTB's physiology and pathogenesis addressed cholesterol as a carbon source during the latency phase [227, 228]. Cholesterol is readily available in infected macrophages and the granuloma. Previous studies have already detected cholesterol in the site of infection [228] and MTB capacity to assimilate it [227]. Shortly after the MFT locus proposal for the novel MFT cofactor, a study of high-density mutagenesis and sequencing for profiling the MTB phenotype response to mutations was published [229]. By mapping random mutagenesis events across the entire genome and correlating these insertion events to the mutant's metabolic fitness to thrive in cholesterol, it was possible to identify novel genes that mediate cholesterol metabolism as an energy source. Among the 42 genes identified as required for cholesterol growth *in vivo*, including some not yet implicated in  $\beta$ -oxidation, the central genes of the MFT cluster were found: Rv0693 (*mftC*), Rv0694 (*mftD*), Rv0695 (*mftE*), and Rv0696 (*mftF*). This seemed to indicate a possible role of the MFT cluster in cholesterol metabolism. However, this study had a severe flaw. To assay differential fitness to grow in cholesterol, Griffin et al. [229] employed



## INTRODUCTION

### Mycofactocin is a predicted RiPP cofactor

minimal media supplemented with 0.1 g L<sup>-1</sup> cholesterol. However, a second carbon source was introduced. By virtue of its lipidic sterol nature, cholesterol is insoluble in water (1.8 mg L<sup>-1</sup> at 30 °C); therefore, 2 g L<sup>-1</sup> ethanol was used as a solvent. A 1988 report indicates that ethanol is a viable carbon source for *Mycobacteria* [230]. While it is true that fast-growing strains like MSMEG are more fit for this purpose, this composition cast a shadow on the essentiality of genes identified by Griffin *et al.* for growth in cholesterol given that a second carbon source, ethanol, is present [229].

Evidence of an *in vivo* relationship between MFT and primary alcohol metabolism was elucidated for the first time by Krishnamoorthy *et al.* [226]. By constructing MSMEG mutants with truncated *mft* genes, it was possible to probe the relevance of MFT in both cholesterol and ethanol metabolism. An  $\Delta mftC$  deletion mutant was unable to grow in all primary alcohols, and complementation restored the phenotype, albeit with a slower growth rate than the wild-type strain. This suggests that the growth phenotype depends on alcohol and MFT, not on cholesterol, as previously suggested [226, 229]. Studies conducted with methanol show a contrasting effect: while the results by Dubey *et al.* have shown twice that MSMEG wild type can grow in methanol as a sole source of carbon [224, 225], Krishnamoorthy *et al.* were unable to replicate this phenotype after 72 h [226].

The same groups investigated the role of MSMEG\_6242 (A0R5M3) from MSMEG as the first presumed MFT-dependent alcohol dehydrogenase. Although not located in the MFT cluster's vicinity, a homolog exists adjacent to the MFT *cluster* in *S. erythraea* NRRL2338 (Figure 9, dark blue arrow). MSMEG\_6242 is located 2 Mbp downstream from the MFT-cluster (Figure 11). Genetic inactivation of the MSMEG\_6242 gene resulted in a mutant unable to grow on ethanol. Furthermore, the transcriptomic analysis indicated that the MSMEG\_6242 transcript is accumulated in the wild-type strain cultured in ethanol compared to a glycerol control. These results suggested that MSMEG\_6242 is involved in ethanol metabolism and that activity depends on MFT as a cofactor [226].

## INTRODUCTION

### Mycofactocin is a predicted RiPP cofactor

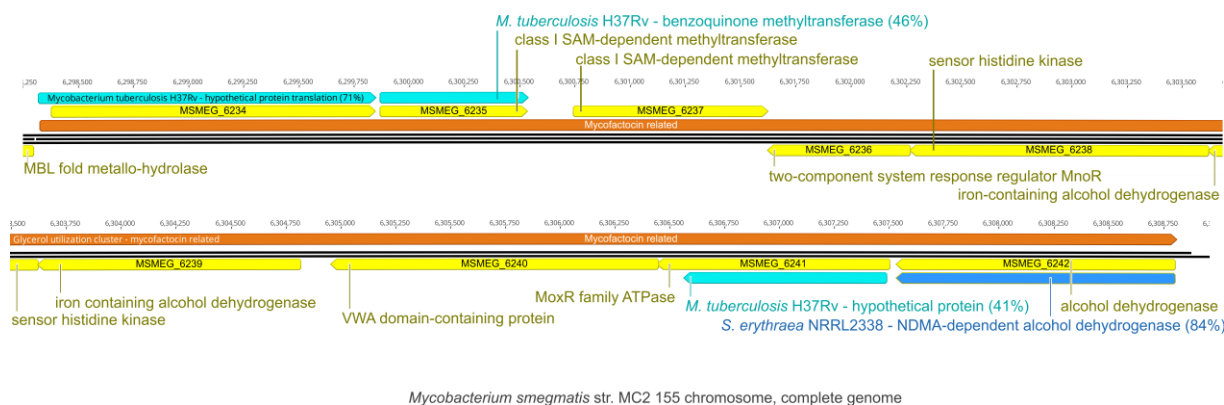


Figure 11: Gene cluster MSMEG\_6234 to MSMEG\_6242 in *M. smegmatis* mc<sup>2</sup> 155, containing the MFT-dependent alcohol dehydrogenase Mno (MSMEG\_6242). Homologs of these CDS can be found in proteins from *M. tuberculosis* H37Rv (cyan) and *S. erythraea* NRRL2338 (blue). Parentheses indicate the identity percentage with a cutoff of >40%.

MSMEG\_6242 shows 99% sequence identity to a characterized methanol dehydrogenase (Mdo) from *Mycobacterium* sp. strain JC1 involved in methylotrophy [224, 231]. Previously known membrane-bound, periplasmic alcohol dehydrogenases of Gram-negative bacteria could use PQQ or NAD<sup>+</sup> as natural cofactors. However, this was not the case for Mdo [232-234]. Heterologously produced MSMEG\_6242 with a C-terminal hexahistidine tag [235] (termed Mno) showed *in vitro* activity with NDMA as artificial redox acceptor and methanol, formaldehyde, ethanol, propanol, or butanol as substrates [224]. This activity contrasted partially to the previously characterized Mdo, unable to oxidize propanol and butanol [234]. Furthermore, the observed activity against formaldehyde suggests an exciting role in which the enzyme can catalyze both steps to assimilate methanol, first by oxidation to yield formaldehyde, from which two molar equivalents can undergo a dismutase reaction to yield two products with a higher and lower oxidation state: formate and a methanol equivalent. The methanol: NDMA oxidoreductase from *Amycolatopsis methanolica* and *M. gastri* was previously reported to catalyze said reactions in the presence of the artificial redox cofactor NDMA, indicating that the natural cofactor is unknown [232].

Supplementing Mdo in a DCPIP-based assay with methanol and extracts from ethanol-cultured MSMEG wild-type, presumed to contain MFT, resulted in a higher specific activity, as measured by DCPIP reduction and discoloration. Lower activity was observed with extracts from an MFT-deficient mutant ( $\Delta mftC$ ) and higher in strains with  $\Delta mftC$  complementation [225]. These results, however, should be taken with care because assays were not performed with purified enzyme [226]. Taken together *in vivo* and *in vitro* results suggest that MSMEG\_6242, or Mno, is a probable MFT-dependent alcohol dehydrogenase that catalyzes the oxidation of primary alcohols to the respective aldehyde, ethanol to acetaldehyde,

## **INTRODUCTION**

### **Mycofactocin is a predicted RiPP cofactor**

for example. The role of Mno in methanol metabolism is still unclear, given the fact that the methylotrophic growth of MSMEG has resulted in opposite results [224-226].

## 7. AIMS OF THIS WORK

Mycofactocin (MFT) is a proposed redox cofactor, universally present in Mycobacteriaceae species, including the etiological agent of tuberculosis, *M. tuberculosis*. The existence of the biosynthetic gene cluster was proposed by bioinformatic analysis, which provided the first steppingstones onto the role of maturases and associated dehydrogenases. During the course of this research, initial studies with the heterologous production of some MFT maturases led to the *in vitro* identification of intermediates and reactions yielding the redox-active precursor premycofactocin (PMFT). Similarly, knock-out, and complementation of the MFT cluster of the model organism MSMEG indicated that MFT is a redox cofactor involved in primary alcohol metabolism. However, despite these advances, no structural characterization of mature MFT has been reported. The role of other MFT enzymes remain unveiled, and the biosynthetic pathway remained incomplete and unconfirmed *in vivo*.

The first publication of this thesis aims at discovering MFT *in vivo* and at the isolation and structure elucidation of the mature molecule. For this, we combined the *in vitro* knowledge of MFT biosynthesis and the finding *in vivo* that MFT is related to ethanol metabolism in order to identify novel intermediates. We planned to compare metabolomic extracts of MSMEG by high-resolution liquid chromatography-mass spectrometry (HR-LC-MS) including applications such as untargeted metabolomics, molecular networking, and isotopic labeling. Comparing growth conditions as well as wild-type and knock-out strains of MFT genes was envisioned to help identify possible MFT-congeners. Isolation of candidate molecules followed by NMR-based structural elucidation was planned to determine the molecular structure of mature MFT congeners.

Another goal of this thesis was the development of culture conditions to increase MFT yield for further enzymatic and a more comprehensive structural and functional characterization. We assumed that – as a redox cofactor – MFT production might depend on oxygen supply in the culture broth. Therefore, we used different oxygen conditions and media compositions to determine possible parameters that influence the MFT yield. We further wanted to know if trends observed in a shake flask experiments could be reproduced in larger scale like in stirred tank reactors.

## 8. MANUSCRIPTS

### 8.1. STRUCTURE ELUCIDATION OF THE REDOX COFACTOR MYCOFACTOCIN REVEALS OLIGO-GLYCOSYLATION BY MftF

Peña-Ortiz, Luis; Graça, Ana Patrícia; Guo, Huijuan; Braga, Daniel; Köllner, Tobias G.; Regestein, Lars; Beemelmans, Christine; Lackner, Gerald.

Chemical Science (2020),11, 5182-5190. DOI: 10.1039/D0SC01172J

#### SUMMARY

*Mycobacterium tuberculosis*, the etiologic agent of tuberculosis (TB), has cofactor-mediated detoxification mechanisms that limit the bacteriostatic effect of anti-TB drugs. Conversely, some prodrugs require to be metabolized by cofactor-dependent mechanisms into the active pharmacological molecule. Novel cofactors could open the door for alternative TB treatments. Mycofactocin (MFT) is a cryptic redox cofactor, belonging to the family of ribosomally produced and post-translationally modified peptides (RiPPs). It has been identified in Mycobacteria and Actinomyces for a previously unobserved redox pool involved in primary alcohol metabolism. Bioinformatics and in vitro studies have proposed a biosynthetic model, but the mature form of the cofactor is still unknown. Here, we integrate <sup>13</sup>C-untargeted metabolomics, molecular networking, and gene knockout studies to discover the mature form of MFT and elucidate its structure. The results demonstrated that the redox-active precursors are decorated with up to nine  $\beta$ -1,4-linked glucose residues. Upon cultivation in ethanol, glucosyl MFT accumulates, with a prevalence of molecules containing a previously unforeseen 2-*O*-methyl glucose moiety. Genetic studies and complementation confirmed the putative MftF glycosyltransferase role, and redox activity in these new moieties was established by activity-based metabolic profiling. NMR structural elucidation characterized the structure of methyl-mycofactocin containing 8 glucose moieties. Our results indicate that methylglucosyl MFT is the mature form of MFT in *M. smegmatis* and will guide future studies into the biochemical and physiological roles of MFT in bacteria.

## CONTRIBUTION TO THE MANUSCRIPT

Luis A. Peña Ortiz contributed to the manuscript by performing mycobacterial cultivation and isotopic labeling in bench and lab-scale, metabolome extraction, and analysis by LC-MS/MS and molecular networking. He was also involved in the preparation and editing of the manuscript.

## ESTIMATED CONTRIBUTION IN PERCENTAGE

Luis A. Peña Ortiz	24
Ana Patrícia Graça	17
Huijuan Guo	16
Daniel Braga	7
Tobias G. Köllner	6
Lars Regestein	5
Christine Beemelmans	5
Gerald Lackner	20

---

Luis Alberto Peña Ortiz

---

Prof. Dr. Christian Hertweck



Showcasing research from Dr. Gerald Lackner's laboratory, Leibniz Institute for Natural Product Research and Infection Biology and Friedrich Schiller University, Germany.

Structure elucidation of the redox cofactor mycofactocin reveals oligo-glycosylation by MftF

A team of researchers around Dr. Gerald Lackner discovered mycofactocin, a redox cofactor from pathogenic mycobacteria involved in alcohol metabolism. It is the first cofactor whose existence had been postulated on the basis of mere bioinformatics and which had remained cryptic for almost a decade. Intensive metabolomics studies eventually led to the identification of the molecule. The elucidation of its chemical structure revealed an unusual sugar decoration. Last but not least, mycofactocin could be a promising target for fighting mycobacterial infections. The authors cordially thank Luo Yu for the artwork.

#### As featured in:



See Gerald Lackner *et al.*,  
*Chem. Sci.*, 2020, 11, 5182.



Cite this: *Chem. Sci.*, 2020, 11, 5182

All publication charges for this article have been paid for by the Royal Society of Chemistry

## Structure elucidation of the redox cofactor mycofactocin reveals oligo-glycosylation by MftF†

Luis Peña-Ortiz,<sup>ab</sup> Ana Patrícia Graça,<sup>ab</sup> Huijuan Guo,<sup>c</sup> Daniel Braga,<sup>ab</sup> Tobias G. Köllner,<sup>d</sup> Lars Regestein,<sup>e</sup> Christine Beemelmanns<sup>bc</sup> and Gerald Lackner<sup>\*ab</sup>

Mycofactocin (MFT) is a redox cofactor belonging to the family of ribosomally synthesized and post-translationally modified peptides (RiPPs) and is involved in alcohol metabolism of mycobacteria including *Mycobacterium tuberculosis*. A preliminary biosynthetic model had been established by bioinformatics and *in vitro* studies, while the structure of natural MFT and key biosynthetic steps remained elusive. Here, we report the discovery of glycosylated MFT by <sup>13</sup>C-labeling metabolomics and establish a model of its biosynthesis in *Mycobacterium smegmatis*. Extensive structure elucidation including NMR revealed that MFT is decorated with up to nine β-1,4-linked glucose residues including 2-O-methylglucose. Dissection of biosynthetic genes demonstrated that the oligoglycosylation is catalyzed by the glycosyltransferase MftF. Furthermore, we confirm the redox cofactor function of glycosylated MFTs by activity-based metabolic profiling using the carveol dehydrogenase LimC and show that the MFT pool expands during cultivation on ethanol. Our results will guide future studies into the biochemical functions and physiological roles of MFT in bacteria.

Received 26th February 2020  
Accepted 18th April 2020

DOI: 10.1039/d0sc01172j

rsc.li/chemical-science

### Introduction

Coenzymes are small molecules indispensable for the catalytic activity of many enzymes. While coenzymes like NAD<sup>+</sup> or FAD are ubiquitous in nature and are essential for the core metabolism of all forms of life, specialized cofactors like pyrroloquinoline quinone (PQQ)<sup>1</sup> and coenzyme F<sub>420</sub><sup>2</sup> are restricted to certain microbial phyla, but typically involved in extraordinary metabolic processes like methylotrophy, methanogenesis, or detoxification processes. Moreover, specialized cofactors serve as model systems for the evolution of cofactors

and their co-evolution with their associated enzyme families. They can be regarded as examples of low-molecular weight natural products that modify, extend or enhance microbial metabolism. Mycobacteria are particularly rich in unusual redox cofactors and antioxidants that contribute to redox balance and metabolic plasticity. For instance, mycothiol<sup>3,4</sup> or ergothioneine<sup>5</sup> protect *Mycobacterium tuberculosis* from oxidative stress and support detoxification pathways. Coenzyme F<sub>420</sub> is involved, *e.g.*, in cell wall biosynthesis<sup>6</sup> or defense against nitrosative stress in mycobacteria.<sup>7</sup> Moreover, some antimycobacterial drugs like pretomanid<sup>8</sup> are administered as prodrugs and will only develop bioactivity after biotransformation by a coenzyme F<sub>420</sub>-dependent reductase.<sup>9</sup> Mycofactocin (MFT) is a putative redox-cofactor whose existence has been postulated on the basis of comparative genomics and bioinformatics.<sup>10,11</sup> Its molecular identity and structure, however, have remained elusive to date. The MFT biosynthetic gene cluster is highly conserved and widespread among mycobacteria. The inactivation of the MFT gene locus in the model species *Mycobacterium smegmatis* (synonym: *Mycobacterium smegmatis*) as well as *M. tuberculosis* resulted in the inability of the mutants to utilize ethanol as a sole source of carbon and further disturbances of mycobacterial redox homeostasis were revealed.<sup>12</sup> Involvement of MFT in methanol metabolism was reported as well.<sup>13</sup> These recent results strongly support the hypothesis that MFT is a redox cofactor and might represent a fitness factor of mycobacteria during some stages of infection.

<sup>a</sup>Junior Research Group Synthetic Microbiology, Leibniz Institute for Natural Product Research and Infection Biology (HKI), Beutenbergstr. 11a, 07745 Jena, Germany. E-mail: gerald.lackner@leibniz-hki.de

<sup>b</sup>Friedrich Schiller University, Beutenbergstr. 11a, 07745 Jena, Germany

<sup>c</sup>Junior Research Group Chemical Biology of Microbe-Host Interactions, Leibniz Institute for Natural Product Research and Infection Biology (HKI), Beutenbergstr. 11a, 07745 Jena, Germany

<sup>d</sup>Department of Biochemistry, Max Planck Institute for Chemical Ecology, Hans-Knöll-Str. 8, 07745 Jena, Germany

<sup>e</sup>Bio Pilot Plant, Leibniz Institute for Natural Product Research and Infection Biology (HKI), Beutenbergstr. 11a, 07745 Jena, Germany

† Electronic supplementary information (ESI) available: ESI Appendix: materials and methods, supplementary figures, supplementary results and discussion (.PDF). Data Set 1: <sup>13</sup>C-labeled compounds (.xlsx). Data Set 2: comparative metabolomics comparing *M. smegmatis* WT, mutant and complement strains (.xlsx). Data Set 3: comparative metabolomics of *M. smegmatis* WT treated with glucose or ethanol (.xlsx). Data Set 4: activity-based metabolic profiling (.xlsx). See DOI: 10.1039/d0sc01172j





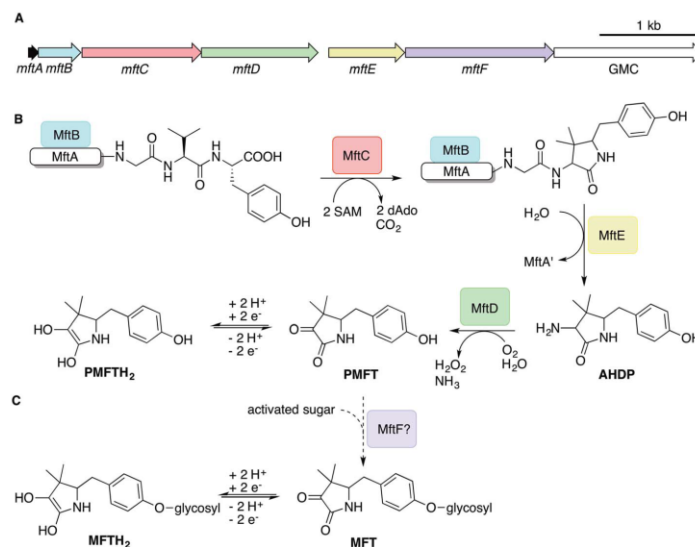


**Fig. 1** Biosynthesis of mycofactocin. (A) Schematic representation of the MFT biosynthetic gene cluster of *M. smegmatis*. Arrows present genes *mftA-F*. The scale bar indicates 1000 base pairs. (B) Current biosynthesis model of MFT revealed by *in vitro* studies. The precursor peptide MftA (WP\_029104568.1) is bound by its chaperone MftB. The rSAM enzyme MftC catalyzes oxidative decarboxylation and cyclization of the core peptide consisting of a C-terminal Val-Tyr dipeptide. The peptidase MftE releases the cyclized core to form AHDP. MftD performs oxidative deamination of AHDP yielding pre-mycofactocin (PMFT), the presumed redox-active core. (C) The putative glycosyltransferase MftF (WP\_011727662.1) was hypothesized to glycosylate premycofactocins. (P)MFT is reduced to (P)MFTH<sub>2</sub> (mycofactocinol) by oxidoreductases. dAdo: 5'-deoxyadenosine, GMC: glucose-methanol-choline oxidoreductase, SAM: S-adenosyl methionine.

The architecture of the MFT gene cluster (Fig. 1A) suggested that the resulting natural product is a ribosomally synthesized and post-translationally modified peptide (RiPP).<sup>14</sup> Several *in vitro* studies have contributed to a preliminary biosynthetic model of MFT (Fig. 1B): the precursor peptide MftA of *M. smegmatis* consisting of 31 amino acids is produced by the ribosome and bound by its chaperone MftB. Subsequently, the terminal core peptide consisting of Val and Tyr is oxidatively decarboxylated and cyclized by the radical SAM enzyme MftC.<sup>15–17</sup> The resulting cyclic core structure is released by the peptidase MftE<sup>18</sup> forming 3-amino-5-[(*p*-hydroxyphenyl)methyl]-4,4-dimethyl-2-pyrrolidinone (AHDP).<sup>19</sup> Just recently, it was shown that MftD, an enzyme homologous to the *l*-lactate dehydrogenase LldD2<sup>20</sup> catalyzes the oxidative deamination of AHDP to yield pre-mycofactocin (PMFT).<sup>21</sup> The same study demonstrated by voltammetry that the  $\alpha$ -keto amide moiety of PMFT is redox-active and can be reduced to PMFTH<sub>2</sub> (midpoint potential:  $-255$  mV). Efficient reduction was also achieved by the action of carveol dehydrogenase using carveol as an electron donor *in vitro*.<sup>21</sup> Therefore, PMFT likely represents the redox-center of MFT, as riboflavin is the redox-active core of FMN and FAD.

Although these current hypotheses are plausible, all these known metabolic intermediates have only been observed *in vitro* and could therefore represent artifacts, making the verification of their relevance *in vivo* urgently desired. Furthermore,

additional steps of MFT biosynthesis, the function of the *mftF* gene as well as the chemical structure of natural MFT awaited experimental clarification. In this study, we confirm the current biosynthetic model of MFT *in vivo*, detected several novel oligoglycosylated MFT congeners and elucidated their structure. We show that MFTs are decorated with a  $\beta$ -1,4-glucan chain and provide genetic evidence that glycosylation is performed by the glycosyltransferase MftF. Finally, we show dependence of MFT formation on ethanol and corroborate its cofactor function by activity-based metabolic profiling.

## Results and discussion

### Discovery of mycofactocins by metabolomics

In order to identify potential mycofactocin congeners in mycobacteria, we used the fast-growing and weakly pathogenic species *M. smegmatis* MC<sup>2</sup> 155 as a model organism and developed a metabolomics approach combining metabolic induction and labeling to specifically trace MFT congeners. Assuming that MFT production would be stimulated by alcohols, we cultivated bacteria in media containing 10 g L<sup>-1</sup> ethanol. Furthermore, we used stable isotope labeling to obtain candidate molecules compatible with the proposed biosynthetic pathway: since the C-terminal core peptide of MftA is composed of Val and Tyr, we reasoned that MFT congeners could be specifically labeled by feeding *L*-Val-<sup>13</sup>C<sub>5</sub> and *L*-Tyr-<sup>13</sup>C<sub>9</sub>.



Intracellular contents were extracted and analyzed by liquid chromatography coupled with high-resolution mass spectrometry (LC-MS). Compounds were detected by *in silico* grouping of co-eluting isotopic peaks and adducts (feature finding). Afterwards,  $^{13}\text{C}$ -labeled compounds were deduced computationally (Data Set 1†). According to the established biosynthetic pathway we expected 13 carbons to remain  $^{13}\text{C}$ -labeled after oxidative decarboxylation of the Val-Tyr core peptide. We therefore searched for compounds that displayed an exchange of 13 carbons, resulting in a mass shift of +13.04362 Da (ESI Fig. S1†). This approach revealed a list of only twelve candidate compounds. Strikingly, the exact mass and proposed sum formula of three of these compounds corresponded to known intermediates of MFT, recently described *in vitro*, namely AHDP, PMFT as well as PMFTH<sub>2</sub>. In addition to these compounds, several labeled molecules with increasing molecular weight were detected. Some co-eluting candidates with a mass difference of +17.02654 could be explained as  $\text{NH}_4^+$  adducts of each other. The remaining nine candidate compounds (Table 1) were grouped based on their chromatographic retention times, eluting closely to either PMFT or PMFTH<sub>2</sub> (approx. 7.2 min and 6.9 min, respectively). Intriguingly, members of the two groups could be arranged in pairs with a mass difference of two hydrogen atoms leading us to assume that each group represented derivatives of either PMFT or PMFTH<sub>2</sub>. Thus, we termed these two clusters of molecules mycofactocinones (MFT) and mycofactocinols (MFTH<sub>2</sub>), respectively. Notably, some mycofactocinols eluted as two chromatographically separated isomers. For instance, the dominant PMFTH<sub>2</sub> eluted at 6.8 min, while the minor isomer eluted at 6.5 min. These two compounds displayed highly similar MS/MS spectra (ESI Fig. S2†) and most likely represent tautomeric forms. For reasons of

simplicity, only the more prevalent isomer was considered during metabolomics studies. We then performed MS/MS networking (Fig. 2), an approach that clusters compounds based on similarity of their MS/MS fragmentation pattern and therefore potentially related chemical scaffolds.<sup>22</sup>

Interestingly, candidates retrieved from  $^{13}\text{C}$ -labeling experiments clustered with further putative MFT congeners. The mass difference between the first candidate mycofactocinol (MFT-1H<sub>2</sub>) with an exact mass of 397.17395 Da and PMFTH<sub>2</sub> was +162.05303 Da, which corresponded to a hexose sugar.

Furthermore, the MS/MS spectrum of MFT-1H<sub>2</sub> (Fig. 2) showed a fragment ion that corresponded to the mass of the putative aglycon ( $m/z$  236.13 [ $\text{M} + \text{H}$ ]<sup>+</sup>), thus supporting the assumption that MFT-1H<sub>2</sub> was a glycosylated derivative of PMFTH<sub>2</sub>. MS/MS networking also revealed a recurrent mass difference of 14.01565 between compounds, indicating that methylation might occur as well. We thus assumed that the MFT candidate molecules could be explained as glycosylated or glycosylated and monomethylated species of PMFT(H<sub>2</sub>). In analogy to coenzyme F<sub>420</sub>-*n*, where *n* indicates the number of glutamyl residues in the side chain,<sup>2</sup> we named the glycosylated molecules MFT-*n*(H<sub>2</sub>) with *n* representing the number of sugar moieties. Monomethylated species were termed methylmycofactocinones (MMFT-*n*) and methylmycofactocinols (MMFT-*n*H<sub>2</sub>), respectively. A targeted search for theoretical mass traces revealed additional members of the MFT-*n*(H<sub>2</sub>) and MMFT-*n*(H<sub>2</sub>) series (Data Set 2†). As expected, the mycofactocinones exhibited MS/MS fragments with a systematic shift by -2.0016 (*e.g.*,  $m/z$  234.11, 396.16, 572.24) (Fig. 2A) demonstrating that the reduction/oxidation indeed takes place in the PMFT moiety. Oligoglycosylation with up to *n* = 9 saccharide units was detected, while seven and eight units appeared to be the most dominant forms. We observed both methylated (MMFT) and unmethylated (MFT) sugar chains, with the methylated series being more prominent. Only monomethylated species were found. Mass fragmentation of MMFT-*n*(H<sub>2</sub>) species was well in agreement with the assumption that the second sugar was the hotspot for methylation. For instance, MS/MS fragmentation of MMFT-8H<sub>2</sub> yielded peaks corresponding to ions of MFT-1H<sub>2</sub> (398.18011) and MMFT-2H<sub>2</sub> (574.24640) suggesting that the methyl group is present in the second sugar moiety (Fig. 2A).

### Structure elucidation of the oligosaccharide moiety

To determine the structure of elongated mycofactocins, we conducted large-scale cultivations. The dominant mycofactocin exhibited the same mass and fragmentation pattern as MMFT-2H<sub>2</sub>, but eluted at a slightly shifted retention time (Fig. S3†). We therefore named this species MMFT-2bH<sub>2</sub>. Due to the low yields and co-elution of contaminants, structural analysis by nuclear magnetic resonance (NMR) was not possible at this stage. However, cellulase ( $\beta$ -1,4-glucanase) treatment degraded the sugar chain of mycofactocin species (*n* > 2), while amylase ( $\alpha$ -1,4-glucanase) did not exhibit any effect (Fig. 3A). This finding strongly suggested that the oligosaccharide chain represents a  $\beta$ -1,4-glucan. Intriguingly, isomer MMFT-2bH<sub>2</sub>, but not

Table 1 MFT candidate molecules obtained by stable isotope labeling of *M. smegmatis* with L-Val- $^{13}\text{C}_9$  and L-Tyr- $^{13}\text{C}_9$ <sup>a</sup>

Name	Sum formula	Exact mass (measured)	RT [min]	Area (mean)
<b>Aglycons</b>				
AHDP	C <sub>13</sub> H <sub>18</sub> N <sub>2</sub> O <sub>2</sub>	234.13683	6.53	44 862
PMFTH <sub>2</sub>	C <sub>13</sub> H <sub>17</sub> NO <sub>3</sub>	235.12084	6.88	49 905
PMFT	C <sub>13</sub> H <sub>15</sub> NO <sub>3</sub>	233.10519	7.22	100 832
<b>Mycofactocinols (MFT-<i>n</i>H<sub>2</sub>)</b>				
MFT-1H <sub>2</sub>	C <sub>19</sub> H <sub>27</sub> NO <sub>8</sub>	397.17367	6.88	53 413
<b>Methylmycofactocinols (MMFT-<i>n</i>H<sub>2</sub>)</b>				
MMFT-2H <sub>2</sub>	C <sub>26</sub> H <sub>39</sub> NO <sub>13</sub>	573.24214	6.89	5722
MMFT-7H <sub>2</sub>	C <sub>36</sub> H <sub>89</sub> NO <sub>38</sub>	1383.50626	6.89	340 064
MMFT-8H <sub>2</sub>	C <sub>62</sub> H <sub>99</sub> NO <sub>43</sub>	1545.55908	6.86	550 390
<b>Methylmycofactocinones (MMFT-<i>n</i>)</b>				
MMFT-7	C <sub>36</sub> H <sub>87</sub> NO <sub>38</sub>	1381.49061	7.25	185 407
MMFT-8	C <sub>62</sub> H <sub>97</sub> NO <sub>43</sub>	1543.54343	7.21	335 701

<sup>a</sup> Mycofactocinols (MFT-*n*H<sub>2</sub>) and mycofactocinones (MFT-*n*) represent glycosylated forms of PMFTH<sub>2</sub> and PMFT, respectively. MMFT-*n*: methylmycofactocinones, MMFT-*n*H<sub>2</sub>: methylmycofactocinols (*n*: number of saccharide moieties). Area values represent the mean of 4 biological replicates. All labeled compounds are shown in Data Set 1, all MFT congeners revealed in this study are shown in Data Set 2.



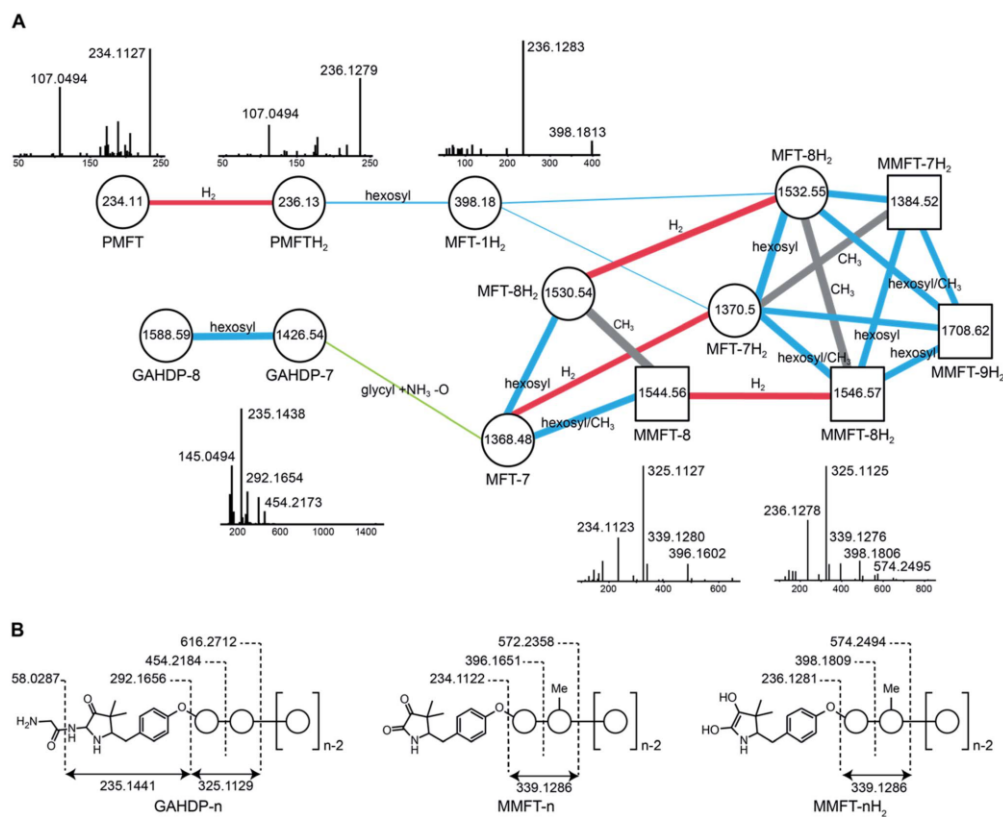


Fig. 2 Discovery and tandem mass spectrometry of MFT congeners. (A) Molecular network of MFT congeners. Nodes (circles) represent chemical compounds. Internal node labels display the precursor mass of compounds ( $m/z$  [ $M + H^+$ ]). External node labels show proposed compound annotations. Edges represent relationships in terms of shared MS/MS fragments. Edge labels show proposed modifications based on precursor mass shifts (blue: hexosylation, red: oxidation/reduction, grey: methylation). Line widths of edges mirror cosine distances. Representative MS/MS spectra of corresponding precursor ions are shown above or below nodes. (B) Schematic representation of mass fragmentation patterns of GAHDP- $n$ , MMFT- $nH_2$  and MMFT- $n$ . Numbers indicate mass-to-charge ratios ( $m/z$ ) of fragments observed. Circles represent hexose moieties. Me: methyl group.

MMFT-2H<sub>2</sub>, accumulated after the enzymatic digest, suggesting that MMFT-2b(H<sub>2</sub>) represents the product of cellulase digestion of MMFT-7/8(H<sub>2</sub>) and shares the identical disaccharide anchor. To further elucidate the structure of MMFT- $nH_2$ , we analyzed enriched fractions of MMFT-2bH<sub>2</sub> and MMFT- $nH_2$  by chemical derivatization and gas chromatography coupled with mass spectrometry (GC-MS). Monosaccharides were released by acid hydrolysis and derivatized by trimethylsilylation (TMS). Comparative analysis of peaks arising from the MMFT- $nH_2$  and MMFT-2bH<sub>2</sub> fractions and carbohydrate standards confirmed the presence of D-glucose (Fig. S4†) and revealed that the methylated sugar present in MMFT- $n(H_2)$  is 2-O-methyl-D-glucose (Fig. S5†). To confirm the glycosidic linkage positions, the oligosaccharide was permethylated before hydrolysis so that only hydroxyl groups involved in glycosidic bond formation

would be free for silylation.<sup>23</sup> This experiment (Fig. S6†) led to the formation of glucose with 2,3,6-O-methyl-1,4-O-TMS modification confirming the 1,4-glycosidic linkage. Additional modification experiments (methanolysis and permethylation) supported the assignments (Fig. S7–S19†). After repeated cultivation we finally obtained MMFT-7/8H<sub>2</sub> in sufficient amounts to record 1D and 2D-NMR spectra (ESI results and discussion, Fig. S20–S27, Tables S1 and S2†). The <sup>1</sup>H NMR spectrum of MMFT-7/8H<sub>2</sub> exhibited a similar five-membered lactam moiety as present in AHDP, but an isolated methine group was shifted to low-field ( $\delta_{H-3}$  4.28 ppm/ $\delta_{C-3}$  76.16 ppm) compared to AHDP ( $\delta_{H-3}$  3.30 ppm/ $\delta_{C-3}$  61.64 ppm). This indicated the amine group connected to C-3 was replaced by a hydroxyl group. The HMBC correlation between H-1' to C-11 suggested the sugar chain to be attached to the hydroxyl group of the tyrosine moiety (Fig. 3B). The  $\beta$ -1,4-glycosidic linkage was





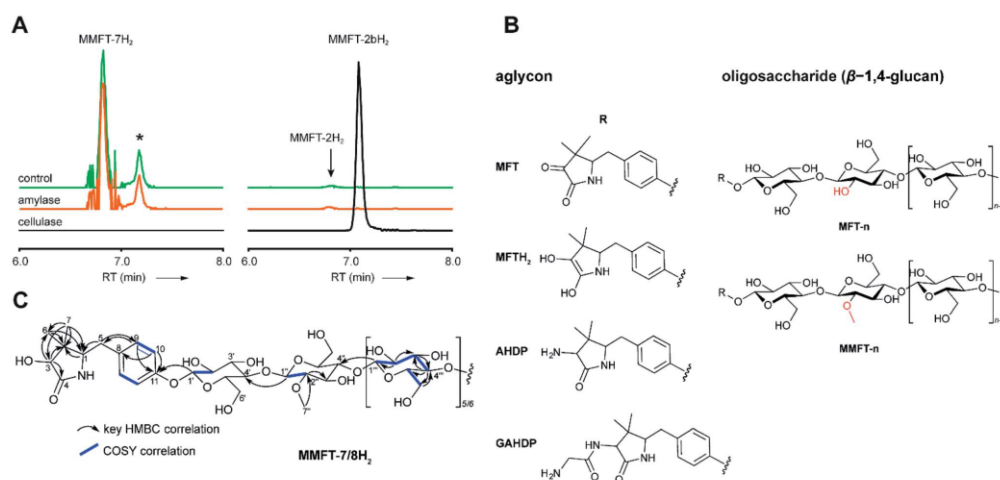


Fig. 3 Structure of mycofactocins. (A) Enzymatic degradation of MMFT-*n* by cellulase. Extracted ion chromatograms (XIC, IM + H<sup>+</sup>) of extract of *M. smegmatis* corresponding to MMFT-7H<sub>2</sub> (*m/z* 1383.50626, left stack) and MMFT-2H<sub>2</sub> or MMFT-2bH<sub>2</sub> (*m/z* 574.24640, right stack) after treatment with cellulase, amylase, or buffer (control) are shown. Asterisk designates a peak corresponding to the M + 2 isotope of MMFT-7. Digestion by cellulase (β-1,4-glycanase) consumes MMFT-*n*H<sub>2</sub> and produces MMFT-2bH<sub>2</sub> suggesting that the oligosaccharide consists of β-1,4-linked glucose. (B) Key COSY and HMBC correlations of MMFT-7/8H<sub>2</sub>. (C) Proposed chemical structures of key mycofactocins and biosynthetic congeners. Mycofactocins are glycosylated by sugar chains consisting of up to nine β-1,4-linked glucose units (*n* ≤ 9). In methylated mycofactocins (MMFT) the second hexose is methylated (2-*O*-methyl-*D*-glucose). The aglycon is PMFT or PMFTH<sub>2</sub> in mycofactocinones or mycofactocinols, respectively. The aglycon is AHDP or GAHDP in biosynthetic precursors AHDP-*n* and GAHDP-*n*, respectively.

confirmed by the HMBC correlations of H-1'' to C-4' and H-1''' to C-4'' and the configuration of the glucose moiety was assigned as β-form by the large coupling constant of anomeric protons ( $J_{H-1'-H-2'} = 8.0$  Hz;  $J_{H-1''-H-2''} = 8.0$  Hz;  $J_{H-1'''-H-2'''} = 8.0$  Hz). The position of the methylated glucose was determined by the observation of a methoxy moiety ( $\delta_{H-7''} = 3.64$  ppm/ $\delta_{C-7''} = 60.55$  ppm) and HMBC correlation of H-7'' to C-2''. The planar structure of MMFT-7/8H<sub>2</sub> is presented in Fig. 3C.

In summary, we propose that the oligosaccharide moiety of MFT is a β-1,4-glucane (cellulose). The methylated hexose present in MMFT-*n*(H<sub>2</sub>) and MMFT-2b(H<sub>2</sub>) was shown to be 2-*O*-methylglucose. The fact that MMFT-2 and MMFT-2b (digested MMFT-*n*) are distinct in retention times points to some degree of structural diversity within MMFTs. Notably, cellulose was shown to be produced by *M. tuberculosis* as a constituent of biofilms after exposure to reductive stress.<sup>24</sup> The production of methylated glucans, like 6-*O*-methylglucose lipopolysaccharides (MGPL), albeit with α-1,4 linkage, is well described in *Mycobacteria*, 2-*O*-methylglucose appears to be less common.<sup>25</sup> Glycosylation is a relatively uncommon modification of cofactors. The most important examples are mycothiol<sup>4</sup> and bacillithiol.<sup>26</sup>

#### Glycine-derived intermediates of MFT biosynthesis

Surprisingly, the MS/MS network (Fig. 2A) revealed two additional compounds (*m/z* 1426.54 and 1588.59) with an unusual mass shift compared to the MFT-*n*(H<sub>2</sub>) candidates. Their mass differences and MS/MS spectra indicated that they represented hepta- and octaglycosylated species sharing a head moiety closely related to

PMFT and PMFT(H<sub>2</sub>). The molecular masses and MS/MS spectra of the compounds could be explained by the assumption that the aglycon corresponded to glycy-AHDP (GAHDP) and these compounds represented the oligoglycosylated forms GAHDP-7 and GAHDP-8. Since the VY core peptide of MftA is preceded by a glycine residue at its N-terminal side it appeared highly likely that the GAHDP-*n* species corresponded to premature cleavage products of the MftC-processed precursor peptide. To corroborate this hypothesis, we fed *M. smegmatis* cultures with a combination of fully <sup>13</sup>C-labeled Gly-<sup>13</sup>C<sub>2</sub>, Val-<sup>13</sup>C<sub>5</sub>, and Tyr-<sup>13</sup>C<sub>9</sub>. Indeed, GAHDP-derived molecules underwent a mass shift of +15.05033 Da, indicating the incorporation of Gly-<sup>13</sup>C<sub>2</sub> (+2.00671 Da) in addition to the decarboxylated Val-Tyr moiety (+13.04362 Da) (Fig. S28†). Targeted searches for GAHDP-*n* as well as AHDP-*n* (lacking the glycy residue) and MAHDP-*n* candidates (AHDP decorated with monomethylated oligosaccharide) revealed three series of oligoglycosylated compounds with similar retention times within each series (Fig. 4, Data Set 2†).

#### Dissection of MFT biosynthesis

In order to test if all MFT candidate compounds were related to MFT biosynthesis, we investigated mutants ( $\Delta$ mftC,  $\Delta$ mftD,  $\Delta$ mftE,  $\Delta$ mftF) created previously<sup>12</sup> of the MFT biosynthesis pathway for the production of candidate molecules (Fig. 4A, Data Set 2†). Indeed, none of the aglycons, nor any of the glycosylated candidates were detected in the  $\Delta$ mftC strain (Fig. 4B). This finding, together with the fact that the genetically complemented strain  $\Delta$ mftC-Comp restored production of MFT



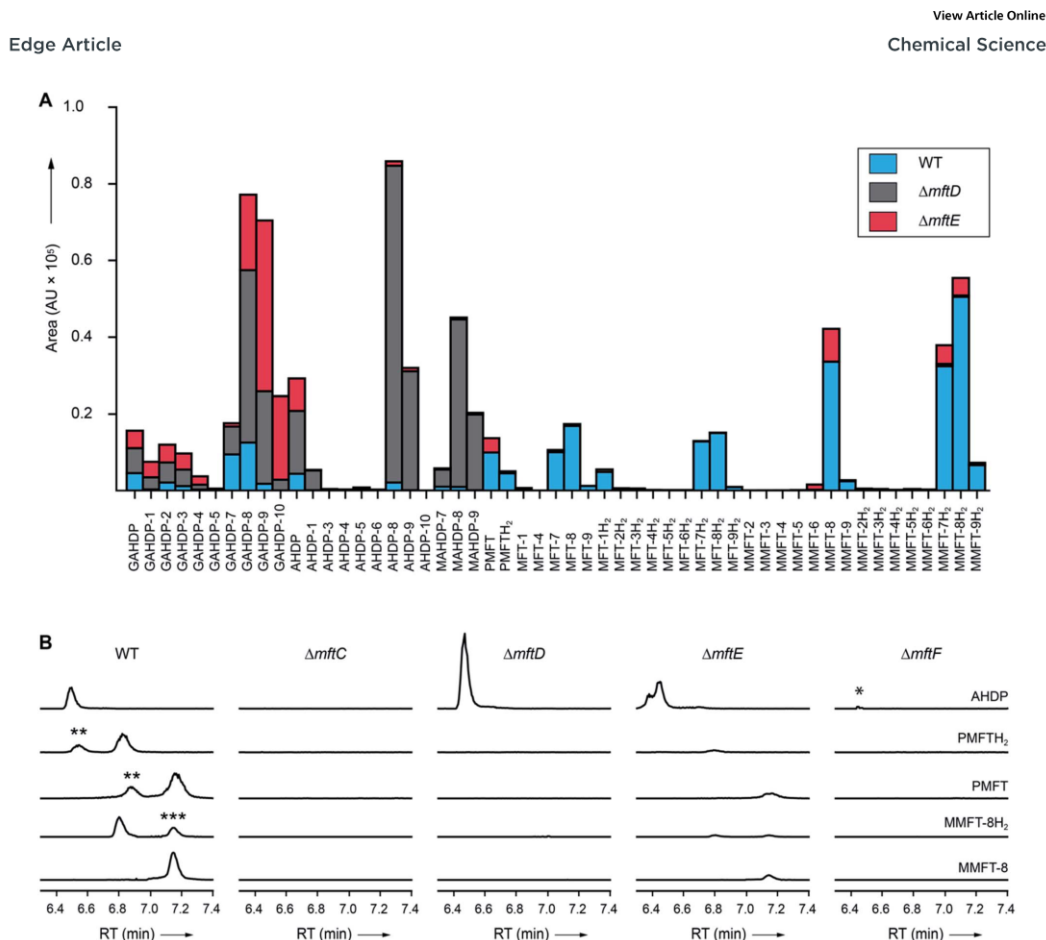


**Fig. 4** Metabolic profile of MFT congeners present in *M. smegmatis*. (A) Distribution of proposed MFT congeners as determined by LC-MS (Data Set 2†). Bars indicate area under the curve of designated species (average of three biological replicates,  $n = 3$ ). Blue: WT, red:  $\Delta mftE$ , gray:  $\Delta mftD$ . The  $\Delta mftE$  mutant produces significantly reduced amounts of MFT congeners compared to WT, but accumulates incorrectly cleaved products (GAHDP- $n$  series).  $\Delta mftD$  is unable to produce PMFT( $H_2$ ) and glycosylated (M)MFT- $n$ ( $H_2$ ), thus accumulating AHDP- $n$  congeners. (B) Extracted ion chromatograms (XIC,  $[M + H]^+$ ) of WT and mutants ( $\Delta mftC$ ,  $\Delta mftD$ ,  $\Delta mftE$ ,  $\Delta mftF$ ) corresponding to AHDP ( $m/z$  235.14411), PMFT ( $m/z$  234.11247), PMFTH $_2$  ( $m/z$  236.12812), MMFT-8 ( $m/z$  1544.55072) and MMFT-8H $_2$  ( $m/z$  1546.56637). \*\*marks minor isomeric forms (Fig. S2†). \*\*\*marks a peak corresponding to the  $M + 2$  isotope of MMFT-8.  $\Delta mftC$  is blocked in biosynthesis of all MFT intermediates,  $\Delta mftF$  abolishes most of the MFT products, but forms trace amounts of AHDP (\*).  $\Delta mftE$  produces most MFT species in lower amounts, while intermediates like AHDP are increasing.  $\Delta mftD$  strongly accumulates AHDP, while MFT congeners are abolished.

congeners (Data Set 2†) represented strong evidence that we indeed identified *bona-fide* MFT-derivatives.

The  $\Delta mftE$  mutant was able to produce mycofactocins, albeit in significantly lower amounts, explaining the previously unexpected phenotypic observation that the  $\Delta mftE$  mutant was able to grow on ethanol, but slower than WT.<sup>12</sup> Intriguingly, the pool of GAHDP- $n$  was strongly increased in the  $\Delta mftE$  strain (Fig. 4A). We thus conclude that MftE can be complemented by an unknown peptidase present in the metabolic background of mycobacteria. Theoretically, an aminopeptidase would be sufficient to degrade the N-terminus of MftA, releasing the AHDP-like core. Peptidases

encoded outside the biosynthetic gene cluster have been observed in other RiPP biosyntheses as well.<sup>27</sup>

However, the removal of the glycine residue might be an apparent bottleneck of the alternative maturation pathway in *M. smegmatis*. Alternatively, GAHDPs could represent shunt products that cannot be further processed. In full agreement with the *in vitro* finding that MftD consumes AHDP to form PMFTH $_2$ ,<sup>21</sup> all metabolites downstream of (M)AHDP- $n$  were abrogated in the  $\Delta mftD$  strain, whereas AHDP- $n$  and GAHDP- $n$  accumulated (Fig. 4). The fact that GAHDP- $n$  increased might suggest that the MftE step is impeded in the absence of MftD as



Chemical Science

View Article Online

Edge Article

well. Genetic dysregulation or cooperative effects between the two enzymes, like complex formation and substrate channeling, might account for this result.

#### Glycosylation of MFT is mediated by MftF

It has been speculated that the putative glycosyltransferase MftF catalyzes a final glycosylation of PMFT (Fig. 1C) to yield the mature cofactor.<sup>21</sup> Our results at this point showed that multiple glucose residues are indeed attached to the aglycon *in vivo*. However, glycosylation appeared already at an early stage as mirrored by the presence of the glycosylated (G)AHDP-*n* series. In order to link oligoglycosylation to a given gene product, we analyzed the  $\Delta mftF$  mutant for the production of glycosylated MFT congeners. Indeed, all glycosylated MFT congeners were abolished in the  $\Delta mftF$  metabolome. Unexpectedly,  $\Delta mftF$  mutants additionally ceased to produce the aglycons PMFT and PMFTH<sub>2</sub>. MftF did, however, produce trace amounts of AHDP, thus showing that at least residual MftC activity was present in the mutant (Fig. 4B). To exclude polar effects, we complemented  $\Delta mftF$  by re-introduction of the *mftF* gene under control of the *mftA* promoter. The restoration of the full MFT metabolite spectrum (Data Set 2†) excluded polar effects and thus verified that MftF was the glycosyltransferase responsible for oligoglycosylation of MFT congeners. The appearance of glycosylated (G)AHDP species in WT together with the drastic decrease of aglycons in  $\Delta mftF$  can be interpreted in a scenario where either glycosylation or the MftF protein itself are essential for the MftD step to efficiently take place *in vivo*. If missing, the biosynthetic machinery may fail to assemble a functional complex or may be unable to recruit the unglycosylated metabolic precursors. The finding that the *mftF* gene is a conserved constituent of MFT biosynthetic loci among different phyla supports the importance of this modification.<sup>11</sup>

The deduced MftF protein of *M. smegmatis* (MSMEG\_1426) consists of 470 amino acids (aa) and belongs to the glycosyltransferase 2 family (GT2) according to PFAM (PF00535) and CAZY searches. These enzymes are known for an inverting mechanism of oligoglycoside formation. This is well in agreement with the proposed  $\beta$ -configuration of the MFT oligosaccharide chain. Sequence alignment (Fig. S29A†) showed a high degree of sequence conservation among mycobacterial species and other actinomycetes (*e.g.*, 92% similarity to MftF of *M. tuberculosis* H37Rv). Prediction of transmembrane domains revealed a single helix spanning residues 324–346 with the N-terminus being located outside of the membrane (Fig. S29B†). The MMFT biosynthetic machinery, however, appears not to be fully encompassed within the MFT cluster since no methyltransferase was found. Future studies are warranted to identify the enzymes involved in MFT oligosaccharide methylation.

#### Cofactor role of mycofactocin

After discovery of the glycosylated mycofactocins, we examined to which extent their production was actually dependent on the presence of ethanol in culture media. We therefore systematically compared the metabolome of *M. smegmatis* WT after ethanol treatment with glucose controls (Data Set 3†).

The results demonstrated that all MFT congeners or intermediates were strongly upregulated upon cultivation on ethanol (median: 34-fold upregulation) (Fig. 5A). These data perfectly support a recent report that MFT is involved in alcohol metabolism.<sup>12</sup>

Finally, we sought to confirm that the MFT congeners identified in this study are indeed coenzymes of MFT-dependent enzymes. To assess this question, we turned to activity-based metabolic profiling.<sup>28</sup> We incubated the extracted metabolome of *M. smegmatis* with the recombinant *L*-carveol dehydrogenase LimC (CAB54559.1) from *Rhodococcus erythropolis* (Fig. S30†), a nicotinoprotein with a non-exchangeable NADH cofactor.<sup>29</sup> This enzyme was proposed to require MFT as an external electron acceptor.<sup>11</sup> A recent study showed that carveol dehydrogenase from *M. smegmatis* was able to reduce PMFT to PMFTH<sub>2</sub> using carveol and internally bound NADH as an electron donor.<sup>21</sup> Likewise, we observed full reduction of all mycofactocinones to mycofactocinols (Fig. 5B, Data Set 4†) by LimC when combined with carveol as a substrate. Controls lacking enzyme or substrate showed weak and no turnover, respectively. The low turnover by LimC alone can be explained by internally bound NADH as reported

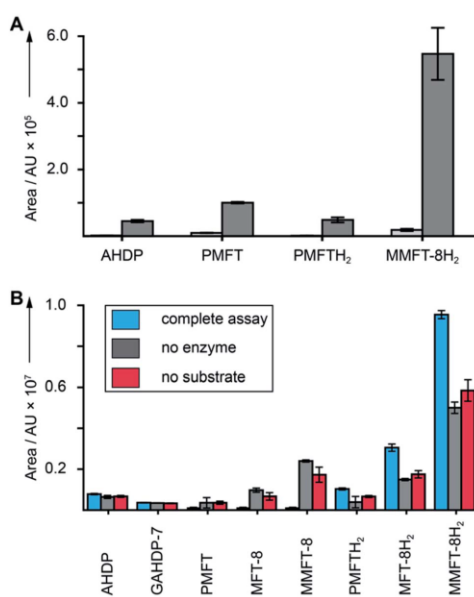


Fig. 5 Cofactor role of mycofactocin. (A) MFT congeners are strongly upregulated (MMFT-8H<sub>2</sub>: 26-fold) on ethanol-containing media. Area under the curve of MFT species produced by *M. smegmatis* treated with ethanol (dark gray) versus glucose controls (light gray) are shown (Data Set 3†). (B) Reduction of mycofactocinones to mycofactocinols by treatment of extracts with LimC and carveol. Blue: complete assay with enzyme and *L*-carveol as substrate. Red: control without substrate, gray: control without enzyme. Bars represent average area under the curve, error bars standard deviation of 3 biological replicates ( $n = 3$ ) for in both charts.





View Article Online

Chemical Science

Edge Article

before.<sup>21</sup> Both the aglycon PMFT as well as the oligoglycosylated MFT-*n* and MMFT-*n* species were completely turned over, while redox-inactive AHDP congeners remained unaffected. These data further validate the notion that all MFT candidates presented here are mycofactocins with full cofactor function. It remains to be clarified if there is a preference for the glycosylated coenzymes or their aglycons in the bacterial cell.

## Conclusion

The redox cofactor mycofactocin has attracted considerable interest since it was postulated by bioinformatics. Despite recent progress made by *in vitro* studies, evidence for mycofactocin congeners in living microorganisms has been missing so far. Our integrated metabolomics approach combining stable isotope labeling, metabolite induction, MS/MS networking as well as genetic dissection of the biosynthetic pathway turned out to be a powerful approach to identify RiPP congeners in bacteria and could inspire similar projects in the future. Using this technique, we discovered natural MFT and found that it is decorated with oligosaccharides consisting of up to nine  $\beta$ -1,4-linked glucose units. Analyses of  $\Delta$ mftF mutants and complement strains revealed that MftF is the glycosyltransferase responsible for the oligoglycosylation observed. Mycofactocins can be isolated in oxidized (mycofactocinones) and reduced forms (mycofactocinols) and are co-substrates of enzymatic reduction by carveol dehydrogenase. These data provide strong evidence that mycofactocins are indeed redox cofactors as proposed earlier.<sup>11,12,21</sup> We, therefore, conclude that we have finally discovered the family of compounds that was tentatively called “mycofactocin” and thus close an important gap of knowledge in the field. Our results will guide further studies into the occurrence, physiological role, and biochemistry of mycofactocins in microorganisms. Finally, these and other studies will inspire future efforts to exploit mycofactocin, e.g., as a disease marker or as a potential drug target for the treatment mycobacterial infections.

## Conflicts of interest

There are no conflicts to declare.

## Acknowledgements

We would like to thank the Carl-Zeiss Foundation and the Leibniz Association as well as the European Regional Development Fund for financial support. CB was kindly supported by the CRC ChemBioSys 1127 (Deutsche Forschungsgemeinschaft). We thank Stefan Kaufmann and Gopinath Krishnamoorthy for kindly providing *M. smegmatis* mutants. We also thank Heike Heinecke for NMR measurements.

## Notes and references

1 J. P. Klinman and F. Bonnot, *Chem. Rev.*, 2014, **114**, 4343–4365.

- C. Greening, F. H. Ahmed, A. E. Mohamed, B. M. Lee, G. Pandey, A. C. Warden, C. Scott, J. G. Oakeshott, M. C. Taylor and C. J. Jackson, *Microbiol. Mol. Biol. Rev.*, 2016, **80**, 451–493.
- N. A. Buchmeier, G. L. Newton, T. Koledin and R. C. Fahey, *Mol. Microbiol.*, 2003, **47**, 1723–1732.
- G. L. Newton, N. Buchmeier and R. C. Fahey, *Microbiol. Mol. Biol. Rev.*, 2008, **72**, 471–494.
- V. Saini, B. M. Cumming, L. Guidry, D. A. Lamprecht, J. H. Adamson, V. P. Reddy, K. C. Chinta, J. H. Mazorodze, J. N. Glasgow, M. Richard-Greenblatt, A. Gomez-Velasco, H. Bach, Y. Av-Gay, H. Eoh, K. Rhee and A. J. C. Steyn, *Cell Rep.*, 2016, **14**, 572–585.
- E. Purwantini and B. Mukhopadhyay, *PLoS One*, 2013, **8**, e81985.
- E. Purwantini and B. Mukhopadhyay, *Proc. Natl. Acad. Sci. U. S. A.*, 2009, **106**, 6333–6338.
- C. K. Stover, P. Warrener, D. R. VanDevanter, D. R. Sherman, T. M. Arain, M. H. Langhorne, S. W. Anderson, J. A. Towell, Y. Yuan, D. N. McMurray, B. N. Kreiswirth, C. E. Barry and W. R. Baker, *Nature*, 2000, **405**, 962–966.
- R. Singh, U. Manjunatha, H. I. Boshoff, Y. H. Ha, P. Niyomrattanakit, R. Ledwidge, C. S. Dowd, I. Y. Lee, P. Kim, L. Zhang, S. Kang, T. H. Keller, J. Jiricek and C. E. Barry III, *Science*, 2008, **322**, 1392–1395.
- R. Ayikpoe, V. Govindarajan and J. A. Latham, *Appl. Microbiol. Biotechnol.*, 2019, **103**, 2903–2912.
- D. H. Haft, *BMC Genomics*, 2011, **12**, 21.
- G. Krishnamoorthy, P. Kaiser, L. Lozza, K. Hahnke, H. J. Mollenkopf and S. H. E. Kaufmann, *mBio*, 2019, **10**, e00190-19.
- A. A. Dubey and V. Jain, *Biochem. Biophys. Res. Commun.*, 2019, **516**, 1073–1077.
- P. G. Arnison, M. J. Bibb, G. Bierbaum, A. A. Bowers, T. S. Bugni, G. Bulaj, J. A. Camarero, D. J. Campopiano, G. L. Challis, J. Clardy, P. D. Cotter, D. J. Craik, M. Dawson, E. Dittmann, S. Donadio, P. C. Dorrestein, K. D. Entian, M. A. Fischbach, J. S. Garavelli, U. Goransson, C. W. Gruber, D. H. Haft, T. K. Hemscheidt, C. Hertweck, C. Hill, A. R. Horswill, M. Jaspars, W. L. Kelly, J. P. Klinman, O. P. Kuipers, A. J. Link, W. Liu, M. A. Marahiel, D. A. Mitchell, G. N. Moll, B. S. Moore, R. Muller, S. K. Nair, I. F. Nes, G. E. Norris, B. M. Olivera, H. Onaka, M. L. Patchett, J. Piel, M. J. Reaney, S. Rebuffat, R. P. Ross, H. G. Sahl, E. W. Schmidt, M. E. Selsted, K. Severinov, B. Shen, K. Sivonen, L. Smith, T. Stein, R. D. Sussmuth, J. R. Tagg, G. L. Tang, A. W. Truman, J. C. Vederas, C. T. Walsh, J. D. Walton, S. C. Wenzel, J. M. Willey and W. A. van der Donk, *Nat. Prod. Rep.*, 2013, **30**, 108–160.
- N. A. Bruender and V. Bandarian, *Biochemistry*, 2016, **55**, 2813–2816.
- B. Khaliullin, P. Aggarwal, M. Bupas, G. R. Eaton, S. S. Eaton and J. A. Latham, *FEBS Lett.*, 2016, **590**, 2538–2548.
- B. Khaliullin, R. Ayikpoe, M. Tuttle and J. A. Latham, *J. Biol. Chem.*, 2017, **292**, 13022–13033.
- N. A. Bruender and V. Bandarian, *J. Biol. Chem.*, 2017, **292**, 4371–4381.



View Article Online

Edge Article

Chemical Science

- 19 R. Ayikpoe, J. Salazar, B. Majestic and J. A. Latham, *Biochemistry*, 2018, **57**, 5379–5383.
- 20 S. Billig, M. Schneefeld, C. Huber, G. A. Grassl, W. Eisenreich and F. C. Bange, *Sci. Rep.*, 2017, **7**, 6484.
- 21 R. S. Ayikpoe and J. A. Latham, *J. Am. Chem. Soc.*, 2019, **141**, 13582–13591.
- 22 M. Wang, J. J. Carver, V. V. Phelan, L. M. Sanchez, N. Garg, Y. Peng, D. D. Nguyen, J. Watrous, C. A. Kapon, T. Luzzatto-Knaan, C. Porto, A. Bouslimani, A. V. Melnik, M. J. Meehan, W. T. Liu, M. Crusemann, P. D. Boudreau, E. Esquenazi, M. Sandoval-Calderon, R. D. Kersten, L. A. Pace, R. A. Quinn, K. R. Duncan, C. C. Hsu, D. J. Floros, R. G. Gavilan, K. Kleigrewe, T. Northen, R. J. Dutton, D. Parrot, E. E. Carlson, B. Aigle, C. F. Michelsen, L. Jelsbak, C. Sohlenkamp, P. Pevzner, A. Edlund, J. McLean, J. Piel, B. T. Murphy, L. Gerwick, C. C. Liaw, Y. L. Yang, H. U. Humpf, M. Maansson, R. A. Keyzers, A. C. Sims, A. R. Johnson, A. M. Sidebottom, B. E. Sedio, A. Klitgaard, C. B. Larson, C. A. Boya P., D. Torres-Mendoza, D. J. Gonzalez, D. B. Silva, L. M. Marques, D. P. Demarque, E. Pociute, E. C. O'Neill, E. Briand, E. J. N. Helfrich, E. A. Granatosky, E. Glukhov, F. Ryffel, H. Houson, H. Mohimani, J. J. Kharbush, Y. Zeng, J. A. Vorholt, K. L. Kurita, P. Charusanti, K. L. McPhail, K. F. Nielsen, L. Vuong, M. Elfeki, M. F. Traxler, N. Engene, N. Koyama, O. B. Vining, R. Baric, R. R. Silva, S. J. Mascuch, S. Tomasi, S. Jenkins, V. Macherla, T. Hoffman, V. Agarwal, P. G. Williams, J. Dai, R. Neupane, J. Gurr, A. M. C. Rodriguez, A. Lamsa, C. Zhang, K. Dorrestein, B. M. Duggan, J. Almaliti, P. M. Allard, P. Phapale, L. F. Nothias, T. Alexandrov, M. Litaudon, J. L. Wolfender, J. E. Kyle, T. O. Metz, T. Peryea, D. T. Nguyen, D. VanLeer, P. Shinn, A. Jadhav, R. Muller, K. M. Waters, W. Shi, X. Liu, L. Zhang, R. Knight, P. R. Jensen, B. O. Palsson, K. Pogliano, R. G. Linington, M. Gutierrez, N. P. Lopes, W. H. Gerwick, B. S. Moore, P. C. Dorrestein and N. Bandeira, *Nat. Biotechnol.*, 2016, **34**, 828–837.
- 23 A. Debettigniesdutz, G. Reznicek, B. Kopp and J. Jurenitsch, *J. Chromatogr.*, 1991, **547**, 299–306.
- 24 A. Trivedi, P. S. Mavi, D. Bhatt and A. Kumar, *Nat. Commun.*, 2016, **7**, 11392.
- 25 G. Stadthagen, T. Sambou, M. Guerin, N. Barilone, F. Boudou, J. Kordulakova, P. Charles, P. M. Alzari, A. Lemassu, M. Daffe, G. Puzo, B. Gicquel, M. Riviere and M. Jackson, *J. Biol. Chem.*, 2007, **282**, 27270–27276.
- 26 G. L. Newton, M. Rawat, J. J. La Clair, V. K. Jothivasan, T. Budiarto, C. J. Hamilton, A. Claiborne, J. D. Helmann and R. C. Fahey, *Nat. Chem. Biol.*, 2009, **5**, 625–627.
- 27 S. Chen, B. Xu, E. Chen, J. Wang, J. Lu, S. Donadio, H. Ge and H. Wang, *Proc. Natl. Acad. Sci. U. S. A.*, 2019, **116**, 2533–2538.
- 28 L. P. de Carvalho, H. Zhao, C. E. Dickinson, N. M. Arango, C. D. Lima, S. M. Fischer, O. Ouerfelli, C. Nathan and K. Y. Rhee, *Chem. Biol.*, 2010, **17**, 323–332.
- 29 M. J. van der Werf, C. van der Ven, F. Barbirato, M. H. Eppink, J. A. de Bont and W. J. van Berkel, *J. Biol. Chem.*, 1999, **274**, 26296–26304.

Open Access Article. Published on 23 April 2020. Downloaded on 8/18/2020 11:07:32 AM.  
This article is licensed under a Creative Commons Attribution 3.0 Unported Licence.





## 8.2. IMPACT OF OXYGEN SUPPLY AND SCALE-UP ON *Mycobacterium smegmatis* CULTIVATION AND MYCOFACTOCIN FORMATION

Peña-Ortiz, Luis; Schlembach, Ivan; Lackner, Gerald; Regestein, Lars.

Frontiers in Bioengineering and Biotechnology (2020),8:593781. DOI:  
10.3389/fbioe.2020.593781

### SUMMARY

Tuberculosis is a recurring threat to public health worldwide. The etiological agent of tuberculosis, *Mycobacterium tuberculosis*, employs cofactor-mediated detoxification mechanisms that enable high-level resistance to commonly used antibiotics. Conversely, some highly effective anti-TB prodrugs require *in vivo* activation by enzymatic mechanisms that require cofactors. Thus, advances in the redox mechanisms of *M. tuberculosis* could pave the way for novel treatments against this deadly disease. Mycofactocin (MFT) is a glycosylated redox cofactor belonging to the ribosomally-produced and post-translationally modified peptides (RiPPs) family of natural products. Further characterization of the cofactor for the structural, enzymatic, and biological role would require higher yields, which we could not achieve by conventional shake flask cultivations. We cultured the non-pathogenic strain *M. smegmatis* mc<sup>2</sup> 155 and modeled different oxygen availability conditions in shake flask cultures and scale-up fermenters. Higher titers of MFT were produced under oxygen-limiting conditions in both complex and mineral media. We found that the level of oxygen supply modulates the yield of MFT and the length of the glycosidic chain. These results allow for reproducible, high yield MFT production and enable further investigations into the biochemical function and physiological role of MFT.

CONTRIBUTION TO THE MANUSCRIPT

Luis A. Peña Ortiz contributed to the manuscript by performing mycobacterial cultivation and sampling, MFT and metabolite extraction, LC-MS measurements, data analysis, and figure production. He was also involved in the preparation and editing of the manuscript.

ESTIMATED CONTRIBUTION IN PERCENTAGE

Luis A. Peña Ortiz	40
Ivan Schlembach	15
Gerald Lackner	15
Lars Regestein	30

---

Luis Alberto Peña Ortiz

---

Prof. Dr. Christian Hertweck



# Impact of Oxygen Supply and Scale Up on *Mycobacterium smegmatis* Cultivation and Mycofactocin Formation

Luis Peña-Ortiz<sup>1</sup>, Ivan Schlembach<sup>2,3</sup>, Gerald Lackner<sup>1</sup> and Lars Regestein<sup>2\*</sup>

<sup>1</sup> Junior Research Group Synthetic Microbiology, Leibniz Institute for Natural Product Research and Infection Biology (HKI), Jena, Germany, <sup>2</sup> Bio Pilot Plant, Leibniz Institute for Natural Product Research and Infection Biology (HKI), Jena, Germany, <sup>3</sup> Faculty of Biological Sciences, Friedrich-Schiller-University, Jena, Germany

## OPEN ACCESS

### Edited by:

Maizirwan Mel,  
International Islamic University  
Malaysia, Malaysia

### Reviewed by:

Mohd Azmir Arifin,  
Universiti Malaysia Pahang, Malaysia  
Johannes Felix Buyel,  
Fraunhofer Society (FHG), Germany

### \*Correspondence:

Lars Regestein  
lars.regestein@leibniz-hki.de;  
lars.regestein@hki-jena.de

### Specialty section:

This article was submitted to  
Bioprocess Engineering,  
a section of the journal  
Frontiers in Bioengineering and  
Biotechnology

Received: 11 August 2020

Accepted: 16 November 2020

Published: 03 December 2020

### Citation:

Peña-Ortiz L, Schlembach I,  
Lackner G and Regestein L (2020)  
Impact of Oxygen Supply and Scale  
Up on *Mycobacterium smegmatis*  
Cultivation and Mycofactocin  
Formation.  
Front. Bioeng. Biotechnol. 8:593781.  
doi: 10.3389/fbioe.2020.593781

Mycofactocin (MFT) is a recently discovered glycosylated redox cofactor, which has been associated with the detoxification of antibiotics in pathogenic mycobacteria, and, therefore, of potential medical interest. The MFT biosynthetic gene cluster is commonly found in mycobacteria, including *Mycobacterium tuberculosis*, the causative agent of tuberculosis. Since the MFT molecule is highly interesting for basic research and could even serve as a potential drug target, large-scale production of the molecule is highly desired. However, conventional shake flask cultivations failed to produce enough MFT for further biochemical characterization like kinetic studies and structure elucidation, and a more comprehensive study of cultivation parameters is urgently needed. Being a redox cofactor, it can be hypothesized that the oxygen transfer rate (OTR) is a critical parameter for MFT formation. Using the non-pathogenic strain *Mycobacterium smegmatis* mc<sup>2</sup> 155, shake flask experiments with online measurement of the oxygen uptake and the carbon dioxide formation, were conducted under different levels of oxygen supply. Using liquid chromatography and high-resolution mass spectrometry, a 4–8 times increase of MFT production was identified under oxygen-limited conditions, in both complex and mineral medium. Moreover, the level of oxygen supply modulates not only the overall MFT formation but also the length of the glycosidic chain. Finally, all results were scaled up into a 7 L stirred tank reactor to elucidate the kinetics of MFT formation. Ultimately, this study enables the production of high amounts of these redox cofactors, to perform further investigations into the role and importance of MFTs.

**Keywords:** mycofactocin, redox cofactor, *Mycobacterium smegmatis*, oxygen limitation, glycosylation, ribosomally synthesized and post-translationally modified peptide, tuberculosis

**Abbreviations:** AGC, Automatic gain control; CTR, Carbon dioxide transfer rate; DOT, Dissolved oxygen tension; LB, Lysogeny Broth; LC-MS, Liquid chromatography–mass spectrometry; MFT, Mycofactocin; MMFT-2b, Methylmycofactocin containing 2 glucose moieties (oxidized); MMFT-2bH<sub>2</sub>, Methylmycofactocin containing 2 glucose moieties (reduced); MMFT-2b(H<sub>2</sub>), Methylmycofactocin containing 2 glucose moieties (reduced and oxidized); MMFT-8, Methylmycofactocin containing 8 glucose moieties (oxidized); MMFT-8H<sub>2</sub>, Methylmycofactocin containing 8 glucose moieties (reduced); MMFT-8(H<sub>2</sub>), Methylmycofactocin containing 8 glucose moieties (reduced and oxidized); OTR, Oxygen transfer rate; PMFT, Premycofactocinone (oxidized); PMFTH<sub>2</sub>, Premycofactocinol (reduced); PMFT(H<sub>2</sub>), Premycofactocin (reduced and oxidized); RQ, Respiratory quotient; STR, Stirred tank reactor;  $\dot{V}_G$ , Gas flow rate [L h<sup>-1</sup>];  $V_L$ , Filling volume of shake flask or STR [L];  $V_{norm}$ , Molar volume of an ideal gas [mol L<sup>-1</sup>];  $y_{CO_2,in}$ , Molar fraction of carbon dioxide in the gas inlet;  $y_{CO_2,out}$ , Molar fraction of carbon dioxide in the off gas;  $y_{O_2,in}$ , Molar fraction of oxygen in the gas inlet;  $y_{O_2,out}$ , Molar fraction of oxygen in the off gas.

# Impact of Oxygen Supply and Scale-Up on *Mycobacterium smegmatis* Cultivation and Mycofactocin Formation

Peña-Ortiz et al.

Mycofactocin Formation

## INTRODUCTION

The genus *Mycobacterium* comprises the highly important etiological agents for human tuberculosis (*Mycobacterium tuberculosis*), bovine tuberculosis (*M. bovis*), and leprosy (*M. leprae*) (Gupta et al., 2018; Parte, 2018). Tuberculosis (TB) is a pulmonary disease, especially relevant for developing countries where multidrug-resistant (MDR-TB) and extensively drug-resistant (XDR-TB) strains are a burden for their development (WHO, 2019). This latter classification is related to the resistance against first-, and second-line antibiotic treatments. Insufficient compliance with the long and cumbersome treatments required facilitates the development of resistance (Nguyen, 2016). *In vitro* studies on TB pathogenesis, mycobacterial physiology, as well as the development of novel treatments, are complicated by the high level of biosafety and the low duplication rate of the pathogen, requiring up to 4 weeks to develop visible colonies on agar plates. For this reason, the non-pathogenic strain *Mycobacterium smegmatis* mc<sup>2</sup> 155 (synonym *Mycobacterium smegmatis*) can be a suitable model (Reyrat and Kahn, 2001; Shiloh and Champion, 2010; Yamada et al., 2018).

Mycobacteria involve unusual redox cofactors for the activation or inactivation of some antibiotics. For instance, the reducing agent mycothiol mediates the degradation of antibiotics like rifampicin and isoniazid, whereas Coenzyme F<sub>420</sub> is involved in the activation of pretomanid (Stover et al., 2000; Rawat et al., 2002; Buchmeier et al., 2003; Singh et al., 2008; Hernick, 2013; Haver et al., 2015). Hence, such compounds arise of medical interest as appealing targets for anti-TB treatments. Therefore, novel redox cofactors present in mycobacteria could open the door to interesting physiological discoveries or even serve as targets for drug development. Mycofactocin (MFT) is a recently identified cofactor, biosynthesized as a ribosomally-produced and post-translationally modified peptide (RiPP) (Ayikpoe et al., 2019; Peña-Ortiz et al., 2020). The discovery of MFT started with the observation that its biosynthetic gene cluster was reminiscent of another bacterial redox cofactor, pyrroloquinoline quinone, and was genomically associated with certain subfamilies of oxidoreductases (Haft, 2011). The MFT locus was found in all species of the genus *Mycobacterium*, is widespread in related Actinobacteria like *Rhodococcus*, but sparsely present in Chloroflexi, Firmicutes, Proteobacteria, and some archaeal species (Haft, 2011; Ayikpoe et al., 2019).

*In vivo* evidence for MFT serving as a cofactor in the conversion of primary alcohols as sole carbon source into aldehydes for further incorporation into the central carbon metabolism has been found (Figure 1A; Dubey and Jain, 2019; Krishnamoorthy et al., 2019). The cofactor would require regeneration to fulfill this role, which can be accomplished by coupling to additional electron acceptors. Typically, in aerobic organisms, oxygen serves as the final electron acceptor. The enzymes and cofactors mediating MFT regeneration are unknown at present. Pioneering *in vitro* studies described the initial steps of MFT biosynthesis until the formation of a redox-active molecule termed premycofactocin (PMFT) (Bruender and Bandarian, 2016, 2017; Khaliullin et al., 2016, 2017; Ayikpoe et al., 2018; Ayikpoe and Latham, 2019). Recently we reported

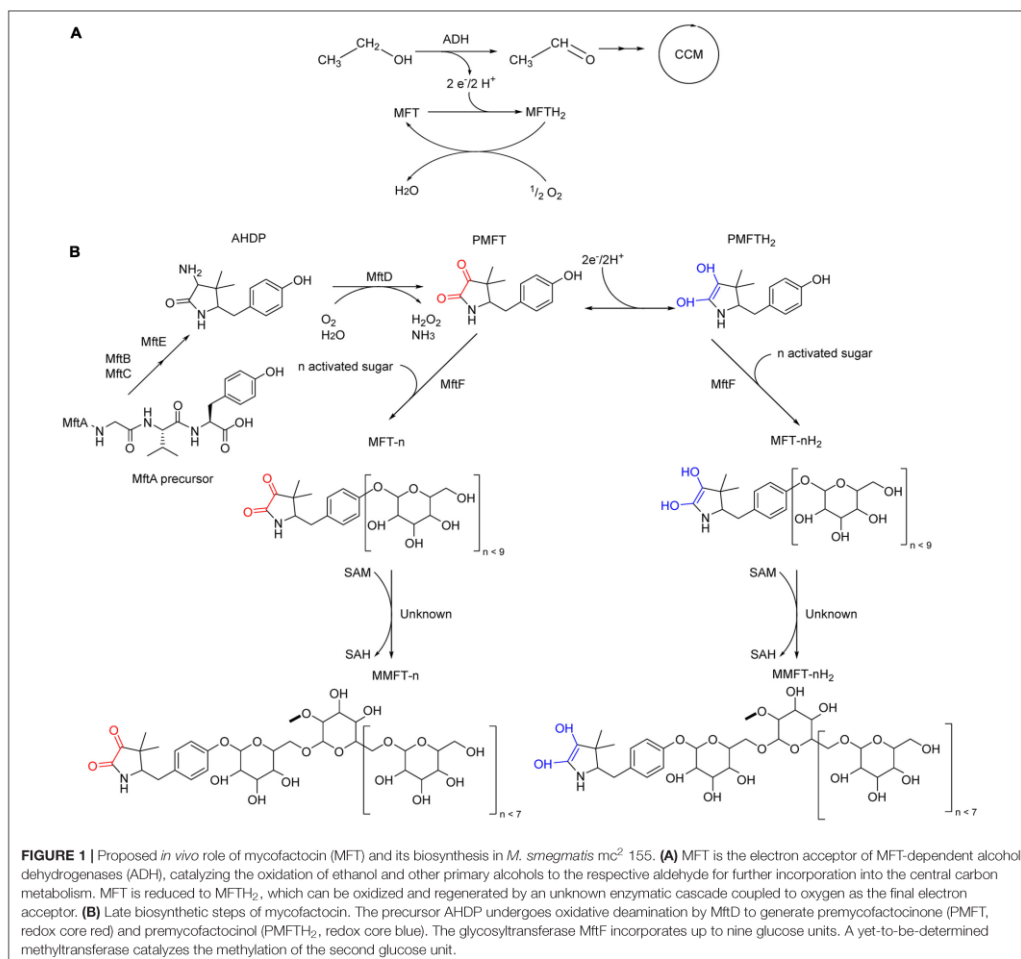
on the discovery of mature MFT *in vivo* (Figure 1B) and showed that PMFT and PMFTH<sub>2</sub> are glycosylated with up to nine glucose residues linked by a β-1,4 glycosidic bond. Species with eight residues are the most abundant ones. This decoration is mediated by the glycosyltransferase MftF with activated glucose as the glycosyl donor. To discriminate against the different congeners, the length of the oligoglycoside chain is indicated by the letter n as in MFT-n. For instance, MFT-8 is decorated with eight glucose units. As a redox cofactor, MFT also exists as oxidized and reduced forms. While MFT-n stands for oxidized mycofactocinones, MFT-nH<sub>2</sub> is used for the corresponding reduced mycofactocinols. To report the sum of oxidized and reduced forms together, the optional hydrogen H<sub>2</sub> is put in parenthesis, e.g., MFT-8(H<sub>2</sub>). In a previous study, we showed that the second glucose unit exists as 2-O-methylglucose (methylmycofactocin, MMFT). MMFT is generally more abundant than non-methylated MFT in *M. smegmatis*. The enzyme responsible for this methylation is not comprised in the MFT gene cluster and is still unknown (Peña-Ortiz et al., 2020), however, it is possible that this modification is catalyzed by a S-adenosyl-L-methionine (SAM)-dependent methyltransferase, with S-adenosyl-L-homocysteine (SAH) as product. We also detected early products from minor reactions, namely glycosylated AHDP (ADHP-n), methyl glycosylated AHDP (MAHDP-n), and glycol-containing AHDP (GAHDP). Lastly, we observed strong upregulation of all MFT species during the cultivation of ethanol as carbon source. Both findings are strong support for the hypothesis that MFTs act as a quinone-like hydrogen carrier during ethanol utilization. Further studies on mycofactocins, like enzyme kinetics or crystallization in complex with mycofactocin-dependent oxidoreductases, would require at least milligrams of the pure cofactor (Peña-Ortiz et al., 2020). Chemical synthesis would be a suitable alternative for premycofactocin production, however, synthesis of its glycosylated versions could be hampered by stereoselectivity at the coupling step and the very finely tuned protection and deprotection required (Palcic, 1999; Williams and Galan, 2017).

For the structure elucidation by nuclear magnetic resonance (NMR), preliminary experiments were conducted to produce methylmycofactocins with eight glucose residues, abbreviated as MMFT-8(H<sub>2</sub>) (Peña-Ortiz et al., 2020). However, the generated amounts of all MFTs were too low to enable experiments beyond the structural elucidation. Therefore, systematic development of the bioprocess for a scalable production was essential. *Mycobacterium* strains are considered strict aerobic or microaerophilic (Moore and James, 1982; Dick et al., 1998; Realini et al., 1998; Lewis and Falkinham, 2015), and the few biotechnological processes available do indicate the importance of oxygen transfer rates (OTRs) in the final product (Hauschild et al., 1994; Lo et al., 2002). Being a redox cofactor involved in aerobic pathways it was reasonable to assume that oxygen availability could have a direct impact on MFT production (Clark and Bushell, 1995; Barberel and Walker, 2000; Gamboa-Suasnavart et al., 2018). In this article, the impact of oxygen supply on production dynamics of MFT from *M. smegmatis* mc<sup>2</sup> 155 is characterized as well as the

# Impact of Oxygen Supply and Scale-Up on *Mycobacterium smegmatis* Cultivation and Mycofactocin Formation

Peña-Ortiz et al.

Mycofactocin Formation



scalability of results from shake flask experiments into stirred tank reactors (STR).

## MATERIALS AND METHODS

### Microbial Strains and Culture Media

*M. smegmatis* was obtained from the Kaufmann laboratory at the Max Planck Institute for Infection Biology in Berlin, Germany. LB complex medium (10 g L<sup>-1</sup> tryptone, 5 g L<sup>-1</sup> yeast extract, 10 g L<sup>-1</sup> NaCl) and Hartman de Bont (Hartmans et al., 1992) mineral medium [2 g L<sup>-1</sup> (NH<sub>4</sub>)<sub>2</sub>SO<sub>4</sub>, 0.1 g L<sup>-1</sup> MgCl<sub>2</sub>·6 H<sub>2</sub>O, 3 g L<sup>-1</sup> Na<sub>2</sub>HPO<sub>4</sub>, 1 g L<sup>-1</sup> KH<sub>2</sub>PO<sub>4</sub>, 10 mL L<sup>-1</sup>] trace

element solution (100 mg L<sup>-1</sup> EDTA, 20 mg L<sup>-1</sup> ZnSO<sub>4</sub>·7 H<sub>2</sub>O, 10 mg L<sup>-1</sup> CaCl<sub>2</sub>·2 H<sub>2</sub>O, 50 mg L<sup>-1</sup> FeSO<sub>4</sub>·7 H<sub>2</sub>O, 2 mg L<sup>-1</sup> Na<sub>2</sub>MoO<sub>4</sub>·2 H<sub>2</sub>O, 2 mg L<sup>-1</sup> CuSO<sub>4</sub>·5 H<sub>2</sub>O, 4 mg L<sup>-1</sup> CoCl<sub>2</sub>·6 H<sub>2</sub>O, 12 mg L<sup>-1</sup> MnCl<sub>2</sub>·7 H<sub>2</sub>O) were used. In all cases, the production of MFT was stimulated by 10 g L<sup>-1</sup> of ethanol at the beginning of the production culture.

### Shake Flask Cultivation With Transfer-Rate Online Measurement (TOM)

For the cultivation of the first seed culture, a single colony was used to inoculate 25 mL of LB with 0.05% tyloxapol (Sigma

Aldrich), and cultured for 48 h to recover cells in suspension without cell clumps. Then, 25 mL of culture broth was inoculated 24 h at a 10% (v/v) ratio from the first seed. Tyloxapol was not used in the second seed. Both seed cultures were conducted at 37°C and 210 rpm with a shaking diameter of 50 mm.

Afterward, a master mix of LB broth pH 7.3 buffered with 250 mM MOPS was inoculated with 25 mL of second seed culture, 2.5 g of sterile ethanol, and volume was brought up to 250 mL with sterile double-distilled water. For the variation of the OTR and, therefore, the oxygen supply of *M. smegmatis*, four different filling volumes of 10, 20, 30, and 40 mL were chosen in 250 mL non-baffled Erlenmeyer flasks. The maximum filling volume of 40 mL reflects a strongly oxygen-limited condition with a calculated maximum OTR of 12.8 mmol L<sup>-1</sup> h<sup>-1</sup> (Meier et al., 2016). The filling volumes of 30, 20, and 10 mL represent the calculated OTRs of 1, 22, and 37 mmol L<sup>-1</sup> h<sup>-1</sup>, respectively. The lowest filling volume of 10 mL ensures fully oxygen-unlimited conditions. Cultivations were performed in an orbital shaker (TOM<sup>®</sup> Kuhner shaker, Switzerland) with a shaking diameter of 25 mm and 210 rpm at 37°C. Every shake flask was equipped with an online monitoring system for oxygen and carbon dioxide measurement. In-house compressed air was supplied at concentrations of CO<sub>2</sub> and O<sub>2</sub> of 0.04% (v/v) and 20.95% (v/v), respectively. The low flow setpoint of the mass flow controller was 11 mL min<sup>-1</sup>, while the high flow setpoint was 55 mL min<sup>-1</sup>. Osmolarity was set at 0.5 Osmol L<sup>-1</sup>. Measurements were performed in 10 min cycles with 3 min of measuring time and 40 s of high flow time. Cultures were prepared in duplicates, one duplicate was sacrificed for measurements after a sharp drop (= decrease of at least 30% in 30 min) in OTR was recorded, while the second sample was taken when OTR was 2 mmol L<sup>-1</sup> h<sup>-1</sup>. Samples were centrifuged; supernatant and pellet were frozen before pH measurement and offline metabolites and MFT measurements as described below. To avoid any impact of evaporation, all measured concentrations are corrected by an evaporation factor. As maximum deviation between duplicate measurements a value below 7% was determined.

### Cultivation in Stirred Tank Bioreactor

Three 300 mL seed cultures were prepared as previously described in 2 L shake flasks, inoculated from a first seed at 10% (v/v) ratio, and cultured for 24 h at 37°C in a 25 mm diameter shaker (Infors HT, Germany). Two were prepared in complex LB medium and one in mineral HdB medium, the latter one supplemented with 10 g L<sup>-1</sup> ethanol as sole carbon source.

The main bench-scale experiments were conducted in three 7 L stirred-tank reactors (diameter = 160 mm) with a filling volume of 3 L at 37°C. All reactors were equipped with one Rushton turbine (diameter = 64 mm). Two STR were done with complex LB medium under oxygen-limited and unlimited conditions and one STR with mineral HdB medium under oxygen-limited conditions. Each STR was inoculated with the corresponding seed culture at a 10% (v/v) ratio with the same production medium. The aeration rate was constant at 0.75 L min<sup>-1</sup> (= 0.25 vvm). Under oxygen-unlimited conditions, the dissolved oxygen tension (DOT) was controlled to maintain a

minimum level of 20% by the stirring rate at 900 rpm. Under oxygen-limited conditions, the agitation rate was 430 rpm to achieve an OTR of 8 mmol L<sup>-1</sup> h<sup>-1</sup>. All STR were buffered with 52.3 g L<sup>-1</sup> (250 mM) MOPS at an initial pH of 7.2 and supplemented with 10 g L<sup>-1</sup> ethanol, 0.5 g L<sup>-1</sup> tyloxapol (Sigma Aldrich), and 1 mL L<sup>-1</sup> antifoam 204 (Sigma Aldrich).

### Analytical Methods

#### Online Measurements in Stirred Tank Bioreactor

For all STR experiments, DOT (Hamilton, United States) and pH were measured online. The O<sub>2</sub>- and CO<sub>2</sub>-concentrations were measured using an off-gas analyzer (Rosemount NGA 2000, Emerson Process Management GmbH&Co., OHG, Haan, Germany) with a paramagnetic sensor and an infrared analyzer. The O<sub>2</sub>-consumption was determined via the OTR, the CO<sub>2</sub>-formation via carbon dioxide transfer rate (CTR), according to the following equations (Anderlei et al., 2004; Regestein et al., 2013):

$$OTR = \frac{\dot{V}_G}{V_L \cdot V_{norm}} \cdot \left( y_{O_2,in} - \frac{1 - y_{O_2,in} - y_{CO_2,in}}{1 - y_{O_2,out} - y_{CO_2,out}} \cdot y_{O_2,out} \right) \quad (1)$$

$$CTR = \frac{\dot{V}_G}{V_L \cdot V_{norm}} \cdot \left( y_{CO_2,out} - \frac{1 - y_{O_2,in} - y_{CO_2,in}}{1 - y_{O_2,out} - y_{CO_2,out}} \cdot y_{CO_2,in} \right) \quad (2)$$

The respiratory quotient (RQ) enables first conclusions about the dominance of oxidative or reductive metabolic pathways and is an indicator for metabolic switches during cultivation:

$$RQ = \frac{CTR}{OTR} \quad (3)$$

#### Offline Metabolite Measurements

Samples of 10 mL were used for metabolites determination. Following harvesting of the cells, supernatant samples were filtered by 0.2 μm and diluted 10-fold with 0.5 mM H<sub>2</sub>SO<sub>4</sub>. A volume of 50 μL was injected in an HPLC system (JASCO International Co., Japan) equipped with a Kromasil 100 C18 (40 mm × 4 mm, 5 μm) precolumn (Dr. Maisch GmbH, Germany) and an Aminex HPX-87H, 300 mm × 7.8 mm, 9 μm ion exclusion column (Bio-Rad, United States), equilibrated at 50°C running in isocratic mode (0.005 mol L<sup>-1</sup> H<sub>2</sub>SO<sub>4</sub> at 0.5 mL min<sup>-1</sup>). Detection was done by refractive index detector and UV (215 nm). Metabolite identification was done based on the retention time of known standards. All samples were analyzed at least in duplicates with deviations below 5%.

#### Offline Mycofactocin Extraction and Measurement

For MFT extraction and determination by high-resolution liquid chromatography-mass spectrometry (LC-MS), all solvents used were of LC-MS grade. A sample (duplicates) volume of 10 mL was filtered through a 0.2 μm regenerated cellulose filter (Sartorius), previously washed thrice with 10 mL LC-MS grade water to remove the wetting agent. After applying vacuum, the biomass lawn was washed in the same manner to remove mass spectrometry (MS) interferences like media salts, antifoam,

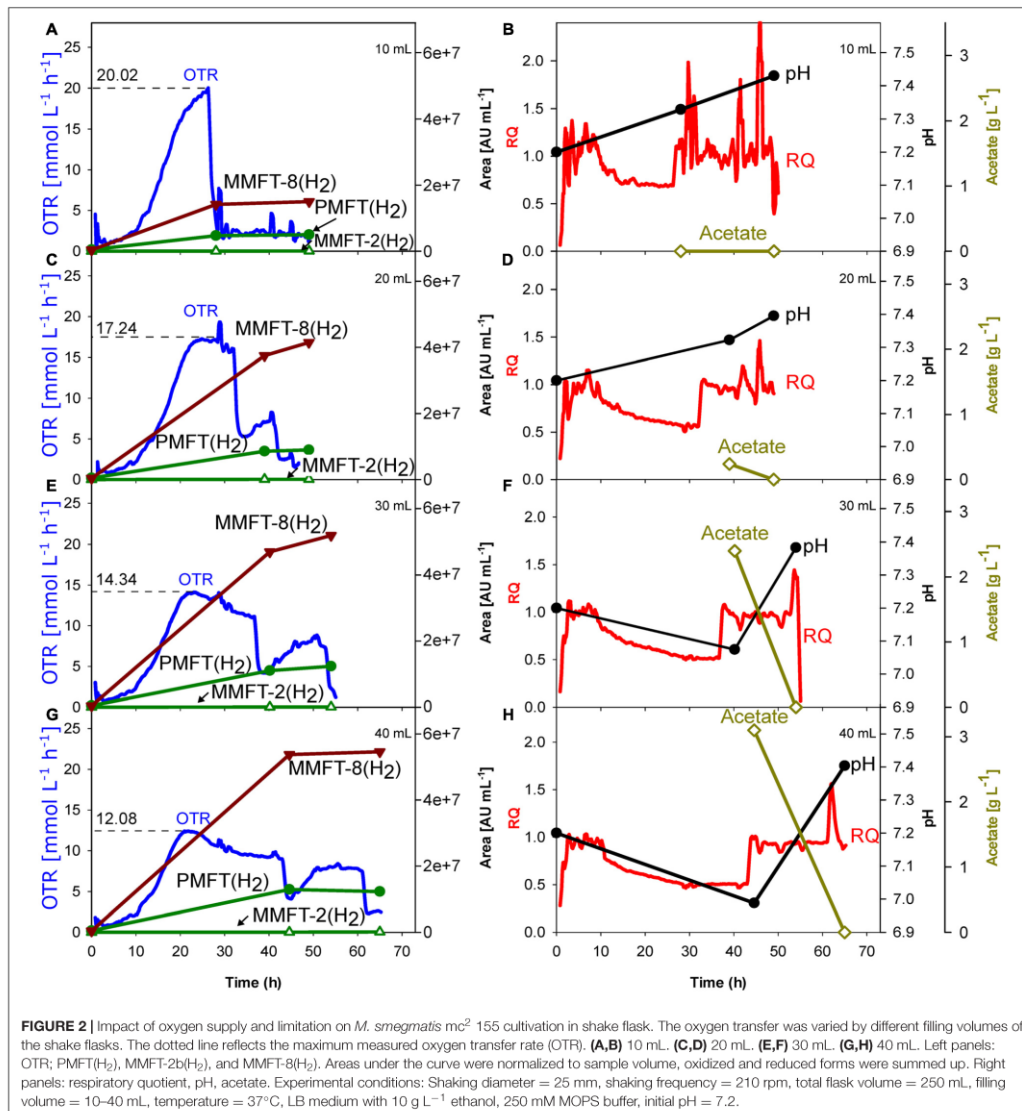
# Impact of Oxygen Supply and Scale-Up on *Mycobacterium smegmatis* Cultivation and Mycofactocin Formation

Peña-Ortiz et al.

Mycofactocin Formation

and tyloxapol. The filter was transferred to a 50 mL centrifuge tube containing 20 mL of cold methanol ( $-20^{\circ}\text{C}$ ) and mixed vigorously on a vortex mixer and an ultrasonic bath for 10 s. The methanolic extract was then transferred to a 100 mL round flask and processed in a rotary evaporator until dryness, then the solids resuspended two times in 500  $\mu\text{L}$  of water and transferred

to a microcentrifuge tube. 1 mL of crude extract was centrifuged twice at  $17,000 \times g$  for 10 min, the supernatant transferred to a new tube and centrifuged again, 600  $\mu\text{L}$  of crude extract was transferred to a glass vial and stored at  $-20^{\circ}\text{C}$ . Before LC-MS measurements, all samples were diluted to a 1:10 ratio in LC-MS water.



# Impact of Oxygen Supply and Scale-Up on *Mycobacterium smegmatis* Cultivation and Mycofactocin Formation

Peña-Ortiz et al.

Mycofactocin Formation

LC-MS measurements of MFT congeners were performed in an Ultimate 3000 UHPLC coupled to a Q Exactive Plus mass spectrometer equipped with a heated electrospray ionization probe (Thermo Fisher Scientific, Germany) as described before (Peña-Ortiz et al., 2020). Metabolite separation was done in an XB-C18 UHPLC column (150 × 2.1 mm, 2.6 μm, 100 Å, Phenomenex) preceded by a SecurityGuard ULTRA precolumn (2 × 2.1 mm, Phenomenex) at 40°C. 10 μl of the sample was injected and separated chromatographically in a mobile phase composed of 0.1% (v/v) formic acid in either water (A) or acetonitrile (B) and a constant flow rate of 300 μL min<sup>-1</sup> as follows: 0–2 min, 2% B; 2–15 min 2–99% B; 15–18 min 99% B. Metabolite separation was followed by full scan (MS<sup>1</sup>) in positive ionization mode at two scan ranges: *m/z* 200–600 and *m/z* 580–2,000 at a resolving power of 70,000 at *m/z* 200, injection time to 100 ms, and automatic gain control (AGC) target to 3 × 10<sup>6</sup>. Further details are presented in **Supplementary Material 6**.

Compound identification by retention time was performed with Compound Discoverer 3.1 (Thermo Fisher Scientific, United States) using the untargeted metabolomics workflow. The default workflow was modified in the Detect Compounds node for a minimum peak intensity of 10,000, and the inclusion of a mass list for targeted identification. The mass list contains molecular mass and retention time of previously identified MFT congeners; maximum RT tolerance for identification was set to 0.25 min. Plotting was done using SigmaPlot 14.0 (Systat Software, Inc., United States). For estimation of PMFT production independent of oxidation state, the areas of PMFT (R<sub>t</sub> 7.2) and PMFTH<sub>2</sub> (R<sub>t</sub> 6.9), MMFT-2 (R<sub>t</sub> 7.1) and MMFT-2bH<sub>2</sub> (R<sub>t</sub> 7.2), as well as MMFT-8 (R<sub>t</sub> 7.2) and MMFT-8H<sub>2</sub> (R<sub>t</sub> 6.8) (Peña-Ortiz et al., 2020) were summed up and designated PMFT(H<sub>2</sub>), MMFT-2b(H<sub>2</sub>) as well as MMFT-8(H<sub>2</sub>), respectively. The relative standard error was 31% between duplicates on average for the major mycofactocin species.

## RESULTS AND DISCUSSION

### Process Characterization in Shake Flask

Although oxygen supply is likely a key factor influencing redox cofactor synthesis, most of the published screening experiments with mycobacteria were performed in a shake flask providing no

information on oxygen supply. Therefore, the initial experiment aimed to elucidate the impact of oxygen supply on metabolic activity and MFT formation. For this reason, *M. smegmatis* mc<sup>2</sup> 155 cultivations were performed in a TOM device which enables online measurement of oxygen uptake and carbon dioxide formation (**Figure 2**). Ethanol (10 g L<sup>-1</sup>) was added as a carbon source to induce MFT production. To determine the impact of decreasing oxygen supply, the filling volume in the shake flasks were increased from 10 to 40 mL, thereby limiting the maximum OTR. The left panels in **Figure 2** outline the OTR and offline MFT measurements. Right panels indicate the online RQ, offline pH-value, and acetate formation. Specific characteristic values of all four experimental conditions are presented in **Table 1**.

To ensure oxygen-unlimited cultivation conditions in the shake flask with the lowest filling volume of 10 mL, the theoretical maximum OTR was previously calculated based on an OTR<sub>max</sub> equation published by Meier et al. (2016). The calculated OTR<sub>max</sub> value under these specific conditions is 31.2 mmol L<sup>-1</sup> h<sup>-1</sup>, representing the theoretical maximum oxygen transfer capacity under the investigated conditions. As the measured oxygen consumption rate never exceeded 20 mmol L<sup>-1</sup> h<sup>-1</sup>, the oxygen demand by the culture was always well below the calculated maximum oxygen transfer capacity. This is finally validated by the shape of the OTR curve (**Figure 2A**), which increases until its maximum value without any visible plateau. This statement is also covered by published OTR curves in literature (Anderlei and Büchs, 2001; Büchs, 2001; Maier and Büchs, 2001; Anderlei et al., 2004).

Moreover, no acetate could be detected in the supernatant which is another indicator for unlimited oxygen supply. However, 20 mL filling volume causes a short oxygen limitation phase, which increases up to 25 h with the increasing filling volume. As visible in **Figures 2C,E,G** the maximum OTR, and thus the metabolic activity decreases from 17 mmol L<sup>-1</sup> h<sup>-1</sup> (for 20 mL) to 12 mmol L<sup>-1</sup> h<sup>-1</sup> (for 40 mL), prolonging the time until the substrate is consumed. In all cases, an RQ between 0.5 and 0.6 was observed, suggesting that ethanol is the main carbon source in the system (Ramon-Portugal et al., 2004). Simultaneously, acetate production increases with the duration of the oxygen-limited phase (plateau length), from 0.24 g L<sup>-1</sup> (for 20 mL) to 3.1 g L<sup>-1</sup> (for 40 mL). The plateau of the OTR curves indicates oxygen-limited conditions. The second peak in the OTR curves is a consequence of the acetate consumption formed before in the

**TABLE 1** | Impact of oxygen-(un)limited conditions on metabolic activity and MFT formation of *M. smegmatis* mc<sup>2</sup> 155 (see **Figure 2**).

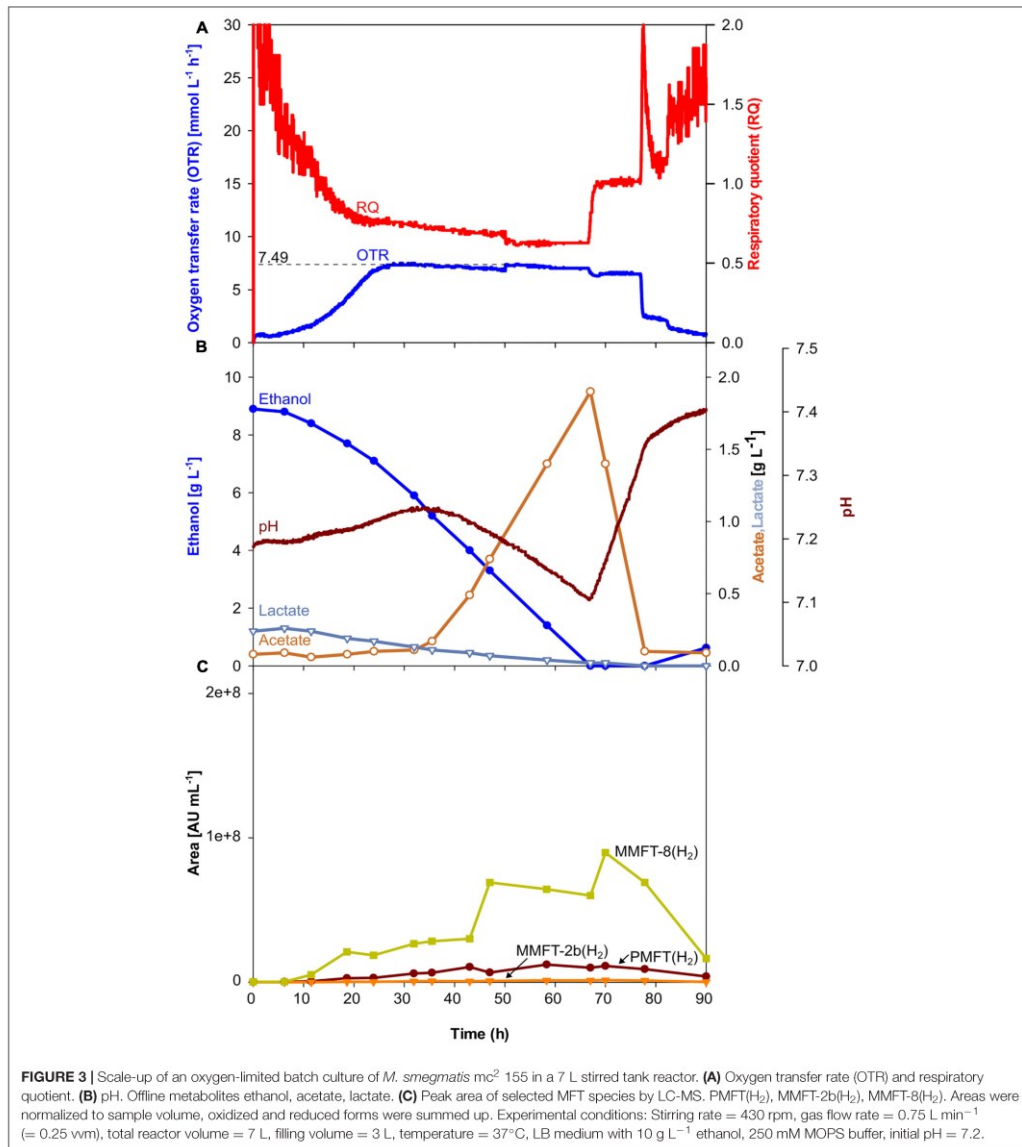
	Oxygen-unlimited		Increasing oxygen limitation	
Filling volume	10 mL	20 mL	30 mL	40 mL
Calculated OTR <sub>max</sub> [mmol L <sup>-1</sup> h <sup>-1</sup> ]	31.2	18.7	13.5	11
Measured OTR <sub>max</sub> [mmol L <sup>-1</sup> h <sup>-1</sup> ]	20.02 ± 0.08	17.24 ± 0.25	14.34 ± 0.01	12.08 ± 0.47
Duration of oxygen-limited phase (= length of the plateau) [h]	0	10	20	25
Time until ethanol depletion [h]	26.1	31.9	36.5	42.9
Generated acetate <sub>max</sub> [g L <sup>-1</sup> ]	0	0.24	2.4	3.1
Premycofactocin <sub>max</sub> PMFT(H <sub>2</sub> ) [Area mL <sup>-1</sup> ]	6,454,441	10,041,793	13,201,682	12,901,731
Methylmycofactocin-2 <sub>max</sub> MMFT-2b(H <sub>2</sub> ) [Area mL <sup>-1</sup> ]	128,868	107,438	100,975	126,746
Methylmycofactocin-8 <sub>max</sub> MMFT-8(H <sub>2</sub> ) [Area mL <sup>-1</sup> ]	19,385,519	46,455,040	55,613,267	57,341,055



Impact of Oxygen Supply and Scale-Up on *Mycobacterium smegmatis* Cultivation and Mycofactocin Formation

Peña-Ortiz et al.

Mycofactocin Formation



oxygen-limited phase. This agrees with a sudden change in the RQ from 0.65 to 1.

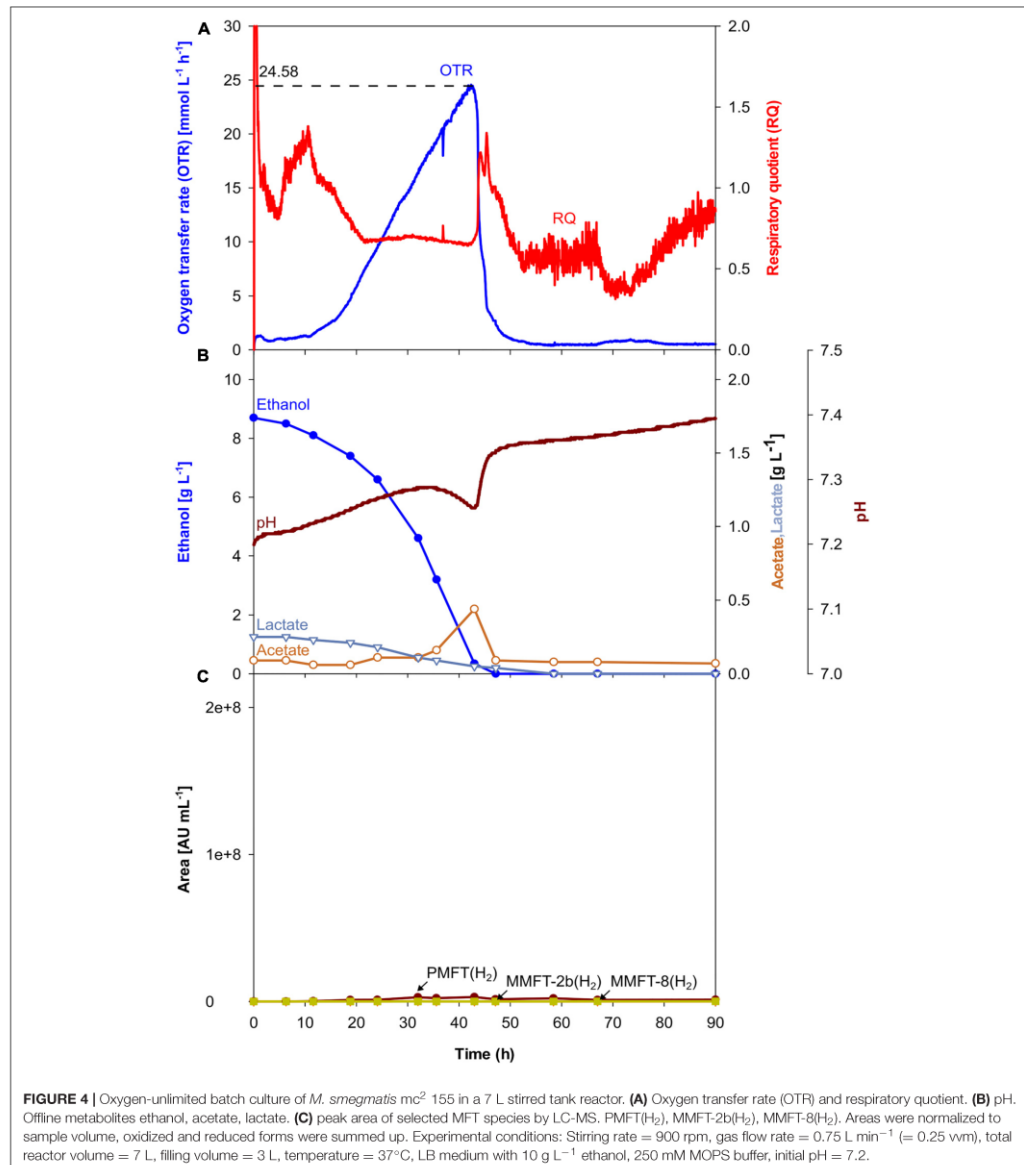
Most important is the impact of the different levels of oxygen supply on the formation of different mycofactocins. To increase visibility, only the key (pre-)mycofactocins PMFT(H<sub>2</sub>),

MMFT-8(H<sub>2</sub>), and MMFT-2b(H<sub>2</sub>) are depicted in **Figure 2**, each pool representing the sum of oxidized and reduced forms. The complete overview of all measured mycofactocins and methylmycofactocins including the biosynthetic precursors AHDP-n and the premature cleavage products GAHDP-n,

# Impact of Oxygen Supply and Scale-Up on *Mycobacterium smegmatis* Cultivation and Mycofactocin Formation

Peña-Ortiz et al.

Mycofactocin Formation



(Peña-Ortiz et al., 2020), can be found in **Supplementary Figures S1, S3–S5**. The comparison of the four different culture conditions in **Figure 2** and **Table 1** show clearly that the absolute amount of produced mycofactocins is increased under

oxygen-limited conditions, especially the long-chained versions MMFT-7(H<sub>2</sub>) and MMFT-8(H<sub>2</sub>) followed by the aglycons PMFT(H<sub>2</sub>). The reduced molecule is the most prevalent form (see also **Supplementary Figure S1**). In all cases, the first offline

samples were taken when OTR dropped for the first time, and RQ switches from 0.65 to 1, which are both indications for ethanol depletion (Ramon-Portugal et al., 2004). It was assumed that the concentrations of mycofactocins are highest at this time point and could decrease after depletion of the main carbon and energy source ethanol. However, as visible in **Figure 2**, all MFT concentrations remain constant or even slightly increase when acetate was consumed in the second growth phase.

Since one aim is to investigate and develop a process for generating sufficient amounts of MFT for further experiments, it was decided to scale up the oxygen-limited cultivation conditions of 40 mL filling volume.

### Impact of Scale-Up Into the 7 L Stirred Tank Reactor

As scale-up criteria from shake flask to STR, the volumetric power input was chosen. The aeration rate was adjusted to 0.25 vvm in all cultivations in the STR to reflect the air diffusion through a cotton plug of a shake flask (Maier and Büchs, 2001). The second important parameter for scale-up based on the volumetric power input is the stirring rate (under aerated conditions) which had to be calculated. The power input under shake flask conditions can be calculated using the fundamental equations for the dimensionless Reynolds and modified Power number (Büchs et al., 2000a,b). Calculations for the STR were based on equations published by Möckel et al. (1983). For better readability, all equations, details of geometry, intermediate calculated results, and assumptions are presented in **Supplementary Material 1**. The calculated value of the stirring rate is 430 rpm, reflecting a power input of 1.48 kW m<sup>-3</sup> under aerated conditions and should result in combination with an aeration rate of 0.25 vvm in a maximum OTR of approx. 12 mmol L<sup>-1</sup> h<sup>-1</sup>. The pH was stabilized by the same buffer system and concentration as under shake flask conditions.

As visible in **Figure 3A**, OTR, and RQ follow a trend comparable to the scaled-up shake flask cultivation depicted in **Figure 2G**. The oxygen was limited at a maximum value of 7.4 mmol L<sup>-1</sup> h<sup>-1</sup> which is lower than it was aimed for. The

main carbon source ethanol was consumed until its depletion after 66.7 h, indicated by a sharp increase of the RQ-value to 1 (**Figures 3A,B**). The shake flask experiments had already shown that acetate is formed as an overflow metabolite. The formation of acetate correlates with the beginning of the oxygen-limited growth phase after approx. 28 h, also indicated by a decreasing pH. The previously produced 1.9 g L<sup>-1</sup> of acetate is taken up in the second growth phase between 66.7 and 77.3 h mirrored by a sharp drop in the OTR curve after its depletion. Based on previous experiences with *M. smegmatis*, biofilm formation was expected and was intended to be controlled by the addition of tyloxapol, a surfactant commonly used in *Mycobacterium* microbiology to disperse and reduce cell clumping, in combination with antifoam for foaming reduction. Their polymeric nature makes these compounds common LC-MS interferences. The filtration and rinsing strategies were successful in removing these compounds for optimal spectra acquisition, but biofilm and subsequent foaming was still observed, due to submerge aeration and especially on high-density complex medium.

Although, all the trends depicted in **Figures 2C–H**, **3C** clearly show that oxygen-limited conditions (after 28 h) have a positive effect on the overall MFT formation, the oxygen-unlimited shake flask experiment presented in **Figure 2A** contains no information about the kinetics of the different mycofactocins during oxygen-unlimited growth. Therefore, an additional experiment was performed under oxygen-unlimited conditions to elucidate ratios and kinetics. The results are depicted in **Figure 4**. As visible in **Figure 4A**, a maximum (unlimited) OTR of 24 mmol L<sup>-1</sup> h<sup>-1</sup> was reached at 41.6 h. Only minor acetate concentrations (0.4 g L<sup>-1</sup>, after 43 h) could be detected, which are likely produced by the biofilm at the reactor wall. Ethanol was fully depleted at 47 h (**Figure 3B**).

The results for MFT formations shown in **Figure 4C** and **Table 2** validate the results of the oxygen-unlimited shake flask experiment (**Figure 2A**) since only minor amounts of all MFT are formed. Moreover, in comparison to the oxygen-unlimited shake flask experiment, all MFT values are even lower, which can be attributed to the strong foam formation, containing visible

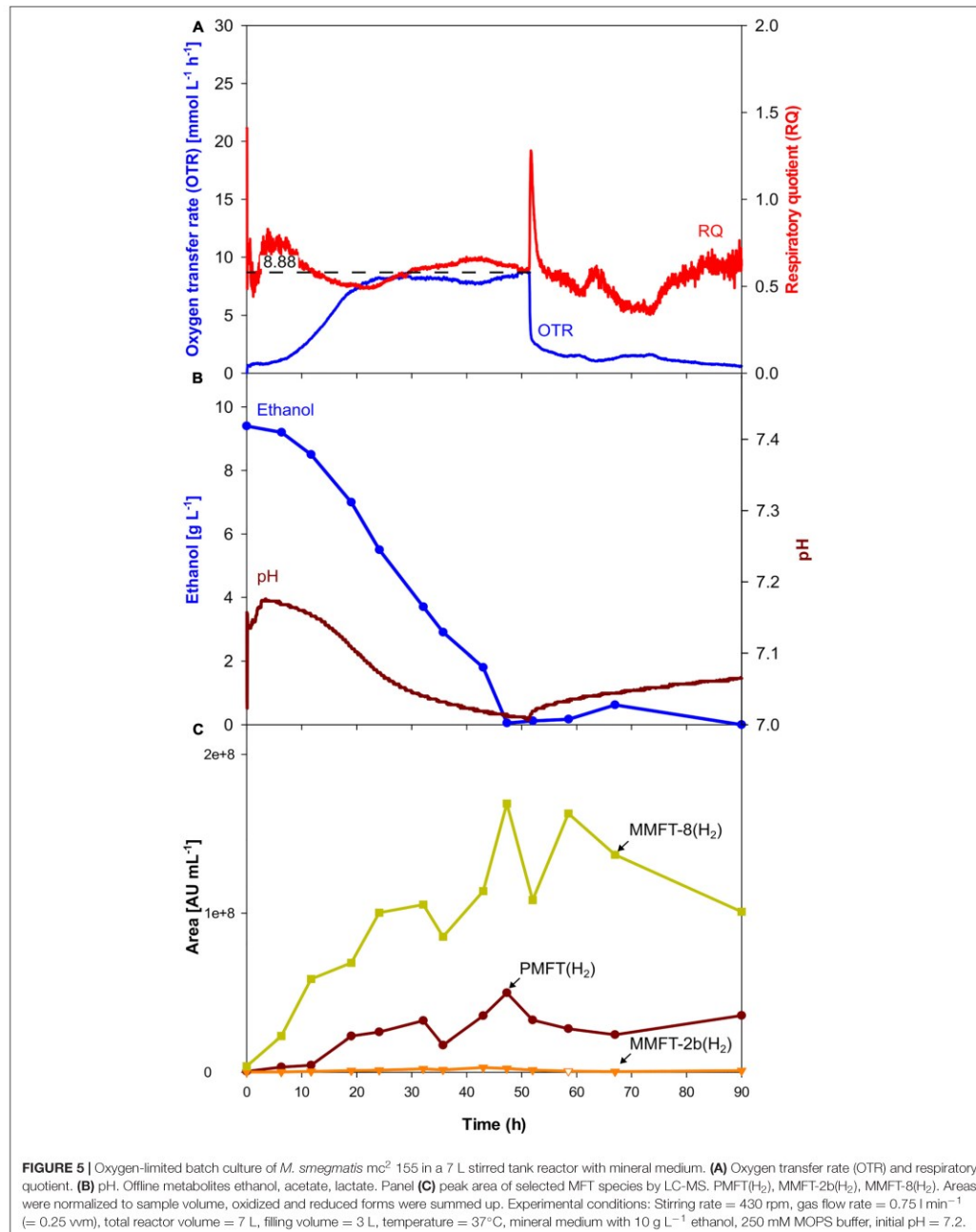
**TABLE 2** | Experimental results of *M. smegmatis* mc<sup>2</sup> 115 cultures in stirred tank reactors.

	Increasing oxygen limitation			
	Complex medium, oxygen-unlimited (Figure 4)	Complex medium, oxygen-limited (Figure 3)	Mineral medium, oxygen-limited (Figure 5)	Complex medium, strongly oxygen-limited (Supplementary Figure S2)
OTR <sub>max</sub> [mmol L <sup>-1</sup> h <sup>-1</sup> ]	24	8	8	2.78
Duration of oxygen-limited phase (= length of the plateau) [h]	0	47	28	> 90
Time to ethanol depletion [h]	47.2	67	51.5	N.A.
Generated acetate <sub>max</sub> [g L <sup>-1</sup> ]	0.4	1.9	0	0.6
Premycofactocin <sub>max</sub> PMFT(H <sub>2</sub> ) [Area mL <sup>-1</sup> ]	3,062,618	12,287,516	49,861,224	299,885
Methylmycofactocin-2 <sub>max</sub> MMFT-2b(H <sub>2</sub> ) [Area mL <sup>-1</sup> ]	153,306	306,667	2,951,352	744,293
Methylmycofactocin-8 <sub>max</sub> MMFT-8(H <sub>2</sub> ) [Area mL <sup>-1</sup> ]	142,371	89,803,844	169,062,399	46,657

Impact of Oxygen Supply and Scale-Up on *Mycobacterium smegmatis* Cultivation and Mycofactocin Formation

Peña-Ortiz et al.

Mycofactocin Formation



# Impact of Oxygen Supply and Scale-Up on *Mycobacterium smegmatis* Cultivation and Mycofactocin Formation

Peña-Ortiz et al.

Mycofactocin Formation

amounts of biomass as well as biofilm formation at the reactor wall (Supplementary Figure S6A).

To elucidate the opposite effect of extremely low oxygen supply on the MFT formation in complex medium, and STR experiment was performed with a maximum OTR of only  $2.5 \text{ mmol L}^{-1} \text{ h}^{-1}$ . Due to the negative results concerning the formation of MFT, the details are only presented in Supplementary Figure S2. Ethanol was consumed very slowly, but, most importantly, none of the longer chained (M)MFT- $n(\text{H}_2)$  species were generated in relevant amounts. Only MMFT-2b( $\text{H}_2$ ) was produced in relatively high amounts (see Table 2). This experimental result clearly demonstrates that an optimal level of oxygen supply is a key parameter to generate MFT but also influences the oligoglycoside chain length of the mycofactocins.

## Impact of Mineral Medium

For further characterization of MFT formation, clearer analytical results, and easier purification, a chemically defined mineral medium Hartmann de Bont (HdB) was tested for further process development as it was used before in several studies involving mycobacteria (Hartmans et al., 1992; Hauschild et al., 1994; Song and Niederweis, 2011; Berney et al., 2012; Greening et al., 2014; Peña-Ortiz et al., 2020). Since previous experiments have proven the positive impact of oxygen limitation, oxygen-limited conditions were also chosen for the experiment presented in Figure 5. As depicted in Figure 5A the OTR increased up to a maximum value of approx.  $8 \text{ mmol L}^{-1} \text{ h}^{-1}$  comparable to the previous oxygen-limited cultivation in complex medium (see Figure 3). With a total duration of 28 h, the oxygen-limited phase is shorter in mineral medium comparing to complex medium (see Table 2), since ethanol is the only available carbon source in mineral medium. Moreover, as indicated by the OTR curve, there is only one growth phase without any acetate formation and therefore no second growth phase. This result is validated by the HPLC measurements, which did not detect any organic acids in the supernatants. As before, a sharp drop in the OTR curve indicates the depletion of ethanol at 51.5 h, mirrored by the HPLC results depicted in Figure 5B.

As visible in Figure 5C, the kinetics of MFT formation looks similar to the results of the oxygen-limited cultivation in complex medium (Figure 3). However, as depicted in Table 2, the maximum amounts of all MFT species are doubled, which makes the oxygen-limited cultivation in the mineral medium the most promising conditions for further MFT production.

## Comparison of Mycofactocin Formation

The previously shown experiments have demonstrated that the positive effect of oxygen-limited conditions can be scaled up into the STR and even higher amounts of MFT could be produced under STR conditions. Besides the maximum OTR, the duration of the oxygen-limited phase is an essential parameter to influence not only the overall MFT formation but also the glycosylation of the different MFT species. As shown in Table 2, the effect of a longer oxygen-limited phase is visible but has to be seen in the context of the maximum OTR. The current results suggest elongating the phase of oxygen-limited conditions, which

could be realized by higher initial concentrations of ethanol, by the addition of ethanol during cultivation (pulsed-batch) as well as by implementing a fed-batch strategy. In every case, the oxygen supply reflected by the OTR should be adjusted between 8 and  $12 \text{ mmol L}^{-1} \text{ h}^{-1}$ . The optimal time point for harvesting seems to be right before ethanol is fully depleted, since especially MMFT-8( $\text{H}_2$ ) concentration started to fluctuate during the metabolic switch from ethanol to acetate. Depending on the chosen level of oxygen supply, the length of the glycosyl chain can be influenced. As stated in Table 2 the purest amounts of the short-chained MMFT-2b( $\text{H}_2$ ) can be generated for levels of very low oxygen supply, realized by OTRs smaller than  $8 \text{ mmol L}^{-1} \text{ h}^{-1}$ . If non-glycosylated PMFT is of interest, mineral medium combined with oxygen-limited conditions will be the most promising conditions.

## CONCLUSION

This study has shown how the formation of different species of MFT is influenced by cultivating *M. smegmatis* under different levels of oxygen supply. On shake flask level, it could be demonstrated that oxygen-limited conditions result in a four times higher amount of longer-chained MFT species and unexpectedly, even promoted drastic changes in the length of the glycosyl chain of MFT. This finding can be used to direct the biosynthesis toward short or elongated MFT species. After scale-up in a 7 L STR, the detected amount of longer-chained MFT species was further increased and even doubled by changing from complex to mineral medium. In addition, the time point of harvesting was identified as another critical parameter since all MFT was degraded after depletion of the carbon sources. A critical open issue is the current need to add antifoam agents in case of submerged aeration to reduce the foam formation. With respect to the overall process to generate pure mycofactocins on a larger scale, antifoam agents are very difficult to remove in a downstream procedure. Therefore, alternative process strategies have to be applied, like pressure fermentation with strongly reduced aeration, to avoid the addition of antifoam agents. Overall, this study represents a milestone for future large-scale production on milligram- to gram-level of MFT congeners and thus sets the stage for upcoming biochemical investigations as well as for more detailed studies into the biosynthesis and physiology of the cofactor.

## DATA AVAILABILITY STATEMENT

The raw data supporting the conclusions of this article will be made available by the authors, without undue reservation.

## AUTHOR CONTRIBUTIONS

LP-O and IS conducted the experiments. GL and LR supervised the study. All authors have written the manuscript under the supervision of LR.

# Impact of Oxygen Supply and Scale-Up on *Mycobacterium smegmatis* Cultivation and Mycofactocin Formation

Peña-Ortiz et al.

Mycofactocin Formation

## FUNDING

We would like to thank the Carl-Zeiss Foundation for funding.

## ACKNOWLEDGMENTS

We would like to thank the Jena School of Microbial Communication (JSMC) for support and Daniel Braga for proofreading the manuscript.

## SUPPLEMENTARY MATERIAL

The Supplementary Material for this article can be found online at: <https://www.frontiersin.org/articles/10.3389/fbioe.2020.593781/full#supplementary-material>

## REFERENCES

- Anderlei, T., and Büchs, J. (2001). Device for sterile online measurement of the oxygen transfer rate in shaking flasks. *Biochem. Eng. J.* 7, 157–162. doi: 10.1016/s1369-703x(00)00116-9
- Anderlei, T., Zang, W., Papaspyrou, M., and Büchs, J. (2004). Online respiration activity measurement (OTR, CTR, RQ) in shake flasks. *Biochem. Eng. J.* 17, 187–194. doi: 10.1016/s1369-703x(03)00181-5
- Ayikpoe, R. S., and Latham, J. A. (2019). MftD Catalyzes the Formation of a Biologically Active Redox Center in the Biosynthesis of the Ribosomally Synthesized and Post-translationally Modified Redox Cofactor, Mycofactocin. *J. Am. Chem. Soc.* 141, 13582–13591. doi: 10.1021/jacs.9b06102
- Ayikpoe, R., Govindarajan, V., and Latham, J. A. (2019). Occurrence, function, and biosynthesis of mycofactocin. *Appl. Microbiol. Biotechnol.* 103, 2903–2912. doi: 10.1007/s00253-019-09684-4
- Ayikpoe, R., Salazar, J., Majestic, B., and Latham, J. A. (2018). Mycofactocin Biosynthesis Proceeds through 3-Amino-5-[(p-hydroxyphenyl)methyl]-4,4-dimethyl-2-pyrrolidinone (AHDPP); Direct Observation of MftE Specificity toward MftA. *Biochemistry* 57, 5379–5383. doi: 10.1021/acs.biochem.8b00816
- Barberel, S. L., and Walker, J. R. L. (2000). The Effect of Aeration upon the Secondary Metabolism of Microorganisms. *Biotechnol. Genet. Eng. Rev.* 17, 281–326. doi: 10.1080/02648725.2000.10647996
- Berney, M., Weimar, M. R., Heikal, A., and Cook, G. M. (2012). Regulation of proline metabolism in mycobacteria and its role in carbon metabolism under hypoxia. *Mol. Microbiol.* 84, 664–681. doi: 10.1111/j.1365-2958.2012.08053.x
- Bruender, N. A., and Bandarian, V. (2016). The Radical S-Adenosyl-L-methionine Enzyme MftC Catalyzes an Oxidative Decarboxylation of the C-Terminus of the MftA Peptide. *Biochemistry* 55, 2813–2816. doi: 10.1021/acs.biochem.6b00355
- Bruender, N. A., and Bandarian, V. (2017). The Creatininase Homolog MftE from *Mycobacterium smegmatis* Catalyzes a Peptide Cleavage Reaction in the Biosynthesis of a Novel Ribosomally Synthesized Post-translationally Modified Peptide (RiPP). *J. Biol. Chem.* 292, 4371–4381. doi: 10.1074/jbc.m116.762062
- Buchmeier, N. A., Newton, G. L., Koledin, T., and Fahey, R. C. (2003). Association of mycothiol with protection of *Mycobacterium tuberculosis* from toxic oxidants and antibiotics. *Mol. Microbiol.* 47, 1723–1732. doi: 10.1046/j.1365-2958.2003.03416.x
- Büchs, J. (2001). Introduction to advantages and problems of shaken cultures. *Biochem. Eng. J.* 7, 91–98. doi: 10.1016/s1369-703x(00)00106-6
- Büchs, J., Maier, U., Milbradt, C., and Zoels, B. (2000a). Power consumption in shaking flasks on rotary shaking machines: I. Power consumption measurement in unbaffled flasks at low liquid viscosity. *Biotechnol. Bioeng.* 68, 589–593. doi: 10.1002/(sici)1097-0290(20000620)68:6<589::aid-bit1>3.0.co;2-j
- Büchs, J., Maier, U., Milbradt, C., and Zoels, B. (2000b). Power consumption in shaking flasks on rotary shaking machines: II. Nondimensional description of specific power consumption and flow regimes in unbaffled flasks at elevated liquid viscosity. *Biotechnol. Bioeng.* 68, 594–601. doi: 10.1002/(sici)1097-0290(20000620)68:6<594::aid-bit2>3.0.co;2-u
- Clark, G. J., and Bushell, M. E. (1995). Oxygen limitation can induce microbial secondary metabolite formation: investigations with miniature electrodes in shaker and bioreactor culture. *Microbiology* 141, 663–669. doi: 10.1099/13500872-141-3-663
- Dick, T., Lee, B. H., and Murugasu-Oei, B. (1998). Oxygen depletion induced dormancy in *Mycobacterium smegmatis*. *FEMS Microbiol. Lett.* 163, 159–164. doi: 10.1111/j.1574-6968.1998.tb13040.x
- Dubey, A. A., and Jain, V. (2019). Mycofactocin is essential for the establishment of methylotrophy in *Mycobacterium smegmatis*. *Biochem. Biophys. Res. Comm.* 516, 1073–1077. doi: 10.1016/j.bbrc.2019.07.008
- Gamboa-Suasnavart, R. A., Valdez-Cruz, N. A., Gaytan-Ortega, G., Reynoso-Cereceda, G. I., Cabrera-Santos, D., López-Griego, L., et al. (2018). The metabolic switch can be activated in a recombinant strain of *Streptomyces lividans* by a low oxygen transfer rate in shake flasks. *Microb. Cell Fac.* 17:189.
- Greening, C., Villas-Boas, S. G., Robson, J. R., Berney, M., and Cook, G. M. (2014). The growth and survival of *Mycobacterium smegmatis* is enhanced by co-metabolism of atmospheric H<sub>2</sub>. *PLoS One* 9:e103034. doi: 10.1371/journal.pone.0103034
- Gupta, R. S., Lo, B., and Son, J. (2018). Phylogenomics and Comparative Genomic Studies Robustly Support Division of the Genus *Mycobacterium* into an Emended Genus *Mycobacterium* and Four Novel Genera. *Front. Microbiol.* 9:67. doi: 10.3389/fmicb.2018.00067
- Haft, D. H. (2011). Bioinformatic evidence for a widely distributed, ribosomally produced electron carrier precursor, its maturation proteins, and its nicotinoprotein redox partners. *BMC Genom.* 12:21. doi: 10.1186/1471-2164-12-21
- Hartmans, S., Kaptein, A., Tramper, J., and De Bont, J. A. M. (1992). Characterization of a *Mycobacterium* sp. and a *Xanthobacter* sp. for the removal of vinyl chloride and 1,2-dichloroethane from waste gases. *Appl. Biotechnol.* 37, 796–801. doi: 10.1007/bf00174848
- Hauschild, I., Schröer, A., Siedersleben, M., and Starnick, J. (1994). The microbial growth of *Mycobacterium aurum* L1 on vinyl chloride with respect to inhibitory and limiting influence of substrate and oxygen. *Water Sci. Technol.* 30, 125–132. doi: 10.2166/wst.1994.0459
- Haver, H. L., Chua, A., Ghode, P., Lakshminarayana, S. B., Singhal, A., Mathema, B., et al. (2015). Mutations in genes for the F420 biosynthetic pathway and a nitroreductase enzyme are the primary resistance determinants in spontaneous in vitro-selected PA-824-resistant mutants of *Mycobacterium tuberculosis*. *Antimicrob. Agents Chemother.* 59, 5316–5323. doi: 10.1128/aac.00308-15
- Hernick, M. (2013). Mycothiol: a target for potentiation of rifampin and other antibiotics against *Mycobacterium tuberculosis*. *Expert Rev. Anti Infect. Ther.* 11, 49–67. doi: 10.1586/eri.12.152
- Khaliullin, B., Aggarwal, P., Bubas, M., Eaton, G. R., Eaton, S. S., and Latham, J. A. (2016). Mycofactocin biosynthesis: modification of the peptide MftA by the radical S-adenosylmethionine protein MftC. *FEBS Lett.* 590, 2538–2548. doi: 10.1002/1873-3468.12249

# Impact of Oxygen Supply and Scale-Up on *Mycobacterium smegmatis* Cultivation and Mycofactocin Formation

Peña-Ortiz et al.

Mycofactocin Formation

- Khaliullin, B., Ayikpoe, R., Tuttle, M., and Latham, J. A. (2017). Mechanistic elucidation of the mycofactocin-biosynthetic radical S-adenosylmethionine protein. *MftC. J. Biol. Chem.* 292, 13022–13033. doi: 10.1074/jbc.m117.795682
- Krishnamoorthy, G., Kaiser, P., Lozza, L., Hahnke, K., Mollenkopf, H. J., and Kaufmann, S. H. E. (2019). Mycofactocin Is Associated with Ethanol Metabolism in *Mycobacteria*. *MBio* 10, e190–e119.
- Lewis, A. H., and Falkinham, J. O. III (2015). Microaerobic growth and anaerobic survival of *Mycobacterium avium*, *Mycobacterium intracellulare* and *Mycobacterium scrofulaceum*. *Int. J. Mycobacteriol.* 4, 25–30. doi: 10.1016/j.ijmyco.2014.11.066
- Lo, C. K., Pan, C. P., and Liu, W. H. (2002). Production of testosterone from phytosterol using a single-step microbial transformation by a mutant of *Mycobacterium* sp. *J. Indus. Microbiol. Biotechnol.* 28, 280–283. doi: 10.1038/sj.jim.7000243
- Maier, U., and Büchs, J. (2001). Characterisation of the gas-liquid mass transfer in shaking bioreactors. *Biochem. Eng. J.* 7, 99–106. doi: 10.1016/s1369-703x(00)00107-8
- Meier, K., Klöckner, W., Bonhage, B., Antonov, E., Regestein, L., and Büchs, J. (2016). Correlation for the maximum oxygen transfer capacity in shake flasks for a wide range of operating conditions and for different culture media. *Biochem. Eng. J.* 109, 228–235. doi: 10.1016/j.bej.2016.01.014
- Möckel, H.-O., Weißgräber, H., and Börner, K. (1983). Der Leistungseintrag in belüfteten Rührsystemen mit niedrigviskosen Medien. *Chemie Technik* 35, 344–347.
- Moore, D. F., and James, A. M. (1982). Growth studies on *Mycobacterium* BCG: oxygen preference. *Microbios* 35, 151–159.
- Nguyen, L. (2016). Antibiotic resistance mechanisms in *M. tuberculosis*: an update. *Arch. Toxicol.* 90, 1585–1604. doi: 10.1007/s00204-016-1727-6
- Palci, M. M. (1999). Biocatalytic synthesis of oligosaccharides. *Curr. Opin. Biotechnol.* 10, 616–624. doi: 10.1016/s0958-1669(99)00044-0
- Parte, A. C. (2018). LPSN - List of Prokaryotic names with Standing in Nomenclature (bacterio.net), 20 years on. *Int. J. Syst. Evol. Microbiol.* 68, 1825–1829. doi: 10.1099/ijsem.0.002786
- Peña-Ortiz, L., Graça, A. P., Guo, H., Braga, D., Köllner, T. G., Regestein, L., et al. (2020). Structure elucidation of the redox cofactor mycofactocin reveals oligo-glycosylation by MftF. *Chem. Sci.* 11, 5182–5190. doi: 10.1039/d0sc01172j
- Ramon-Portugal, F., Pingaud, H., and Strehaiano, P. (2004). Metabolic transition step from ethanol consumption to sugar/ethanol consumption by *Saccharomyces cerevisiae*. *Biotechnol. Lett.* 26, 1671–1674. doi: 10.1007/s10529-004-3520-5
- Rawat, M., Newton, G. L., Ko, M., Martinez, G. J., Fahey, R. C., and Av-Gay, Y. (2002). Mycothiol-deficient *Mycobacterium smegmatis* mutants are hypersensitive to alkylating agents, free radicals, and antibiotics. *Antimicrob. Agents Chemother.* 46, 3348–3355. doi: 10.1128/aac.46.11.3348-3355.2002
- Realini, L., De Ridder, K., Palomino, J., Hirschel, B., and Portaels, F. (1998). Microaerophilic conditions promote growth of *Mycobacterium genavense*. *J. Clin. Microbiol.* 36, 2565–2570. doi: 10.1128/jcm.36.9.2565-2570.1998
- Regestein, L., Giese, H., Zavrel, M., and Büchs, J. (2013). Comparison of two methods for designing calorimeters using stirred tank reactors. *Biotechnol. Bioeng.* 110, 180–190. doi: 10.1002/bit.24601
- Reyrat, J. M., and Kahn, D. (2001). *Mycobacterium smegmatis*: an absurd model for tuberculosis? *Trends Microbiol.* 9, 472–474. doi: 10.1016/s0966-842x(01)02168-0
- Shiloh, M. U., and Champion, P. A. (2010). To catch a killer. What can mycobacterial models teach us about *Mycobacterium tuberculosis* pathogenesis? *Curr. Opin. Microbiol.* 13, 86–92. doi: 10.1016/j.mib.2009.11.006
- Singh, R., Manjunatha, U., Boshoff, H. I. M., Ha, Y. H., Niyomrattanakit, P., Ledwidge, R., et al. (2008). PA-824 kills nonreplicating *Mycobacterium tuberculosis* by intracellular NO release. *Science* 322, 1392–1395. doi: 10.1126/science.1164571
- Song, H., and Niederweis, M. (2011). Uptake of Sulfate but Not Phosphate by *Mycobacterium tuberculosis* Is Slower than That for *Mycobacterium smegmatis*. *J. Bacteriol.* 194, 956–964. doi: 10.1128/jb.06132-11
- Stover, C. K., Warrener, P., Vandevanter, D. R., Sherman, D. R., Arain, T. M., Langhorne, M. H., et al. (2000). A small-molecule nitroimidazopyran drug candidate for the treatment of tuberculosis. *Nature* 405, 962–966. doi: 10.1038/35016103
- WHO (2019). *Global tuberculosis report 2019*. Geneva: World Health Organization.
- Williams, R., and Galan, M. C. (2017). Recent Advances in Organocatalytic Glycosylations. *Eur. J. Org. Chem.* 2017, 6247–6264. doi: 10.1002/ejoc.201700785
- Yamada, H., Yamaguchi, M., Igarashi, Y., Chikamatsu, K., Aono, A., Murase, Y., et al. (2018). Mycolicibacterium smegmatis, Basonym Mycobacterium smegmatis, Expresses Morphological Phenotypes Much More Similar to *Escherichia coli* Than *Mycobacterium tuberculosis* in Quantitative Structome Analysis and CryoTEM Examination. *Front. Microbiol.* 9:1992. doi: 10.3389/fmicb.2018.01992

**Conflict of Interest:** The authors declare that the research was conducted in the absence of any commercial or financial relationships that could be construed as a potential conflict of interest.

Copyright © 2020 Peña-Ortiz, Schlembach, Lackner and Regestein. This is an open-access article distributed under the terms of the Creative Commons Attribution License (CC BY). The use, distribution or reproduction in other forums is permitted, provided the original author(s) and the copyright owner(s) are credited and that the original publication in this journal is cited, in accordance with accepted academic practice. No use, distribution or reproduction is permitted which does not comply with these terms.

## 9. SUPPLEMENTARY RESULTS

### 9.1. THE ROLE OF MYCOFACTOCIN IN LACTATE METABOLISM

The gene *mftD* encodes the MFT putative PMFT maturase, which generates the redox core of PMFT in a two-step reaction: the amino group is oxidized in the presence of molecular oxygen to yield an imino group, which can then spontaneously hydrolyze to generate an  $\alpha$ -diketo-amide [181]. This reaction is similar to in the biosynthesis of the endogenous cofactors PPQ, TPQ, TTQ, CTQ, and LTQ, in which oxidative processes at the aminosemiquinone intermediate of a tyrosine or tryptophan side chain occur. However, while this reaction is spontaneous in these cofactors, MFT requires the enzyme MftD [133, 236]. Based on sequence similarity, the original annotation of *mftD* was an MFT-dependent L-lactate dehydrogenase (L-LDH) [178]. Before the role of MftD in MFT maturation had been established, the possible role of MftD in lactate metabolism was investigated.

Lactate dehydrogenases oxidize lactate into pyruvate for incorporation into the CCM and can be grouped based on their cofactor use, either NAD<sup>+</sup>-dependent (nLDHs) or NAD<sup>+</sup>-independent (iLDHs) [237]. Therefore, it is presumed that iLDHs are quinone dependent, and under this hypothesis, MftD would then be part of the redox pool MFT with the respiratory chain. While the MSMEG genome only encodes *mftD*, also termed *lldD1*/MSMEG\_1424, there are two possible candidates in MTB: *mftD/lldD1*/Rv0694 and *lldD2*/Rv1872c. This presumed metabolic redundancy in MTB could have been relevant for the pathogenesis of TB and survival during latency, as macrophages and other innate immune cells produce lactate by the Warburg effect, providing the intracellular pathogen with a carbon source [196].

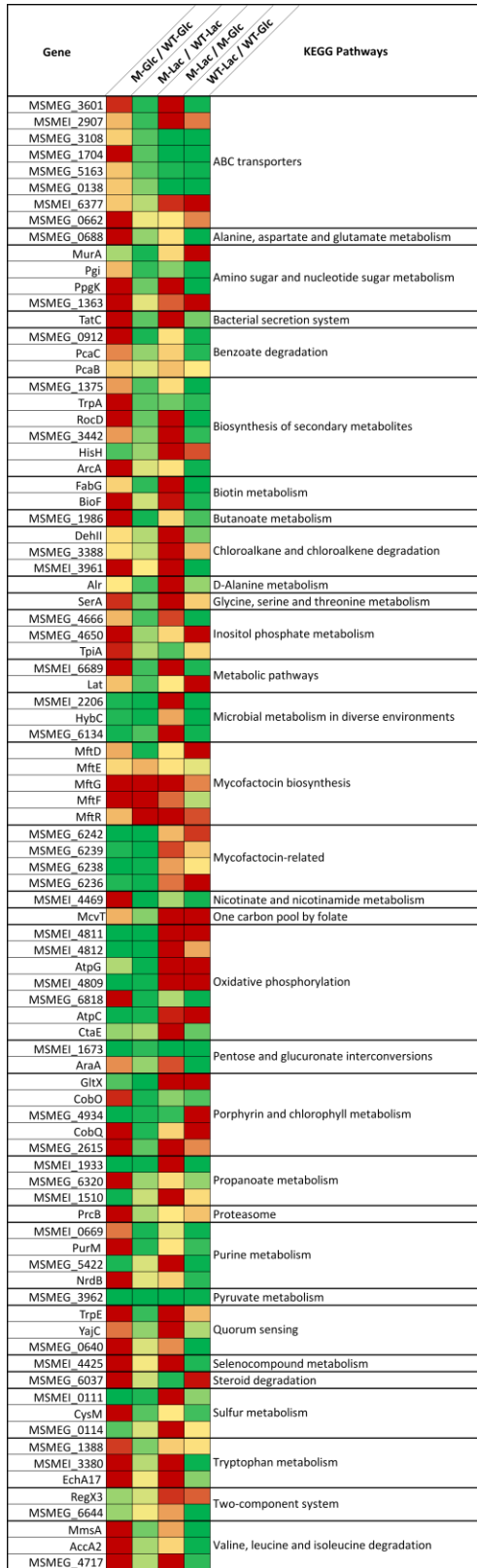
This environment is acidic, glucose-depleted, and some of the available carbon sources are triacylglycerides [10, 238]. *In vitro*, pyruvate metabolism was found to proceed by a reverse rearrangement of the methylcitrate cycle. This study indicates that *lldD2* is expressed constitutively. However, no upregulation was observed with lactate as a carbon source. *lldD1* (*mftD*) was only upregulated with pyruvate as the sole carbon source, signaling a possible role in its metabolism and coupling to the CCM [198].

To elucidate whether MFT is associated with L-lactate metabolism, proteome extracts from *M. smegmatis* wild-type and  $\Delta mftAB$  mutant strain in either lactate or glucose as sole carbon source were analyzed by a bottom-up proteomics approach (section 13.1). Heatmap of identified MFT proteins and those features with a significance score ( $p$ -value / log<sub>2</sub> ratio) <0.05 in the  $\Delta mftAB$  versus WT treatment in lactose are shown in Figure 12.

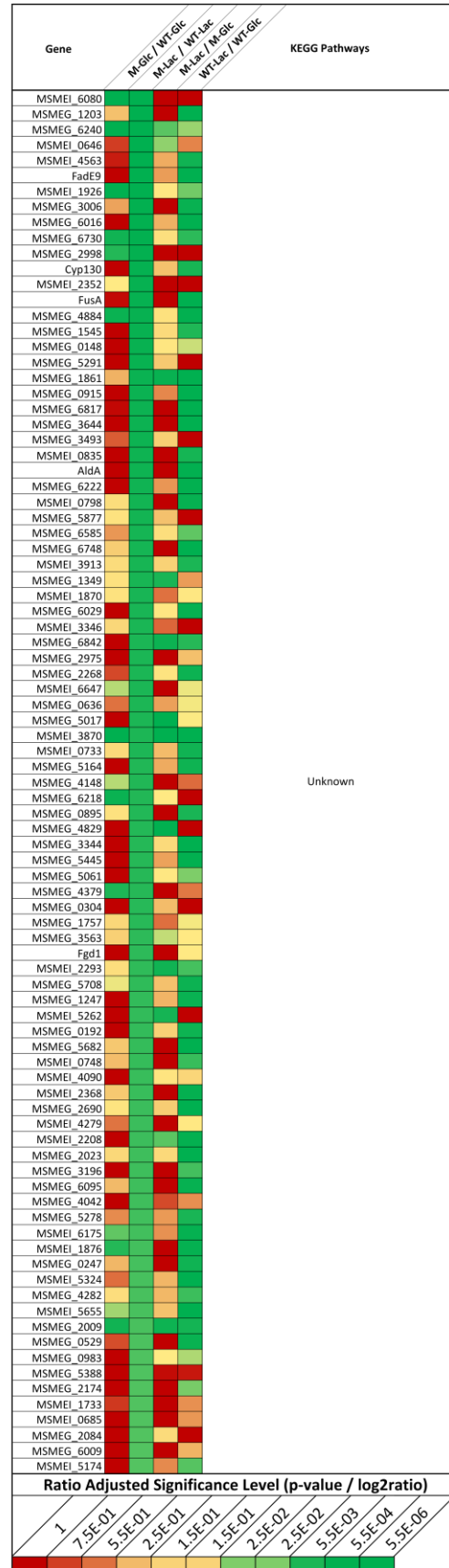


## SUPPLEMENTARY RESULTS

### The role of mycofactocin in lactate metabolism



(A)



**SUPPLEMENTARY RESULTS**  
**The role of mycofactocin in lactate metabolism**

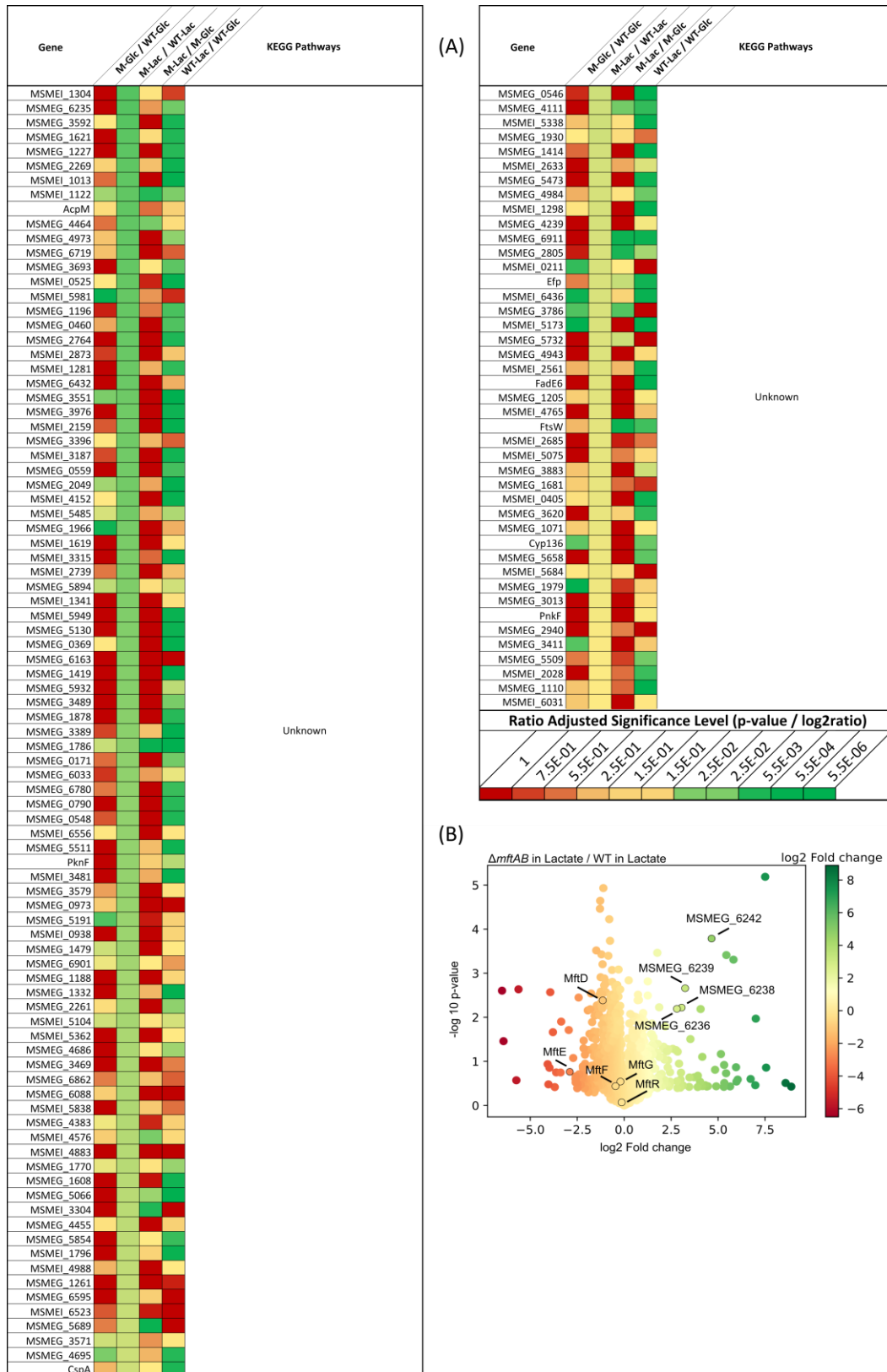


Figure 12: KEGG metabolic pathway enrichment (A) of features with ratio significance level  $<0.05$  OR annotated as MFT maturases. Lac = lactate, Glc = glucose. (B) Butterfly plot of features in lactate as sole carbon source. Statistically significant features upregulated in the mutant strain appear in the top right side of the chart.  $P$ -value calculated by two-tailed Student' t-test.

Peptides corresponding to the MFT biosynthesis pathway (Figure 12, black star) were identified as MftR (54% coverage), MftD (48% coverage), MftE (12% coverage). MftF (24%

**SUPPLEMENTARY RESULTS**  
**The role of mycofactocin in lactate metabolism**

coverage) and the putative glucose-methanol-choline dehydrogenase, tentatively annotated as MftG (28% coverage). Raw values are included in Table 2. For the *verum* experiment under lactate as sole carbon source all other values except MftD and MftR are negative, indicating upregulation in the wild-type strain, albeit not statistically significant ( $p$ -value  $> \alpha$ ).

Protein or gene	M-Glu / WT-Glu		M-Lac / WT-Lac		Putative annotation
	Log2Fold	$p$ -value	Log2Fold	$p$ -value	
MftG	-1.216	0.2884	-1.106	0.4019	Glucose-methanol-choline oxidoreductase
MftD	-1.340	0.1298	-2.204	<b>0.0041</b>	AHDP oxidase
MftE	8.117	0.3954	-2.721	0.4090	MFT peptidase
MftF	1.132	0.7956	-1.242	0.4963	MFT glucosyltransferase
MftR	2.423	0.3244	1.011	0.9662	Transcriptional regulator, TetR family protein
<i>MSMEG_6236</i>	6.308	0.01703	6.999	<b>0.00643</b>	Two-component system, regulatory protein
<i>MSMEG_6238</i>	21.181	<b>0.00016</b>	8.329	<b>0.00603</b>	Putative two-component system sensor kinase
<i>MSMEG_6239</i>	13.260	0.02160	9.487	<b>0.00220</b>	1,3-propanediol dehydrogenase
<i>MSMEG_6242</i>	25.005	<b>0.00001</b>	25.158	<b>0.00016</b>	Alcohol dehydrogenase, iron-containing
<i>MSMEG_3962</i>	-2.840	<b>0.00014</b>	1.650	<b>0.00410</b>	Lactate 2-monooxygenase

Table 2: Log2fold and  $p$ -value (2-tailed t-test) of MFT biosynthesis proteins and putative MFT-dependent dehydrogenases. Values in bold indicate statistical significance,  $\alpha = 0.01$ .

MftD, initially annotated as an MFT-dependent L-lactate dehydrogenase but later reassigned as an AHDP oxidase [181], was the only MFT biosynthetic gene showing statistically significant results upregulation (2.2-fold,  $p$ -value 0.0041) in the wild-type strain compared to  $\Delta mftAB$ . While the introduced genetic defect does not affect the integrity of the *mftD* gene, it was hypothesized that the lack of its presumed natural cofactor might result in significant upregulation in the wild-type strain. This and the lack of significant changes in the ion abundance of other peptides belonging to the MFT pathway does not allow inference of whether MFT or proteins associated with the MFT biosynthesis are upregulated in the presence of lactate as the sole carbon source. However, these results confirm that MftD is not involved in lactate metabolism as hypothesized in light of its role in MFT biosynthesis.

Interestingly, probable MFT-dependent dehydrogenases (Figure 12, white star) were found to be statistically upregulated in the mutant strain in either lactate or glucose as sole carbon source (Table 2). Statistical significance in these features is stronger compared to those associated with MFT biosynthesis (Figure 12, black star). The cluster *MSMEG\_6236* to

## SUPPLEMENTARY RESULTS

### The role of mycofactocin in lactate metabolism

MSMEG\_6242 (Figure 11) was previously found to be upregulated only in WT strains compared to  $\Delta mftC$  treated with ethanol or cholesterol:ethanol. MSMEG\_6242 was indispensable for ethanol metabolism combined with MFT [226], and *in vitro* activity was observed with purified enzymes against methanol and formaldehyde [224]. In our dataset, a 25-fold upregulation in the wild-type strain was found with strong statistical support, regardless of whether the carbon source is glucose or lactate (*p*-value 0.00001).

Taken together, the upregulation of the MSMEG\_6242 and nearby genes occur in both glucose and lactate. Our results suggests that the products of the MSMEG\_6236 to MSMEG\_6242 cluster are involved in the metabolism of both carbon sources. It is possible that these proteins are implicated in metabolic pathways, the coupling of cofactor-dependent steps to the membrane-bound electron transport chain, or in a cofactor regeneration system. Our results confirm that MftD is not an L-lactate dehydrogenase as initially suggested. MSMEG\_3962 (Figure 12, green star) was found to be upregulated in all carbon sources and independent of whether MFT was truncated or not. MSMEG\_3962 and MSMEG\_2512, the latter one found in the data set but with a significance level  $>0.05$ , are both putative L-lactate-2-monooxygenase. These enzymes catalyze the conversion of L-lactate to acetate, carbon dioxide and water [239, 240], possibly being the responsible enzymes for lactate assimilation as sole carbon source. Furthermore, MSMEG\_3962 was found upregulated in a hydrogenase *hyd2* mutant, possibly relating lactate metabolism, and scavenging of atmospheric  $H_2$  [241].

Further studies were conducted with the *mftD* gene from *M. smegmatis* (MSMEG\_1424). The gene was artificially synthesized and codon-optimized for production in an *E. coli* BL21(DE3) host. While expression in a pET28(a) vector was unsuccessful, the protein was produced in a pMAL vector as an 85.5 kDa maltose-binding protein (MBP) fusion. The crude protein lysate and purified fraction containing the recombinant protein from the MBP affinity column are shown in Figure 13A. Recombinant MftD was used to verify DL-lactate dehydrogenase activity *in vitro* with lactate and other  $\alpha$ -hydroxy acids with different number of carbon atoms (two in glycolic acid to six in 2-hydroxyhexanoic acid), as well as aromatic and indol-containing side chains. A 50 mM phosphate buffer pH 7.1 was used with 1 mM  $\alpha$ -hydroxy acid substrate, and 0.1 mM DCPIP ( $\lambda_{max}$  600 nm) as artificial redox acceptor and as a colorimetric readout for positive dehydrogenase activity as previously used [242, 243]. The reaction was initiated by adding a master mix of all components to the aliquoted enzyme. Discoloration of DCPIP was only observed with L-lactate, but not with D-lactate or other

**SUPPLEMENTARY RESULTS**  
**The role of mycofactocin in lactate metabolism**

$\alpha$ -hydroxy acids (Figure 13B). The results were compared with those from a protein extract of the same production strain transformed with the empty plasmid, MBP:LacZ, to confirm the observed activity from the insert and not the MBP tag.

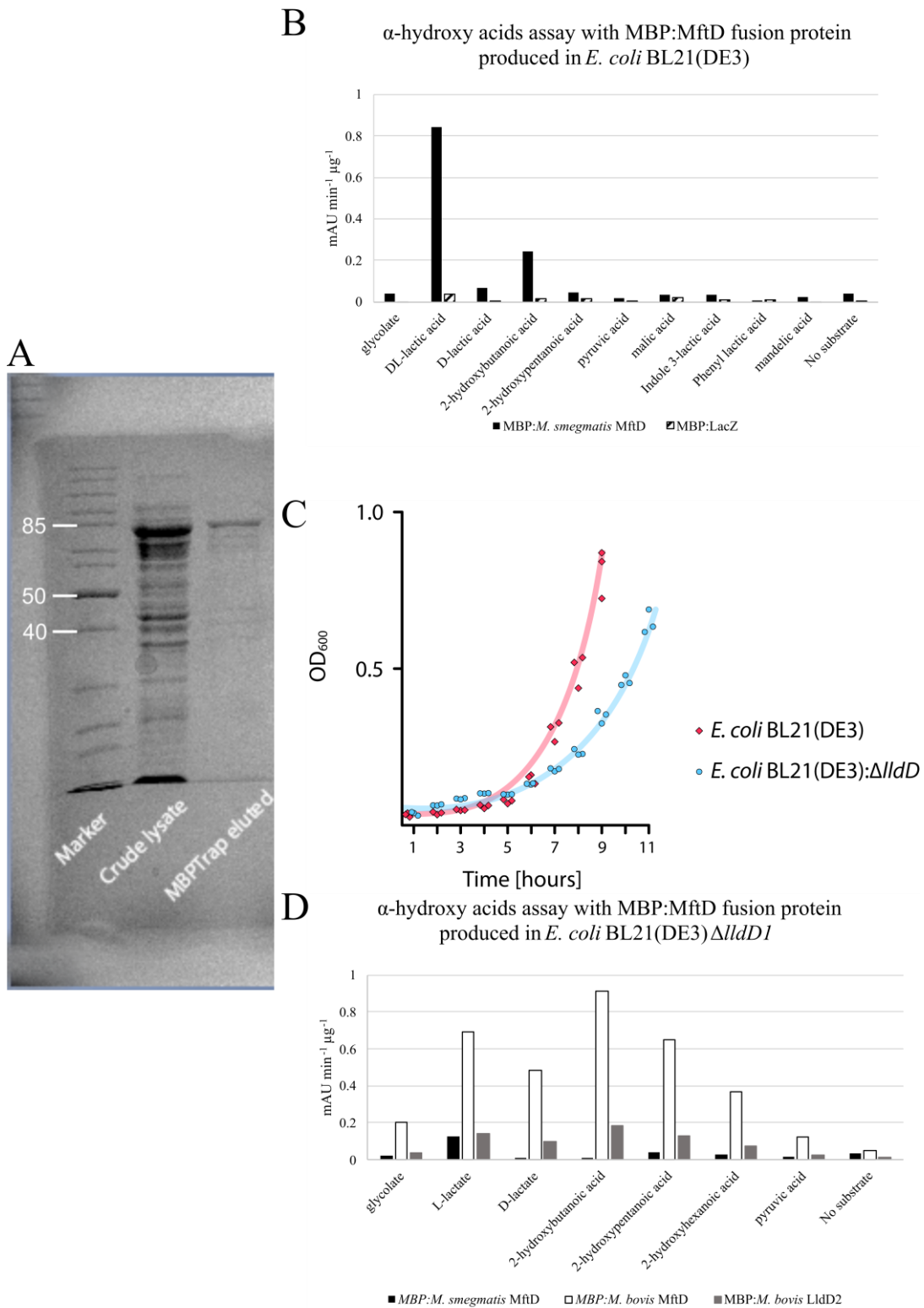


Figure 13: Lactate dehydrogenase activity of MftD. (A): purification by affinity chromatography of the MBP: *M. smegmatis* MftD fusion protein. Protein marker size units in kDa (PageRuler Unstained Protein Ladder) (B) *M. smegmatis* MftD with various  $\alpha$ -hydroxy acids and DCPIP as the final electron acceptor. (C): growth curve of the *E. coli* BL21(DE3)  $\Delta$ lldD (courtesy Dr. Daniel Braga). (D): *M. smegmatis*, and *M. bovis* MftD and LldD2 with various  $\alpha$ -hydroxy acids and DCPIP as the final electron acceptor.

## SUPPLEMENTARY RESULTS

### The enzymatic activity of MFT-dependent alcohol dehydrogenase and glucose-methanol-choline oxidoreductase

As seen in Figure 13A, following affinity chromatography MBP:MftD coelutes with other background proteins. In-gel trypsin digestion followed by mass spectrometry for peptide identification was performed [244] and identified WP\_000586962.1 (LldD2 quinone dependent L-lactate dehydrogenase) as a possible enzyme responsible for lactate metabolism. An *E. coli* BL21(DE3)  $\Delta lldD$  strain was constructed with scarless recombineering [245] to reduce the background activity. Growth was only slightly delayed in the new mutant strain with lactate as the sole carbon source in minimal media M9 (Figure 13C).

The *M. smegmatis* *mftD*-containing vector was transformed on the *E. coli* BL21(DE3)  $\Delta lldD$ . Following protein purification as before no activity with *M. smegmatis* MftD was observed. The genes MBBSGS4\_0634 (*mftD*) and MBBSGS4\_1859 (*lldD2*), encoding for possible lactate dehydrogenases in *M. bovis* BCG S4 Jena were also transformed and produced. Activity with the *M. bovis* MftD was still observed, while no DCPIP reduction was observed with LldD2 (Figure 13D). Further insights into the proteomics results, WP\_001102108.1 was also found in the *E. coli* background, encoding for the YkgE uncharacterized iron-containing protein. While LldD2 is the canonical FMN-dependent L-lactate dehydrogenase, catalyzing its oxidation to pyruvate, YkgE is part of the *ykgEFG* gene cluster. These genes are homologues of the lactate utilization cluster *lutABC* in *B. subtilis* [246] and previously involved in *E. coli* lactate metabolism. A double  $\Delta lldD \Delta ykgE$  mutant was reported to be unable to metabolize L-lactate [247]. Therefore, YkgE is inferred to be another protein involved in lactate metabolism, while MftD did not exhibit any lactate dehydrogenase activity.

### 9.2. THE ENZYMATIC ACTIVITY OF MFT-DEPENDENT ALCOHOL DEHYDROGENASE AND GLUCOSE-METHANOL-CHOLINE OXIDOREDUCTASE

To further probe the relationship between MFT and the putative MFT-dependent alcohol dehydrogenase, the gene MSMEG\_6242 was expressed in a pET28(a) vector and produced the recombinant protein heterologously in *E. coli* BL21(DE3). This gene encodes a putative MFT-dependent alcohol dehydrogenase [224, 225]. An enzymatic assay was performed, based on the oxidation of either 100 mM methanol or ethanol to the respective aldehyde. 200  $\mu$ M DCPIP or NDMA ( $\lambda_{\max}$  440 nm) was incorporated as an artificial redox acceptor and 35  $\mu$ M NAD<sup>+</sup>, NADP, FAD<sup>+</sup>, or NADH to account for possible missing secondary redox partner. The buffer employed is 50 mM phosphate buffer pH 7.2. If under the conditions of this assay alcohol dehydrogenase activity is observed, the artificial redox cofactors are then replaced with

## SUPPLEMENTARY RESULTS

**The enzymatic activity of MFT-dependent alcohol dehydrogenase and glucose-methanol-choline oxidoreductase**  
stoichiometric quantities of the putative natural cofactor MFT, in sufficient amounts for enough catalytic turnover to be measured by LC-MS.

The reaction was initiated by adding a master mix of all components to the aliquoted enzyme. While the recombinant MSMEG\_6242 was successfully produced (46 kDa, Figure 14A), no turnover was visible with NDMA in any of the conditions observed, neither with methanol nor ethanol or the addition of secondary redox partners (Figure 14B). This result contradicts the observations that MSMEG\_6242, or Mno, has alcohol methanol oxidase activity *in vitro* [224]. In this scenario, methanol is oxidized to formaldehyde, while electrons are taken up by NDMA, reducing the electron acceptor in the process. However, DCPIP reduction was observed in the presence of NADH. To query the observed oxidation of DCPIP, the assay was repeated with each component removed as a control, namely without enzyme, without substrate or without NADH (*verum*). No reaction was observed in the absence of enzyme, methanol, or ethanol. However, with NADH alone discoloration was present, indicating that reduction of DCPIP can occur from NADH (Figure 14D). Additional studies must be followed to further establish positive alcohol dehydrogenase activity of MSMEG\_6242 as it was previously reported [224, 225].

SUPPLEMENTARY RESULTS

The enzymatic activity of MFT-dependent alcohol dehydrogenase and glucose-methanol-choline oxidoreductase

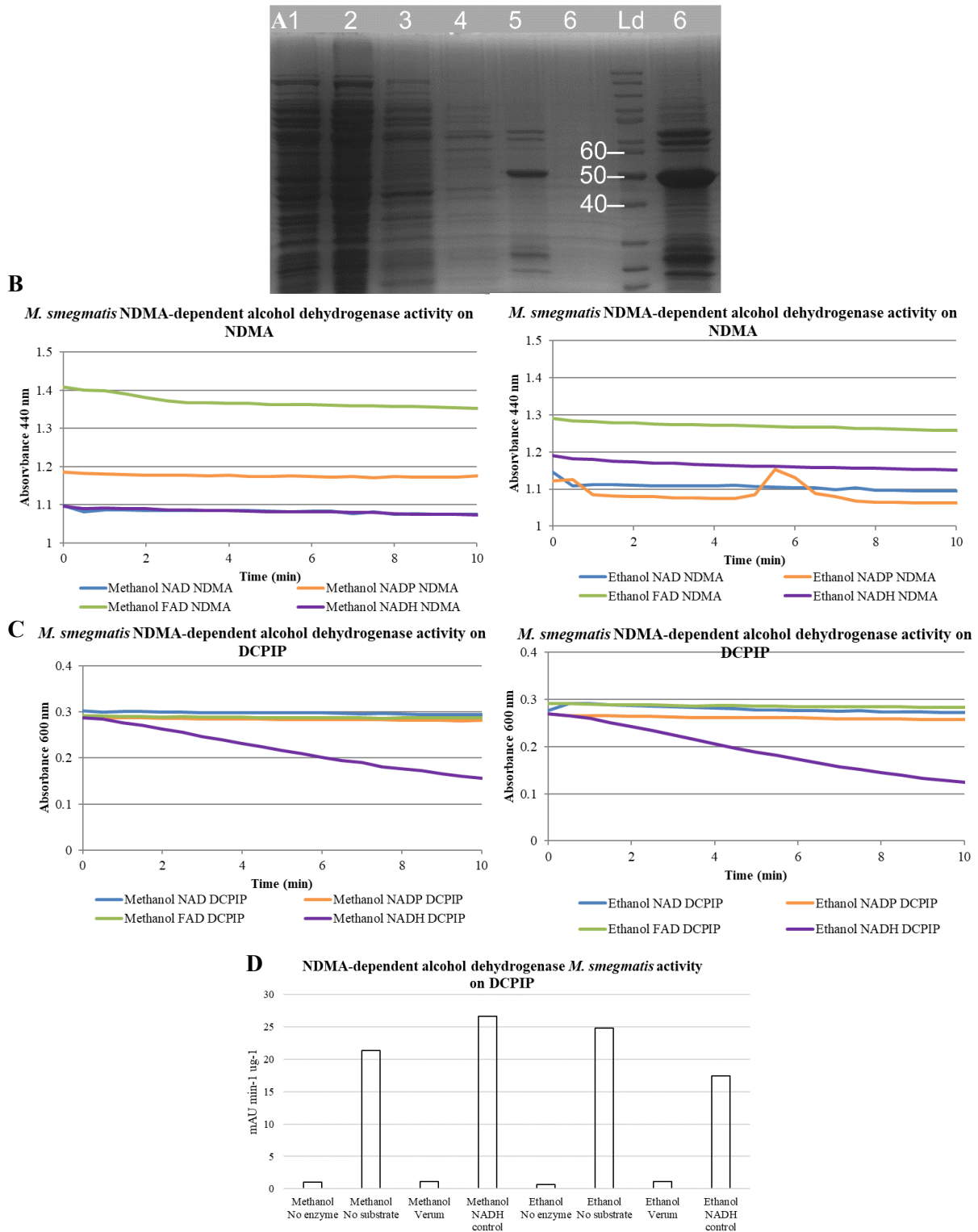


Figure 14: Production and enzymatic assay of MSMEG\_6242 in *E. coli* BL21(DE3). (A) SDS-PAGE depicting the fractions of the recombinant enzyme purification by affinity chromatography. Lane 1: crude lysate; 2: NiNTA column flowthrough; 3: 20 mM imidazole wash; 4: 50 mM imidazole wash; 5: eluted fraction with 300 mM imidazole; 6: centrifugal concentrator (MWCO 3 kDa) flowthrough; 7: concentrated protein. Protein marker size units in kDa (PageRuler Unstained Protein Ladder). Alcohol dehydrogenase oxidation with recombinant MSMEG\_6242 and NDMA (B) or DCPIP (C) as artificial redox acceptor. (D). Decoloration of oxidized DCPIP only occurs in the presence of reduced NADH.



**Process development for mycofactocin production in mineral media with supplementation**

## 9.3. PROCESS DEVELOPMENT FOR MYCOFACTOCIN PRODUCTION IN MINERAL MEDIA WITH SUPPLEMENTATION

More comprehensive studies on the biochemistry of MFT, for example enzyme kinetics and crystallography, as well as protein-ligand interactions with MFT-dependent reductases and oxidases require high quantities of the cofactor. These studies are important, for example, to determine a possible role of MFT in TB pathogenesis and dormancy, or to elucidate the interaction between MFT and the cytochrome electron transport chain. Too low quantities would lead to few catalytic cycles, which would make a response signal in the method studied ambiguous with respect to, for example, oxidation or reduction of the artificial redox cofactor mediated by background components and not the enzyme under study. An alternative would be to establish a regeneration assay, which is not straightforward and would also require further insights on the biochemistry of the cofactor.

Our studies on MFT characterization in MSMEG were performed in a shake flask or Petri dishes containing sterile filters inoculated with a preculture, then placed over solid media. This method led to low quantities of the cofactor for further studies and is cumbersome to upscale for larger yields. Large-scale production is usually performed in bioreactors, where aeration, agitation, nutrient depletion, and product formation can be monitored using online or offline analytical methods. However, as scale and biomass concentration increase, the broth rheology changes, so oxygen transfer becomes the main limiting factor. In order to increase the yield of MFT available from the wild-type MSMEG strain we performed some preliminary studies in a stirred tank reactor with posterior process characterization in shake flask with online oxygen measuring.

A higher availability of cofactors and the implementation of regeneration systems are both important steps in their large-scale commercial exploitation, particularly for enzymes such as dehydrogenases and oxidases [248]. For example, PQQ-dependent, NAD(P)-dependent, or FAD-dependent glucose oxidase/dehydrogenase are employed in glucose and alcohol sensors for monitoring in blood and food products. The cofactor is immobilized with the enzyme during production. The electrons generated by the reaction are used for an electrochemical or colorimetric response with an artificial redox cofactor or with a peroxidase, respectively [214, 249-251]. The coenzyme F<sub>420</sub> has been proposed for applications in methanogenesis and bioremediation using microorganisms, and in industrial catalysis with F<sub>420</sub>-dependent enzymes for the development and production of biopharmaceuticals and agro-industrial compounds. The availability of the cofactor was recognized as a significant barrier for commercial applications [82]. Metabolic

## SUPPLEMENTARY RESULTS

### Process development for mycofactocin production in mineral media with supplementation

engineering in the natural host was previously used to increase the F<sub>420</sub> cofactor titer, with a ten-fold increase compared to wild-type achieved by both overexpression of the biosynthetic genes *fbiABC* and increased iron and sulfur availability for the radical SAM *fbiC*, identified as the limiting step [252]. Given that MFT also involves a radical SAM-mediated MftC reaction, is hypothesized that iron and sulfur supplementation would positively affect MFT production.

While efforts are being undertaken to overexpress some of the MFT genes, wild-type MSMEG was cultivated in a 7 L STR fermenter with 3 L mineral media HdB filling volume [253] at 37°C and pH 7 under control with 100 g L<sup>-1</sup> ammonium hydroxide or phosphoric acid. Aeration was set at 0.75 L min<sup>-1</sup> (=0.25 vvm) to replicate the air supply in a shake flask through a cotton plug [254], and agitation was left to automatic control to achieve the maximum OTR possible under this aeration. In the three experiments performed under this setting, the maximum stirring rate was between 421 and 488 rpm at the OTR<sub>max</sub> point. The sole carbon source was 10 g L<sup>-1</sup> ethanol. Neither tyloxapol nor antifoam agents were applied to simplify downstream processing, which resulted in significant foam formation. As such, biomass measurements were not reliable and were omitted from the dataset. For metabolomic extraction, 25 mL broth were centrifuged, and the biomass treated in 20 mL LC-MS-grade methanol for extraction. The methanolic extract was then dried under reduced pressure, resuspended twice in LC-MS-grade water and centrifuged in each step to remove insoluble particulates and cell debris. Then, the aqueous extract was resuspended at a 1:10 ratio and 10 µL injected for LC-MS measurement as described [236, 255]. To simplify data analysis, areas were normalized to sample volume, and oxidized and reduced MFTs were summed and evaluated as one entity. This is a reasonable compromise, given that the extraction methodology is unlikely to induce degradation of the oligoglucosyl chain but might impact the extracellular redox status of MFT, biasing our results if expressed in MFT<sup>red/ox</sup> ratios.

Figure 15 describes the first experiment, the culture of MSMEG in HdB mineral media at an oxygen supply of 0.75 L min<sup>-1</sup>. An OTR<sub>max</sub> of 14.8 mmol L<sup>-1</sup> h<sup>-1</sup> was achieved at 27.8 h, followed by a 22 h plateau at ≈5 mmol L<sup>-1</sup> h<sup>-1</sup> until the carbon source was depleted (Figure 15A). At the OTR<sub>max</sub> the MFT production had increased 6× for PMFT(H<sub>2</sub>), 61× for MMFT-2b(H<sub>2</sub>), and 7× for MMFT-8(H<sub>2</sub>) compared to the base (26 h). Interestingly, the OTR<sub>max</sub> and the MFT production peak coincide with an increase in the ethanol consumption rate, observed in the slope of the ethanol trace.

## SUPPLEMENTARY RESULTS

### Process development for mycofactocin production in mineral media with supplementation

According to [256] one of the possible explanations for this plot shape is diauxic growth, fueled by the production of overflow metabolites such as acetate or lactate, only minimal amounts of acetate were observed, and no lactate was produced (Figure 15B). Another other possible explanation, as predicted from test microorganisms under various environmental stressors, is a non-carbon source limitation [256]. Because the system is pH controlled by phosphoric acid, and ammonium was added in abundance, neither phosphate nor nitrogen are expected to be the limiting factor. Therefore, it could be reasonable to correlate the depletion of a metabolite or a micronutrient with the MFT production but hampered by its lack thereof, for example additional micronutrients or vitamins.

To elucidate whether additional media components change the OTR trace, eliminates the substrate limitation phase, and increases the MFT yield, we performed two additional cultivations with HdB media supplementation. Given the previous positive results with iron and sulfur supplementation for F<sub>420</sub> overproduction without genetic manipulation [252] we decided to increase the concentration of micronutrients by adding 10× the concentration of trace elements (Section 13.1.1). Iron and sulfur supplementation (ferric ammonium citrate, ferric citrate, ferrous sulfate) was 0.1 mg mL<sup>-1</sup> per compound, in addition to 1 mM L-cysteine [252]. While the OTR<sub>max</sub> was 16.76 mmol L<sup>-1</sup> h<sup>-1</sup> at 40 h (instead of 27.8 h in the basal media without supplementation, Figure 15), the maximum MFT was achieved at 46 hours. The fold change between the base production (28 h) and this peak was 26× for PMFT(H<sub>2</sub>), 53× for MMFT-2b(H<sub>2</sub>), and 60× for MMFT-8(H<sub>2</sub>). As before, the OTR drop to <5 mmol L<sup>-1</sup> h<sup>-1</sup> was simultaneous with an increase in ethanol consumption rate. However, ethanol consumption was much slower, being depleted at 70.3 h compared to 57.5 h in the base media with standard composition of trace elements. While lactate was not observed, 0.17 g L<sup>-1</sup> acetate were produced after 10 hours in the absence of oxygen-limiting conditions (Figure 16B). However, the OTR trace does not show a plateau concurrent with diauxic growth and acetate does not accumulate, suggesting perhaps that ethanol and acetate are being co-metabolized. Additionally, at the peak of acetate production, MFT yield increased significantly, with a higher proportion of long-chain methyl mycofactocin compared to short-chain MMFT(H<sub>2</sub>) and PMFT(H<sub>2</sub>).

While the titer of MFT was increased with additional micronutrients and additional iron and sulfur, the OTR plateau previously described as a non-carbon source limitation was still there. As a next step, we proceeded to supplement the mineral media with a solution of vitamins according to Wolfe [257] and 5 g L<sup>-1</sup> amino acids (proteinogenic amino acids except for

## SUPPLEMENTARY RESULTS

### Process development for mycofactocin production in mineral media with supplementation

glutamate due to instability and tyrosine due to solubility) to evaluate if this composition removes the suspected microelement deficiency.

As before, supplementation of vitamins and amino acids had a negligible effect on  $OTR_{max}$  (16.39  $mmol L^{-1} h^{-1}$  at 40 h, Figure 17A). Due to data corruption, it was not possible to determine maximum stirring rate, but is reasonable to assume that is similar as before. The production peak at 48 h followed the  $OTR_{max}$  and the fold change between the base (32.2 h) and the peak was 5× for PMFT( $H_2$ ), 6× for MMFT-2b( $H_2$ ), and 36× for MMFT-8( $H_2$ ). Visually, foam formation was significant in this reactor from the beginning, and oxygen transfer could have been impaired. It is reasonable to suggest that vitamins and amino acids have a much higher stimulating effect on cell fitness than micronutrients, resulting in higher biomass achieved and higher foam formation. This media composition resulted in the highest acetate production (0.24  $g L^{-1}$  at 23.3 h) and similar ethanol depletion as in the base media (Figure 17B), and the highest measurement of MMFT-8( $H_2$ ), with  $1.05 \times 10^8$  arbitrary units (AU) per  $mL^{-1}$ .

With all our experiments showing a  $OTR$  peak followed by a plateau, we concluded that none of the media compositions employed solved the substrate limitation, predicted from the previously characterized trace shape under various conditions [254]. A summary of the observed process parameters and MFT formation is described in Table 3.

<b>HdB broth supplementation, oxygen-unlimited batch culture</b>	<b>Base broth 1X TES</b>	<b>1X TES 10X iron-sulfur</b>	<b>1X TES, vitamins, and amino acids</b>
<i>Figure</i>	Figure 15	Figure 16	Figure 17
<i><math>OTR_{max}</math> (<math>mmol L^{-1} h^{-1}</math>)</i>	14.58 at 27.8 h	16.76 at 53,4 h	16.39 at 39.8 h
<i>Time until ethanol depletion (h)</i>	57.5	70.3	57.35
<i>Generated acetate [<math>g L^{-1}</math>]</i>	0.10	0.17	0.24
<i><math>Premycofactocin_{max}</math> PMFT(<math>H_2</math>) [<math>AU mL^{-1}</math>]</i>	$6.92 \times 10^6$	$1.67 \times 10^7$	$5.15 \times 10^6$
<i>Methyl-mycofactocin-2<math>_{max}</math> MMFT-2b(<math>H_2</math>) [<math>AU mL^{-1}</math>]</i>	$2.0 \times 10^7$	$4.19 \times 10^6$	$1.88 \times 10^6$
<i>Methyl-mycofactocin-8<math>_{max}</math> MMFT-8b(<math>H_2</math>) [<math>AU mL^{-1}</math>]</i>	$3.54 \times 10^7$	$7.16 \times 10^7$	$1.05 \times 10^8$

Table 3: impact of mineral media supplementation on process parameters and MFT formation in MSMEG. TES = trace element solution.

SUPPLEMENTARY RESULTS

Process development for mycofactocin production in mineral media with supplementation

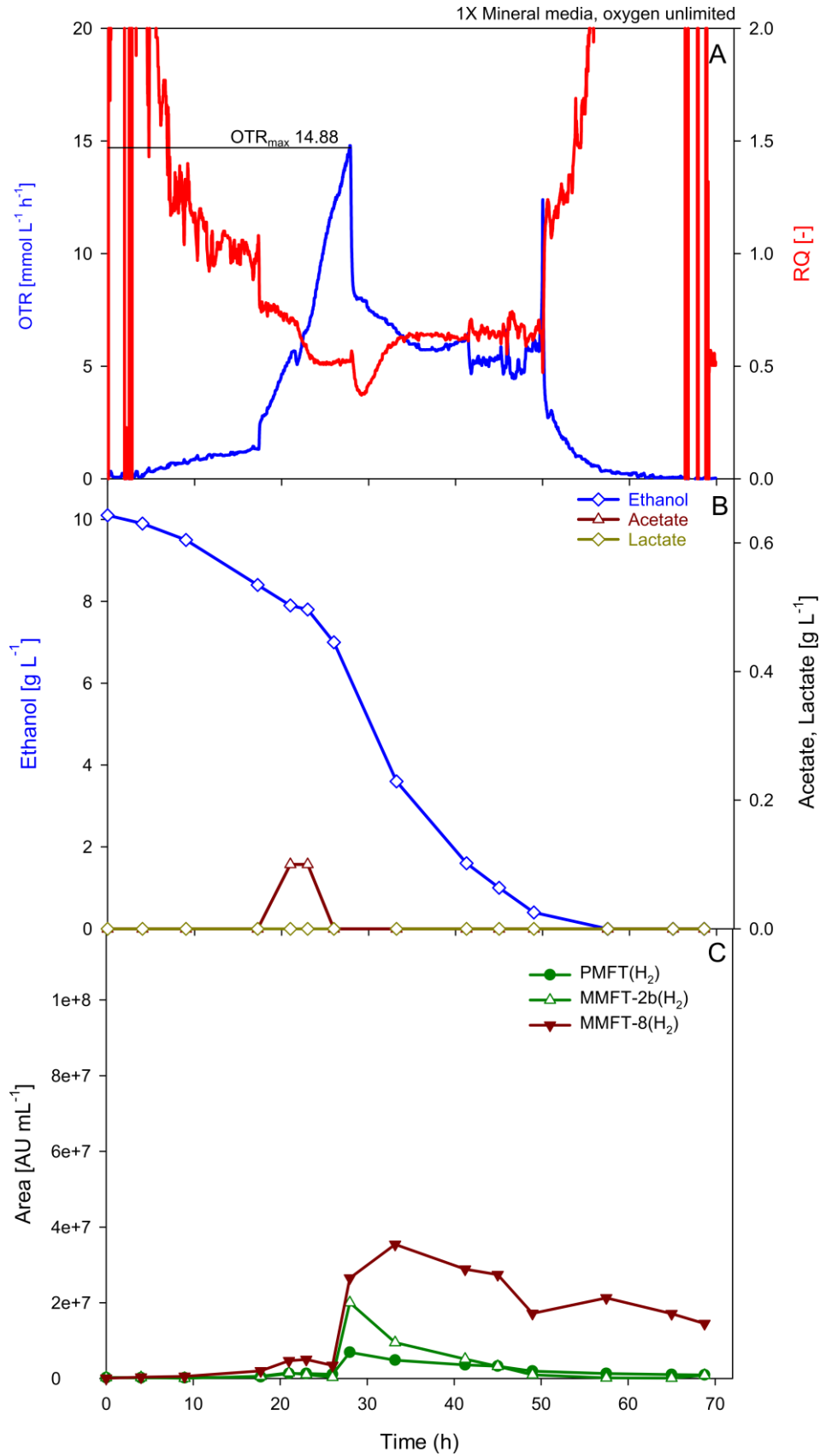


Figure 15: Oxygen-unlimited batch culture of MSMEG in a 3 L mineral media filling volume stirred tank reactor. (A) Oxygen transfer rate (OTR) and respiratory quotient. (B) Offline metabolites ethanol, acetate, lactate. (C) the peak area of MFT by the sum of reduced and oxidized species PMFT(H<sub>2</sub>), MMFT-2b(H<sub>2</sub>), MMFT-8(H<sub>2</sub>). Areas were normalized to sample volume. Experimental conditions: stirring rate = system controlled – max 488 rpm, gas flow rate = 0.75 L min<sup>-1</sup>, total reactor volume = 7 L, filling volume = 3 L, temperature 37°C, HdB medium with 10 g L<sup>-1</sup> ethanol, pH 7, controlled with 100 g L<sup>-1</sup> NaOH or H<sub>3</sub>PO<sub>4</sub>.

Process development for mycofactocin production in mineral media with supplementation

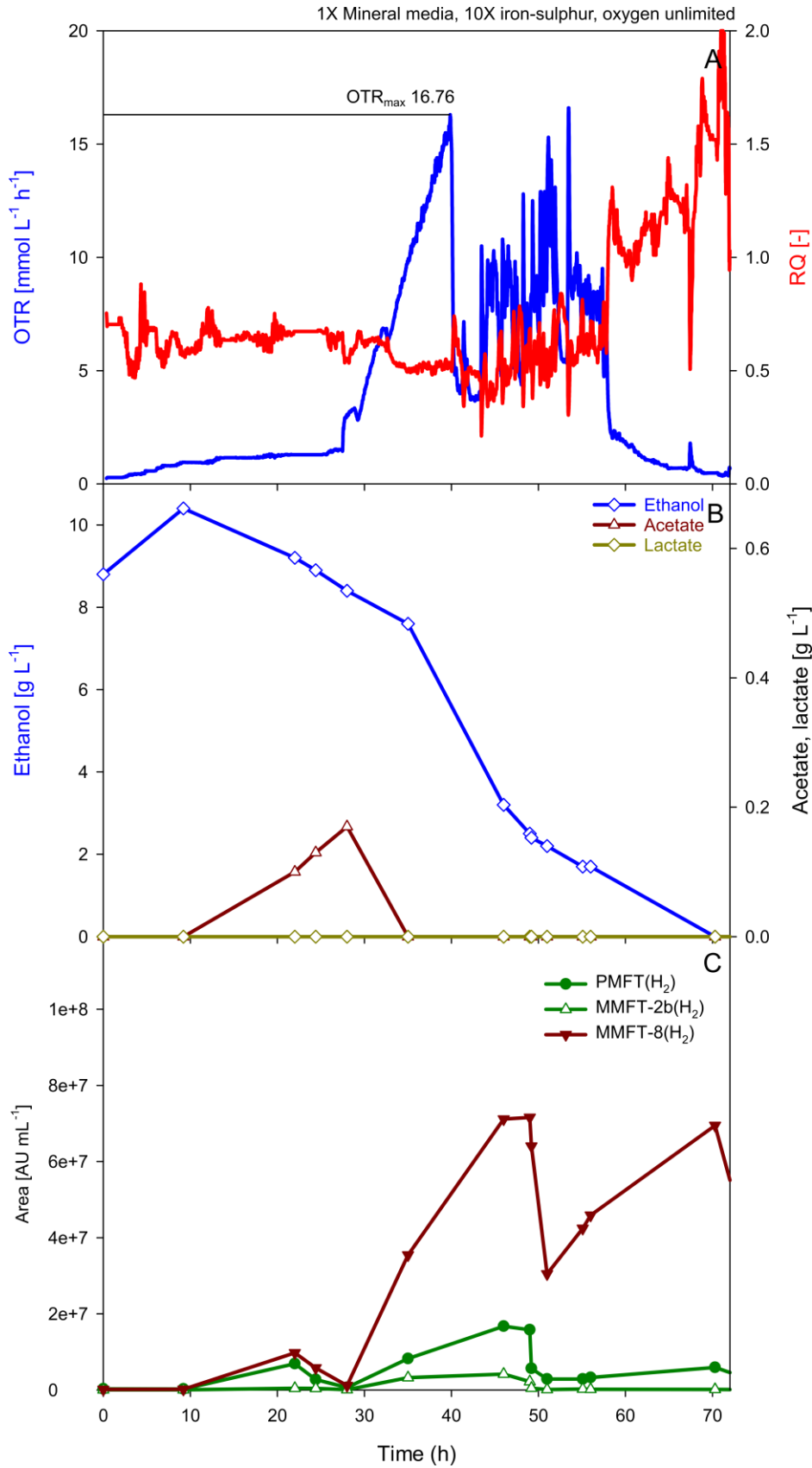


Figure 16: Oxygen-unlimited batch culture of MSMEG in a 3 L mineral media supplemented with iron and sulfur. (A) Oxygen transfer rate (OTR) and respiratory quotient. (B) Offline metabolites ethanol, acetate, lactate. (C) the peak area of MFT by the sum of reduced and oxidized species PMFT(H<sub>2</sub>), MMFT-2b(H<sub>2</sub>), MMFT-8(H<sub>2</sub>). Areas were normalized to sample volume. Experimental conditions: stirring rate = system controlled – max 421 rpm, gas flow rate = 0.75 L min<sup>-1</sup>, total reactor volume = 7 L, filling volume = 3 L, temperature 37°C, HdB medium with 10 g L<sup>-1</sup> ethanol, iron and sulfur according to text. pH 7, controlled with 100 g L<sup>-1</sup> NaOH or H<sub>3</sub>PO<sub>4</sub>.

Process development for mycofactocin production in mineral media with supplementation

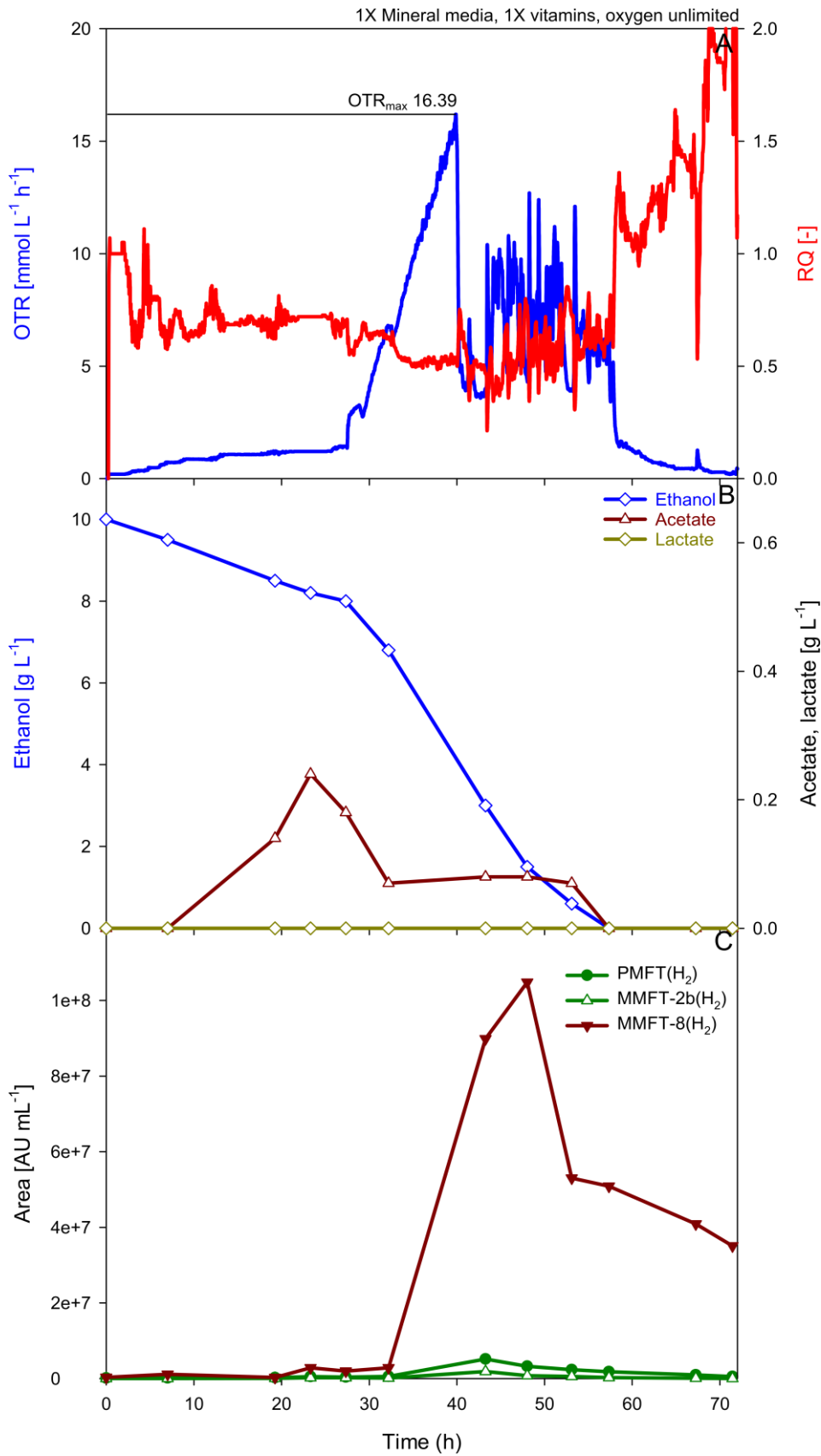


Figure 17: Oxygen-unlimited batch culture of MSMEG in a 3 L mineral media supplemented with vitamins and amino acids. (A) Oxygen transfer rate (OTR) and respiratory quotient. (B) Offline metabolites ethanol, acetate, lactate. (C) the peak area of MFT by the sum of reduced and oxidized species PMFT(H<sub>2</sub>), MMFT-2b(H<sub>2</sub>), MMFT-8(H<sub>2</sub>). Areas were normalized to sample volume. Experimental conditions: stirring rate = system controlled, gas flow rate = 0.75 L min<sup>-1</sup>, total reactor volume = 7 L, filling volume = 3 L, temperature 37°C, HdB medium with 10 g L<sup>-1</sup> ethanol, vitamins, and amino acids according to text. pH 7, controlled with 100 g L<sup>-1</sup> NaOH or H<sub>3</sub>PO<sub>4</sub>.

**Process development for mycofactocin production in mineral media with supplementation**

Uncertainties in the MFT process development in MSMEG were compounded by the general lack of information regarding the conditions for cases when the goal is a specific chemical entity. These conditions are essential to determine the importance of oxygen in the media and proper process transfer and comparability. For example, while a report on high-yield production of the coenzyme F<sub>420</sub> in wild-type MSMEG includes details about the type and operation of the STR used [258], a follow-up by other authors using metabolic engineering for the same purpose lacks information about the cultivation vessel, the filling volume, and the agitation and aeration conditions employed [252]. Other report, such as involving the production of mycolactones from *M. ulcerans*, lacks filling volume in STR conditions [259]. Furthermore, biotechnological applications are sparse with this genus. This work in STR culture of MSMEG is a substantial contribution to the field by providing a path to upscale MFT production without genetic manipulation and resulting in reproducible data that can be used for further applications [255]. Reproducibility is the key, and container geometry and shaking frequency have the largest impact on the transfer method development and upscaling [260]. However, the few biotechnological processes involving mycobacterial strains suggest the importance of oxygen transfer rates in the final product [261, 262]. For example, microbial transformation of plant-based sterols is achieved by *M. neoaurum* NRRL B-3805 in an eco-friendly, more robust process compared to chemical methods [263]. Formation of androst-4-ene-3,17-dione is promoted by high dissolved oxygen tension (>40%), while its abiotic reduction to the final product, testosterone, follows when dissolved oxygen tension reaches zero [262]. Bioremediation of vinyl chloride, a precursor to polyvinyl chloride polymers (PVC) with cytotoxic properties, has been achieved with *M. aurum* L1 with optimal oxygen concentrations of 2,5 mgL<sup>-1</sup> and inhibition occurring at air-saturated concentrations ( $\geq 7$  mg L<sup>-1</sup>) [261]. The steroid precursor biosynthesis process described by [264] incorporates microtiter plate, shake flask, and STR characterization within a volumetric oxygen transfer coefficient ( $k_L a$ ) to determine the OTR achieved. In the previously referred report on wild-type F<sub>420</sub> production [258], while foaming was reported and a second overhead impeller was used to control foam, no comparison was described. Therefore, the experiments here performed represent a source of inline data on the oxygen consumption of *M. smegmatis* with ethanol as carbon source for further biotechnological processes.



## SUPPLEMENTARY RESULTS

### Completeness of MFT extraction from complex media broths

#### 9.4. COMPLETENESS OF MFT EXTRACTION FROM COMPLEX MEDIA BROTHS

The extraction of MFT involves the recovery of biomass by centrifugation or filtration with additional washing steps, followed by extraction with 20 mL ice-cold methanol or solvent mixture (60% acetonitrile: 20% methanol 20: water 0.1% formic acid) and incubation for 1 hour at room temperature for cell lysis. The extract is then dried, and MFT is re-extracted in water from the cell debris twice. The aqueous extract is then centrifuged twice to remove particulate matter prior to LC-MS measurement [236, 255]. This protocol was implemented for speed, ease of use, and scalability. It involves two extraction steps, from biomass to the alcoholic extract using solvent and from dried extract to sample using water. The possibility that product losses occurred, either in the extraction vessel or in the cell debris pellet due to saturation in the aqueous phase was studied.

To elucidate whether significant MFT is still present in the different stages of the extraction process, we cultured wild-type MSMEG at a 10% preinoculum ratio in 150 mL LB complex media broth in a 500 mL flask ( $\varnothing$  105 mm), supplemented with 0.5 g L<sup>-1</sup> tyloxapol and 10 g L<sup>-1</sup> ethanol. Cells were cultured for 50 hours at 37°C at 200 rpm in a 25 mm throw shaker. A theoretical OTR<sub>max</sub> of 14 mmol L<sup>-1</sup> h<sup>-1</sup> was calculated [265]. Triplicate aliquots of 5, 10, and 20 mL were filtered through a prewashed 0.2  $\mu$ L regenerated cellulose filter. The filter was then placed in a centrifugal tube prefilled with cold methanol and processed as described before [255]. The dried methanolic extract was resuspended thrice in 500  $\mu$ L LC-MS water. However, unlike the published protocol, these fractions were not pooled together but treated individually (labeled as H<sub>2</sub>O 1, H<sub>2</sub>O 2, H<sub>2</sub>O 3 in Figure 18, respectively). The flask was rinsed with 500  $\mu$ L MeOH to recover unextracted MFT (MeOH wash, Figure 18), and the samples were centrifuged 10 minutes at maximum speed. The supernatant was then isolated, and the pellet from the aqueous extract was resuspended in MeOH to recover MFT from the cell debris pellet (MeOH 1, MeOH 2, MeOH 3). All samples were centrifuged at least twice to remove precipitates and resuspended in LC-MS water at a 1:10 ratio; 10  $\mu$ L were injected and measured as before [255].

Following incubation, the culture's optical density was 2.46 at 600 nm, and the dry weight was 1.15 mg mL<sup>-1</sup> (average of three replicates). In the initial protocol, the two aqueous extracts are combined for particulates centrifugation and LC-MS injection. Our results indicate that these two fractions together contain >88% of the recoverable MFT, making further extractions unnecessary. Besides, minor or no detectable MFT was found in the container vessel used for drying under reduced pressure, nor in the pellet following water extraction. The recovered MFT increases proportional to the culture volume used, which indicates that the process is

**SUPPLEMENTARY RESULTS**  
**Completeness of MFT extraction from complex media broths**

reproducible for 1 mL culture or 1.15 mg biomass per mL solvent without achieving observable saturation of the alcoholic extract.

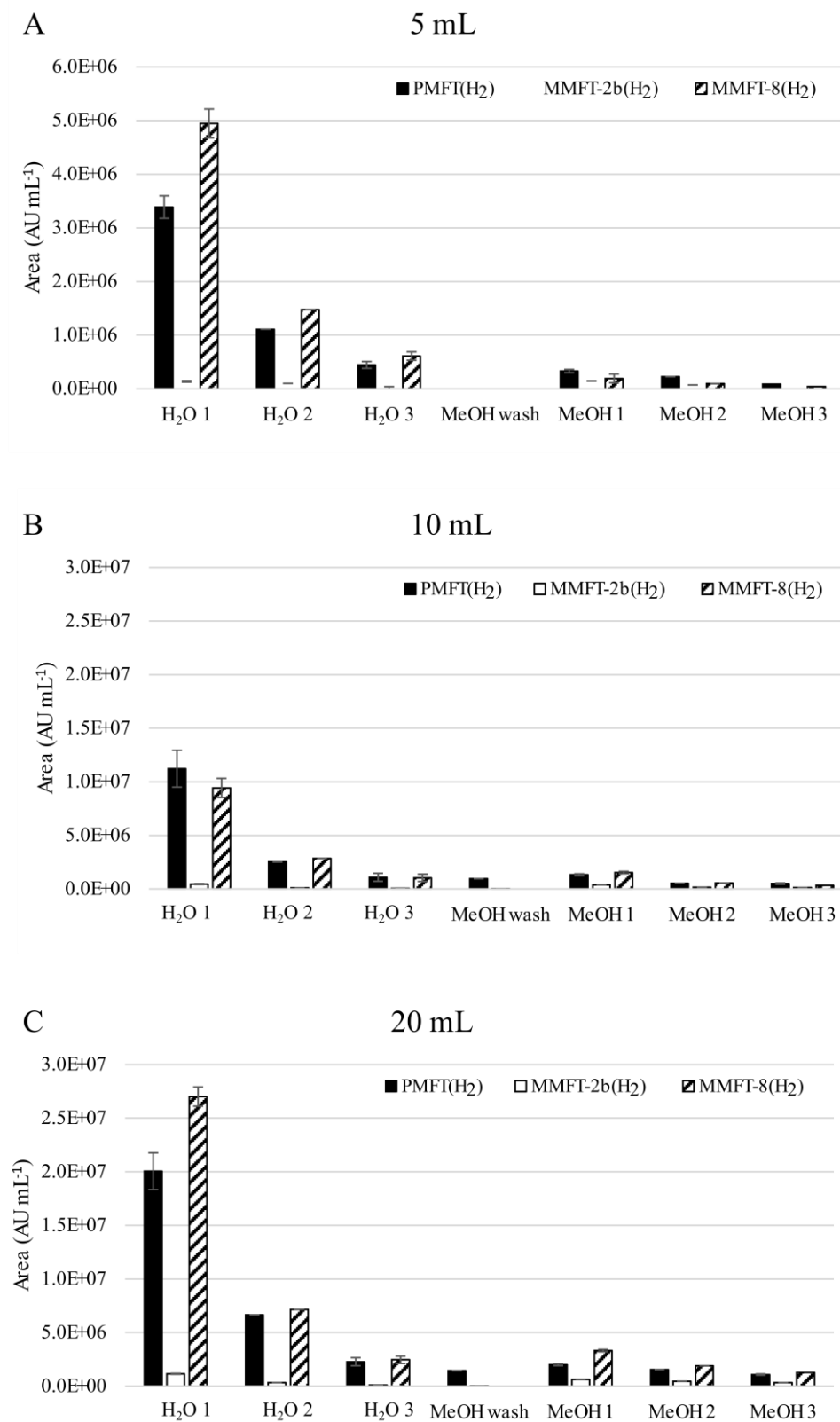


Figure 18: Estimation of the MFT yield in the different steps of the extraction process. MFT was extracted from (A): 5 mL culture; (B): 10 mL culture; (C): 20 mL culture.

## SUPPLEMENTARY RESULTS

### Completeness of MFT extraction from complex media broths

Furthermore, it was studied whether one-hour biomass incubation with methanol was sufficient to extract MFT from the biomass. For this, 5 mg of a wild-type MSMEG frozen pellet, previously cultured in complex media supplemented with 10 g L<sup>-1</sup> ethanol and oxygen-limiting conditions were used. MFT was extracted with 20 mL MeOH and left standing at room temperature, and without agitation, for 30, 60, 120 minutes, or 20 hours at 4°C. Then, the methanolic extract was dried, resuspended twice in water, and the fractions were pooled, centrifuged twice, and diluted 1:10 for LC-MS measurement. We observed that, in this case, the precursor PMFT(H<sub>2</sub>) abundance is higher compared to the long-chain MMFT-8(H<sub>2</sub>); this could be an artifact of the previous pellet storage at -20°C, resulting in glucosyl chain degradation. No discernible difference was assessed between 60 and 120 minutes, while 30 minutes resulted in half the abundance compared to 60 minutes of incubation. An overnight (20 hours) incubation resulted in product loss. These results, although performed with 5 mg frozen bacterial biomass, indicate that incubation time between 1 and 2 hours do not largely affect the amount of MFT measured, while shorter times result in an underestimation and excessively long times could result in degradation or abiotic oxidation.

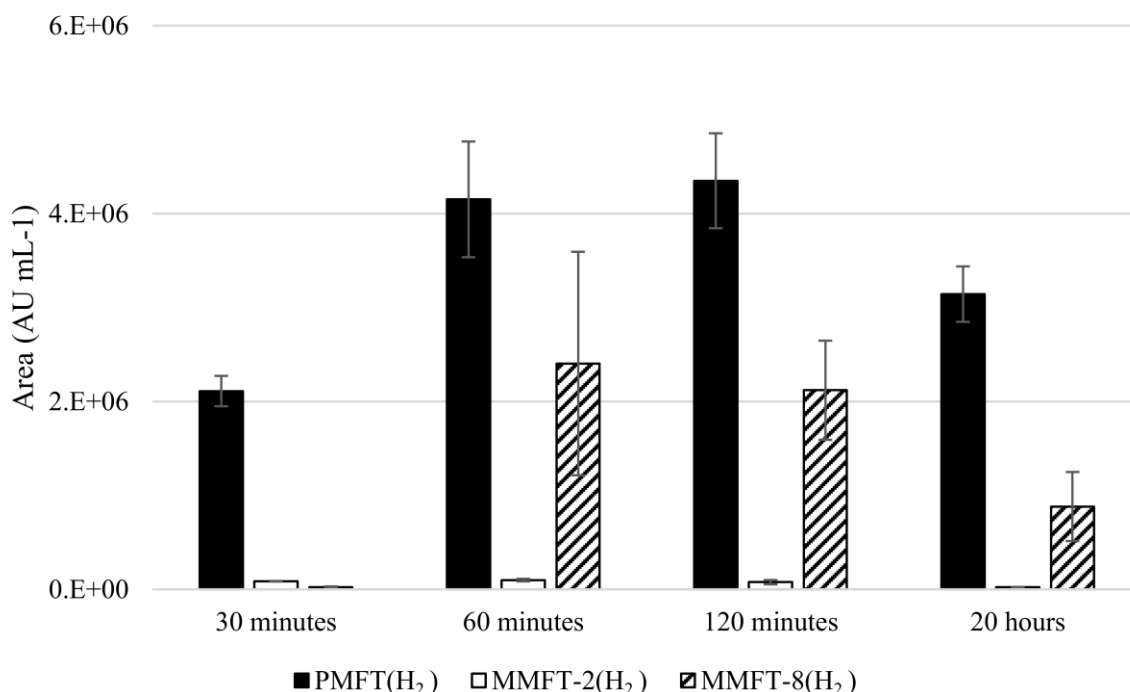


Figure 19: Impact of incubation time on the MFT yield from a 5 mg frozen MSMEG pellet.

## 10. DISCUSSION

### 10.1. STRUCTURE ELUCIDATION OF THE REDOX COFACTOR MYCOFACTOCIN

The objective of this thesis was the *in vivo* discovery of mature MFT, the role of the putative glycosyltransferase MftF and the scale-up production in a stirred tank reactor (STR). As depicted by Haft [179], the canonical MFT cluster contains the biosynthetic genes *mftABCF*, encoding the precursor peptide, chaperone/binding protein, radical SAM, and glycosyltransferase, respectively. Other genes positively associated but not universally present are *mftED* encoding an AHDP peptidase and deaminase, respectively, and putative MFT-dependent oxidoreductases. Following the *in vitro* work that characterized the gene products and reactions catalyzed by *mftABCDE* [181, 183-187], and the identification of MFT as a cofactor in the metabolism of primary alcohols [225, 226] the nature of the post-translational modification catalyzed by MftF was characterized, which led to the identification *in vivo* of previously unknown glucosylated MFT, which we consider is the mature form of the cofactor. Furthermore, genetic knockout and complementation experiments led to discovering MFT congeners and premature forms, which could be significant for the formulation of a biosynthetic pathway. Following the nomenclature for other redox-susceptible congeners, with the suffix -ol for reduced forms and -one for oxidized (for example, ubiquinol and ubiquinone), reduced molecules were termed mycofactocinol, while mycofactocinone are oxidized. [236].

We started from the observation that the core peptide of MFT is composed of the dipeptide Val29 and Tyr30 [201]. Additionally, the biosynthetic genes cluster was previously shown associated with ethanol metabolism [226]. Consequently, we cultured MSMEG in mineral media Hartmann de Bond with 10 g L<sup>-1</sup> ethanol. This media was previously used to characterize carbon assimilation in mycobacterial strains [253, 261, 266] Supplementation with 0.5 g L<sup>-1</sup> tyloxapol was done to reduce the formation of biofilms and cell clumps, which would induce different morphologies and phenotypes. However, its polymeric nature interference with the acquisition of high-quality MS spectra, especially at high *m/z*. To overcome these challenges, and while not recommended for quantitative cellular metabolite determination [267, 268], we implemented a culture technique on sterile regenerated cellulose 0.2 µm, inoculated with a liquid preinoculum, and then rinsed under sterile conditions with autoclaved water followed by vacuum filtration to remove culture broth traces. Incubation and metabolite extraction from the biomass lawn with cold solvent mixture allowed us to recover MS-compatible metabolites without salt or tyloxapol interference [269].

## Structure elucidation of the redox cofactor mycofactocin

To isotopically enrich Val and Tyr peptides/proteins and facilitate the identification of MFT congeners by HR-LC-MS, we incorporated  $^{12}\text{C}_5$ -Val and  $^{12}\text{C}_9$ -Tyr, or the isotopically enriched  $^{13}\text{C}_5$ -Val and  $^{13}\text{C}_9$ -Tyr. The previously identified mycofactocin intermediates AHDP (predicted  $m/z$   $[\text{M}+\text{H}]^+$  235.14411), PMFT (predicted  $m/z$   $[\text{M}+\text{H}]^+$  234.11247), and PMFTH<sub>2</sub> (predicted  $m/z$   $[\text{M}+\text{H}]^+$  236.12812) were identified as molecules with a +13.04362 Da mass shift compared to the unlabeled isotopologue, indicating full incorporation of the labeled amino acid ( $^{13}\text{C}_{14}$ ) minus  $\approx 1$  Da from MftC-mediated Tyr oxidative decarboxylation [183, 184]. After identifying the MFT intermediaries, we performed MS/MS acquisition and molecular networking in GNPS [270] to identify novel MFT intermediaries (Figure 20). The results were visualized and annotated in Cytoscape [271]. The features matching the PMFT (observed  $m/z$  234.1121,  $\Delta 1.5$  ppm) and PMFTH<sub>2</sub> (observed  $m/z$  236.1278,  $\Delta 1.3$  ppm) were located in *M. smegmatis* metabolome samples cultured in ethanol as sole carbon source (red node) and separated by a mass difference of 2.021 Da, which can be explained as the two electrons involved in a redox exchange ( $\text{H}_2 = 2.0151$  Da). The PMFTH<sub>2</sub> feature is connected with a novel congener,  $m/z$  398.1805, by a mass difference of 162.052 Da. This value can be attributed to the incorporation of a single hexose moiety ( $\text{C}_6\text{H}_{12}\text{O}_6 - \text{H}_2\text{O} = 162.0529$  Da). Since the precursor is PMFTH<sub>2</sub>, the resulting ion must be reduced as well. As such, this product was termed MFT-1H<sub>2</sub> (predicted  $m/z$   $[\text{M}+\text{H}]^+$  398.18095,  $\Delta 1.9$  ppm), the first mature MFT congener containing a hexosyl moiety discovered *in vivo*. Tandem liquid chromatography-mass spectrometry (LC-MS/MS) with *in silico* prediction of product ions indicated that the glycosylation occurred on the phenyl moiety of PMFT, a relatively uncommon position for *O*-glycosylation in peptides.

PMFTH<sub>2</sub> was also found networked with an unknown  $m/z$  225.1487 by a 10.958 Da edge. We were unable to assign an annotation to this feature. We concluded that it is not MFT-related because it is only present in *M. smegmatis* metabolomic extracts in glucose (green node), and it is not labeled, *i.e.*, do not arise from  $^{13}\text{C}$ -TyrVal. Furthermore, the retention time is 10.5 minutes, while the other putative mycofactocins range from 5.5 to 7.2 min. Upon close analysis of the MS/MS spectra, it reveals an  $m/z$  107.0858 peak, which could be the reason for the positive clustering. Later updates in the GNPS database analysis revealed that this feature was annotated as 5-(6-methyl-7-oxooctyl)furan-2(5H)-one (predicted  $m/z$   $[\text{M}+\text{H}]^+$  225.14852).

## Structure elucidation of the redox cofactor mycofactocin

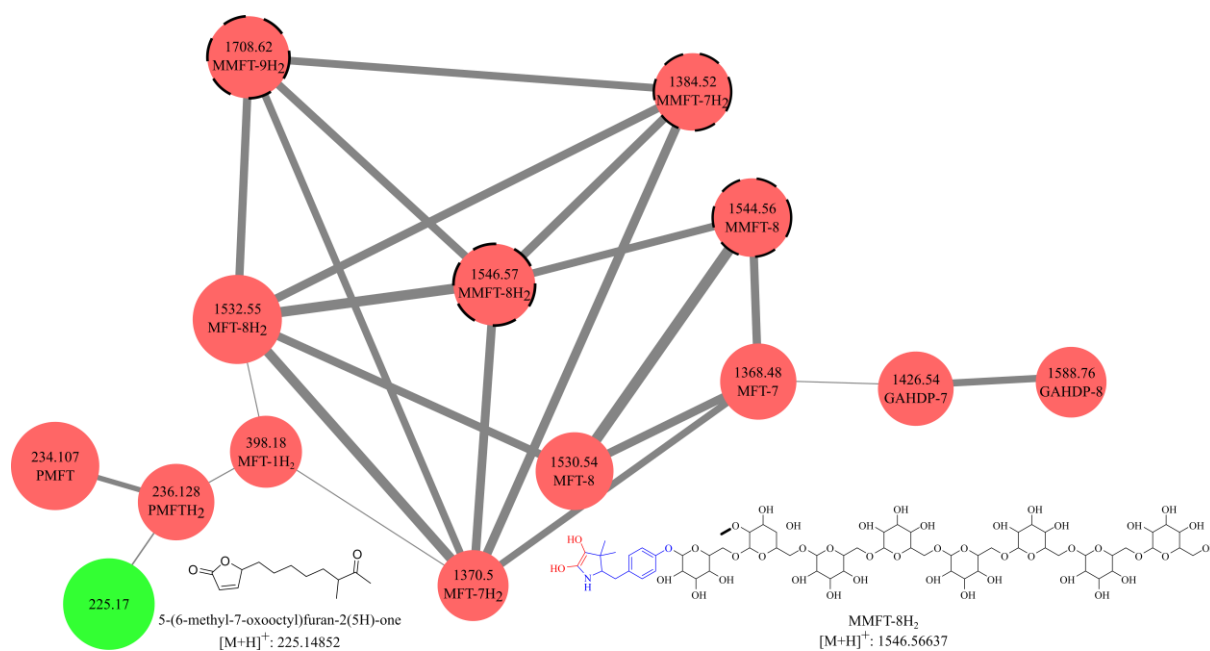


Figure 20: Molecular networking of mycofactocin, generated with GNPS [270] and data visualization by Cytoscape [271]. Nodes are colored based on the carbon source in the culture media, red in ethanol and green in glucose. Edge thickness represent the cosine score, a value of how identical the spectra are. As a representative mycofactocin, MMFT-8H<sub>2</sub> structure is indicated with redox core atoms and bonds in red with the premycofactocin (PMFT) precursor in blue. Position of the methyl moiety in 2-*O*-methylglucose in bold.

With the discovery of MFT-1H<sub>2</sub>, we set up to determine the existence of other MFT molecules that were not identified in the first analysis. An initial network generated with settings for high-resolution Orbitrap instruments (precursor ion mass tolerance and fragment ion mass tolerance = 0.02 Da) resulted in a network with four nodes: PMFT, PMFTH<sub>2</sub>, MFT-1H<sub>2</sub>, and the aforementioned 225.17 feature. Using the default settings (precursor ion mass tolerance = 2 Da and fragment ion mass tolerance = 0.5 Da) we decreased stringency, a key parameter to identify long-glycosyl chain MFTs. While mass accuracy may be lower for ions at higher  $m/z$  values, top-down (without enzymatic digestion) analysis of glycosyl chains is diffculted by higher lability in electrospray ionization of *O*-glycosidic bonds as the one described here [272] and of the glycosidic linkages between each hexose [273, 274]. Therefore, MS/MS results in more characterizable product ions from the aglycon and short-chain MFT rather than from mature long-chain MFT.

The mass difference between MFT-1H<sub>2</sub> and its two connected nodes,  $m/z$  1370.50 and  $m/z$  1532.55 are both a multiple of 162.0529, indicating six and seven incorporations, respectively. Therefore, accounting for the initial glycosyl moiety, these two ions are termed MFT-7H<sub>2</sub> and MFT-8H<sub>2</sub>, respectively. Interestingly, while some ions incorporate multiples of  $m/z$  162, the most intense ions are multiple of  $m/z$  176, corresponding to a hexose and methyl group (162 Da + 14 Da). Tandem mass spectrometry of methyl mycofactocin (MMFT-*n*), later verified by nuclear magnetic resonance (NMR)-based structural elucidation identified the hexose

**Structure elucidation of the redox cofactor mycofactocin**

incorporation as a glucosyl moiety linked by  $\beta$ -1-4 glycosidic bonds and confirmed a monomethylation in the second sugar group and its second hydroxyl moiety, 2-*O*-methylglucose. An orthogonal confirmation was obtained by performing enzymatic digestion of long-chained MFT (MMFT-7) by two possible exogenous, commercial glucosyl hydrolases with different stereoselectivity:  $\alpha$ -amylase (specific for 1,4- $\alpha$ -D-glycosidic bond) and cellulase (specific for 1,4- $\beta$ -D-glycosidic bond). The nature and importance of this post-translational modification in the context of other cofactors is discussed in a subsequent section.

An ion matching the prediction of MFT-7 was connected to a three-member network with an  $m/z$   $\Delta$ 58.08. A glycyly moiety could explain this mass difference. In the MFT precursor MftA, the core dipeptide Val29, and Tyr30 are preceded by Gly28. Isotopic labeling with  $^{13}\text{C}_2$ -Gly and gene knock-out studies allowed us to conclude that these ions correspond to premature cleavage products of MftA, following MftC processing. We termed this product glycyly-AHDP (GAHDP), possibly arising from an unspecific peptidase cleaving the dipeptide Cys28-Gly29. Because it originates from an MFT species with seven glucosyl moieties, this new feature is termed GAHDP-7; a similar feature with a  $\Delta m/z$  of 162 could be identified as additional glycosylation to form GAHDP-8. Observing the existence of glycosylated GAHDP (GAHDP-*n*), we hypothesized that the glycosylated precursor AHDP (AHDP-*n*) could exist as well. A manual search with the predicted mass-to-charge ratio for the possible AHDP-1 (predicted  $m/z$   $[\text{M}+\text{H}]^+$  397.19693), up until and including AHDP-10 (predicted  $m/z$   $[\text{M}+\text{H}]^+$  1855.67236) congeners confirmed their existence, albeit in minimum amounts. The low ion abundance explains the lack of data-dependent MS/MS spectra required for molecular networking and their absence in the network.

The main genes involved in MFT biosynthesis and maturation, *mftC-F*, were knocked-out individually to probe the relationship between gene expression and accumulation of the MFT congeners. Then, metabolomic extracts were produced as before and analyzed by LC-MS. The ion intensity was compared to that in an extract from wild-type. Figure 21 shows the biosynthetic model leading to the formation of glycosylated MFT and short-chain intermediates. The color-code relates to the mutant/wild-type ratio.

As expected, the inactivation of the radical SAM enzyme MftC diminished or eliminated the formation of all measured products, confirming that the radical SAM-mediated decarboxylation and cyclization is the first step in the biosynthetic pathway. Similarly, all glucosylated products (AHDP-*n*, GAHDP-*n*, MFT-*n*, MMFT-*n*) were downregulated in a

## DISCUSSION

### Structure elucidation of the redox cofactor mycofactocin

glycosyltransferase-deficient *ΔmftF* mutant. Furthermore, the mature forms of MFT, both methylated and nonmethylated, are downregulated by any biosynthetic gene inactivation. Interestingly, AHDP is still synthesized in slightly higher amounts in an *ΔmftE* mutant when compared to WT. The deletion of the AHDP oxidase gene *mftD* induced the accumulation of AHDP, a logical outcome resulting from PMFT biosynthesis blockage.

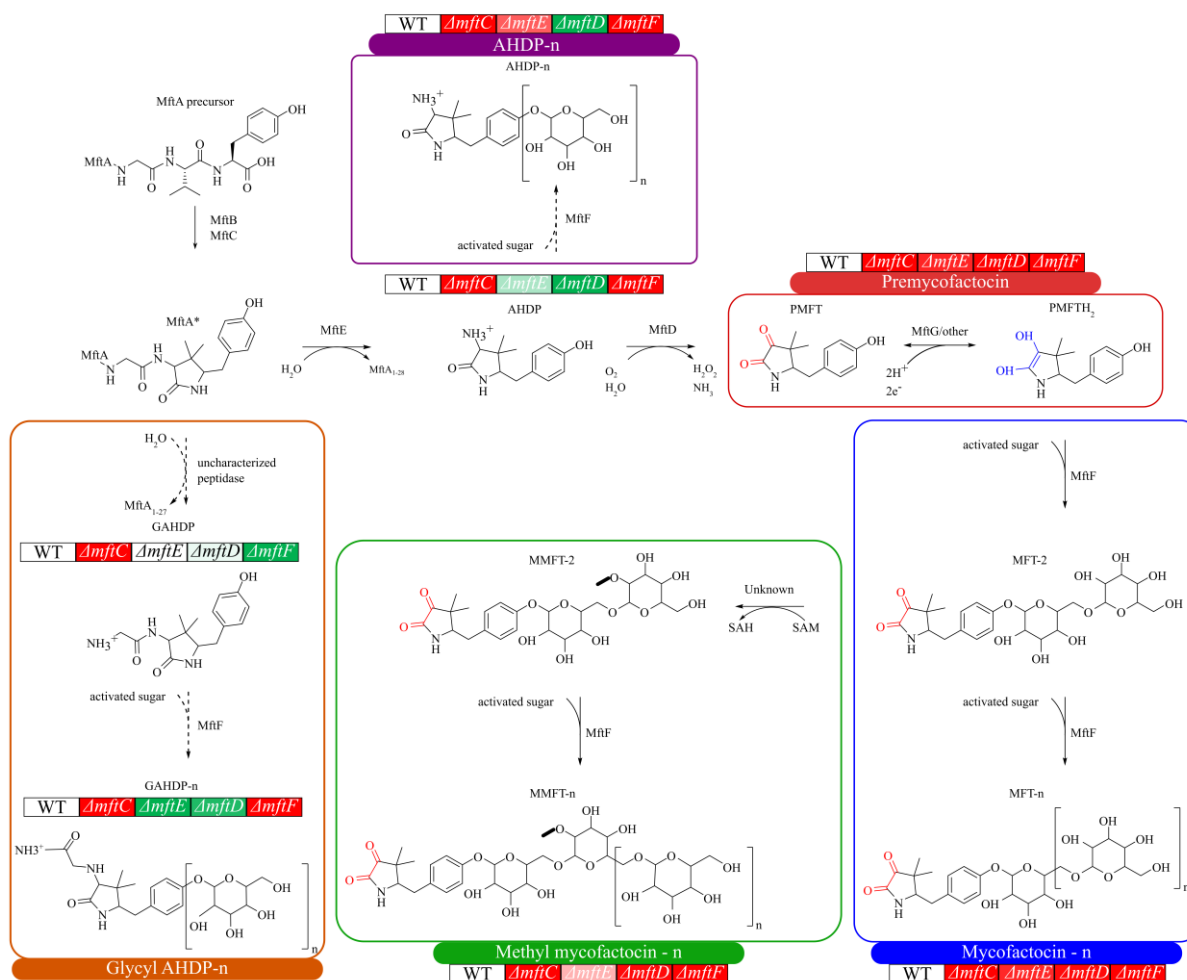


Figure 21: Mycofactocin and methylmycofactocin biosynthesis. Dashed lines indicate side-reactions. Atoms and bonds in the redox active moiety are highlighted in red (diketone) or blue (dihydroxyl). A bold bond indicates methyl moieties. Relative abundance mutant strains *ΔmftC*, *ΔmftE*, *ΔmftD*, or *ΔmftF*, is shown in color scale: white: wild-type, red: lower abundance than in the wild-type, green: higher abundance than in wild-type. SAM: S-adenosylmethionine. SAH: S-adenosylhomocysteine. NDP: nucleotide diphosphate.

In the wild-type strain and in low quantities compared to MFT-n and MMFT-n, GAHDP accumulates in an *ΔmftE* mutant. This is consistent with the existence of an uncharacterized peptidase that cleaves the Cys28-Gly29 bond in MftA\*. Furthermore, AHDP is accrued when *mftD* is truncated. The accumulation of glycosylated AHDP-n and GAHDP-n in this mutant indicates that PMFT, AHDP, and GAHDP are sugar moieties acceptors. These moieties could suggest a different biosynthetic order than the one proposed by other researchers [201], as described below (Section 10.3).



**Mycofactocin glucosyltransferase catalyzes an unusual O-glucosylation of a modified N-terminal tyrosine**

By virtue of the glucosyl chain discovered here, we can consider this as the tail moiety of MFT, in a similar vein as the charged polyglutamyl tail of coenzyme F<sub>420</sub>, or the AMP handle for ATP or NAD(P)<sup>+</sup>, or the isoprenyl chain of certain quinones (Figure 4). As previously mentioned, cofactor polyglutamylation and chain length are related to substrate and cofactor binding affinity in the corresponding enzyme and results in different enzymatic kinetics. Experimentally, this conclusion was reached by combining kinetic analysis, requiring a high yield of F<sub>420</sub> produced in a recombinant overproducer *M. smegmatis* strain and heterologously-produced F<sub>420</sub>-dependent oxidoreductases, combined with *in silico* structural studies of publicly available oxidoreductases crystal structures [99-101]. It is possible to suggest that the glucosyl tail of MFT is also related to the modulation of activity and substrate turnover, with additional variability across taxa.

## 10.2. MYCOFACTOCIN GLUCOSYLTRANSFERASE CATALYZES AN UNUSUAL O-GLUCOSYLATION OF A MODIFIED N-TERMINAL TYROSINE

Glycosyltransferases (GT) are enzymes that couple nucleotide monophosphate (NMP) or nucleotide diphosphate (NDP) sugar moieties to an acceptor molecule. Glycosyltransferases are part of nature's chemical arsenal for chemical diversity of proteins, lipids, and secondary metabolites, further exemplified by a relative donor and acceptor molecule promiscuity. In natural products and novel therapeutic proteins and antibodies, glycosylation can influence and improve physicochemical properties that determine its druggability [275, 276].

Most nucleotide-active sugars are in an  $\alpha$ -anomeric form, but the product has a  $\beta$ -anomeric configuration. This configuration is termed "invertin." Maintaining the stereochemistry from donor moiety to product is termed a "retaining" configuration [277]. Structurally, a limited set of three-dimensional folds have been observed, termed from GT-A to GT-D, associated with either an invertin or retaining mechanism; no correlation between fold type and bond mechanism has been identified [278, 279]. In eukaryotes, glycosylation is a common phenomenon associated with protein folding and stability, metabolism regulation, and cell-to-cell adhesion [280]. For prokaryotes, glycosylation is the process through which many cell wall polymers are produced, as well as extracellular structures involved in adherence, auto aggregation, biofilm formation, and pathogenesis [281]. Besides structural glycosylation, prokaryotic protein glycosylation has been acquired notoriety for potential relevance in pathogenic genera such as *Campylobacter* sp., *Helicobacter* sp., *Haemophilus* sp., among others [282]. Interestingly, only 10 NDP-active sugars are substrates for most eukaryotic glycosylation pathways, while prokaryotic glycosylation is much more diverse [283, 284].

**Methylated mycofactocin and the biosynthetic order of mycofactocin production**

The glycosyltransferase MftF is annotated as a GT-A fold-containing GT superfamily 2 [285]; this superfamily involves GTs with an inverting mechanism that is involved in the synthesis of  $\beta$ -linked polysaccharides such as cellulose, chitin, and hyaluronan with a UDP-activated donor monosaccharide [279, 286-288]. Our group confirmed that in MSMEG MftF encodes a MFT glycosyltransferase, catalyzing the transfer of up to nine glucosyl residues to PMFT(H<sub>2</sub>) in a  $\beta$ -1,4 configuration. We also observed the existence of the glycosylated precursor AHDP and glyceryl-containing AHDP (GAHDP). Their presence in a *ΔmftE* indicates that PMFT, AHDP, and GAHDP are suitable acceptors for the glucosidic chain [236]. Nuclear magnetic resonance-based structural elucidation of a methylated MFT, MMFT-8, indicated that the glucosidic chain is located in the phenyl moiety of the decarboxylated tyrosine.

While *N*-glycosylation of serine and threonine residues is the most common protein glycosylation pattern, *O*-glycosylation is more common in glycosylated natural products biosynthesis. *C*- and *S*-glycosylation are less frequent motifs in nature [275, 289-291]. Tyrosine glycosylation is, however, a relatively rare case. It was first observed in insect and rabbit tissue, where it was suggested to serve as a tyrosine reservoir mechanism during development [289, 292-294]. Another *O*-glucosyl tyrosine residue found in nature is the S-layer protein SpA of the Gram-positive bacterium *Paenibacillus alvei* [289]. *Yersinia ruckeri*, the causative agent of enteric redmouth disease in farmed and free-living fish, encodes a virulence factor in a protein complex termed antifeeding prophage (Afp). A glycosyltransferase domain in Afp was found responsible for non-reversible tyrosine glycosylation and inactivation in zebrafish embryos of RhoA, a GTPase essential for cytoskeleton organization [295].

In addition to the aforementioned *in vivo* events, glycosylation of phenolic molecules has been performed by chemical synthesis to improve physicochemical properties of potential therapeutic peptides [296]. Our results indicate that MftF is another example of *O*-glucosidation on the phenyl moiety of the modified Val29-Tyr30 dipeptide present in PMFT(H<sub>2</sub>). Therefore, MFT is a new addition to the large group of glycosylated natural products [275].

### 10.3. METHYLATED MYCOFACTOCIN AND THE BIOSYNTHETIC ORDER OF MYCOFACTOCIN PRODUCTION

To our surprise, we found that the most abundant glycosylated MFT showed methylation in one of the glycosidic residues. Enzymatic digestion with cellulase ( $\beta$ -1,4-glucanase) enriched a compound that we termed MMFT-2b, decorated with two glucose moieties and one methyl

**Methylated mycofactocin and the biosynthetic order of mycofactocin production**

group, indicating that the glycosidic bond between MFT-1 and MMFT-2 cannot be hydrolyzed, possibly because of the presence of the methyl moiety. The methylation position on the second glucose was confirmed by NMR-based structural elucidation [236].

Methyltransferases catalyze the transfer of a methyl group from a donor to an acceptor atom. Most methyltransferases use SAM as a donor group, releasing SAH in the process, however simple donors such as methanol or complex such as methylcobalamin or methyltetrahydrofolate are involved [297]. Methylation is commonly associated with epigenetic gene regulation by modulating histone tails' uncoiling (catalyzed by methylamines), while natural products methyltransferases are involved in methanogenesis in Archaea, cell components biosynthesis, and of secondary metabolites such as pigments and signaling molecules [297, 298]. Three structurally-distinct classes have been characterized: type I (classic Rossmann type with seven strands twisted in a  $\beta$ -sheet structure), class II (shorter  $\beta$ -sheets composed by strands forming various turns and loops, characterized by the SET domain), and class III (transmembrane). Class II is associated only with histone lysine methylation [298], and class III with cobalamin and C-terminal cysteine residues of signaling molecules [299, 300]. Oxygen is the most common acceptor atom for half of the known enzymes in this clade, followed by amine, thiosulfoxide, and halide moieties [298].

Methylglycosylations, where the acceptor atom is a sugar group, are uncommon modifications present in bacteria, fungi, algae, plants, and in some worms and molluscs. As a tailoring modification it is involved in methylation of cell wall and membrane glycopeptidolipids and lipopolysaccharides; few natural products are described with this moieties [299]. As being part of the cell surface, methylated glycans could be epitopes for recognition by innate immune mechanisms [300]. Most of the knowledge in methyltransferases acting on sugars comes from mycobacterial strains. *M. smegmatis* contains a large number of open reading frames annotated as methyltransferases involved, among others, in the biosynthesis of polymethylated polysaccharides (PMPS), which form complexes with long-chain fatty acids during fatty acid metabolism [66] and mycolic acid biosynthesis [301]. Two classes of  $\alpha$ -1,4 PMPS have been identified, methylglucose polysaccharides (MGPL) containing between fifteen and twenty units of unmethylated glucose and 6-*O*-methylglucose. The non-reducing end is capped with 3-*O*-methylglucose, and some methylglucose moieties are branched and contain acetate, propionate, or isobutyrate. MGPL are only present in the slow-growing, more pathogenic group mycobacteria. At the same time, the fast-growing species also possess methylmannose polysaccharides (MMP), ten to thirteen unbranched

**Methylated mycofactocin and the biosynthetic order of mycofactocin production**

3-*O*-methylmannoses with an unmethylated mannose at the non-reducing end, and a methyl aglycon capping the reducing end [302]. In addition, other methylated components in the mycobacterial cell envelope are glycopeptidolipids (GLPs), comprised of a long methoxy fatty acid chain, an acetylated tripeptide amino alcohol (D-Phe-D-*allo*-Thr-D-Ala-L-alaninol), and methylated rhamnose in several positions. It was shown that several methyltransferases encoded by *mtf* genes are involved in the methylation of rhamnose, first 3-*O*, then 4-*O*, followed by 2-*O*-methyl rhamnose [66, 303, 304]. Furthermore, the association of glucose or mannose-based PMPS with fatty acids for cell membrane conformation could point towards a similar binding affinity of MFT and MFT-dependent enzymes with membrane or cell wall components for anchoring or preventing extracellular diffusion. The methylation of the second glucosyl moiety is highly puzzling. It could be related to a novel, not-yet-characterized mycobacterial 2-*O*-glucosyl methyltransferase involved in the biosynthesis of MFT. From our enzymatic characterization, the fact that exoglucanases cannot completely degrade the last two units of methyl MFT could relate to methylation as a protective mechanism to prevent complete degradation of MFT [236]. However, the commercial enzymes employed are of different biological origin. It remains to be seen if endogenous *M. smegmatis* cellulase is not impaired by 2-*O*-methylglucose. All-in-all, the 2-*O*-methylglucose moiety in the  $\beta$ -1,4 glucosyl linkage of MFT here reported is an addition to the repertoire of methylated polysaccharide species in the *Mycobacterium* genus. However, the responsible enzyme and mechanism remain to be elucidated.

Unfortunately, these results cannot completely elucidate a logical order for the precursors leading to mature MFT biosynthesis. Studies on the biosynthesis of both MMPs and MGPLs could be an inspiration for deciphering this. Substrate specificity studies were performed with  $\alpha$ -1,4-mannosyltransferase and the rSAM 3-*O*-methyltransferase, the enzymes believed to participate in chain elongation and methylation and found in MSMEG cell-free extracts, respectively. It was found that the mannosyltransferase was only active on MMP precursors containing more than 3-*O*-methylmannoses, which suggests that mannosylation occurs before methylation for the chain to be elongated under the conditions tested [301]. In a similar vein, 3-*O*-methyltransferase and 6-*O*-methyltransferase were found in the soluble protein fraction from *M. phlei* and methylate the respective hydroxyl groups in MGPL precursors  $\alpha$ -1,4-glucooligosaccharides. Therefore, the biosynthesis of MMP would proceed in a similar way as for MGPL, with glycosylation followed by methylation in a second step [301, 305]. However, the biosynthesis of GLP has not been completely elucidated so far, and the question remains on whether the characterized methyltransferases act posterior to glycosylation, as is for

## Methylated mycofactocin and the biosynthetic order of mycofactocin production

MGPL and MMP, or whether the oligosaccharide chain is methylated elsewhere and then transferred to the tripeptide [299].

Since the formation of the redox core is vital for fulfilling the MFT role *in vivo*, other researchers have proposed that the logical mechanism is the oxidative deamination catalyzed by MftD first, followed by glucosylation by MftF [200]. However, an alternative pathway might exist in which MftF first glycosylates AHDP before the oxidative deamination catalyzed by MftD and posterior methylation (Figure 22). This pathway would also explain why AHDP and GAHDP are possible acceptors for the glucosyltransferase to form AHDP-*n* and GAHDP-*n*, respectively. The biological advantage of this mechanism would be to prevent premature oxidation or reduction of the nascent MFT, before it acquires the glucosyl tailoring moiety. Furthermore, it is still unclear whether glucosylation occurs consecutively or the entire (methyl)glucosyl chain is transferred simultaneously to the PMFT or AHDP precursor. This latter case would imply the existence of two glycosyltransferases, one that forms the glucosyl tail *ex situ* and a second one that transfer moiety to the MFT precursor. Efforts are being made to answer this and other questions, for example, to determine whether in other organisms with the MFT BGC the nature of the glucosyl tail, chain distribution, and methylation is similar to MSMEG.

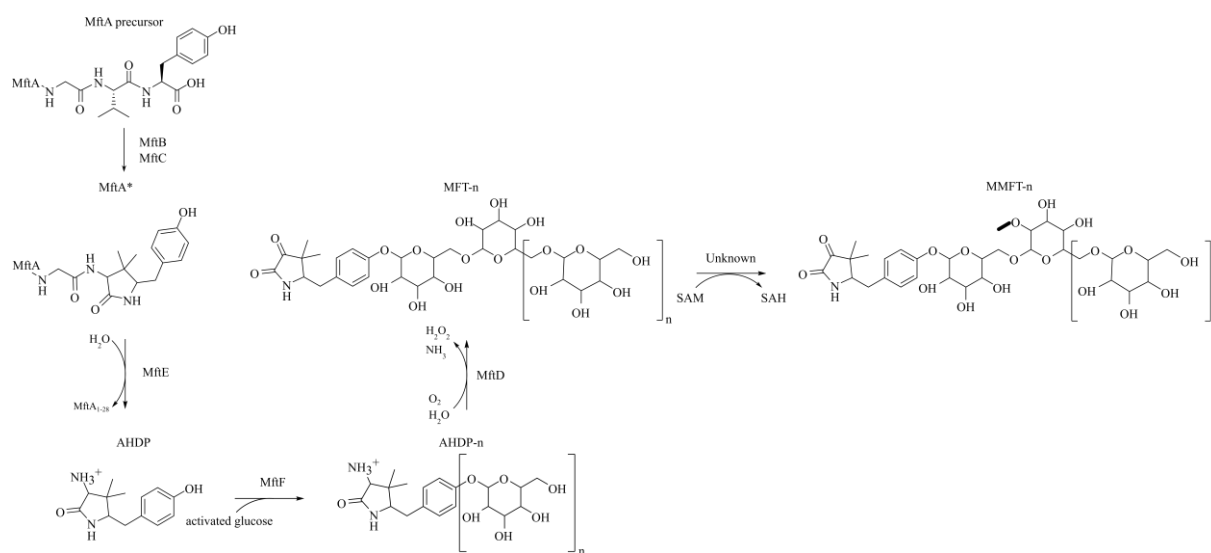


Figure 22: Proposed order of mycofactocin biosynthesis and (methyl) oligoglucosylation.

Another puzzling question is the *raison d'etre* for the methylation. We can obtain inspiration in the argumentation provided for methyl bacillithiol and methyl mycothiol, the latter not yet discovered *in vivo* but previously produced by solid-phase synthesis and enzymatically accepted mycothiol disulfide reductase [64]. It can be proposed that the  $\gamma$ -glutamyl-cysteine or L-cysteinyl-D-glucosamine present in BSH and MSH offers autocatalytic and proteolytic

**Methylated mycofactocin and the biosynthetic order of mycofactocin production**

protection of the cysteine residue. With this modification in place and in case of metabolic need, cysteine can still be redirected to other pathways by specialized transpeptidases [62]. Therefore, protection from hydrolases could be a hypothetical purpose of the methylation. Even though no mycobacteria strain is known to use cellulose ( $\beta$ -1,4-glucose oligosaccharides) *in vitro* as a carbon source, all Mycobacteria genomes have, at least, one cellulase-encoding gene, except *M. leprae* [306-308]. It is possible that, under unknown environmental cues, these cellulases are produced to degrade the glucan chains of MFT, either as a mechanism for redox modulation if chain length is correlated with enzyme kinetics, as a precursor to regenerate long-chain MFT at a later stage or to use the released glucose as an energy source. Whether native cellulases are active against MMFT-2 and release PMFT(H<sub>2</sub>) is a topic for future biochemical characterization.

While we know little regarding the possible activities of MFT-dependent oxidoreductases and dehydrogenases, it is likely that they are coupled to the known redox pool and further into the membrane-bound oxidative phosphorylation to generate energy. Furthermore, the knowledge of mycofactocin would have to reconcile itself with a question at a later stage: is there a relationship between the pathogenesis of TB and MFT? Additional studies into the catalytic activities of MFT-dependent redox enzymes, especially under various conditions and models to simulate TB conditions, are particularly important to answer this critical question. While the role of MFT in ethanol consumption in MSMEG has been shown, which is highly likely to occur also in MTB, there is not yet a relation between MFT and TB. It has been reported that alcohol consumption results in an increased risk of TB and drug resistant TB. Notably, about 10% of TB cases globally were attributed to alcohol misuse [309]. The TB and alcohol relationship is not only grounded on the social symptoms and consequences of alcohol consumption (increased poverty, crowded dwellings, and limited treatment compliance, for example) [309]. Biologically, alcohol leads to impairment of the immune system by suppressing phagocytosis and macrophage' oxidative burst, resulting in increased susceptibility of TB acquisition and reactivation of latent TB. Furthermore, alcoholism limits cytokines' production, affecting macrophage and T-cell response to MTB infection [310]. The vascularization of MTB-containing granulomas could allow the pathogen to access ethanol as a carbon source through the blood [311-313], raising the hypothesis of whether MFT could be associated with increased MTB pathogenesis and TB progression due to high alcohol consumption.

**Impact of Oxygen Supply and Scale-Up on *Mycobacterium smegmatis* Cultivation and Mycofactocin Formation**10.4. IMPACT OF OXYGEN SUPPLY AND SCALE-UP ON *Mycobacterium smegmatis* CULTIVATION AND MYCOFACTOCIN FORMATION

With the discovery of short-chain and long-chain MFT a new question arose regarding the role of the different chain lengths. In *M. smegmatis*, we discovered that long-chain MMFT with eight glucosyl moieties are the most abundant congeners, followed by nine and seven [236]. This situation could reflect the oligoglutamyl moiety of F<sub>420</sub>, which was found more extended (five to eight units) in Mycobacteria and Chloroflexi, and slightly shorter in Proteobacteria and methanogens with cytochromes (three to six) and methanogens without cytochromes (two to three) [314-316]. There is a general lack of knowledge of enzymatic properties and chain-dependent in putative MFT-dependent alcohol dehydrogenases and GMC oxidoreductases. Such studies require significant quantities of the cofactor and a regeneration system. However, our results indicate that MFT yield is too low in the wild-type model organism studied. Furthermore, structural crystallography of some heterologously produced MFT-dependent oxidoreductases has been previously published [223], which could be greatly benefited in the future from ligand soaking studies with the pure cofactor [317]. While studies are being undertaken to increase the MFT titer by metabolic engineering, we first scaled-up the culture volume to achieve higher MFT quantities, without the need for genetic manipulation.

To properly model the parameters of MFT production in an STR, we cultured *M. smegmatis* in LB broth in an orbital shaker equipped with transfer-rate online measurement (TOM) of oxygen [255], also termed respiratory activity monitoring system (RAMOS) when carbon dioxide is incorporated [318]. The system provides a measurement of the oxygen transfer rate (OTR) and carbon transfer rate (CTR, volume carbon dioxide formed per oxygen consumed), expressing the oxygen transfer (and therefore, consumption) from the atmosphere to the cells and carbon dioxide release, or production [256, 318]. Experimental analysis of auxotrophic mutants, in which a nutrient or microelement deficiency is known, showed that the OTR versus time plot's shape could be correlated with biological phenomena such as substrate or oxygen limitation, product inhibition, or diauxic growth. Therefore, the OTR plot shape allows for quick inferences regarding the organism's metabolic behavior in question [256]. The OTR and CTR quotient is the respiratory quotient (RQ), a useful variable for monitoring and diagnosing the metabolic state of the culture and carbon source assimilation [319]. An RQ of 1 indicates that substrate and product, mostly biomass, have the same degree of reduction and is often the basepoint when glucose or acetate is the main carbon source. A value higher than one indicates that the product is more reduced than the substrate, such as carboxylic acids, while lower values

## DISCUSSION

### Impact of Oxygen Supply and Scale-Up on *Mycobacterium smegmatis* Cultivation and Mycofactocin Formation

indicate that the substrate is more reduced than the product [320]. When ethanol is the main carbon source, the RQ reaches a value of around 0.55, which we frequently observed during the main culture phase [321].

We employed variations in the filling volume, from 10 to 40 mL in 10 mL steps, to simulate different oxygen levels in the shake flask. To reduce flask-to-flask variability LB (complex medium) was pre-inoculated, supplemented with 0.5 g L<sup>-1</sup> tyloxapol and 250 mM MOPS buffer for a pH 7.2, and then dispensed into each flask. We observed that at the lowest filling volume (highest oxygen availability), OTR<sub>max</sub> was 20.02 mmol L<sup>-1</sup> h<sup>-1</sup>. This plot's shape correlated with the proposed shape for a normal fermentation (single peak, asymmetrical shape), while oxygen limitation and diauxic growth are present at a filling volume of 20 mL, as evidenced by the two OTR peaks with a broad plateau. At the highest filling volume (and lowest oxygen availability), OTR<sub>40mL</sub> was 12.08 mmol L<sup>-1</sup> h<sup>-1</sup>, with measured OTR<sub>30 mL</sub> of 14.34 mmol L<sup>-1</sup> h<sup>-1</sup> and OTR<sub>20 mL</sub> of 17.24 mmol L<sup>-1</sup> h<sup>-1</sup>. Furthermore, our shake flasks and stirred tank reactor (STR) results confirm that ethanol is the main carbon source, as evidenced from the RQ ≈ 0.6 during most of the fermentation and the sudden increase in RQ to a value of 1 followed by a steady decrease was observed simultaneously with offline metabolite measurements indicating that ethanol was depleted.

While MFT was found through all conditions tested, a consistent increase of the long-chain MMFT-8(H<sub>2</sub>) was observed directly proportional with increasing oxygen limitation in shake flasks (4.8-fold in 20 mL, 8.6-fold in 30 mL, 11.8-fold in 40 mL), while the ratios of the precursors PMFT(H<sub>2</sub>) (20 mL: 3.1-fold; 30 mL: 6.1; 40 mL: 8.0-fold) and MMFT-2b(H<sub>2</sub>) (20 mL: 1.7-fold; 30 mL: 2.4-fold; 40 mL: 3.9-fold) increased in a similar but less dramatic way. The same increase was observed in the overflow metabolite acetate, with no production observed under oxygen-unlimited conditions (OTR<sub>max</sub>) and a maximum yield of 3.1 g L<sup>-1</sup> in oxygen-limiting conditions (OTR<sub>min</sub>).

Since we found the highest long-chain MFT production at the OTR<sub>min</sub> of 12.08 mmol L<sup>-1</sup> h<sup>-1</sup>, we used the volumetric power as input from scale-up, from shake flask to a 7L STR filled with 3L complex media (LB broth) filling volume. Aeration was set to 0.25 vvm, to reflect the air diffusion through a classical cotton plug in a shake flask [254]. Furthermore, the oxygen intake (integral under the curve) at the OTR<sub>min</sub> reference point can be converted to the OTR<sub>max</sub> at which the STR would be limited, for which a value of 430 rpm should result in this OTR. The actual value achieved was 7.4 mmol L<sup>-1</sup> h<sup>-1</sup>, which is lower than



## DISCUSSION

### Impact of Oxygen Supply and Scale-Up on *Mycobacterium smegmatis* Cultivation and Mycofactocin Formation

intended but within the  $\pm 5 \text{ mmol L}^{-1} \text{ h}^{-1}$  considered reasonable for similar models [265]. Despite the supplementation with  $0.5 \text{ g L}^{-1}$  tyloxapol as a surfactant and  $1 \text{ mL L}^{-1}$  antifoam 204, foaming and biofilm formation was significant and could also account for the decreased OTR. Known foaming consequences include decreased cell viability, a more cumbersome and costly downstream process, and, as worst-case scenario, contamination of the fermenter system and overall loss in process productivity [322].

While the results between shake flask at  $\text{OTR}_{\text{min}}$  and complex media STR are comparable, the longer bioprocess performed on STR following the depletion of ethanol and the increase of RQ from 0.6 to 1 indicates that MMFT-8( $\text{H}_2$ ) quickly and steadily degrades from its apex without a clear increase in species with a shorter chain. To model the opposite conditions (oxygen-unlimited), the system was set at 900 rpm. As expected, not only was acetate meagerly produced, leading to a lack of diauxic growth phase and lower pH variation, but the MFT titer of the aglycon and the species monitored was significantly inferior to the same media and inoculum conditions in oxygen-limiting conditions. In this experiment,  $\text{OTR}_{\text{max}}$  was  $24.58 \text{ mmol L}^{-1} \text{ h}^{-1}$ , still within a  $\pm 5 \text{ mmol L}^{-1} \text{ h}^{-1}$  range compared to the shake flask experiment.

Chemically, LB broth is not a defined media, with lot-to-lot variability due to its components. We performed an additional STR cultivation in HdB broth, a mineral, chemically-defined media, and oxygen-limiting conditions owing to the increased MFT titer observed. OTR and RQ remained similar to the complex broth experiment and between the established parameters for the desired conditions and carbon source. Interestingly, higher MFT yields were observed in mineral media. However, the broth's heterogeneous composition, mainly by foaming, made it impossible for us to achieve reliable biomass quantification. It is possible that in the complex broth, owing to its higher nutrient concentration, foaming was more prevalent in comparison with the mineral media.

While the STR in complex media and  $\text{OTR}_{\text{min}}$  yielded a high acetate titer, acetate was not observed at any point during the fermentation in mineral media in oxygen-limiting conditions. In contrast, it was observed in our preliminary studies in oxygen unlimited conditions. Acetate production is explainable by the overflow metabolism, termed “aerobic fermentation,” a product of limitation in the oxidative phosphorylation machinery during the catabolism of high-energy precursors aerobic conditions. This leads to the additional redox potential being eliminated by secretion of metabolic intermediates that can later be still rerouted to the CCM [323-325]. The phosphate acetyltransferase-acetyl kinase pathway (Pta-AckA) is responsible

**Impact of Oxygen Supply and Scale-Up on *Mycobacterium smegmatis* Cultivation and Mycofactocin Formation**

for acetate formation in *E. coli* and MTB by converting acetyl-CoA to acetyl phosphate, followed by dephosphorylation and secretion [326, 327]. When acetate or another overflow metabolite is present, it is expected that its assimilation results in a second OTR peak, leading to a second, albeit shorter, growth phase with the concomitant increase in the oxygen transfer rate. This phenomenon is ubiquitous among bacteria, yeast, and eukaryotic cells, and the secreted product varies depending on the microorganism.

The term overflow metabolism is employed in bacteria, where the major product, for example, in *E. coli* is acetate and in *Streptococcus bovis* is lactate. Historically, the term Warburg effect applies to eukaryotic cells, and particularly cancerous cell lines, where high rates of glycolysis, instead of being correctly directed to oxidative phosphorylation results in poor ATP production. To address this, the central carbon metabolites are produced as an overflow mechanism [323]. The production of ethanol by *S. cerevisiae* and other yeasts is termed the Crabtree effect. In this case acetaldehyde and lactate are the overflow metabolites, and results in reduced viability, sugar-induced cell death and process productivity in commercial fermentation [323, 328]. All-in-all, the three phenomena refer to the same process: the uncoupling of ATP formation (ATP homeostasis) in response to substrate availability and glycolysis rate [328].

A particularly interesting situation occurs in mycobacterial strains. *In vivo*, MTB produces lactate, acetate and other compounds in a guinea pig model [11], however an early study indicates that, unlike fatty acids, these do not positively influence cell growth [192, 329]. *In vitro*, secretion and assimilation of acetate occurred at a high rate, simultaneous with co-assimilation of simpler carbon sources such as glucose [327]. These results suggest that MTB adapts its metabolic pathways in host tissues for energy assimilation and depending on carbon source availability. These two processes are coupled to electron acceptors such as succinate and fumarate [192] and possibly to additional cofactors.

Together, this indicates a high degree of control between the overflow metabolism pathways in response to environmental cues, namely substrate availability [192] but possibly also oxygen, owing to its low availability and oxidative conditions during active infection [44]. A similar situation could occur in the fast-growing species *M. smegmatis*, since our STR results [255] only show production of acetate and no lactate, suggesting that acetate is the main product of overflow metabolism, increasing during the first OTR peak of the culture and decreasing in parallel with the second peak. Production and the second peak are only present in cultures under

**Impact of Oxygen Supply and Scale-Up on *Mycobacterium smegmatis* Cultivation and Mycofactocin Formation**

oxygen-limitation (filling volume >20 mL), and negligible amounts were produced in complex media STR under high aeration, correlating with previous observations [323]. Studies on MTB demonstrated that acetate is produced by a pathway homologous to the *E. coli* Pta-AckA fermentative mechanism [325] and that MTB can assimilate various carbon sources simultaneously [330]. It is possible to speculate that acetate and ethanol are metabolized simultaneously in the experiments we performed.

In this thesis, we have discovered the novel redox cofactor MFT, starting from the observation from previous researchers that alterations in the MFT maturase genes result in the inability to grow in primary alcohols, namely ethanol, but in a lower degree shorter ( $C_1$ ) and longer ( $C_3$ ) alcohols [226]. We have described the *in vivo* existence in *M. smegmatis* of the previous *in vitro* characterized intermediates, in addition to the last post-translational modification that results in the most abundant MFT species. Furthermore, we observed a relationship between oxygen transfer rate and MFT titer, with consequences for the high-yield production of the cofactor by biological means and without genetic manipulation.

## 11. CONCLUSION & OUTLOOK

Excluding some intracellular parasites, the almost universal presence of NAD<sup>+</sup>/NADH conversion emphasizes its relevance in maintaining intracellular redox conditions required to sustain metabolic reactions within almost all cells. However, the wide range of possible substrates available in different environments and the complex catabolic and anabolic requirements associated with each environment make additional cofactors necessary to couple redox reactions. The presence of various redox pools is a consequence of the diversification of energy substrates such as chemoautotroph metabolism and life evolution under various oxygenic conditions. Therefore, novel cofactors are an exciting field of research that opens new avenues for studying the biochemistry that sustains life in different niches, such as in pathogenic microorganisms.

We have discovered mycofactocin, a novel cofactor in the medically important genus *Mycobacterium* and other environmental microbes. Mycofactocin is the glucosylated form of premycofactocin, decorated with up to nine  $\beta$ -1,4-linked glucose residues. Additionally, we have also discovered that the second unit of the glucosyl chain is a 2-*O*-methylglucose, present in the most abundant MFT congeners from MSMEG. This discovery is a breakthrough as it reveals *in vivo* the existence of a novel cofactor previously partially described only *in vitro*. These tailoring moieties, the variable glucosyl chain, and the methylation could be similarly diverse across the taxa carrying an MFT gene cluster, as other cofactors with a flexible tail length such as F<sub>420</sub> and the prenylated quinones ubiquinone or menaquinone. Such aspect remains to be elucidated and surely will be the focus of future investigations.

Our results allow for inferences regarding a possible biosynthetic order, in which AHDP is first glucosylated prior to oxidative deamination. This hypothesis contrasts with the proposals by previous researchers in which glucosylation is posterior to oxidative deamination, however further studies are required. Together, the discovery of the responsible methyltransferase, the scope of glucosyl/methyl MFT in fitness characterization, and the enzymology of MFT-dependent dehydrogenases/oxidases are some of the follow-up steps on the research of this novel cofactor. While the main feature of cofactors is not being consumed during metabolism, further *in vitro* characterization requires both higher cofactor availability and a regeneration system to devolve the reduced cofactor to its oxidized form, or vice versa. Our STR modeling indicates that mineral media and oxygen limiting conditions at an OTR of  $\approx 12 \text{ mmol L}^{-1} \text{ h}^{-1}$  provides the highest titer of a long-chain, methylated MFT. The methods we have described here to identify the mycofactocin congeners by high-resolution mass

## CONCLUSION & OUTLOOK

spectrometry, enabling physiological characterization of strains deficient in the putative MFT-dependent enzymes in the short chain alcohol dehydrogenases clade. Finally, we have provided a set of MFT precursors and congeners that can be now investigated in other MFT producing strains such as MTB. We have discovered the mature of mycofactocin, a novel cofactor proposed more than ten years ago, and with this breakthrough further studies are possible to determine more properties of MFT in mycobacterial biochemistry, with an outlook towards elucidating possible roles in MTB life cycle and TB pathogenesis.

## 12. REFERENCES

1. Rastogi, N., E. Legrand, and C. Sola, *The mycobacteria: an introduction to nomenclature and pathogenesis*. Rev Sci Tech, 2001. **20**(1): p. 21-54.
2. Gupta, R.S., B. Lo, and J. Son, *Phylogenomics and Comparative Genomic Studies Robustly Support Division of the Genus Mycobacterium into an Emended Genus Mycobacterium and Four Novel Genera*. Front Microbiol, 2018. **9**: p. 67.
3. George, K.M., et al., *Mycolactone: a polyketide toxin from Mycobacterium ulcerans required for virulence*. Science, 1999. **283**(5403): p. 854-7.
4. Torrado, E., et al., *Evidence for an intramacrophage growth phase of Mycobacterium ulcerans*. Infect. Immun., 2007. **75**(2): p. 977-87.
5. WHO, *Global tuberculosis report 2019*. 2019, Geneva: World Health Organization.
6. Smith, I., *Mycobacterium tuberculosis pathogenesis and molecular determinants of virulence*. Clin Microbiol Rev, 2003. **16**(3): p. 463-496.
7. Comas, I., et al., *Out-of-Africa migration and Neolithic coexpansion of Mycobacterium tuberculosis with modern humans*. Nat. Genet., 2013. **45**(10): p. 1176-82.
8. Kleinnijenhuis, J., et al., *Innate immune recognition of Mycobacterium tuberculosis*. Clin. Dev. Immunol., 2011. **2011**: p. 405310-405310.
9. Marrakchi, H., M.-A. Lanéelle, and M. Daffé, *Mycolic Acids: Structures, Biosynthesis, and Beyond*. Chem. Biol., 2014. **21**(1): p. 67-85.
10. Martin, C.J., A.F. Carey, and S.M. Fortune, *A bug's life in the granuloma*. Semin Immunopathol, 2016. **38**(2): p. 213-220.
11. Somashekar, B.S., et al., *Metabolic Profiling of Lung Granuloma in Mycobacterium tuberculosis Infected Guinea Pigs: Ex vivo 1H Magic Angle Spinning NMR Studies*. J. Proteome Res., 2011. **10**(9): p. 4186-4195.
12. Somashekar, B.S., et al., *Metabolomic Signatures in Guinea Pigs Infected with Epidemic-Associated W-Beijing Strains of Mycobacterium tuberculosis*. J. Proteome Res., 2012. **11**(10): p. 4873-4884.
13. Shin, J.-H., et al., *1H NMR-based Metabolomic Profiling in Mice Infected with Mycobacterium tuberculosis*. J. Proteome Res., 2011. **10**(5): p. 2238-2247.
14. Fernández-García, M., et al., *Comprehensive Examination of the Mouse Lung Metabolome Following Mycobacterium tuberculosis Infection Using a Multiplatform Mass Spectrometry Approach*. J. Proteome Res., 2020. **19**(5): p. 2053-2070.
15. Lillebaek, T., et al., *Molecular evidence of endogenous reactivation of Mycobacterium tuberculosis after 33 years of latent infection*. J. Infect. Dis., 2002. **185**(3): p. 401-4.
16. Lerner, T.R., et al., *Mycobacterium tuberculosis replicates within necrotic human macrophages*. J Cell Biol, 2017. **216**(3): p. 583-594.
17. Chhabra, N., et al., *Pharmacotherapy for multidrug resistant tuberculosis*. J Pharmacol Pharmacother, 2012. **3**(2): p. 98-104.
18. Koch, A., V. Mizrahi, and D.F. Warner, *The impact of drug resistance on Mycobacterium tuberculosis physiology: what can we learn from rifampicin?* Emerg. Microbes & Infect., 2019. **3**(1): p. 1-11.
19. Levin, M.E. and G.F. Hatfull, *Mycobacterium smegmatis RNA polymerase: DNA supercoiling, action of rifampicin and mechanism of rifampicin resistance*. Mol. Microbiol., 1993. **8**(2): p. 277-85.
20. Williams, D.L., et al., *Characterization of rifampin-resistance in pathogenic mycobacteria*. Antimicrob. Agents Chemother., 1994. **38**(10): p. 2380-6.
21. McKenzie, D., et al., *The effect of nicotinic acid amide on experimental tuberculosis of white mice*. J Lab Clin Med, 1948. **33**(10): p. 1249-53.
22. FitzPatrick, F.K., *Nicotinamide in Murine Tuberculosis*. Exp. Biol. Med., 1955. **88**(1): p. 54-56.
23. Slayden, R.A. and C.E. Barry, *The genetics and biochemistry of isoniazid resistance in Mycobacterium tuberculosis*. Microb. Infect., 2000. **2**(6): p. 659-669.
24. Vilchèze, C. and J.W.R. Jacobs, *The Mechanism of Isoniazid Killing: Clarity Through the Scope of Genetics*. Annu. Rev. Microbiol., 2007. **61**(1): p. 35-50.

25. Zhang, Y., et al., *Role of acid pH and deficient efflux of pyrazinoic acid in unique susceptibility of Mycobacterium tuberculosis to pyrazinamide*. J. Bacteriol., 1999. **181**(7): p. 2044-2049.
26. Zhang, Y. and D. Mitchison, *The curious characteristics of pyrazinamide: a review*. Int. J. Tuberc. Lung Dis., 2003. **7**(1): p. 6-21.
27. Lamont, E.A., N.A. Dillon, and A.D. Baughn, *The Bewildering Antitubercular Action of Pyrazinamide*. Microbiol. Mol. Biol. Rev., 2020. **84**(2): p. e00070-19.
28. Gopal, P., et al., *Pyrazinoic Acid Inhibits Mycobacterial Coenzyme A Biosynthesis by Binding to Aspartate Decarboxylase PanD*. ACS Infect. Dis., 2017. **3**(11): p. 807-819.
29. Sayahi, H., et al., *Pyrazinamide, but not pyrazinoic acid, is a competitive inhibitor of NADPH binding to Mycobacterium tuberculosis fatty acid synthase I*. Bioorg. Med. Chem. Lett., 2011. **21**(16): p. 4804-4807.
30. Blanchard, J.S., *Molecular mechanisms of drug resistance in Mycobacterium tuberculosis*. Annu. Rev. Biochem., 1996. **65**(1): p. 215-239.
31. Shepherd, R.G., et al., *Structure-activity studies leading to ethambutol, a new type of antituberculous compound*. Ann. N. Y. Acad. Sci., 1966. **135**(2): p. 686-710.
32. Takayama, K. and J.O. Kilburn, *Inhibition of synthesis of arabinogalactan by ethambutol in Mycobacterium smegmatis*. Antimicrob. Agents Chemother., 1989. **33**(9): p. 1493-1499.
33. Deng, L., et al., *Recognition of multiple effects of ethambutol on metabolism of mycobacterial cell envelope*. Antimicrob. Agents Chemother., 1995. **39**(3): p. 694-701.
34. Johnsson, K. and P.G. Schultz, *Mechanistic Studies of the Oxidation of Isoniazid by the Catalase Peroxidase from Mycobacterium tuberculosis*. J. Am. Chem. Soc., 1994. **116**(16): p. 7425-7426.
35. Banerjee, A., et al., *inhA, a gene encoding a target for isoniazid and ethionamide in Mycobacterium tuberculosis*. Science, 1994. **263**(5144): p. 227-230.
36. Lei, B., C.-J. Wei, and S.-C. Tu, *Action Mechanism of Antitubercular Isoniazid: Activation by Mycobacterium tuberculosis KatG, isolation, and characterization of InhA inhibitor*. J. Biol. Chem., 2000. **275**(4): p. 2520-2526.
37. Mahapatra, S., et al., *A Novel Metabolite of Antituberculosis Therapy Demonstrates Host Activation of Isoniazid and Formation of the Isoniazid-NAD<sup>+</sup> Adduct*. Antimicrob. Agents Chemother., 2012. **56**(1): p. 28-35.
38. DeBarber, A.E., et al., *Ethionamide activation and sensitivity in multidrug-resistant Mycobacterium tuberculosis*. PNAS, 2000. **97**(17): p. 9677-9682.
39. Zhu, C., et al., *Molecular mechanism of the synergistic activity of ethambutol and isoniazid against Mycobacterium tuberculosis*. J. Biol. Chem., 2018. **293**(43): p. 16741-16750.
40. Nguyen, L., *Antibiotic resistance mechanisms in M. tuberculosis: an update*. Arch. Toxicol., 2016. **90**(7): p. 1585-604.
41. Du Preez, I. and D.T. Loots, *Novel insights into the pharmacometabonomics of first-line tuberculosis drugs relating to metabolism, mechanism of action and drug-resistance*. Drug Metab. Rev., 2018. **50**(4): p. 466-481.
42. Hoagland, D.T., et al., *New agents for the treatment of drug-resistant Mycobacterium tuberculosis*. Adv. Drug Del. Rev., 2016. **102**: p. 55-72.
43. Cooke, M.S., et al., *Oxidative DNA damage: mechanisms, mutation, and disease*. FASEB J, 2003. **17**(10): p. 1195-1214.
44. Slauch, J.M., *How does the oxidative burst of macrophages kill bacteria? Still an open question*. Mol. Microbiol., 2011. **80**(3): p. 580-583.
45. Beckman, J.S., et al., *Apparent hydroxyl radical production by peroxynitrite: implications for endothelial injury from nitric oxide and superoxide*. PNAS, 1990. **87**(4): p. 1620-1624.
46. Shastri, M.D., et al., *Role of Oxidative Stress in the Pathology and Management of Human Tuberculosis*. Oxid Med Cell Longev, 2018. **2018**: p. 7695364-7695364.
47. McNaught, A.D., et al., *IUPAC Compendium of Chemical Terminology*. 1997: International Union of Pure and Applied Chemistry.
48. Wolfenden, R. and M.J. Snider, *The Depth of Chemical Time and the Power of Enzymes as Catalysts*. Acc. Chem. Res, 2001. **34**(12): p. 938-945.
49. Radzicka, A. and R. Wolfenden, *A proficient enzyme*. Science, 1995. **267**(5194): p. 90-3.
50. Tsuchiya, Y., et al., *Protein CoAlation and antioxidant function of coenzyme A in prokaryotic cells*. Biochem. J., 2018. **475**(11): p. 1909-1937.

51. Hansen, R.E., D. Roth, and J.R. Winther, *Quantifying the global cellular thiol–disulfide status*. PNAS, 2009. **106**(2): p. 422-427.
52. Akerboom, T.P., M. Bilzer, and H. Sies, *The relationship of biliary glutathione disulfide efflux and intracellular glutathione disulfide content in perfused rat liver*. J. Biol. Chem., 1982. **257**(8): p. 4248-52.
53. Wu, G., et al., *Glutathione Metabolism and Its Implications for Health*. J. Nutr., 2004. **134**(3): p. 489-492.
54. Chakravarthi, S., C.E. Jessop, and N.J. Bulleid, *The role of glutathione in disulphide bond formation and endoplasmic-reticulum-generated oxidative stress*. EMBO Rep, 2006. **7**(3): p. 271-275.
55. Dickerhof, N., L. Paton, and A.J. Kettle, *Oxidation of bacillithiol by myeloperoxidase-derived oxidants*. Free Radical Biol. Med., 2020. **158**: p. 74-83.
56. Hiras, J., et al., *Physiological Studies of Chlorobiaceae Suggest that Bacillithiol Derivatives Are the Most Widespread Thiols in Bacteria*. mBio, 2018. **9**(6): p. e01603-18.
57. Newton, G.L., et al., *Bacillithiol is an antioxidant thiol produced in Bacilli*. Nat. Chem. Biol., 2009. **5**(9): p. 625-7.
58. Ung, K.S.E. and Y. Av-Gay, *Mycothiols-dependent mycobacterial response to oxidative stress*. FEBS Lett., 2006. **580**(11): p. 2712-2716.
59. Spies, H.S. and D.J. Steenkamp, *Thiols of intracellular pathogens. Identification of ovothiol A in Leishmania donovani and structural analysis of a novel thiol from Mycobacterium bovis*. Eur. J. Biochem., 1994. **224**(1): p. 203-13.
60. Newton, G.L., et al., *Distribution of thiols in microorganisms: mycothiol is a major thiol in most actinomycetes*. J. Bacteriol., 1996. **178**(7): p. 1990-1995.
61. Newton, G.L., et al., *The Structure of U17 Isolated from Streptomyces clavuligerus and its Properties as an Antioxidant Thiol*. Eur. J. Biochem., 1995. **230**(2): p. 821-825.
62. Newton, G.L. and M. Rawat, *N-methyl-bacillithiol, a Novel Thiol from Anaerobic Bacteria*. mBio, 2019. **10**(1).
63. Haft, D.H. and M.K. Basu, *Biological systems discovery in silico: radical S-adenosylmethionine protein families and their target peptides for posttranslational modification*. J. Bacteriol., 2011. **193**(11): p. 2745-55.
64. Stewart, M.J.G., et al., *Mycothiols disulfide reductase: solid phase synthesis and evaluation of alternative substrate analogues*. Org. Biomol. Chem., 2008. **6**(2): p. 385-390.
65. Kumar, A., S. Kumar, and B. Taneja, *The structure of Rv2372c identifies an RsmE-like methyltransferase from Mycobacterium tuberculosis*. Acta Crystallogr D Biol Crystallogr, 2014. **70**(Pt 3): p. 821-32.
66. Ripoll-Rozada, J., et al., *Biosynthesis of mycobacterial methylmannose polysaccharides requires a unique 1-O-methyltransferase specific for 3-O-methylated mannosides*. PNAS, 2019. **116**(3): p. 835-844.
67. Warrior, T., et al., *N-methylation of a bactericidal compound as a resistance mechanism in Mycobacterium tuberculosis*. PNAS, 2016. **113**(31): p. E4523-E4530.
68. Hernick, M., *Mycothiols: a target for potentiation of rifampin and other antibiotics against Mycobacterium tuberculosis*. Expert. Rev. Anti Infect. Ther., 2014. **11**(1): p. 49-67.
69. Newton, G.L., et al., *Characterization of Mycobacterium smegmatis Mutants Defective in 1-d-myo-Inosityl-2-amino-2-deoxy- $\alpha$ -d-glucopyranoside and Mycothiol Biosynthesis*. Biochem. Biophys. Res. Commun., 1999. **255**(2): p. 239-244.
70. Rawat, M., et al., *Mycothiols-deficient Mycobacterium smegmatis mutants are hypersensitive to alkylating agents, free radicals, and antibiotics*. Antimicrob. Agents Chemother., 2002. **46**(11): p. 3348-55.
71. Vilcheze, C., et al., *Mycothiols biosynthesis is essential for ethionamide susceptibility in Mycobacterium tuberculosis*. Mol. Microbiol., 2008. **69**(5): p. 1316-29.
72. Buchmeier, N.A., et al., *Association of mycothiol with protection of Mycobacterium tuberculosis from toxic oxidants and antibiotics*. Mol. Microbiol., 2003. **47**(6): p. 1723-32.
73. Buchmeier, N.A., G.L. Newton, and R.C. Fahey, *A mycothiol synthase mutant of Mycobacterium tuberculosis has an altered thiol-disulfide content and limited tolerance to stress*. J. Bacteriol., 2006. **188**(17): p. 6245-52.



74. Stover, C.K., et al., *A small-molecule nitroimidazopyran drug candidate for the treatment of tuberculosis*. Nature, 2000. **405**(6789): p. 962-6.
75. Manjunatha, U.H., et al., *Identification of a nitroimidazo-oxazine-specific protein involved in PA-824 resistance in Mycobacterium tuberculosis*. PNAS, 2005. **103**(2): p. 431-436.
76. Matsumoto, M., et al., *OPC-67683, a nitro-dihydro-imidazooxazole derivative with promising action against tuberculosis in vitro and in mice*. PLoS Med, 2006. **3**(11): p. e466.
77. Singh, R., et al., *PA-824 Kills Nonreplicating Mycobacterium tuberculosis by Intracellular NO Release*. Science, 2008. **322**(5906): p. 1392-1395.
78. Nasto, B., *Not-for-profit to launch antibiotic against drug-resistant tuberculosis*. Nat. Biotechnol., 2019.
79. Eirich, L.D., G.D. Vogels, and R.S. Wolfe, *Distribution of coenzyme F420 and properties of its hydrolytic fragments*. J. Bacteriol., 1979. **140**(1): p. 20-7.
80. Coats, J.H., et al., *Discovery, production, and biological assay of an unusual flavenoid cofactor involved in lincomycin biosynthesis*. J. Antibiot., 1989. **42**(3): p. 472-474.
81. McCormick, J.R.D. and G.O. Morton, *Identity of cosynthetic factor I of Streptomyces aureofaciens and fragment FO from coenzyme F420 of Methanobacterium species*. J. Am. Chem. Soc., 1982. **104**(14): p. 4014-4015.
82. Greening, C., et al., *Physiology, Biochemistry, and Applications of F420- and Fo-Dependent Redox Reactions*. Microbiol. Mol. Biol. Rev., 2016. **80**(2): p. 451-93.
83. Jirapanjawan, T., et al., *The redox cofactor F420 protects mycobacteria from diverse antimicrobial compounds and mediates a reductive detoxification system*. Appl. Environ. Microbiol., 2016.
84. Haver, H.L., et al., *Mutations in genes for the F420 biosynthetic pathway and a nitroreductase enzyme are the primary resistance determinants in spontaneous in vitro-selected PA-824-resistant mutants of Mycobacterium tuberculosis*. Antimicrob. Agents Chemother., 2015. **59**(9): p. 5316-23.
85. Fischer, J.D., et al., *The structures and physicochemical properties of organic cofactors in biocatalysis*. J. Mol. Biol., 2010. **403**(5): p. 803-24.
86. Yu, Y., X. Liu, and J. Wang, *Expansion of Redox Chemistry in Designer Metalloenzymes*. Acc. Chem. Res, 2019. **52**(3): p. 557-565.
87. Richter, M., *Functional diversity of organic molecule enzyme cofactors*. Nat Prod Rep, 2013. **30**(10): p. 1324-45.
88. Okeley, N.M. and W.A. van der Donk, *Novel cofactors via post-translational modifications of enzyme active sites*. Chem. Biol., 2000. **7**(7): p. R159-R171.
89. Davidson, V.L., *Protein-Derived Cofactors*, in *Comprehensive Natural Products III*. 2020. p. 40-57.
90. Denessiouk, K.A., V.-V. Rantanen, and M.S. Johnson, *Adenine recognition: A motif present in ATP-, CoA-, NAD-, NADP-, and FAD-dependent proteins*. Proteins: Struct. Funct. Genet., 2001. **44**(3): p. 282-291.
91. Nikiforov, A., V. Kulikova, and M. Ziegler, *The human NAD metabolome: Functions, metabolism and compartmentalization*. Crit. Rev. Biochem. Mol. Biol., 2015. **50**(4): p. 284-297.
92. Preiner, M., et al., *The Future of Origin of Life Research: Bridging Decades-Old Divisions*. Life, 2020. **10**(3).
93. Nitschke, W. and M.J. Russell, *Beating the acetyl coenzyme A-pathway to the origin of life*. Philos Trans R Soc Lond B Biol Sci, 2013. **368**(1622): p. 20120258.
94. Pearlman, Samuel M., Z. Serber, and James E. Ferrell, *A Mechanism for the Evolution of Phosphorylation Sites*. Cell, 2011. **147**(4): p. 934-946.
95. Hemmann, J.L., et al., *The one-carbon carrier methylofuran from Methylobacterium extorquens AM1 contains a large number of  $\alpha$ - and  $\gamma$ -linked glutamic acid residues*. J. Biol. Chem., 2016. **291**(17): p. 9042-9051.
96. Chistoserdova, L., *Wide Distribution of Genes for Tetrahydromethanopterin/Methanofuran-Linked C1 Transfer Reactions Argues for Their Presence in the Common Ancestor of Bacteria and Archaea*. Front. Microbiol, 2016. **7**(1425).
97. Sybesma, W., et al., *Controlled Modulation of Folate Polyglutamyl Tail Length by Metabolic Engineering of Lactococcus lactis*. Appl. Environ. Microbiol., 2003. **69**(12): p. 7101-7107.

98. Hemmann, J.L., et al., *Methylfuran is a prosthetic group of the formyltransferase/hydrolase complex and shuttles one-carbon units between two active sites*. PNAS, 2019. **116**(51): p. 25583-25590.
99. Lawrence, S.A., et al., *Mammalian Mitochondrial and Cytosolic Polyglutamate Synthetase Maintain the Subcellular Compartmentalization of Folates*. J. Biol. Chem., 2014. **289**(42): p. 29386-29396.
100. Ney, B., et al., *Cofactor Tail Length Modulates Catalysis of Bacterial F420-Dependent Oxidoreductases*. Front. Microbiol, 2017. **8**(1902).
101. Kirk, C.D., et al., *The affinity of pea cotyledon 10-formyltetrahydrofolate synthetase for polyglutamate substrates*. Phytochemistry, 1994. **35**(2): p. 291-296.
102. Søballe, B. and R.K. Poole, *Microbial ubiquinones: multiple roles in respiration, gene regulation and oxidative stress management*. Microbiology (Reading), 1999. **145**(8): p. 1817-1830.
103. Brunsveld, L., H. Waldmann, and D. Huster, *Membrane binding of lipidated Ras peptides and proteins — The structural point of view*. Biochim. Biophys. Acta, 2009. **1788**(1): p. 273-288.
104. Fischer, J.D., G.L. Holliday, and J.M. Thornton, *The CoFactor database: organic cofactors in enzyme catalysis*. Bioinformatics, 2010. **26**(19): p. 2496-2497.
105. Zhou, Y., et al., *Determining the extremes of the cellular NAD(H) level by using an Escherichia coli NAD(+)-auxotrophic mutant*. Appl. Environ. Microbiol., 2011. **77**(17): p. 6133-6140.
106. Bockwolfdt, M., et al., *Identification of evolutionary and kinetic drivers of NAD-dependent signaling*. PNAS, 2019. **116**(32): p. 15957-15966.
107. Grose, J.H., et al., *Evidence that feedback inhibition of NAD kinase controls responses to oxidative stress*. PNAS, 2006. **103**(20): p. 7601-7606.
108. Xiao, W., et al., *NAD(H) and NADP(H) Redox Couples and Cellular Energy Metabolism*. Antioxid. Redox Signal, 2018. **28**(3): p. 251-272.
109. Begley, T.P., et al., *The biosynthesis of nicotinamide adenine dinucleotides in bacteria*, in *Cofactor Biosynthesis*. 2001. p. 103-119.
110. Panozzo, C., et al., *Aerobic and anaerobic NAD<sup>+</sup> metabolism in Saccharomyces cerevisiae*. FEBS Lett., 2002. **517**(1-3): p. 97-102.
111. Kurnasov, O., et al., *NAD Biosynthesis: identification of the tryptophan to quinolinate pathway in bacteria*. Chem. Biol., 2003. **10**(12): p. 1195-1204.
112. Sauve, A.A., et al., *Chemistry of Gene Silencing: The Mechanism of NAD<sup>+</sup>-Dependent Deacetylation Reactions*. ACS Biochem, 2001. **40**(51): p. 15456-15463.
113. Bieganowski, P. and C. Brenner, *Discoveries of Nicotinamide Riboside as a Nutrient and Conserved NRK Genes Establish a Preiss-Handler Independent Route to NAD<sup>+</sup> in Fungi and Humans*. Cell, 2004. **117**(4): p. 495-502.
114. Foster, J.W. and A.M. Baskowsky-Foster, *Pyridine nucleotide cycle of Salmonella typhimurium: in vivo recycling of nicotinamide adenine dinucleotide*. J. Bacteriol., 1980. **142**(3): p. 1032-5.
115. Macheroux, P., B. Kappes, and S.E. Ealick, *Flavogenomics--a genomic and structural view of flavin-dependent proteins*. FEBS J., 2011. **278**(15): p. 2625-34.
116. Pimviriyakul, P. and P. Chaiyen, *Chapter One - Overview of flavin-dependent enzymes*, in *The Enzymes*, P. Chaiyen and F. Tamanoi, Editors. 2020, Academic Press. p. 1-36.
117. Shah, M.V., et al., *Cofactor F420-Dependent Enzymes: An Under-Explored Resource for Asymmetric Redox Biocatalysis*. Catalysts, 2019. **9**(10).
118. Kalyanaraman, B., C.C. Felix, and R.C. Sealy, *Semiquinone anion radicals of catechol(amine)s, catechol estrogens, and their metal ion complexes*. Environ. Health Perspect., 1985. **64**: p. 185-98.
119. Johnson, B.J., et al., *Structural snapshots from the oxidative half-reaction of a copper amine oxidase: implications for O<sub>2</sub> activation*. J. Biol. Chem., 2013. **288**(39): p. 28409-28417.
120. Song, Y. and G.R. Buettner, *Thermodynamic and kinetic considerations for the reaction of semiquinone radicals to form superoxide and hydrogen peroxide*. Free Radic Biol Med, 2010. **49**(6): p. 919-962.
121. Basset, G.J., et al., *Phylloquinone (Vitamin K1): Occurrence, Biosynthesis and Functions*. Mini Rev Med Chem, 2017. **17**(12): p. 1028-1038.

122. Nowicka, B. and J. Kruk, *Occurrence, biosynthesis and function of isoprenoid quinones*. Biochim Biophys Acta, 2010. **1797**(9): p. 1587-605.
123. Aussel, L., et al., *Biosynthesis and physiology of coenzyme Q in bacteria*. Biochim. Biophys. Acta, 2014. **1837**(7): p. 1004-1011.
124. van Beilen, J.W.A. and K.J. Hellingwerf, *All Three Endogenous Quinone Species of Escherichia coli Are Involved in Controlling the Activity of the Aerobic/Anaerobic Response Regulator ArcA*. Front. Microbiol, 2016. **7**(1339).
125. Sharma, P., et al., *Kinase activity of ArcB from Escherichia coli is subject to regulation by both ubiquinone and demethylmenaquinone*. PLoS One, 2013. **8**(10): p. e75412-e75412.
126. Knaggs, A.R., A.R. Knaggs, and A.R. Knaggs, *The biosynthesis of shikimate metabolites*. Nat. Prod. Rep., 1999. **16**(4): p. 525-560.
127. Meganathan, R., *Ubiquinone biosynthesis in microorganisms*. FEMS Microbiol. Lett., 2001. **203**(2): p. 131-139.
128. Degli Esposti, M., *A Journey across Genomes Uncovers the Origin of Ubiquinone in Cyanobacteria*. Genome Biol Evol, 2017. **9**(11): p. 3039-3053.
129. Lichtenthaler, H.K., *The 1-Deoxy-D-Xylulose-5-Phosphate Pathway of Isoprenoid Biosynthesis in Plants*. Annu. Rev. Plant Physiol. Plant Mol. Biol., 1999. **50**: p. 47-65.
130. Lange, B.M., et al., *Isoprenoid biosynthesis: the evolution of two ancient and distinct pathways across genomes*. PNAS, 2000. **97**(24): p. 13172-7.
131. Unden, G. and J. Bongaerts, *Alternative respiratory pathways of Escherichia coli: energetics and transcriptional regulation in response to electron acceptors*. Biochim Biophys Acta, 1997. **1320**(3): p. 217-34.
132. Davidson, V.L., *Generation of protein-derived redoxcofactors by posttranslational modification*. Mol. BioSyst., 2011. **7**(1): p. 29-37.
133. Klinman, J.P. and F. Bonnot, *Intrigues and intricacies of the biosynthetic pathways for the enzymatic quinocofactors: PQQ, TTQ, CTQ, TPQ, and LTQ*. Chem Rev, 2014. **114**(8): p. 4343-65.
134. Janes, S., et al., *A new redox cofactor in eukaryotic enzymes: 6-hydroxydopa at the active site of bovine serum amine oxidase*. Science, 1990. **248**(4958): p. 981-987.
135. Dooley, D.M., *Structure and biogenesis of topaquinone and related cofactors*. J Biol Inorg Chem, 1999. **4**(1): p. 1-11.
136. Mu, D., et al., *Tyrosine codon corresponds to topa quinone at the active site of copper amine oxidases*. J. Biol. Chem., 1992. **267**(12): p. 7979-82.
137. Cai, D. and J.P. Klinman, *Evidence of a self-catalytic mechanism of 2,4,5-trihydroxyphenylalanine quinone biogenesis in yeast copper amine oxidase*. J. Biol. Chem., 1994. **269**(51): p. 32039-42.
138. McIntire, W.S., et al., *A new cofactor in a prokaryotic enzyme: tryptophan tryptophylquinone as the redox prosthetic group in methylamine dehydrogenase*. Science, 1991. **252**(5007): p. 817-24.
139. Wang, Y., et al., *MauG, a Novel Diheme Protein Required for Tryptophan Tryptophylquinone Biogenesis*. ACS Biochem, 2003. **42**(24): p. 7318-7325.
140. Datta, S., et al., *Structure of a quinohemoprotein amine dehydrogenase with an uncommon redox cofactor and highly unusual crosslinking*. PNAS, 2001. **98**(25): p. 14268-73.
141. Grau-Bové, X., I. Ruiz-Trillo, and F. Rodriguez-Pascual, *Origin and evolution of lysyl oxidases*. Sci Rep, 2015. **5**: p. 10568-10568.
142. Wang, S.X., et al., *A Crosslinked Cofactor in Lysyl Oxidase: Redox Function for Amino Acid Side Chains*. Science, 1996. **273**(5278): p. 1078-1084.
143. Bollinger, J.A., D.E. Brown, and D.M. Dooley, *The Formation of Lysine Tyrosylquinone (LTQ) Is a Self-Processing Reaction. Expression and Characterization of a Drosophila Lysyl Oxidase*. ACS Biochem, 2005. **44**(35): p. 11708-11714.
144. Ortega, M.A. and W.A. van der Donk, *New Insights into the Biosynthetic Logic of Ribosomally Synthesized and Post-translationally Modified Peptide Natural Products*. Cell Chem Biol, 2016. **23**(1): p. 31-44.
145. Arnison, P.G., et al., *Ribosomally synthesized and post-translationally modified peptide natural products: overview and recommendations for a universal nomenclature*. Nat Prod Rep, 2013. **30**(1): p. 108-60.

146. Oman, T.J. and W.A. van der Donk, *Follow the leader: the use of leader peptides to guide natural product biosynthesis*. Nat. Chem. Biol., 2010. **6**(1): p. 9-18.
147. Kuipers, O.P., et al., *Protein engineering of lantibiotics*. Antonie Van Leeuwenhoek, 1996. **69**(2): p. 161-170.
148. Burkhart, B.J., et al., *A prevalent peptide-binding domain guides ribosomal natural product biosynthesis*. Nat. Chem. Biol., 2015. **11**(8): p. 564-70.
149. Dunbar, K.L. and D.A. Mitchell, *Revealing nature's synthetic potential through the study of ribosomal natural product biosynthesis*. ACS Chem Biol, 2013. **8**(3): p. 473-87.
150. Simons, A., K. Alhanout, and R.E. Duval, *Bacteriocins, Antimicrobial Peptides from Bacterial Origin: Overview of Their Biology and Their Impact against Multidrug-Resistant Bacteria*. Microorganisms, 2020. **8**(5): p. 639.
151. Zhu, W. and J.P. Klinman, *Biogenesis of the peptide-derived redox cofactor pyrroloquinoline quinone*. Curr. Opin. Chem. Biol., 2020. **59**: p. 93-103.
152. Hauge, J.G., *Glucose Dehydrogenase of Bacterium Anitratum: An Enzyme with a Novel Prosthetic Group*. J. Biol. Chem., 1964. **239**: p. 3630-9.
153. Goodwin, P.M. and C. Anthony, *The biochemistry, physiology and genetics of PQQ and PQQ-containing enzymes*. Adv. Microb. Physiol., 1998. **40**: p. 1-80.
154. Buurman, E.T., et al., *The role of magnesium and calcium ions in the glucose dehydrogenase activity of Klebsiella pneumoniae NCTC 418*. Arch. Microbiol., 1990. **153**(5): p. 502-5.
155. Jia, D., et al., *Pyrroloquinoline-quinone suppresses liver fibrogenesis in mice*. PLoS One, 2015. **10**(3): p. e0121939.
156. Kim, J., et al., *The inhibitory effect of pyrroloquinoline quinone on the amyloid formation and cytotoxicity of truncated alpha-synuclein*. Mol Neurodegener, 2010. **5**: p. 20.
157. Zhang, Y. and P.A. Rosenberg, *The essential nutrient pyrroloquinoline quinone may act as a neuroprotectant by suppressing peroxynitrite formation*. Eur. J. Neurosci., 2002. **16**(6): p. 1015-1024.
158. Huang, Y., N. Chen, and D. Miao, *Effect and mechanism of pyrroloquinoline quinone on anti-osteoporosis in Bmi-1 knockout mice-Anti-oxidant effect of pyrroloquinoline quinone*. Am J Transl Res, 2017. **9**(10): p. 4361-4374.
159. Kong, L., et al., *Pyrroloquinoline quinone inhibits RANKL-mediated expression of NFATc1 in part via suppression of c-Fos in mouse bone marrow cells and inhibits wear particle-induced osteolysis in mice*. PLoS One, 2013. **8**(4): p. e61013.
160. Steinberg, F., et al., *Pyrroloquinoline quinone improves growth and reproductive performance in mice fed chemically defined diets*. Exp Biol Med (Maywood), 2003. **228**(2): p. 160-6.
161. Rucker, R., et al., *Is pyrroloquinoline quinone a vitamin?* Nature, 2005. **433**(7025): p. E10-E11.
162. Killgore, J., et al., *Nutritional importance of pyrroloquinoline quinone*. Science, 1989. **245**(4920): p. 850-2.
163. Ames, B.N., *Prolonging healthy aging: Longevity vitamins and proteins*. PNAS, 2018. **115**(43): p. 10836-10844.
164. Goosen, N., R.G. Huinen, and P. van de Putte, *A 24-amino-acid polypeptide is essential for the biosynthesis of the coenzyme pyrrolo-quinoline-quinone*. J. Bacteriol., 1992. **174**(4): p. 1426-7.
165. Barr, I., et al., *Demonstration That the Radical S-Adenosylmethionine (SAM) Enzyme PqqE Catalyzes de Novo Carbon-Carbon Cross-linking within a Peptide Substrate PqqA in the Presence of the Peptide Chaperone PqqD*. J. Biol. Chem., 2016. **291**(17): p. 8877-8884.
166. Sofia, H.J., et al., *Radical SAM, a novel protein superfamily linking unresolved steps in familiar biosynthetic pathways with radical mechanisms: functional characterization using new analysis and information visualization methods*. Nucleic Acids Res., 2001. **29**(5): p. 1097-106.
167. Broderick, J.B., et al., *Radical S-adenosylmethionine enzymes*. Chem Rev, 2014. **114**(8): p. 4229-317.
168. Quevillon, E., et al., *InterProScan: protein domains identifier*. Nucleic Acids Res., 2005(33 (Web Server issue)): p. W116-W120.
169. Berman, H.M., et al., *The Protein Data Bank*. Nucleic Acids Res., 2000. **28**: p. 235-242.
170. Frey, P.A., *Radical Mechanisms of Enzymatic Catalysis*. Annu. Rev. Biochem., 2001. **70**(1): p. 121-148.
171. Shen, Y.Q., et al., *Distribution and properties of the genes encoding the biosynthesis of the bacterial cofactor, pyrroloquinoline quinone*. ACS Biochem, 2012. **51**(11): p. 2265-75.

172. Martins, A.M., et al., *A two-component protease in *Methylorubrum extorquens* with high activity toward the peptide precursor of the redox cofactor pyrroloquinoline quinone*. J. Biol. Chem., 2019. **294**(41): p. 15025-15036.
173. Magnusson, O.T., et al., *Quinone biogenesis: Structure and mechanism of PqqC, the final catalyst in the production of pyrroloquinoline quinone*. PNAS, 2004. **101**(21): p. 7913-7918.
174. Mahanta, N., G.A. Hudson, and D.A. Mitchell, *Radical S-Adenosylmethionine Enzymes Involved in RiPP Biosynthesis*. ACS Biochem, 2017. **56**(40): p. 5229-5244.
175. Benjdia, A., C. Balty, and O. Berteau, *Radical SAM Enzymes in the Biosynthesis of Ribosomally Synthesized and Post-translationally Modified Peptides (RiPPs)*. Front. Chem., 2017. **5**.
176. Kensch, P.R., et al., *Practical and theoretical advances in predicting the function of a protein by its phylogenetic distribution*. J R Soc. Interface, 2007. **5**(19): p. 151-170.
177. Basu, M.K., J.D. Selengut, and D.H. Haft, *ProPhylo: partial phylogenetic profiling to guide protein family construction and assignment of biological process*. BMC Bioinform, 2011. **12**: p. 434.
178. Haft, D.H., *Bioinformatic evidence for a widely distributed, ribosomally produced electron carrier precursor, its maturation proteins, and its nicotinoprotein redox partners*. BMC Genom., 2011. **12**: p. 21.
179. van Belkum, M.J., L.A. Martin-Visscher, and J.C. Vederas, *Structure and genetics of circular bacteriocins*. Trends Microbiol., 2011. **19**(8): p. 411-418.
180. Vogels, G.D. and C. Van der Drift, *Degradation of purines and pyrimidines by microorganisms*. Bacteriol Rev, 1976. **40**(2): p. 403-468.
181. Ayikpoe, R.S. and J.A. Latham, *MftD Catalyzes the Formation of a Biologically Active Redox Center in the Biosynthesis of the Ribosomally Synthesized and Post-translationally Modified Redox Cofactor, Mycofactocin*. J. Am. Chem. Soc., 2019.
182. Skinnider, M.A., et al., *Genomic charting of ribosomally synthesized natural product chemical space facilitates targeted mining*. PNAS, 2016. **113**(42): p. E6343-E6351.
183. Khaliullin, B., et al., *Mycofactocin biosynthesis: modification of the peptide MftA by the radical S-adenosylmethionine protein MftC*. FEBS Lett., 2016. **590**(16): p. 2538-48.
184. Bruender, N.A. and V. Bandarian, *The Radical S-Adenosyl-l-methionine Enzyme MftC Catalyzes an Oxidative Decarboxylation of the C-Terminus of the MftA Peptide*. ACS Biochem, 2016. **55**(20): p. 2813-6.
185. Khaliullin, B., et al., *Mechanistic elucidation of the mycofactocin-biosynthetic radical S-adenosylmethionine protein, MftC*. J. Biol. Chem., 2017. **292**(31): p. 13022-13033.
186. Bruender, N.A. and V. Bandarian, *The Creatininase Homolog MftE from *Mycobacterium smegmatis* Catalyzes a Peptide Cleavage Reaction in the Biosynthesis of a Novel Ribosomally Synthesized Post-translationally Modified Peptide (RiPP)*. J. Biol. Chem., 2017. **292**(10): p. 4371-4381.
187. Ayikpoe, R., et al., *Mycofactocin Biosynthesis Proceeds through 3-Amino-5-[(p-hydroxyphenyl)methyl]-4,4-dimethyl-2-pyrrolidinone (AHDP); Direct Observation of MftE Specificity toward MftA\**. ACS Biochem, 2018.
188. Sievers, F., et al., *Fast, scalable generation of high-quality protein multiple sequence alignments using Clustal Omega*. Mol. Syst. Biol., 2011. **7**(1).
189. Sievers, F. and D.G. Higgins, *Clustal Omega for making accurate alignments of many protein sequences*. Protein Sci., 2018. **27**(1): p. 135-145.
190. Guindon, S., et al., *New Algorithms and Methods to Estimate Maximum-Likelihood Phylogenies: Assessing the Performance of PhyML 3.0*. Syst. Biol., 2010. **59**(3): p. 307-321.
191. Le, S.Q. and O. Gascuel, *An Improved General Amino Acid Replacement Matrix*. Mol. Biol. Evol., 2008. **25**(7): p. 1307-1320.
192. Cook, G.M., et al., *Energetics of Respiration and Oxidative Phosphorylation in *Mycobacteria**. Microbiol Spectr, 2014. **2**(3).
193. Diskin, C. and E.M. Pålsson-McDermott, *Metabolic Modulation in Macrophage Effector Function*. Front Immunol, 2018. **9**: p. 270-270.
194. Ratter, J.M., et al., *In vitro and in vivo Effects of Lactate on Metabolism and Cytokine Production of Human Primary PBMCs and Monocytes*. Front Immunol, 2018. **9**(2564).

195. Appelberg, R., et al., *The Warburg effect in mycobacterial granulomas is dependent on the recruitment and activation of macrophages by interferon- $\gamma$* . Immunology, 2015. **145**(4): p. 498-507.
196. Billig, S., et al., *Lactate oxidation facilitates growth of Mycobacterium tuberculosis in human macrophages*. Sci Rep, 2017. **7**(1): p. 6484.
197. Zimmermann, M., et al., *Integration of Metabolomics and Transcriptomics Reveals a Complex Diet of Mycobacterium tuberculosis during Early Macrophage Infection*. mSystems, 2017. **2**(4).
198. Serafini, A., et al., *Mycobacterium tuberculosis requires glyoxylate shunt and reverse methylcitrate cycle for lactate and pyruvate metabolism*. Mol. Microbiol., 2019.
199. Trivedi, A., et al., *Thiol reductive stress induces cellulose-anchored biofilm formation in Mycobacterium tuberculosis*. Nat Commun, 2016. **7**: p. 11392.
200. Ayikpoe, R.S., *New Insights into Mycofactocin Biosynthesis, Structure and Function*, in Faculty of Natural Sciences and Mathematics. 2019, University of Denver.
201. Ayikpoe, R., V. Govindarajan, and J.A. Latham, *Occurrence, function, and biosynthesis of mycofactocin*. Appl. Microbiol. Biotechnol., 2019.
202. Deng, W., C. Li, and J. Xie, *The underlying mechanism of bacterial TetR/AcrR family transcriptional repressors*. Cell. Signal., 2013. **25**(7): p. 1608-13.
203. Peterson, E.J.R., et al., *Path-seq identifies an essential mycolate remodeling program for mycobacterial host adaptation*. Mol. Syst. Biol., 2019. **15**(3).
204. Lubelski, J., et al., *Biosynthesis, immunity, regulation, mode of action and engineering of the model lantibiotic nisin*. Cell. Mol. Life Sci., 2008. **65**(3): p. 455-76.
205. Lees, G.J. and G.R. Jago, *Role of Acetaldehyde in Metabolism: A Review I. Enzymes Catalyzing Reactions Involving Acetaldehyde*. J. Dairy Sci., 1978. **61**(9): p. 1205-1215.
206. Antranikian, G. and S. Elleuche, *Bacterial group III alcohol dehydrogenases - function, evolution and biotechnological applications*. OA Alcohol, 2013. **1**(1).
207. Krozowski, Z., *The short-chain alcohol dehydrogenase superfamily: Variations on a common theme*. J. Steroid Biochem. Mol., 1994. **51**(3): p. 125-130.
208. Chen, L., et al., *Redox Balance in Lactobacillus reuteri DSM20016: Roles of Iron-Dependent Alcohol Dehydrogenases in Glucose/ Glycerol Metabolism*. PLoS One, 2016. **11**(12): p. e0168107-e0168107.
209. Cavener, D.R., *GMC oxidoreductases: A newly defined family of homologous proteins with diverse catalytic activities*. J. Mol. Biol., 1992. **223**(3): p. 811-814.
210. Cotruvo, J.A., *The Chemistry of Lanthanides in Biology: Recent Discoveries, Emerging Principles, and Technological Applications*. ACS Cent Sci, 2019. **5**(9): p. 1496-1506.
211. Cavener, D.R., *GMC oxidoreductases. A newly defined family of homologous proteins with diverse catalytic activities*. J. Mol. Biol., 1992. **223**(3): p. 811-4.
212. Wongnate, T. and P. Chaiyen, *The substrate oxidation mechanism of pyranose 2-oxidase and other related enzymes in the glucose-methanol-choline GMC superfamily*. FEBS J., 2013. **280**(13): p. 3009-3027.
213. Romero, E. and G. Gadda, *Alcohol oxidation by flavoenzymes*. Biomol. Concepts, 2014. **5**(4): p. 299-318.
214. Ferri, S., K. Kojima, and K. Sode, *Review of Glucose Oxidases and Glucose Dehydrogenases: A Bird's Eye View of Glucose Sensing Enzymes*. J. Diabetes Sci. Technol, 2011. **5**(5): p. 1068-1076.
215. Sutzl, L., et al., *The GMC superfamily of oxidoreductases revisited: analysis and evolution of fungal GMC oxidoreductases*. Biotechnol Biofuels, 2019. **12**: p. 118.
216. Iida, K., et al., *Expansion and evolution of insect GMC oxidoreductases*. BMC Evol. Biol., 2007. **7**(1).
217. Zheng, Y., et al., *Physiological Effect of XoxG(4) on Lanthanide-Dependent Methanotrophy*. mBio, 2018. **9**(2): p. e02430-17.
218. Takahashi, K., et al., *Membrane-associated glucose-methanol-choline oxidoreductase family enzymes PhcC and PhcD are essential for enantioselective catabolism of dehydrodiconiferyl alcohol*. Appl. Environ. Microbiol., 2015. **81**(23): p. 8022-36.
219. Anthony, C. and L.J. Zatman, *The microbial oxidation of methanol. 2. The methanol-oxidizing enzyme of Pseudomonas sp. M 27*. Biochem. J., 1964. **92**(3): p. 614-21.

220. Jahn, B., et al., *Understanding the chemistry of the artificial electron acceptors PES, PMS, DCPIP and Wurster's Blue in methanol dehydrogenase assays*. J. Biol. Inorg. Chem., 2020. **25**(2): p. 199-212.
221. Pichersky, E., J.P. Noel, and N. Dudareva, *Biosynthesis of plant volatiles: nature's diversity and ingenuity*. Science (New York, N.Y.), 2006. **311**(5762): p. 808-811.
222. van der Werf, M.J., et al., *Stereoselective carveol dehydrogenase from Rhodococcus erythropolis DCL14. A novel nicotinoprotein belonging to the short chain dehydrogenase/reductase superfamily*. J. Biol. Chem., 1999. **274**(37): p. 26296-304.
223. Haft, D.H., et al., *Mycofactocin-associated mycobacterial dehydrogenases with non-exchangeable NAD cofactors*. Sci Rep, 2017. **7**: p. 41074.
224. Dubey, A.A., S.R. Wani, and V. Jain, *Methylotrophy in Mycobacteria: Dissection of the Methanol Metabolism Pathway in Mycobacterium smegmatis*. J. Bacteriol., 2018. **200**(17).
225. Dubey, A.A. and V. Jain, *Mycofactocin is essential for the establishment of methylotrophy in Mycobacterium smegmatis*. Biochem. Biophys. Res. Commun., 2019.
226. Krishnamoorthy, G., et al., *Mycofactocin Is Associated with Ethanol Metabolism in Mycobacteria*. mBio, 2019. **10**(3).
227. Pandey, A.K. and C.M. Sasseti, *Mycobacterial persistence requires the utilization of host cholesterol*. PNAS, 2008. **105**(11): p. 4376-80.
228. Gatfield, J. and J. Pieters, *Essential Role for Cholesterol in Entry of Mycobacteria into Macrophages*. Science, 2000. **288**(5471): p. 1647-1651.
229. Griffin, J.E., et al., *High-resolution phenotypic profiling defines genes essential for mycobacterial growth and cholesterol catabolism*. PLoS Pathog, 2011. **7**(9): p. e1002251.
230. Tsukamura, M., *Utilisation of ethanol as sole carbon source by Mycobacterium marinum*. Tubercle, 1988. **69**(2).
231. Dubey, A.A. and V. Jain, *MnoSR Is a Bona Fide Two-Component System Involved in Methylotrophic Metabolism in Mycobacterium smegmatis*. Appl. Environ. Microbiol., 2019. **85**(13): p. e00535-19.
232. Bystrykh, L.V., et al., *Formaldehyde dismutase activities in Gram-positive bacteria oxidizing methanol*. Microbiology, 1993. **139**(9): p. 1979-1985.
233. Van Ophem, P.W., J. Van Beeumen, and J.A. Duine, *Nicotinoprotein [NAD(P)-containing] alcohol/aldehyde oxidoreductases. Purification and characterization of a novel type from Amycolatopsis methanolica*. Eur. J. Biochem., 1993. **212**(3): p. 819-26.
234. Park, H., et al., *Identification and functional characterization of a gene for the methanol : N,N'-dimethyl-4-nitrosoaniline oxidoreductase from Mycobacterium sp. strain JCI (DSM 3803)*. Microbiology, 2009. **156**(2): p. 463-471.
235. Singh, M.I. and V. Jain, *Tagging the Expressed Protein with 6 Histidines: Rapid Cloning of an Amplicon with Three Options*. PLoS One, 2013. **8**(5): p. e63922.
236. Peña-Ortiz, L., et al., *Structure elucidation of the redox cofactor mycofactocin reveals oligoglycosylation by MftF*. Chem Sci, 2020.
237. Garvie, E.I., *Bacterial lactate dehydrogenases*. Microbiol Rev, 1980. **44**(1): p. 106-39.
238. Warner, D.F., *Mycobacterium tuberculosis metabolism*. Cold Spring Harb Perspect Med, 2014. **5**(4): p. a021121.
239. Giegel, D.A., C.H. Williams, and V. Massey, *L-lactate 2-monooxygenase from Mycobacterium smegmatis. Cloning, nucleotide sequence, and primary structure homology within an enzyme family*. J. Biol. Chem., 1990. **265**(12): p. 6626-6632.
240. Nikitushkin, V.D., et al., *Metabolic profiling of dormant Mycolicibacterium smegmatis cells' reactivation reveals a gradual assembly of metabolic processes*. Metabolomics, 2020. **16**(2): p. 24.
241. Greening, C., et al., *The growth and survival of Mycobacterium smegmatis is enhanced by co-metabolism of atmospheric H<sub>2</sub>*. PLoS One, 2014. **9**(7): p. e103034.
242. Zhao, R., et al., *NAD-dependent lactate dehydrogenase catalyses the first step in respiratory utilization of lactate by Lactococcus lactis*. FEBS Open Bio, 2013. **3**: p. 379-386.
243. Stansen, C., et al., *Characterization of a Corynebacterium glutamicum lactate utilization operon induced during temperature-triggered glutamate production*. Appl. Environ. Microbiol., 2005. **71**(10): p. 5920-8.

244. Shevchenko, A., et al., *In-gel digestion for mass spectrometric characterization of proteins and proteomes*. Nat Protoc, 2006. **1**(6): p. 2856-60.
245. Reisch, C.R. and K.L. Prather, *The no-SCAR (Scarless Cas9 Assisted Recombineering) system for genome editing in Escherichia coli*. Sci Rep, 2015. **5**: p. 15096.
246. Chai, Y., R. Kolter, and R. Losick, *A widely conserved gene cluster required for lactate utilization in Bacillus subtilis and its involvement in biofilm formation*. J. Bacteriol., 2009. **191**(8): p. 2423-30.
247. Chauhiac, D., et al., *Removing chiral contamination of lactate solutions by selective metabolism of the D-enantiomer*. Biotechnol. Lett., 2015. **37**(12): p. 2411-8.
248. Wang, X., et al., *Cofactor NAD(P)H Regeneration Inspired by Heterogeneous Pathways*. Chem, 2017. **2**(5): p. 621-654.
249. Xie, W., L. Bülow, and B. Xie, *Pyrroloquinoline quinone glucose dehydrogenase adopted in thermometric analysis for enhancement of glucose determination*. J. Therm. Anal. Calorim., 2018. **134**(3): p. 1913-1919.
250. Loughran, M.G., J.M. Hall, and A.P.F. Turner, *Development of a pyrroloquinoline quinone (PQQ) mediated glucose oxidase enzyme electrode for detection of glucose in fruit juice*. Electroanalysis, 1996. **8**(10): p. 870-875.
251. Vijayakumar, A.R., et al., *Alcohol biosensors based on coupled oxidase-peroxidase systems*. Anal. Chim. Acta, 1996. **327**(3): p. 223-234.
252. Bashiri, G., et al., *Metabolic engineering of cofactor F420 production in Mycobacterium smegmatis*. PLoS One, 2010. **5**(12): p. e15803.
253. Hartmans, S., et al., *Characterization of a Mycobacterium sp. and a Xanthobacter sp. for the removal of vinyl chloride and 1,2-dichloroethane from waste gases*. Appl. Microbiol. Biotechnol., 1992. **37**(6): p. 796-801.
254. Maier, U. and J. Büchs, *Characterisation of the gas-liquid mass transfer in shaking bioreactors*. Biochem Eng J, 2001. **7**(2): p. 99-106.
255. Peña-Ortiz, L., et al., *Impact of Oxygen Supply and Scale Up on Mycobacterium smegmatis Cultivation and Mycofactocin Formation*. Front. Bioeng. Biotechnol., 2020. **8**.
256. Anderlei, T. and J. Büchs, *Device for sterile online measurement of the oxygen transfer rate in shaking flasks*. Biochem Eng J, 2001. **7**(2): p. 157-162.
257. Wolin, E.A., M.J. Wolin, and R.S. Wolfe, *Formation of methane by bacterial extracts*. J. Biol. Chem., 1963. **238**: p. 2882-6.
258. Isabelle, D., D.R. Simpson, and L. Daniels, *Large-scale production of coenzyme F420-5,6 by using Mycobacterium smegmatis*. Appl. Environ. Microbiol., 2002. **68**(11): p. 5750-5.
259. Cadapan, L.D., et al., *Suspension cultivation of Mycobacterium ulcerans for the production of mycolactones*. FEMS Microbiol. Lett., 2001. **205**(2): p. 385-9.
260. Hecht, A., et al., *A minimum information standard for reproducing bench-scale bacterial cell growth and productivity*. Commun. Biol., 2018. **1**(1): p. 219.
261. Hauschild, I., et al., *The microbial growth of Mycobacterium aurum L1 on vinyl chloride with respect to inhibitory and limiting influence of substrate and oxygen*. Water Sci Technol, 1994. **30**(9): p. 125-132.
262. Lo, C.K., C.P. Pan, and W.H. Liu, *Production of testosterone from phytosterol using a single-step microbial transformation by a mutant of Mycobacterium sp.* J Ind Microbiol Biotechnol, 2002. **28**(5): p. 280-283.
263. Rodriguez-Garcia, A., et al., *Complete genome sequence of 'Mycobacterium neoaurum' NRRL B-3805, an androstenedione (AD) producer for industrial biotransformation of sterols*. J. Biotechnol., 2016. **224**: p. 64-5.
264. Marques, M.P., J.M. Cabral, and P. Fernandes, *A microwell platform for the scale-up of a multistep bioconversion to bench-scale reactors: sitosterol side-chain cleavage*. Biotechnol J, 2010. **5**(4): p. 402-12.
265. Meier, K., et al., *Correlation for the maximum oxygen transfer capacity in shake flasks for a wide range of operating conditions and for different culture media*. Biochem Eng J, 2016. **109**: p. 228-235.
266. Song, H. and M. Niederweis, *Uptake of Sulfate but Not Phosphate by Mycobacterium tuberculosis Is Slower than That for Mycobacterium smegmatis*. J. Bacteriol., 2011. **194**(5): p. 956-964.



## REFERENCES

267. Bennett, B.D., et al., *Absolute quantitation of intracellular metabolite concentrations by an isotope ratio-based approach*. Nat Protoc, 2008. **3**(8): p. 1299-311.
268. Lu, W., et al., *Metabolite Measurement: Pitfalls to Avoid and Practices to Follow*. Annu. Rev. Biochem., 2017. **86**: p. 277-304.
269. Bolten, C.J., et al., *Sampling for metabolome analysis of microorganisms*. Anal Chem, 2007. **79**(10): p. 3843-9.
270. Wang, M., et al., *Sharing and community curation of mass spectrometry data with Global Natural Products Social Molecular Networking*. Nat. Biotechnol., 2016. **34**(8): p. 828-837.
271. Shannon, P., et al., *Cytoscape: a software environment for integrated models of biomolecular interaction networks*. Genome Res., 2003. **13**(11): p. 2498-504.
272. Petho, L., G. Mezo, and G. Schlosser, *Overcharging Effect in Electrospray Ionization Mass Spectra of Daunomycin-Tuftsins Bioconjugates*. Molecules, 2019. **24**(16).
273. Zaia, J., *Mass spectrometry of oligosaccharides*. Mass Spectrom. Rev., 2004. **23**(3): p. 161-227.
274. Suzuki, H., et al., *Computationally and Experimentally Derived General Rules for Fragmentation of Various Glycosyl Bonds in Sodium Adduct Oligosaccharides*. Anal. Chem., 2009. **81**(3): p. 1108-1120.
275. Liang, D.M., et al., *Glycosyltransferases: mechanisms and applications in natural product development*. Chem Soc Rev, 2015. **44**(22): p. 8350-74.
276. Kightlinger, W., et al., *Synthetic Glycobiology: Parts, Systems, and Applications*. ACS Synth Biol, 2020. **9**(7): p. 1534-1562.
277. Sinnott, M.L., *Catalytic mechanism of enzymic glycosyl transfer*. Chem. Rev., 1990. **90**(7): p. 1171-1202.
278. Coutinho, P.M., et al., *An evolving hierarchical family classification for glycosyltransferases*. J. Mol. Biol., 2003. **328**(2): p. 307-17.
279. Campbell, J.A., et al., *A classification of nucleotide-diphospho-sugar glycosyltransferases based on amino acid sequence similarities*. Biochem. J., 1997. **326**(3): p. 929-939.
280. Spiro, R.G., *Protein glycosylation: nature, distribution, enzymatic formation, and disease implications of glycopeptide bonds*. Glycobiology, 2002. **12**(4): p. 43R-56R.
281. Yakovlieva, L. and M.T.C. Walvoort, *Processivity in Bacterial Glycosyltransferases*. ACS Chem Biol, 2019.
282. Schäffer, C., P. Messner, and M. Pohlschroder, *Emerging facets of prokaryotic glycosylation*. FEMS Microbiol. Rev., 2017. **41**(1): p. 49-91.
283. Thibodeaux, C.J., C.E. Melançon, and H.-w. Liu, *Unusual sugar biosynthesis and natural product glycodiversification*. Nature, 2007. **446**(7139): p. 1008-1016.
284. Dell, A., et al., *Similarities and differences in the glycosylation mechanisms in prokaryotes and eukaryotes*. Int J Microbiol, 2010. **2010**: p. 148178.
285. Berg, S., et al., *The glycosyltransferases of Mycobacterium tuberculosis—roles in the synthesis of arabinogalactan, lipoarabinomannan, and other glycoconjugates*. Glycobiology, 2007. **17**(6): p. 35R-56R.
286. Lairson, L.L., et al., *Glycosyltransferases: Structures, Functions, and Mechanisms*. Annu. Rev. Biochem., 2008. **77**(1): p. 521-555.
287. Thibodeaux, C.J., C.E. Melancon, 3rd, and H.W. Liu, *Natural-product sugar biosynthesis and enzymatic glycodiversification*. Angew Chem Int Ed Engl, 2008. **47**(51): p. 9814-59.
288. Finn, R.D., et al., *The Pfam protein families database*. Nucleic Acids Res., 2008. **36**: p. D281-D288.
289. Zarschler, K., et al., *Protein tyrosine O-glycosylation--A rather unexplored prokaryotic glycosylation system*. Glycobiology, 2010. **20**(6): p. 787-798.
290. Joshi, H.J., et al., *SnapShot: O-Glycosylation Pathways across Kingdoms*. Cell, 2018. **172**(3): p. 632-632.e2.
291. Reily, C., et al., *Glycosylation in health and disease*. Nat. Rev. Nephrol., 2019. **15**(6): p. 346-366.
292. Chen, P.S., H.K. Mitchell, and M. Neuweg, *Tyrosine glucoside in Drosophila busckii*. Insect Biochem., 1978. **8**(4): p. 279-286.
293. Kramer, K.J., et al., *Tyrosine metabolism for cuticle tanning in the tobacco hornworm, Manduca sexta (L.) and other lepidoptera: Identification of  $\beta$ -d-glucopyranosyl-O-l-tyrosine and other metabolites*. Arch. Biochem. Biophys., 1980. **205**(1): p. 146-155.

294. Rodriguez, I.R. and W.J. Whelan, *A novel glycosyl-amino acid linkage: Rabbit-muscle glycogen is covalently linked to a protein via tyrosine*. *Biochem. Biophys. Res. Commun.*, 1985. **132**(2): p. 829-836.
295. Jank, T., et al., *Tyrosine glycosylation of Rho by Yersinia toxin impairs blastomere cell behaviour in zebrafish embryos*. *Nat. Commun.*, 2015. **6**(1): p. 7807.
296. Wadzinski, T.J., et al., *Rapid phenolic O-glycosylation of small molecules and complex unprotected peptides in aqueous solvent*. *Nat. Chem.*, 2018. **10**(6): p. 644-652.
297. Ragsdale, S.W., *Catalysis of methyl group transfers involving tetrahydrofolate and B(12)*. *Vitam Horm*, 2008. **79**: p. 293-324.
298. Liscombe, D.K., G.V. Louie, and J.P. Noel, *Architectures, mechanisms and molecular evolution of natural product methyltransferases*. *Nat. Prod. Rep.*, 2012. **29**(10).
299. Staudacher, E., *Methylation--an uncommon modification of glycans*. *Biol. Chem.*, 2012. **393**(8): p. 675-85.
300. Wohlschlagel, T., et al., *Methylated glycans as conserved targets of animal and fungal innate defense*. *PNAS*, 2014. **111**(27): p. E2787-E2796.
301. Jackson, M. and P.J. Brennan, *Polymethylated polysaccharides from Mycobacterium species revisited*. *J. Biol. Chem.*, 2009. **284**(4): p. 1949-53.
302. Mendes, V., et al., *Biosynthesis of mycobacterial methylglucose lipopolysaccharides*. *Nat. Prod. Rep.*, 2012. **29**(8).
303. Jeevarajah, D., et al., *Methylation of GPLs in Mycobacterium smegmatis and Mycobacterium avium*. *J. Bacteriol.*, 2004. **186**(20): p. 6792-9.
304. Patterson, J.H., et al., *Identification of a methyltransferase from Mycobacterium smegmatis involved in glycopeptidolipid synthesis*. *J. Biol. Chem.*, 2000. **275**(32): p. 24900-6.
305. Kamisango, K., A. Dell, and C.E. Ballou, *Biosynthesis of the mycobacterial O-methylglucose lipopolysaccharide. Characterization of putative intermediates in the initiation, elongation, and termination reactions*. *J. Biol. Chem.*, 1987. **262**(10): p. 4580-4586.
306. Medie, F.M., et al., *Genome analyses highlight the different biological roles of cellulases*. *Nat. Rev. Microbiol.*, 2012. **10**(3): p. 227-234.
307. Van Wyk, N., et al., *Characterization of a mycobacterial cellulase and its impact on biofilm- and drug-induced cellulose production*. *Glycobiology*, 2017. **27**(5): p. 392-399.
308. Varrot, A., et al., *Mycobacterium tuberculosis Strains Possess Functional Cellulases*. *J. Biol. Chem.*, 2005. **280**(21): p. 20181-20184.
309. Rehm, J., et al., *The association between alcohol use, alcohol use disorders and tuberculosis (TB). A systematic review*. *BMC Public Health*, 2009. **9**: p. 450-450.
310. Imtiaz, S., et al., *Alcohol consumption as a risk factor for tuberculosis: meta-analyses and burden of disease*. *Eur. Respir. J.*, 2017. **50**(1): p. 1700216.
311. Jones, A.W., *Variability of the blood:breath alcohol ratio in vivo*. *J. Stud. Alcohol*, 1978. **39**(11): p. 1931-9.
312. Labianca, D.A. and G. Simpson, *Statistical analysis of blood- to breath-alcohol ratio data in the logarithm-transformed and non-transformed modes*. *Eur J Clin Chem Clin Biochem*, 1996. **34**(2): p. 111-7.
313. Uusi-Mäkelä, M. and M. Rämetsä, *Hijacking Host Angiogenesis to Drive Mycobacterial Growth*. *Cell Host Microbe*, 2018. **24**(4): p. 465-466.
314. Bair, T.B., D.W. Isabelle, and L. Daniels, *Structures of coenzyme F420 in Mycobacterium species*. *Arch. Microbiol.*, 2001. **176**(1): p. 37-43.
315. Gorris, L.G. and C. van der Drift, *Cofactor contents of methanogenic bacteria reviewed*. *BioFactors*, 1994. **4**(3-4): p. 139-45.
316. Ney, B., et al., *The methanogenic redox cofactor F420 is widely synthesized by aerobic soil bacteria*. *ISME J*, 2017. **11**(1): p. 125-137.
317. Hassell, A.M., et al., *Crystallization of protein-ligand complexes*. *Acta Crystallogr. D*. 2006. **63**(1): p. 72-79.
318. Anderlei, T., et al., *Online respiration activity measurement (OTR, CTR, RQ) in shake flasks*. *Biochem Eng J*, 2004. **17**(3): p. 187-194.
319. Franzén, C.J., E. Albers, and C. Niklasson, *Use of the inlet gas composition to control the respiratory quotient in microaerobic bioprocesses*. *Chem. Eng. Sci.*, 1996. **51**(13): p. 3391-3402.

## REFERENCES

320. Heyman, B., et al., *Online monitoring of the respiratory quotient reveals metabolic phases during microaerobic 2,3-butanediol production with Bacillus licheniformis*. Eng. Life Sci., 2020. **20**(3-4): p. 133-144.
321. Ramon-Portugal, F., H. Pingaud, and P. Strehaiano, *Metabolic transition step from ethanol consumption to sugar/ethanol consumption by Saccharomyces cerevisiae*. Biotechnol. Lett., 2004. **26**(21): p. 1671-4.
322. Routledge, S.J., *Beyond de-foaming: the effects of antifoams on bioprocess productivity*. Comput Struct Biotechnol J, 2012. **3**: p. e201210014-e201210014.
323. Vazquez, A., *A Historical View of Overflow Metabolism*, in *Overflow Metabolism: From Yeast to Marathon Runners*. 2018. p. 1-6.
324. Pinhal, S., et al., *Acetate Metabolism and the Inhibition of Bacterial Growth by Acetate*. J. Bacteriol., 2019. **201**(13): p. e00147-19.
325. el-Mansi, E.M. and W.H. Holms, *Control of carbon flux to acetate excretion during growth of Escherichia coli in batch and continuous cultures*. J Gen Microbiol, 1989. **135**(11): p. 2875-83.
326. Enjalbert, B., et al., *Acetate fluxes in Escherichia coli are determined by the thermodynamic control of the Pta-AckA pathway*. Sci Rep, 2017. **7**(1): p. 42135.
327. Rücker, N., et al., *Acetate Dissimilation and Assimilation in Mycobacterium tuberculosis Depend on Carbon Availability*. J. Bacteriol., 2015. **197**(19): p. 3182-3190.
328. de Alteriis, E., et al., *Revisiting the Crabtree/Warburg effect in a dynamic perspective: a fitness advantage against sugar-induced cell death*. Cell Cycle, 2018. **17**(6): p. 688-701.
329. Bloch, H. and W. Segal, *Biochemical differentiation of Mycobacterium tuberculosis grown in vivo and in vitro*. J. Bacteriol., 1956. **72**(2): p. 132-141.
330. de Carvalho, L.P., et al., *Metabolomics of Mycobacterium tuberculosis reveals compartmentalized co-catabolism of carbon substrates*. Chem. Biol., 2010. **17**(10): p. 1122-31.

## 13. ANNEX

## 13.1. PROTOCOL FOR PROTEOMIC ANALYSIS OF MYCOBACTERIAL STRAINS

Kindly provided by the Molecular and Applied Microbiology research group at the Leibniz Institute for Natural Product Research and Infection Biology – Hans Knöll Institute (HKI).

## 13.1.1. Reagents

	Component	Concentration
Lysogeny broth (LB)	Tryptone	10 g L <sup>-1</sup>
	Yeast extract	5 g L <sup>-1</sup>
	NaCl	5 g L <sup>-1</sup>
Hartman's de Bont (HdB)	(NH <sub>4</sub> ) <sub>2</sub> SO <sub>4</sub>	2 g L <sup>-1</sup>
	MgCl <sub>2</sub> ·7H <sub>2</sub> O	0.1 g L <sup>-1</sup>
	Na <sub>2</sub> HPO <sub>4</sub>	3 g L <sup>-1</sup>
	KH <sub>2</sub> PO <sub>4</sub>	1 g L <sup>-1</sup>
	Trace element solution 100X	10 g L <sup>-1</sup>
	Carbon source 100X	10 g L <sup>-1</sup>
HdB trace element solution* 100X	EDTA	1 g L <sup>-1</sup>
	CaCl <sub>2</sub> ·2H <sub>2</sub> O	0.1 mg L <sup>-1</sup>
	Na <sub>2</sub> MoO <sub>4</sub> ·2H <sub>2</sub> O	0.02 g L <sup>-1</sup>
	CoCl <sub>2</sub> ·6H <sub>2</sub> O	0.04 g L <sup>-1</sup>
	MnCl <sub>2</sub> ·4H <sub>2</sub> O	0.12 g L <sup>-1</sup>
	ZnSO <sub>4</sub> ·7H <sub>2</sub> O	0.2 g L <sup>-1</sup>
	FeSO <sub>4</sub> ·7H <sub>2</sub> O	0.5 g L <sup>-1</sup>
	CuSO <sub>4</sub> ·5H <sub>2</sub> O	0.02 g L <sup>-1</sup>
Lysis buffer	SDS	10 g L <sup>-1</sup>
	NaCl	150 mM
	TEAB	100 mM
	cOmplete™ ULTRA Protease Inhibitor Cocktail (Roche)	1 tablet in 10 mL <sup>-1</sup>
	Phosphostop (Roche)	1 tablet in 10 mL <sup>-1</sup>
	TEAB	Trimethylammonium bicarbonate (Thermo)
Cation exchange	Pierce Strong Cation Exchange Kit	NA
Benzonase	Benzonase (Novagen)	250 U mL <sup>-1</sup>
Reduction buffer	TCEP	500 mM
	TEAB	100 mM
Alkylation buffer	2-chloroacetamide (CAA)	0.0292 g, 625 mM
	TEAB	500 µL, 100 mM
Protein precipitation	Chilled MeOH (-20°C)	NA
	Chilled chloroform (-20°C)	NA
	Chilled ultrapure water	NA
Resuspension buffer	2,2,2-trifluoroethanol	5%
	TEAB (optional)	100 mM
Resolubilization buffer	Trifluoroacetic acid	0.05%
	Acetonitrile	2%
rLysC 1 µg µL <sup>-1</sup>	rLysC (Promega V1671)	15 µg
	Acetic acid	15 µL, 50 mM
Trypsin 2 µg µL <sup>-1</sup>	Trypsin Gold (Promega V5280)	100 µg
	Acetic acid	50 µL, 50 mM

**Protocol for proteomic analysis of mycobacterial strains***13.1.2. Protocol*

1. Prepare a preculture in LB broth of wild-type *M. smegmatis* and a knockout  $\Delta mftAB$  strain.
2. Incubate at 37°C until an OD 2.
3. Centrifuge the preculture at 4000 rpm for 30 min and discard the supernatant. Resuspend in HdB base media and centrifuge again to wash the cells from LB components.
4. Repeat 3 times and discard the supernatant.
5. Dilute the pellet to an OD of 0.65 – 0.7 and inoculate 100 mL HdB at a 1/100 ratio in a properly sized flask. Supplement the media with 0.5 g L<sup>-1</sup> tyloxapol and either 10 g L<sup>-1</sup> glucose or lactate as the sole carbon source.
6. Incubate at 37°C until an OD 2.
7. Split the culture in 3x50 mL polypropylene conical tubes with 30 mL culture. Centrifuge for 4000 rpm for 30 min and discard the supernatant.
8. Repeat 2 times with 10 mL HdB base media and discard the supernatant.
9. Resuspend the washed pellet in 600 µL lysis buffer or more if necessary, to ensure complete dissolution.
10. Transfer to a Bead Beater compatible screw-cap tube with 0.5 g small glass beads (Ø 0.5 mm) and 3-4 individual large glass beads (Ø 4 mm).
11. Lyse the cells in a Bead Beater with a standard protocol (5000 rpm for 20 seconds) with 5 minutes incubation in ice between cycles. Repeat 5 times. Centrifuge and transfer the supernatant to a new tube, all following centrifugation steps should be done 15 minutes at maximum speed and 4°C.
12. In this step, to remove potential traces of tyloxapol, use the Pierce Strong Cation Exchange kit following the manufacturer's recommendations. Resuspend the precipitated protein pellet in the kit purification buffer and sonicate in the water bath for 15 minutes. Elute 2 times in 50 µL TEAB.
13. Add 0.4 µL benzonase, incubate at 37°C and mix thoroughly through the time in an ultrasonic bath with ultrasound ON. Centrifuge and transfer to a new tube.
14. Quantify protein concentration in the supernatant with the Direct Detect system and TEAB as blank. Dilute if required (lineal concentration range 0.25 – 5 µg µL<sup>-1</sup>). Take 100 µg and complete to 100 µL with TEAB in a new tube.
15. Add 2 µL reduction buffer and mix.
16. Add 2 µL alkylation buffer and mix.
17. Incubate in a preheated thermomixer at 70°C and 500 rpm in darkness for 30 minutes.
18. Freeze at -20°C for 15 minutes. Precipitate protein as follows.
19. Add 400 µL chilled MeOH (-20°C) and mix.
20. Add 100 µL chilled chloroform (-20°C) and mix.
21. Add 300 µL ultra-pure, ice-cold water, and mix.
22. Incubate at -20°C for 5 minutes.
23. Centrifuge for 5 minutes.

**Protocol for proteomic analysis of mycobacterial strains**

24. Discard the top aqueous layer, without disturbing the protein interphase.
25. Add 400  $\mu\text{L}$  chilled MeOH ( $-20^{\circ}\text{C}$ ) and mix thoroughly. Centrifuge 5 minutes again.
26. Discard the organic supernatant containing chloroform. Dry in a Speedvac for 5 minutes without excessive drying. Resuspend in 100  $\mu\text{L}$  resuspension buffer, sonicate in the water bath for 15 minutes.
27. Add 2  $\mu\text{L}$  1  $\mu\text{g}$   $\mu\text{L}^{-1}$  rLysC for a protease: protein ratio 1:50. Mix gently and incubate 2 hours at  $37^{\circ}\text{C}$ .
28. Add 2  $\mu\text{L}$  2  $\mu\text{g}$   $\mu\text{L}^{-1}$  trypsin for a protease: protein ratio 1:25. Mix gently and incubate 16 hours at  $37^{\circ}\text{C}$ .
29. Evaporate in SpeedVac until dryness
30. Resolubilize in 25  $\mu\text{L}$  resolubilization buffer by pipetting up and down several times, 15 minutes with sonication in a water bath, and vortex.
31. Filter through a 0.2  $\mu\text{m}$  spin filter (Merck UFC30LG25) at 18,000 g for 15 minutes at  $4^{\circ}\text{C}$ .
32. Transfer to an LC-MS-compatible vial for bottom-up proteomic analysis as follows.

*13.1.3. LC-MS protocol*

LC-MS/MS analysis was carried out on an Ultimate 3000 nano RSLC system coupled to a Q Exactive HF mass spectrometer (both Thermo Fisher Scientific, Waltham, MA, USA). Peptide trapping for 5 min on an Acclaim Pep Map 100 column (2 cm x 75  $\mu\text{m}$ , 3  $\mu\text{m}$ ) at 5  $\mu\text{L}/\text{min}$  was followed by separation on an analytical Acclaim Pep Map RSLC nano column (50 cm x 75  $\mu\text{m}$ , 2  $\mu\text{m}$ ). Eluents A (0.1% [v/v] formic acid in water) and B (0.1% [v/v] formic acid in 90/10 acetonitrile/water [v/v]) were mixed as follows: 0-4 min at 4% B, 60 min at 12% B, 120 min at 16% B, 150 min at 25% B, 175 min at 35% B, 200 min at 60% B, 210-215 min at 96% B, 215.1-240 min at 4% B. Positively charged ions were generated at 2.2 kV using a Nanospray Flex Ion Source (Thermo Fisher Scientific) and monitored at  $m/z$  300-1500,  $R=120,000$  full width at half maximum (FWHM) using a maximum injection time (IT<sub>max</sub>) of 120 ms and an automatic gain control (AGC) target of  $3e6$ . Precursor ions were selected for fragmentation in a data-dependent manner (Top15,  $z=2-5$ ) at an isolation width of  $m/z$  1.6 amu for higher-energy collisional dissociation (HCD) fragmentation at 30% normalized collision energy (NCE). MS<sub>2</sub> ions were scanned at  $R=15,000$  FWHM (IT<sub>max</sub>=75 ms, AGC=  $2e5$ ) using a dynamic exclusion of precursor ions for 30 s. The LC-MS/MS instrument was controlled by Chromeleon 7.2, QExactive HF Tune 2.8, and Xcalibur 4.0 software.

#### Protein database search

Tandem mass spectra were searched against the UniProt reference proteome database (2018/09/13; <https://www.uniprot.org/proteomes/UP000000757>) of *Mycobacterium smegmatis* ATCC 700084 using Proteome Discoverer (PD) 2.2 (Thermo) and the algorithms of Mascot 2.4 (Matrix Science, UK), Sequest HT (version of PD2.2) and MS Amanda 2.0. Two missed cleavages were allowed for the tryptic digestion. The precursor mass tolerance was set to 10 ppm and the fragment mass tolerance was set to 0.02 Da. Modifications were defined as dynamic Met oxidation and protein *N*-term acetylation as well as static Cys carbamidomethylation. A strict false discovery rate (FDR) < 1% on both peptide and protein level were required for positive protein hits. The Percolator node of PD2.2 and a reverse decoy database was used for q value validation of spectral matches. Only rank 1 proteins and peptides of the top scored proteins were counted. The Minora algorithm of PD2.2 was applied for relative protein abundance quantification.

#### 14. ACKNOWLEDGMENTS

My family is my support, role models, encouragers, advocates, and fanatics, and for them, this achievement is greatly owed. Mom and dad have been an inspiration of hard-work and dedication, my compass, and my guide as a scientist and an adult. My sister, Ana, always my little princess, your encouragement and passion for my work recharges my batteries. To them, I dedicate this work.

I want to thank Dr. Gerald Lackner for inviting me to join the new Synthetic Microbiology research group as the first doctoral student. Our fruitful discussions, Friday afternoons scanning spectra after spectra, and shared surprises along the way have been rewarded with the publications here presented and planted the seed for years of exciting discoveries in novel cofactors. I look forward to his prolific scientific career, of which I am happy to be part. I want to thank Prof. Dr. Christian Hertweck for his support through the years, sharp observations on my presentations, and his critical review of the present work.

On this adventure, I was joined by a wonderful group of scientific researchers. With Patricia Graça, we embarked on the adventure of a lifetime, and without her hard work and tenacious spirit for excellence (and cleanliness), this work would not have been possible. I eagerly wait for her results. I wish plenty of success to Patricia and Mark Ellerhorst in the next phase of the mycofactocin research. I anticipate enlightening results that will answer many questions that this project has opened. I also want to thank Dr. Sirinthra Thiengmag for her hard work, friendship, and good memories during our time in Jena and even funnier memories in Zurich.

The Synthetic Microbiology research group is a *zettelkasten* with many drawers, and together we connect knowledge in biochemistry, microbiology, and synthetic biology. I want to thank the F<sub>420</sub> drawer for their experience and support: Dr. Daniel Last and Mahmudul Hasan for their support and fruitful discussions for the past and future projects. Special thanks go to Dr. Daniel Braga for his formidable breadth of knowledge and sharpshooter eye with critical review. And thank you to the Therapeutic Microbes and Balance of the Microverse team: Dr. Alexandre Chamas, Martha Sporniak, and Alexander Mauz. Together, I hope our group has been instructive and welcoming to the students that have come through our doors looking for knowledge, especially those in the mycofactocin project: Sandesh Neupane, Rita Müller, and Daniela Winkler.

I want to thank the co-authors of our publications, members of the Chemical Biology of Microbe-Host Interactions Dr. Christine Beemelmans and Dr. Huijuan Guo for bringing their



## ACKNOWLEDGMENTS

scientific expertise to this project. Dr. Tobias Köllner at the Max Plank Institute for Chemical Biology for his GC-MS measurements and instruction. Furthermore, our reports were invaluable helped by the scientific staff at the Bio-Pilot Plant. I want to thank Dr. Lars Regestein, Dr. Ivan Schlembach, Dr. Bettina Bardl, Michael Cyrulies, and collaborators for their invaluable support, insightful discussion, and thorough training. And Dr. Thomas Krüger at the Molecular and Applied Microbiology research group for his training in gel-free proteomics and data analysis. Our research at the HKI would not be possible without our administration, purchase, IT, and colleagues in other departments, and I thank them for their hard work and dedication.

During my time at the Hans Knöll Institute and at Jena, I have come to meet and make friendships with an incredible group of hard-working scientists, colleagues, and persons. Thank you to my dear Farzaneh, Carito, Hendrik and Irina, Kiara, Kendra and Alberto, Martin, Lia, Felicia, Evgeni, Iuliia, Derek and Laura, Hally, Martha, and Laura, Juan Camilo, Johana, and so many more. It is now time to say so long, farewell, auf Wiedersehen, and good night. Our paths will cross again someday.

Coming to Jena was a rewarding decision, but John has always encouraged me to go forward unafraid, way before this project started and, many times, more convinced than myself. He is my biggest cheerleader with pompoms, the voice in my head that reminds me that everything has a beginning, a purpose, and a destination. I will always be grateful to life and destiny to be part of his life and happy to have him in mine.

**15. SELBSTÄNDIGKEITSERKLÄRUNG**

Ich versichere, dass ich die vorliegende Arbeit selbstständig und ohne andere als die angegebenen Hilfsmittel verfasst habe. Die aus fremden Quellen direkt oder indirekt übernommenen Gedanken sind als solche gekennzeichnet.

Jena, den 29.09.2021

---

Luis Alberto Peña Ortiz

## 16. CURRICULUM VITÆ

**Personal Data**

**Name:** Luis Alberto Peña Ortiz  
**Date and place of birth:** March 7<sup>th</sup>, 1987, in Bogotá, Colombia

**Scientific Publications**

Peña-Ortiz, Luis; Graça, Ana Patrícia; Guo, Huijuan; Braga, Daniel; Köllner, Tobias G.; Regestein, Lars; Beemelmans, Christine; Lackner, Gerald. Structure elucidation of the redox cofactor mycofactocin reveals oligo-glycosylation by MftF. *Chem. Sci.*, 2020,11, 5182-5190. DOI: 10.1039/D0SC01172J

Peña-Ortiz, Luis; Schlembach, Ivan; Lackner, Gerald; Regestein, Lars. Impact of Oxygen Supply and Scale Up on *Mycobacterium smegmatis* Cultivation and Mycofactocin Formation. *Front. Bioeng. Biotechnol.*,2020, 8:593781. DOI: 10.3389/fbioe.2020.593781

**Scientific Presentations**

Poster presentation at the Annual Meeting of the Association for General and Applied Microbiology (VAAM). Title of the poster “Biosynthesis and Oligo-Glycosylation of the Redox Cofactor Mycofactocin in *Mycolicibacterium smegmatis*”. March 8<sup>th</sup> – 11<sup>th</sup>, 2020, in Leipzig, Germany.

Poster presentation at the VAAM Workshop "Biology of Microorganisms Producing Natural Products". Title of the poster “Approximation to the heterologous expression and structure elucidation of the proposed cofactor mycofactocin”. September 15<sup>th</sup> – 19<sup>th</sup>, 2019, in Jena, Germany.

Speaker of the Jena School for Microbial Communication (JSMC) workshop “Untargeted metabolomics using high-resolution LC-MS”. January 31<sup>st</sup> – February 01<sup>st</sup>, 2018, in Jena, Germany.

Member of the organizing committee of the JSMC 8<sup>th</sup> International Conference on Microbial Communication for Young Scientists. March 19<sup>th</sup> – 22<sup>nd</sup>, 2018, in Jena, Germany.

Poster presentation at the VAAM Workshop "Emerging Trends in Natural Product Biotechnology". Title of the poster “Heterologous production of the Mycobacteria-associated cofactor mycofactocin”. September 20<sup>th</sup>, 2018, in Dortmund, Germany.

Scientific talk at the International Leibniz Research School (ILRS) symposium. Title of the talk: “Characterization of an L-lactate dehydrogenase putatively related to a cryptic cofactor in *Mycobacterium smegmatis*”. May 7<sup>th</sup> – 8<sup>th</sup>, 2018, in Jena, Germany.